中國醫藥大學藥學院
藥物化學研究所博士論文

指 導 教 授： 郭 盛 助　教 授

共同指導教授： 楊 寧 蓀　教 授

吳 金 濱　教 授

(I)新穎喹諾酮 CMQ 經活性氧和粒腺體路徑誘發前列腺癌細胞凋亡和有絲分裂災難
(Novel quinolone CMQ induces apoptosis and mitotic catastrophe in prostate cancer cells via reactive oxygen species- and mitochondria-dependent pathways)

(II)CMQ 增強樹突細胞為基礎之癌症疫苗的功效
(CMQ augments efficacy of dendritic cell-based cancer vaccines)

(III)特定植物萜類和木酚素具有強效的抗急性呼吸道症狀病毒之活性
(Specific plant terpenoids and lignoids possess potent antiviral activities against severe acute respiratory syndrome coronavirus)

研究生： 溫 致 群

Chih-Chun Wen

中 華 民 國 100 年 7 月

中國醫藥大學藥學院藥物化學研究所
博士學位考試

(I)新穎喹諾酮 CMQ 經活性氧和粒腺體路徑誘發前列腺癌細胞凋亡和有絲分裂災難

(II)CMQ 增強樹突細胞為基礎之癌症疫苗的功效

(III)特定植物萜類和木酚素具有強效的抗急性呼吸道症狀病毒之活性

(I)Novel quinolone CMQ induces apoptosis and mitotic catastrophe in prostate cancer cells via reactive oxygen species- and mitochondria-dependent pathways
(II)CMQ augments efficacy of dendritic cell-based cancer vaccines
(III)Specific plant terpenoids and lignoids possess potent antiviral activities against severe acute respiratory syndrome coronavirus

指　導　老　師　：　郭　盛　助　教授
共同指導老師　：　楊　寧　蓀　教授
　　　　　　　　　　吳　金　濱　教授
研　　究　　生　：　溫　致　群

　　本論文係 溫 致 群 同學於中國醫藥大學藥學院藥物化學研究所完成之博士論文，經考試委員審查及口試合格，特此證明。

論文口試委員審定書

考試委員：

所　　　　　長：

中 華 民 國 100 年 7 月 11 日

Acknowledgement

大學廖志中老師在學習過程中的指正和生活上的打氣幫忙。我很想再感謝的就是我的良師益友中興大學簡世昌教授，感謝他在婚禮的幫忙和博士班歷程中，不斷地提供精神和生活上的灌溉，也提供了許多科學上的指導，非常感謝。

攻讀博士的過程中，太多的人需要感謝。首先，想要感謝在中研院楊寧蓀實驗室裡曾經幫忙或一起工作過的同事們，謝謝我的難兄難弟魏紋祈魏傑克，很高興看到你的卓越成長和感謝你給我的幫忙；謝謝繪名鞋姊在實驗和生活上的幫忙，謝謝現任同事們碧雪、莉婷、永祥、薇婷、Arul、Tina、Blue、小倩、聖晏、詠宗、怡君、書翊、佳奇、小昭和年輕有為的章杰，感謝楊寧蓀實驗室的前同事們曹小曹、徐師傅、琇慧、文經、Terry、小美、瑩筑、雅玲、文心學姊、小米茶、淑貞、王正方博士、Kandan、、Vani、Steve、顏伯任(Robert)、趙嶸、坤珀、育生、青晉、靜芳、淑敏；也感謝中研院其他實驗室所有曾經幫過我的人，謝謝聿智、永志、阿伯、洪博、慶豐、俊維、佳穎、逸人、恩豪、進賢、秋萍、育雯、瑀心、世川、怡均、清毅、郭博、秉忠、小佑、恬岉、志翰、小賴、奕枚、包子、宗遠、政權、慧玲、啟彰、智揚、俊杰、皎君、書甄、秉智、凱偉、子軒、均宇、偉君，謝謝你們的陪伴和幫忙。另外，我也想特別感謝中國醫藥大學曾經幫助過我的貴人謝謝立琛常常不辭辛勞地幫忙，真心地非常感謝你的熱心幫助，謝謝學長姐們俊仁美華夫婦、勝宏學長、健源學長，謝謝同學們momo、華鑫、元照、亮董和怡倩的幫忙，謝謝學弟妹們泰霖、士鳴，也特別感謝廖紋瑩蟲蟲時常的鼎力相助。此外，我想感謝我的死黨，恭喜也謝謝黎雁行博士，謝謝大熊、芭樂。還有一直情義相挺的 Kenny 和老大，謝謝你們在我需要幫忙時，幫助我！

最後，我想將這份論文獻給我最重要的親人們！首先，是我最親愛的父母親，爸媽，您們是很偉大也是全世界最好的爸媽，很謝謝您們這麼地相信和栽培著我，謝謝你們，沒有你們，就沒有這份論文，謝謝爸爸和媽媽！再來，我想要將這份論文獻給我在天國的叔叔（乾爸），謝謝您一直鼓勵我，我真的很希望您可以看到我畢業的那一刻，謝謝 K 爸，我也想謝謝我的乾媽，謝謝乾媽一路的支持和鼓勵；我也想獻給我在天上的爺爺和奶奶，希望您們能夠感到高興。再者，我想要謝謝我的大哥致遠，謝謝你一直都支持你的弟弟，我感受的到，哥，謝謝你！也謝謝我的兩個妹妹致儀和致絹，相信你們也會為我高興，謝謝你們！還要謝謝我的另一爸媽我的岳父岳母，不但不嫌棄我，更願意將他們最寶貴的掌上明珠許配給我，也僅以這份論文獻給您們！在這最後的最後，壓軸中的壓軸，我想要以這份論文獻給剛成為我最親密的家人岳穎，謝謝你當初在眾多競爭者中選擇了我一個窮學生，謝謝你在我學習歷程中的支持，謝謝你走進我的生命中，更謝謝你給我機會在民國一百年完成了與妳的終身大事和學業，謝謝你成為我生命中的一部份，沒有你就沒有這份論文，謝謝我最棒的老婆！
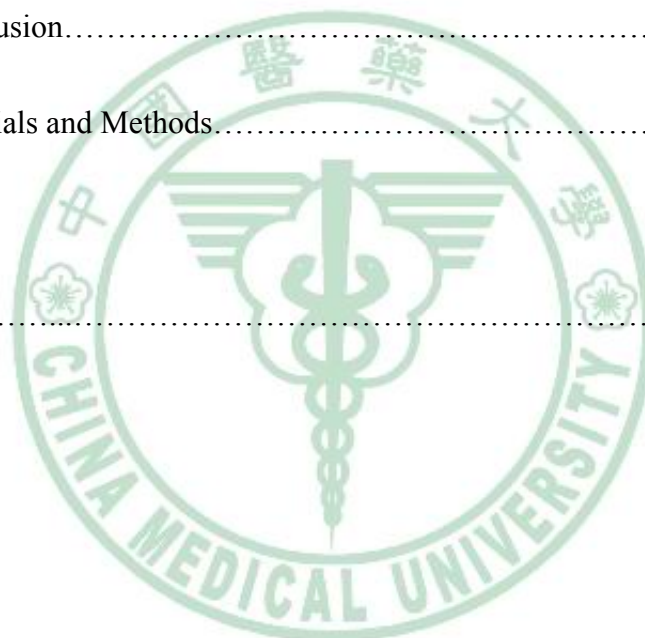
Table of Contents

Abbreviation

2P4Q	2-phenyl-4-quinolone
ABC	ATP binding cassette
AIF	Apoptosis-inducing factor
ALL	acute lymphoblastic leukemias
APC	antigen-presenting cell
ATCC	American Type Culture Collection
BMDC	bone marrow-derived dendritic cells
BrdU	5-bromo-2-deoxyuridine
CBE	75% ethanol extract from *Cibotium barometz*
CBM	methanol extract from *Cibotium barometz*
CEA	carcinoembryogenic antigen
CICD	caspase-independent cell death
CC_{50}	the cytotoxic concentration (CC_{50}) of test compounds that
CCR7	CC chemokine receptor 7
CMQ	2- (3-chlorophenyl)- 6, 7-methylenedioxyquinolin-4-one
concn	concentration
COX-2	cyclooxygenase-2
CPE	cytopathogenic effect
CRT	calreticulin
CTCL-CMQ	Dendritic cells were pulsed with CMQ-treated tumor cell lysate
CTL	cytotoxic T lymphocyte
CTH	*n*-hexane extract from *Cassia tora*
DAMPs	damage-Associated Molecular Patterns

DAPI	4',6-diamidino-2-phenylindole
DBM	methanol extract from *Dioscorea batatas*
DCs	dendritic cells
DMSO	dimethyl sulfoxide
DR	death receptor
DSB	double strand breaks
DTT	dithiothreitol
EC_{50}	the effective concentration (EC_{50}) for the inhibition of viral
ELISA	Enzyme-linked immunosorbent assay
END	endoreduplication
ER	endoplasmic reticulum
Eq. 1	Equation 1
Eq. 2	Equation 2
F-T	4-6 cycles of freezing-thawing
FBS	fetal bovine serum
FITC	fluorescein isothiocyanate
FMKp	a bacterial membrane fragment of *Klebsiella pneumonia*
FMQ	2-(3-fluorophenyl)-6,7-methylenedioxyquinolin-4-one
FRET	fluorescence energy transfer
GM-CSF	granulocyte macrophage colony-stimulating factor
GSH	*n*-hexane extract from *Gentiana scabra*
H_2DCFDA	dichlorodihydrofluorescein diacetate
HMGB1	high-mobility group box 1
HSP70	heat shock protein 70

HSP90	heat shock protein 90
IAP	inhibitor of apoptosis
ICD	immunogenic cell death
I.D.	intradernally
IL-1β	interleukin-1β
IL-4	interleukin-4
IL-6	interleukin-6
IL-10	interleukin-10
IL-12	interleukin-12
iNOS	inducible nitric oxide synthase
I.N	intranodally
Irra	irradiation (60 Gray)
I.T.	intratumorally
I.V.	intravenously
DX	doxorubicin
KLH	keyhole limpet hemocyanin
mAb	monoclonal antibodies
maDC	matured DC
MBAs	microtubule-binding agents
MC	mitotic catastrophe
MDAs	microtubule-depolymerizing agents
MDDC,	monocyte-derived dendritic cells
MDR	multidrug resistance
MFI	mean fluorescence intensity

MHC	major histocompatibility complex
MRP	multidrug resistance-associated protein
MTAs	microtubule-targeting agents
MTT	3-(4,5-dimethylthiazol-2-yl)-2,5-diphenyltetrazolium bromide
NAC	N-acetyl cysteine
N.C.	not calculable
NCCD	nomenclature committee on cell death
NF-κB	nuclear factor kappa B
NIC	niclosamide
NMDA	N-nethyl D-aspartate
NSCLC	non-small-cell lung carcinomas
N.T.	not tested
OD	Optical density
PBMC	peripheral blood mononuclear cells
PBST	PBS containing 0.1% Tween 20
PCD	Programmed cell death
PDB	Protein Data Bank
PE	phycoerythrin
PI	propidium iodide
PMSF	phenylmethylsulfonnylfluoride
PSMA	prostate-specific membrane antigen
PTX	paclitaxel
S.C.	subcutaneously
SCID	severe combined immunodeficient
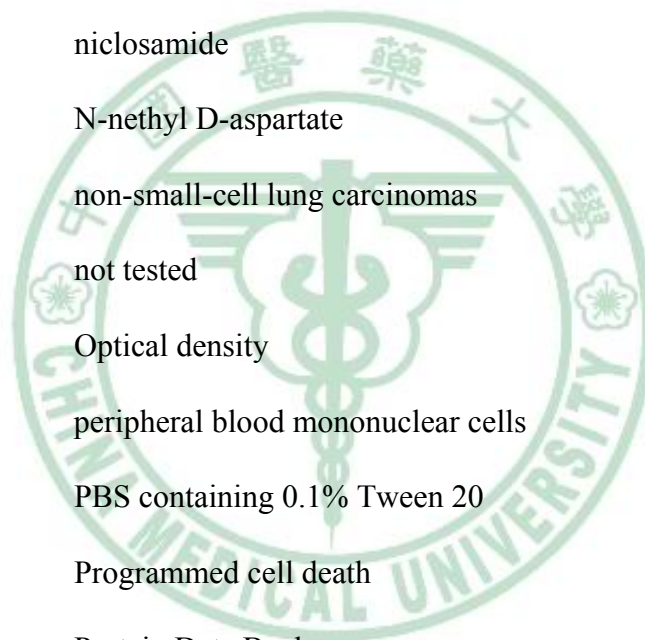
S.D.	standard deviation
SI	Selective index
ROS	reactive oxygen species
SARS	severe acute respiratory syndrome
SARS -CoV	SARS coronavirus
TAAs	tumor-associated antigens
TBAs	tubulin-binding asgents
TCH	*n*-hexane extract from *Taxillus chinensis*
TCLs	tumor cell lysates
TCL-C	DCs pulsed with colchicne-treated tumor cell lysate for 12h,
TCL-CMQ	DCs pulsed with CMQ-treated tumor cell lysate for 12h,
TCL-DMSO	DCs pulsed with DMSO-treated tumor cell lysate for 12h,
TCL-DX	DCs pulsed with DX-treated tumor cell lysate for 12h,
TCL-FMQ	DCs pulsed with FMQ-treated tumor cell lysate for 12h,
TCM	traditional Chinese medicines
TNF-α	tumor necrosis factor-α
T_{Reg}	regulatory T cells
V	vincristine
VAL	valinomycin
Z-IETD-FMK	caspase-8 inhibitor
Z-VAD-FMK	caspase family inhibitor

Figures

XII

XIII

Tables

中文摘要

第一部分：

在第一個研究部分，我們利用 CMQ 作為候選藥物探討在 p53 基因表達的前列腺癌 LNCaP 細胞和 p53 基因缺乏的前列腺癌 PC-3 細胞的抗癌活性。體外結果顯示 CMQ 可抑制這兩種癌細胞的增生，這種抑制效果與微管解聚效果和 G2/M 細胞週期中止有關。CMQ 在 LNCaP 細胞引起嚴重的凋亡 (apoptosis) 效果，但是，在 PC-3 細胞則引起核內複製 (endoreduplication) 和延後性的細胞死亡。細胞週期的封鎖被發現與升高的活性氧 (reactive oxygen species, ROS) 的升高量有關，進而啟動了粒腺體凋亡路徑及後續的 caspase-3 和 caspase-9 的活化。此外，CMQ 可以活化 LNCaP 細胞中的 Caspase-8，在 PC-3 細胞則不然。腹腔內注射 CMQ 有效性抑制在帶有 LNCaP 和 PC-3 之免疫不全小鼠之癌細胞生長。這些實驗結果顯示 CMQ 在這兩種前列腺癌細胞具有可區分的抗癌效果。

關鍵詞：CMQ；2-phenyl-4-quinolone；細胞凋亡；有絲分裂災難；抗癌活性

第二部分：

　　損害相關分子模式(damage-Associated Molecular Patterns, DAMPs)和免疫性的細胞死亡(immunogenic cell death, ICD)相關，而且能促進樹突狀細胞(dendritic cells, DCs)的成熟和抗原呈現。特定的微管解聚劑(microtubule-depolymerizing agents, MDAs)例如秋水仙素已經被發現能抗癌和活化樹突狀細胞。在這個部分的研究，我們評估三種了 MDAs，包括秋水仙素和兩種 2-phenyl-4-quinolone (2P4Q)衍生物，誘發在癌細胞免疫性細胞死亡的能力及活化樹突狀細胞和增加 T 細胞的能力。這三個測試的 MDAs 可以使 HSP70 (heat shock protein 70)、HSP90 (heat shock protein 90)和 HMGB1 (high-mobility group box 1)的 DAMPs 增加，但卻不能增加 calreticulin（CRT）的表現量。樹突狀細胞加上經由 MDAs 處理過內的腫瘤細胞裂解液 (tumor cell lysates, TCLs)為基礎的樹突狀細胞疫苗有效地抑制癌細胞生長和增加小鼠存活率，並且對癌細胞具有細胞毒性 T 淋巴球(cytotoxic T lymphocyte, CTL)的活性。在體內利用抗體刪除的實驗中，顯示 CD8$^+$ T 細胞和自然殺手細胞才是主要影響此項抗癌活性的主要細胞，而非 CD4$^+$ T 細胞。此外，在處理和刺激樹突狀細胞的過程中，加入白介素-4 (interleukin-4, IL-4)和顆粒細胞巨噬細胞群落刺激因子(granulocyte macrophage colony-stimulating factor, GM-CSF)可以有效地增加白介素-12 (interleukin-12, IL-12)和降低白介素-10 (interleukin-10, IL-10)

的分泌量。在另一方面，MDAs 也可以引起樹突狀細胞表面標記成熟表現，和增加 CD4$^+$ T 細胞和 CD8$^+$ T 細胞與樹突狀細胞(DCs)之增生。綜觀來說，MDAs 包括臨床使用的秋水仙素可以引起免疫性細胞死亡，MDA 處理過內的腫瘤裂解液(tumor cell lysates, TCLs)為基礎的樹突狀細胞疫苗可以產生強效的抗癌免疫活性。這個研究方法也許可以在未來臨床上癌症疫苗發展的指標。

關鍵詞：免疫性的細胞死亡；2-phenyl-4-quinolone；樹突細胞；秋水仙素；癌症疫苗

第三部分：

　　為避免抗嚴重急性呼吸道症候群(severe acute respiratory syndrome, SARS)這種致命疾病的捲土重來，發展抗嚴重急性呼吸道症候群冠狀病毒(SARS coronavirus, SARS-CoV)藥物是重要的。在這個研究中，利用 SARS-CoV 感染 Vero E6 細胞所產生的細胞病變效應(cytopathogenic effect,CPE)為測定法來評估超過兩百個植化物和超過兩百個中草藥萃取物之抗 SARS-CoV 活性。植化物中，十個雙萜類化合物、兩個倍半萜類化合物、兩個三萜類化合物、五個木酚素類化合物、薑黃素和兩個參考有效控制組 niclosamide 和 valinomycin 在濃度 3.3-10 µM 皆為 CPE 抑制劑. 六種植化萃取物在濃度 25-200 µg/ml 也為強的抑制劑，分別為從龍膽（*Gentiana scabra*）萃取的 GSH、從淮山藥（*Dioscorea batatas*）萃取的 DBM、從決明子（*Cassia tora*）萃取的 CTH、從桑寄生（*Taxillus chinensis*）萃取的 TCH 和從狗脊（*Cibotium barometz*）萃取的 CBE 和 CBM。並針對二十二個化合物和六個植物萃取物進行抑制 50 %Vero E6 細胞增殖的樣品濃度(CC_{50})和抑制 50 %病毒繁殖的樣品濃度(EC_{50})之測定。最有效的植化物 **1**、**5**、**6**、**8**、**14** 和 **16** 其選擇性指數值(Selective index values, SI, SI= $CC_{50/}$ EC_{50})分別為 58、>510、111、193、180 和>667。CBE、GSH、DBM、CTH 和 TCH 這五種最有效萃取物其 SI 分別為> 59.4、> 57.5、> 62.1、> 59.4 和 > 92.9。 Betulinic acid (**13**) 和 savinin (**16**) 是 SARS-CoV 3CL 蛋

白質酶競爭性抑制劑，其 K_i 值 分別為 $8.2 \pm 0.7\ \mu M$ 和 $9.1 \pm 2.4\ \mu M$。

CBM 和 DBM 也顯示能制 SARS-CoV 3CL 蛋白質酶活性，其 IC_{50} 分別為

$39\ \mu g/ml$ 和 $44\ \mu g/ml$。我們的研究顯示特定的雙萜類化合物、木酚素類化

合物和這六種化合物具有強效的抗 SARS 效果。

關鍵詞：嚴重急性呼吸道症候群；萜類；木酚素類；植物萃取物；3CL

蛋白質酶

Abstract

Part I.

In this study, we investigated the effect of 2- (3-chlorophenyl)- 6, 7-methylenedioxyquinolin-4-one (CMQ) as a drug candidate for anti-tumor activities in p53-expressing LNCaP cells and p53-null PC-3 cells of prostate cancers. *In vitro* results showed that CMQ-1 inhibited tumor cell growth in both cell types, and the inhibition was associated with microtubule-depolymerizing activity and G2/M cell cycle arrest in both cell lines. Intriguingly, CMQ triggered a strong apoptotic activity in LNCaP cells but induced an endoreduplication activity and delayed cell death in the tested PC-3 cells. The cell cycle blockade was found to be associated with an elevated level of reactive oxygen species (ROS), followed by activation of the mitochondrial apoptotic pathway, with subsequent consecutive activation of caspases-9 and -3. In addition, CMQ significantly activated caspase-8 in LNCaP cells but not in PC-3 cells. Intraperitoneal injection of CMQ significantly suppressed tumor growth in SCID mice bearing LNCaP or PC-3 xenografts. Our findings suggest that CMQ may display differential antitumor activities in different prostate cancers, and this may have clinical applications.

Keywords: CMQ, 2-phenyl-4-quinolone, apoptosis, mitotic catastrophe, anti-tumor activity

Part II.

Damage-associated molecular patterns (DAMPs) are associated with immunogenic cell death and have the ability to enhance maturation and antigen presentation of dendritic cells (DCs). Specific microtubule-depolymerizing agents (MDAs) such as colchicine have been shown to confer anti-cancer activity and also trigger activation of DCs. In the second section, we evaluated the ability of three MDAs (colchicine and two 2-phenl-4-quinolone analogues) to induce immunogenic cell death in test tumor cells, activate DCs, and augment T-cell proliferation activity. Three test phytochemicals considerably increased the expression of DAMPs including HSP70, HSP90 and HMGB1, but had no effect on expression of calreticulin (CRT). DC vaccines pulsed with MDA-treated tumor cell lysate (TCLs) had a significantly inhibitory effect on tumor growth, showed cytotoxic T-lymphocyte activity against tumors, and increased the survival rate of test mice. In vivo antibody depletion experiments suggested that $CD8^+$ T cells and NK cells, but not $CD4^+$ T cells, were the main effector cells responsible for the observed anti-tumor activity. In addition, culture of DCs with GM-CSF and IL-4 during the pulsing and stimulation period significantly increased the production of IL-12 and decreased production of IL-10. On the other hand, MDAs also induced phenotypic maturation of DCs and augmented $CD4^+$ and $CD8^+$ T-cell proliferation when co-cultured with DCs. Taken together, specific MDAs including the clinical drug, colchicine, can induce immunogenic cell death in tumor cells,

and DCs pulsed with MDA-treated tumor cell lysates (TCLs) can generate potent anti-tumor immunity in mice. This approach may warrant future clinical evaluation as a cancer vaccine.

Part III.

Development of anti-severe acute respiratory syndrome associated coronavirus (SARS-CoV) agents is pivotal to prevent the reemergence of the life-threatening disease, SARS. In this study, more than 200 phytocompounds and more than 200 extracts from Chinese medicinal herbs were evaluated for activity against anti-severe acute respiratory syndrome associated coronavirus (SARS-CoV) activities using a cell-based assay measuring SARS-CoV–induced cytopathogenic effect on Vero E6 cells. Ten diterpenoids, two sesquiterpenoids, two triterpenoids, five lignoids, curcumin and reference controls, niclosamide and valinomycin were potent inhibitors at concentrations between 3.3 and 10 µM. Six herbal extracts, one each from *Gentiana scabra*, *Dioscorea batatas*, *Cassia tora* and *Taxillus chinensis* (designated as GSH, DBM, CTH and TCH, respectively), and two from *Cibotium barometz* (designated as CBE and CBM), were found to be potent inhibitors of SARS-CoV at concentrations between 25 and 200 µg/ml. The concentrations of the 22 compounds and six extracts to inhibit 50% of Vero E6 cell proliferation (CC_{50}) and viral replication (EC_{50}) were measured. The selective index values ($SI = CC_{50}/EC_{50}$) of the most potent compound **5** and **16** were >510 and >667, respectively. In addition, the resulting selective index values of the most effective extracts CBE, GSH, DBM, CTH and TCH were > 59.4, > 57.5, > 62.1, > 59.4, and > 92.9, respectively. Betulinic acid (**13**) and savinin (**16**) were competitive inhibitors of SARS-CoV 3CL protease with K_i values = 8.2

± 0.7 and 9.1 ± 2.4 µM, respectively. Among these extracts, CBM and DBM also showed significant inhibition of SARS-CoV 3CL protease activity with IC_{50} values of 39 µg/ml and 44 µg/ml, respectively. Our findings suggest that specific abietane-type diterpenoids and lignoids as well as these six herbal extracts exhibit strong anti-SARS-CoV effects.

Keywords: SARS; terpenoids; lignoids; phytoextracts; 3CL protease

Part I. Novel quinolone CMQ induces apoptosis and mitotic catastrophe in prostate cancer cells via reactive oxygen species (ROS)- and mitochondria-dependent pathways

Chapter 1. Introduction

1.1. Epidemiology of prostate cancer

Cancer is probably the most extensive public health problem in the world including Taiwan. Prostate cancer is the most frequently diagnosed malignancy and the second leading cause of cancer-related deaths in men in the United States (*1-3*). In 2010, prostate cancer alone accounts for approximately 28 % of incidental cases and for 11 % of total cancer deaths in men (**Figure 1**) (*3*). Although the incidence of prostate cancer is lower in Asian countries, however, this type of cancer is one of the top 10 fatal cancers in Taiwan (**Table 1**) (*4*). Regional and early diagnosed tumors can be treated by radiation therapy and prostatectomy. However, it has been reported that numerous patients treated with prostatectomy suffer relapse (*5, 6*). The androgen-ablation therapy may be effective for the patients with relapsed disease at the initial stage, but the cancers eventually progress to hormone-refractory prostate cancer and metastasize to other organs, , leaving a majority of

the sufferers dead within a few years (*2, 7, 8*). To date, there is no effective treatment for locally advanced or metastatic prostate cancer. Therefore, it is particularly important to discover effective therapeutic agents that can treat androgen-dependent or/and androgen-independent prostate cancers without further progression and high mortality. In this context, many novel approaches for the treatment of prostate cancer are currently under development, including new androgen receptor antagonists, cytotoxic agents, antimitotic drugs, antiangiogenic agents, and immune-based therapies (*2*). Based on this rationale and importance, in this study, we investigate a novel quinolone derivative, CMQ, as a candidate anti-tumor agent in prostate cancer cells.
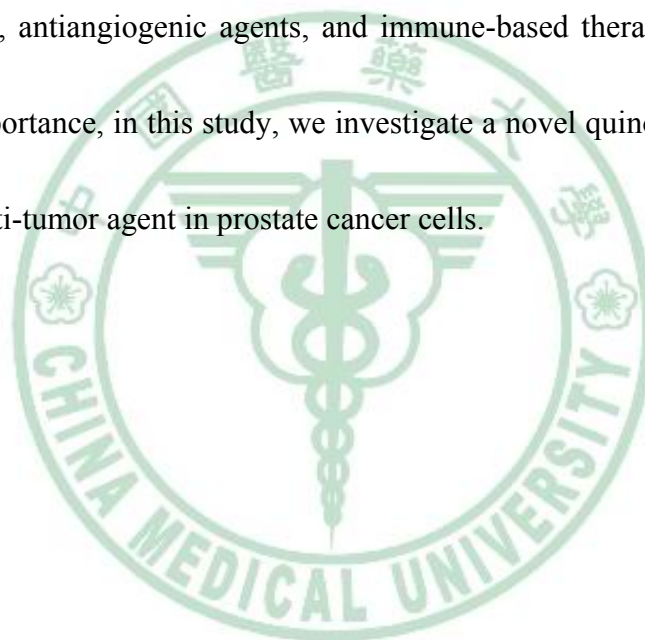
Estimated New Cases*

	Males			Females			
Prostate	217,730	28%		Breast	207,090	28%
Lung & bronchus	116,750	15%		Lung & bronchus	105,770	14%
Colon & rectum	72,090	9%		Colon & rectum	70,480	10%
Urinary bladder	52,760	7%		Uterine corpus	43,470	6%
Melanoma of the skin	38,870	5%		Thyroid	33,930	5%
Non-Hodgkin lymphoma	35,380	4%		Non-Hodgkin lymphoma	30,160	4%
Kidney & renal pelvis	35,370	4%		Melanoma of the skin	29,260	4%
Oral cavity & pharynx	25,420	3%		Kidney & renal pelvis	22,870	3%
Leukemia	24,690	3%		Ovary	21,880	3%
Pancreas	21,370	3%		Pancreas	21,770	3%
All Sites	**789,620**	**100%**		**All Sites**	**739,940**	**100%**

Estimated Deaths

	Males			Females			
Lung & bronchus	86,220	29%		Lung & bronchus	71,080	26%
Prostate	32,050	11%		Breast	39,840	15%
Colon & rectum	26,580	9%		Colon & rectum	24,790	9%
Pancreas	18,770	6%		Pancreas	18,030	7%
Liver & intrahepatic bile duct	12,720	4%		Ovary	13,850	5%
Leukemia	12,660	4%		Non-Hodgkin lymphoma	9,500	4%
Esophagus	11,650	4%		Leukemia	9,180	3%
Non-Hodgkin lymphoma	10,710	4%		Uterine Corpus	7,950	3%
Urinary bladder	10,410	3%		Liver & intrahepatic bile duct	6,190	2%
Kidney & renal pelvis	8,210	3%		Brain & other nervous system	5,720	2%
All Sites	**299,200**	**100%**		**All Sites**	**270,290**	**100%**

Figure 1. Ten leading cancer types for the estimated new cancer cases and deaths, by sex, United States, 2010. [Adopted from Jemal et al. (*3*)]

Table 1. Ten leading cancer types for the estimated cancer–caused deaths, by sex, Taiwan, 2009.

	Estimated deaths caused by cancer (2009 in Taiwan)					
	Male			Female		
Ranking	Location	deaths	%	Location	deaths	%
1	Liver & intrahepatic bile duct	5,467	21.6	Lung and bronchus	2,615	22.8
2	Lung and bronchus	5,336	21.1	Liver & intrahepatic bile duct	2,292	20.0
3	Colon and rectum	2,562	10.1	Colon and rectum	1,969	17.2
4	Oral cavity	2,103	8.3	Breast	1,588	13.9
5	Stomach	1,457	5.8	Stomach	825	7.2
6	Esophagus	1,369	5.4	Uterine corpus	657	5.7
7	Prostate cancer	936	3.7	Pancreas	609	5.3
8	Pancreas	871	3.4	Ovary	435	3.8
9	Leukemia	571	2.3	Non-Hodgkin lymphoma	372	3.2
10	Non-Hodgkin lymphoma	542	2.1	Leukemia	353	3.1
	Others	4,070	16.1	Others	2,918	25.5
	All sites	25,284	100		14,633	100

The table was modified from Department of Health, Executive Yuan, Taiwan.

(http://www.doh.gov.tw/CHT2006/DM/DM2_p01.aspx?class_no=25&level_no=1&doc_no=76013).

4

1.2. The structure of microtubules and microtubule-binding agents (MBAs)

In general, antimitotic drugs constitute a class of anticancer drugs that target the microtubule system (*9, 10*). A particularity of microtubule-binding agents compared to other categories of anticancer drugs is their various structural diversity and in many cases, their structural complexity (**Figure 2**). As shown in **Figure 3a**, microtubules, the key components of cytoskeletal filaments in all eukaryotic cells, are composed of a backbone of α- and β- tubulin heterodimers (*9-11*). To the best of our knowledge, in terms of drugs which interfere the tubulin polymerization, there are typically three binding-domains within microtubule structures (**Figure 3b**). Microtubule dynamics and stability, strongly associated with the rearrangement of depolymerization and polymerization, as shown in **Figure 3c**, are critical for cells undergoing replication and division where microtubule architecture vividly changes. Microtubules are also associated with various intracellular components, including mitochondria, the endoplasmic reticulum, the Golgi apparatus and lysosomes. As seen in **Figure 4a** and **4b**, the mitotic spindle microtubules allow the appropriate alignment of chromosomes during metaphase, followed by the equal distribution of chromatids between the two daughter cells during anaphase (*12*). An increasing number of chemically diverse substances, originating from natural sources, have been discovered bound to tubulin and/or microtubules, interacting with microtubule

polymerization, leading to mitosis arrest, resulting in apoptosis of cancer cells or other types of cell deaths (*9, 11, 13, 14*). According to their interference with microtubule dynamics and stability, antimitotic drugs are classified into two distinct groups, as summarized in **Table 2**. Microtubule-stablizing agents or microtubule-polymerizing agents, which bind to fully formed microtubules and promote polymerization of tunulin subunits, include the taxanes, such as paclitaxel and doxetaxel, and the epothilones. The second group, microtubule-destabilizing agents or microtubule-depolymerizing agents (MDAs), which bind mainly to the tubulin dimer and inhibit their polymerization into microtubules, include the vinca alkaloids, such as vincristine, vinblastine, and colchicine. Both the taxanes and the vinca alkaloids are currently used as chemotherapeutic drugs for various human cancers, whereas agents binding to the colchicine-binding site have been recognized as potential targets (*14, 15*). Although there are numerous microtubule-binding agents in clinical use (**Table 2**), the long-term use of many MBAs may result in drug resistance (**Table 3**). Therefore, it is vitally important to discover and develop new drug candidates to improve this difficult situation.
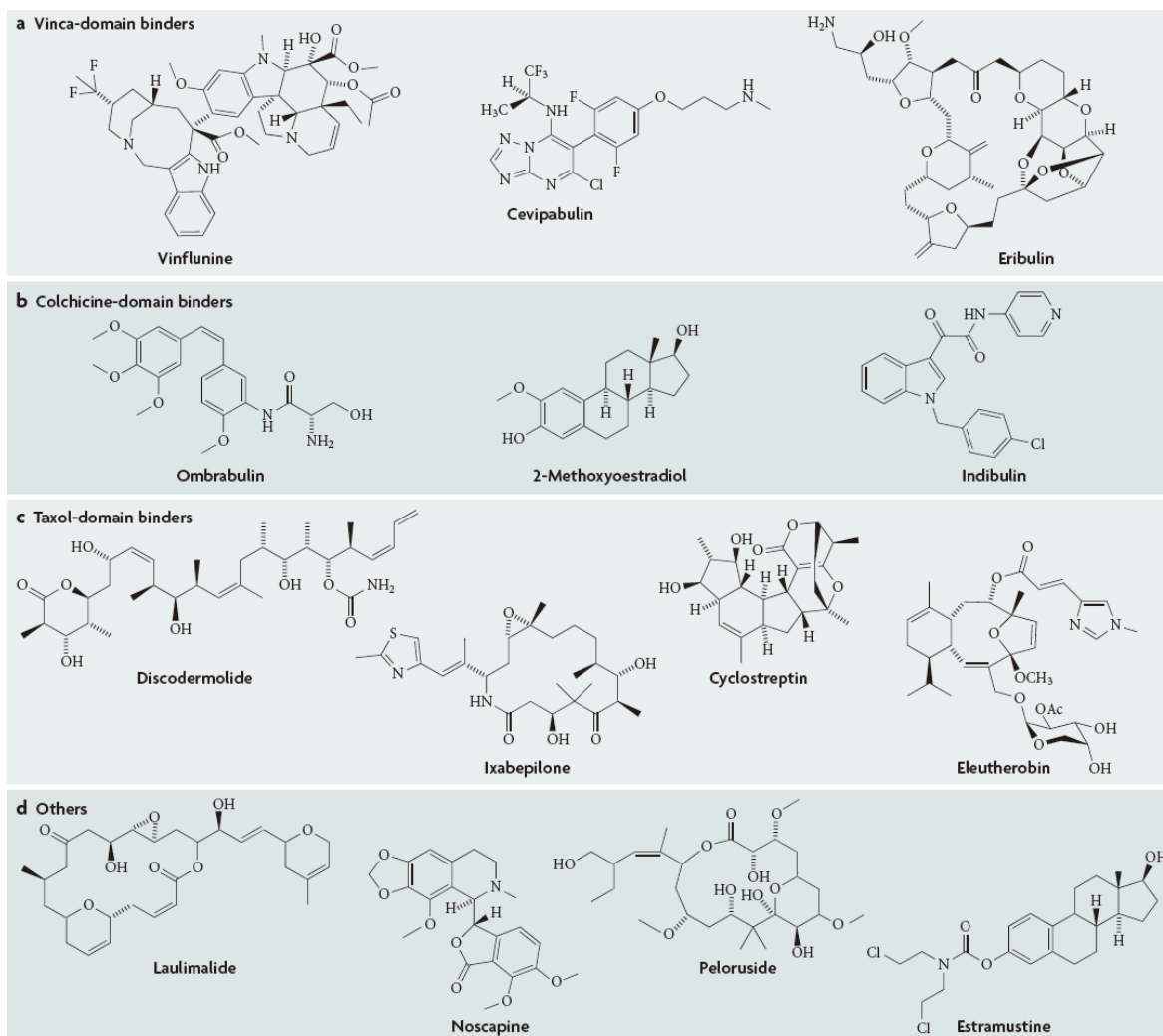
Figure 2. Various chemical structures of microtubule-binding agents, grouped according to their binding domains. a: vinca-domain binders; b: colchicine-domain binders; c: taxol-domain binders; d: others.

This figure shows the extreme chemical diversity and the complexity of these agents. This figure is adopted from Dumontet et al. (*10*)
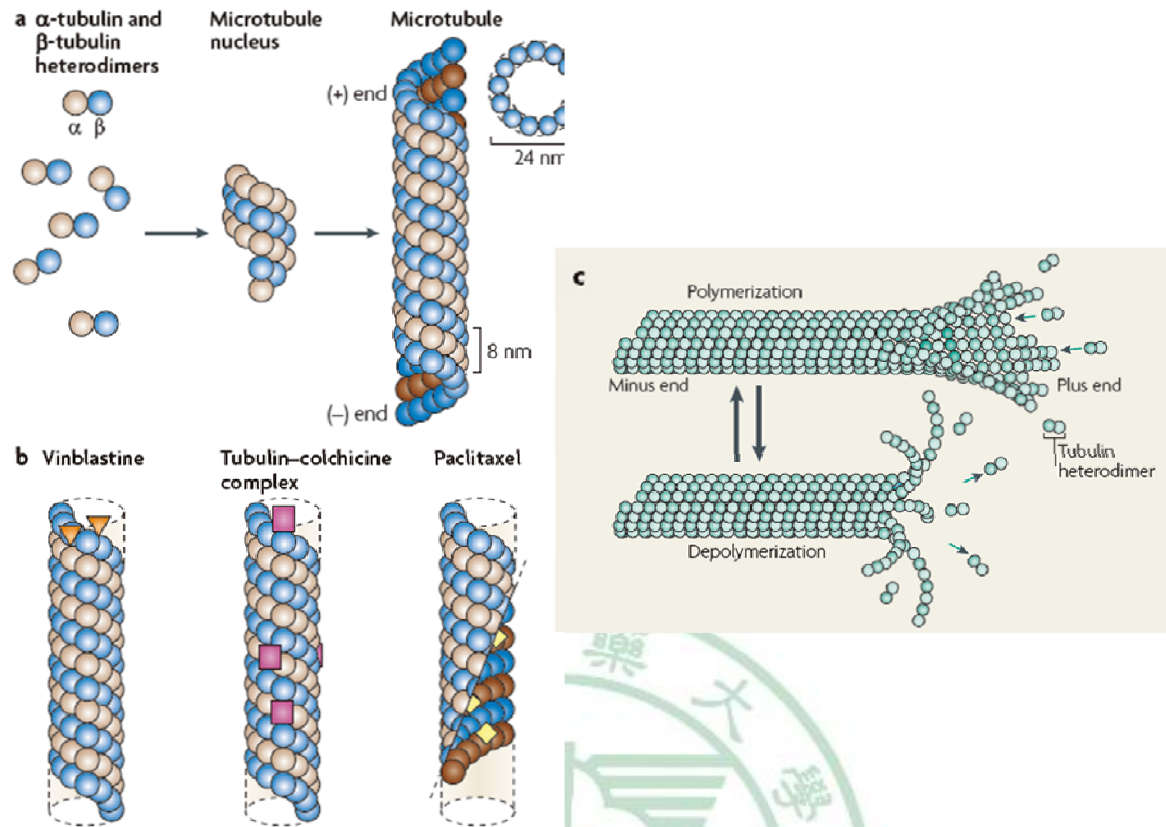
Figure 3. The formation of microtubules and the binding sites for microtubule inhibitors.

(a) The formation of microtubules. The soluble tubulin dimers, each containing one α-tubulin peptide and one β-tubulin peptide, polymerize to form a microtubule nucleus. Additional dimers are added head-to-tail; resulting microtubules are highly dynamic structures with a (+) end, characterized by an exposed β-tubulin peptide and a (−) end, characterized by an exposed α-tubulin peptide. **(b) The binding sites of different microtubule inhibitors.** Three binding sites of microtubule inhibitors are shown (orange triangles, purple squares and yellow diamonds). While vinca alkaloids bind to microtubule

ends, colchicine binds to soluble dimers, which are incorporated incorporated into the microtubules. Taxanes, such as paclitaxel, bind along the interior surface of the microtubules. The figures (a) and (b) are adopted from Dumontet et al. (*10*). **(c) The dynamics and stability of microtubules.** Microtubules are dynamic polymers assembled from tubulin heterodimers, which are organized so that the microtubules have an intrinsic polarity. Microtubules undergo periods of polymerization and depolymerization and interconvert randomly between these states, a property known as dynamic instability. This figure (c) was adopted from Walczak et al. (*12*).
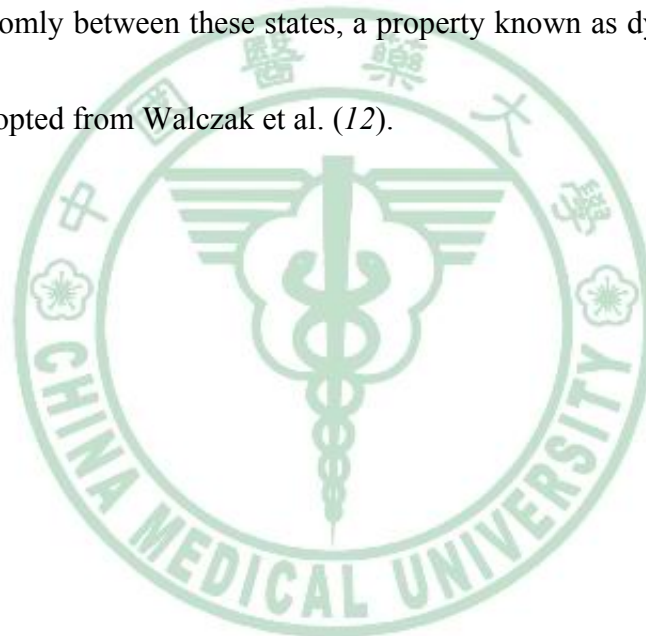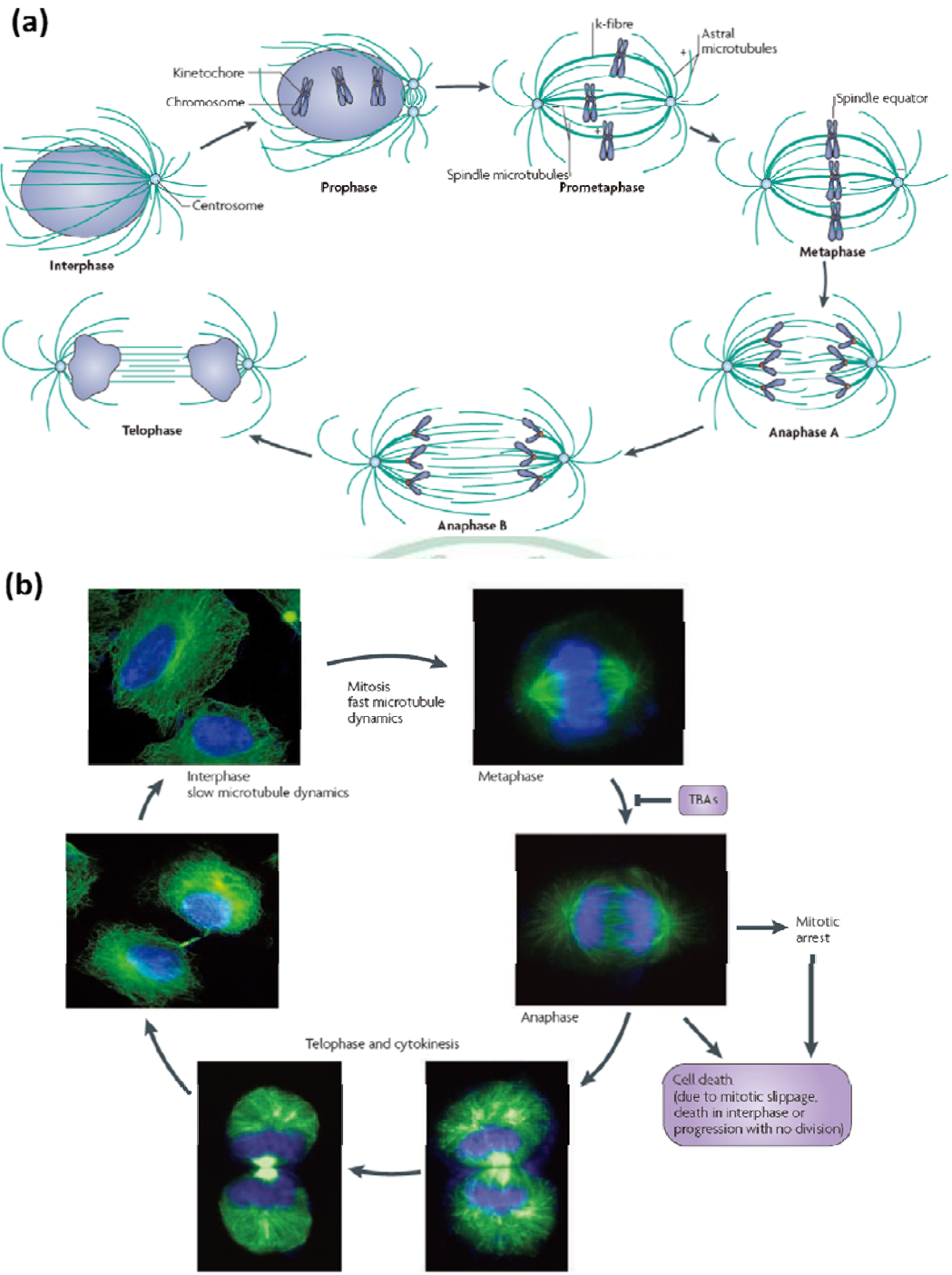
Figure 4. The role of the microtubules in cell cycle.

(a) The structure of the mitotic spindle during mitosis. Mitosis is staged into individual

phases. During prometaphase, the spindle microtubules are connected with kinetochore

(k)-fibres (bundles of stabilized microtubules) and the kinetochores on the chromosomes, allowing the chromosome to align at the spindle equator,; this defines metaphase. The microtubules are uniformly oriented with their minus (-) ends at the centrosome and their plus (+) ends extending towards the spindle equator, where they often overlap. The astral microtubules emanate from the centrosomes and extend their plus (+) ends towards the cell's cortex. The movement of the chromosomes towards the poles occurs during anaphase A, and the two spindle poles separate during anaphase B. The nuclear envelope begins to reform and the DNA begins to decondense during telophase. An organized central spindle bundle of microtubules is also present. This figure is adopted from Walczak et al. (*12*). **(b) The microtubule changes during the cell cycle.** The structures of microtubule (shown in green) undergo marked morphological changes to regulate specific functions throughout the cell cycle. Microtubule dynamics vary during the cell cycle, being most dynamic during mitosis and least dynamic in interphase cells. Most of tubulin-binding agents (TBAs) act upon the dynamics of the spindle microtubules, which are important for normal spindle function. Disruption of spindle microtubules causes mitotic arrest, leading to cell death through various mechanisms. DNA is shown in blue. This figure is adopted from Kavallaris et al.   (*11*)

Table 2. Anti-mitotic drugs including microtubule-polymerizing agents and microtubule-depolymerizing agents currently in clinical use

Microtubule-polymerizing/-stabilizing agents		
Compound class	**Compound**	**Clinical status**
Taxanes (taxol-domain binder)	Paclitaxel	Approved for ovarian cancer, breast cancer and NSCLC; in clinical trials for various solid tumour types
	Docetaxel	Approved for NSCLC, breast, prostate, stomach, head and neck cancer; in clinical trials for various solid tumour types
	Cabazitaxel	Approved for metastatic hormone-resistant prostate cancer
	Nab-paclitaxel	Approved for breast cancer; in clinical trials for various solid tumours. Clinical trials for prostate cancer
	Larotaxel	Phase III trials for pancreatic cancer
Epothilones (taxol-domain binder)	Ixabepilone	Approved for breast cancer; in clinical trials for solid tumours
Mcrotubule-depolymerizing/-destabilizing agents		
Compound class	**Compound**	**Clinical status**
Vinca alkaloids (vinca-domain binder)	Vincristine	Approved for ALL, lymphomas, various solid tumours; in clinical trials for various tumour types
	Vinblastine	Approved for lymphomas and various solid tumours; in clinical trials for various tumour types
	Vinorelbine	Approved for breast cancer and NSCLC; in clinical trials for various tumour types
	Vindesine	Approved for ALL, lymphomas and lung cancer; in clinical trials for various tumour types
	Vinflunine	Approved for bladder cancer; in clinical trials for breast cancer in combination with trastuzumab
Dolastatins (vinca-domain binder)	Romidepsin	Approved for cutaneous T cell lymphoma; in clinical trials for myeloma, lymphoma and solid tumours
Halichondrin (vinca-domain binder)	Eribulin	Phase III trials for advanced breast cancer
Combretastatins (colchicine-domain binder)	Ombrabulin	Phase III trials for sarcoma

This table was modified from Dumontet et al. (*10*)

Table 3. Characteristics of microtubule-binding agents.

Agent	Sensitivity to ABC efflux pumps	Sensitivity to β-tubulin content
Vinca alkaloids	MDR sensitive MRP sensitive	Sensitive to βIII-tubulin content
Cryptophycins	MDR insensitive	Not determined
Dolastatins	MDR sensitive	Not determined
Taxanes	MDR sensitive MRP2 and MRP7 sensitive	Sensitive to βIII-tubulin content
Epothilones	MDR sensitive	No
Discodermolides	MDR sensitive MRP1 sensitive	Sensitive to βIII-tubulin content
Cyclostreptin	MDR insensitive	Not determined
Laulimalides	MDR insensitive	Not determined
Taccalonolide	MDR insensitive	More active if high βIII-tubulin content
Peloruside	MDR insensitive	Not determined
Hemiasterlin	MDR insensitive	Not determined
Combretastatins	MDR insensitive	Yes
2-Methoxyoestradiol	MDR insensitive	Inactive against βI-tubulin

ABC, ATP binding cassette; MDR, multidrug resistance; MRP, multidrug resistance-associated protein.

This table is adopted from Dumontet et al.(*10*)

1.3. Cell death including apoptosis and mitotic catastrophe

Various types of cell death have recently been defined and classified by the Nomenclature Committee on Cell Death (NCCD); these include apoptosis, autophagy, necrosis, cornification, and atypical cell death such as mitotic catastrophe (*16*). Programmed cell death (PCD) is a natural process for removing unwanted cells such as those with aberrant substratum attachment, potentially harmful mutations, or abnormal alterations in cell-cycle control (*17*). Apoptosis, a major type of PCD, is essentially a regulating mechanism by which cells undergo programmed cell death (*18*). In many malignant cells, the normal process for removing unwanted cells is deregulated (*17*). Anti-apoptotic mechanisms contribute to the development of cancer and to the resistance of cancer cells to anticancer chemotherapies. An increasing number of studies have demonstrated that promoting apoptosis is a good strategy for cancer drug discovery (*17, 19-22*). To date, at least two major apoptotic pathways have been described previously: the intrinsic and the extrinsic pathway (see **Figure 5**) (*18, 19, 23*). The intrinsic pathway is a mitochondrion-mediated process, influencing mitochondrial permeability and resulting in cytochrome c release and activation of caspase-9. The extrinsic apoptotic pathway, on the other hand, is triggered by the binding of specific ligands such as Fas ligands and TRAIL (tumor-necrosis factor-related apoptosis-inducing ligand) to membrane death receptors (DRs) such as Fas (CD95/APO-1), DR4 (TRAIL-R1), and DR5 (TRAIL-R2), resulting in

14

recruitment of adaptor molecules and initiating activation of caspase-8 as well as distal executioner caspases including caspase-3. Additionally, the endoplasmic reticulum stress pathway is recognized as the third pathway to induce apoptosis (*24*). On the other hand, the p53 tumor suppressor functions as a key regulator of both intrinsic and extrinsic pathways (*18*). However, although current chemotherapeutic drugs can induce apoptosis, there is still an urgent need to find candidate drugs that will target an apoptotic pathway with a less adverse effect for practical, more productive cancer chemotherapy.

Mitotic catastrophe is a type of cell death characterized by the occurrence of aberrant mitosis with the formation of large multi-nucleated cells, which may be morphologically distinguishable from apoptotic cells (*25-27*). However, mitotic catastrophe is a term sometimes used restrictively to illustrate a type of cell death that occurs during or after a defective mitosis, which takes place through apoptosis or necrosis, rather than a cell death itself (*25, 26, 28*). Moreover, it may be associated with complicated mechanisms of induction, as shown in **Figure 6**. Several antitumor drugs and ionizing radiation have been shown to induce mitotic catastrophe (*26*), but precisely how the ensuing lethality is controlled or what mechanisms are involved is less characterized. The type of cell death caused by antitumor therapy may be evaluated by the mechanisms of action of the antitumor agents, the dosing regimen, and perhaps the genetic background of the cells under treatment with anti-cancer agents. For example, oxaliplatin can trigger different

types of cell death such as mitotic catastrophe and apoptosis in esophageal cancer cells

(*29*). The proteasome inhibitor Bortezomib induces cell death via mitotic catastrophe and

apoptosis in B-cell lymphoma cell lines (*30*). Doxorubicin may induce one of two distinct

modes of cell death: apoptosis or cell death through mitotic catastrophe accompanied by

senescence-like phenotype (*31*). The wild-type of p53 promotes apoptosis or senescence,

whereas mitotic catastrophe is independent of p53 (*25, 26*). Mitotic catastrophe may be

regarded as a delayed response of p53-mutant or p53-null tumors that are resistant to some

damage especially for DNA damage (see **Figure 7**). In this context, characterization of the

mechanisms of treatment-induced mitotic catastrophe should contribute to further

improvement of the anti-tumor chemotherapy, due to the fact that the majority of solid

tumors bear an inactive p53 protein (*25*).
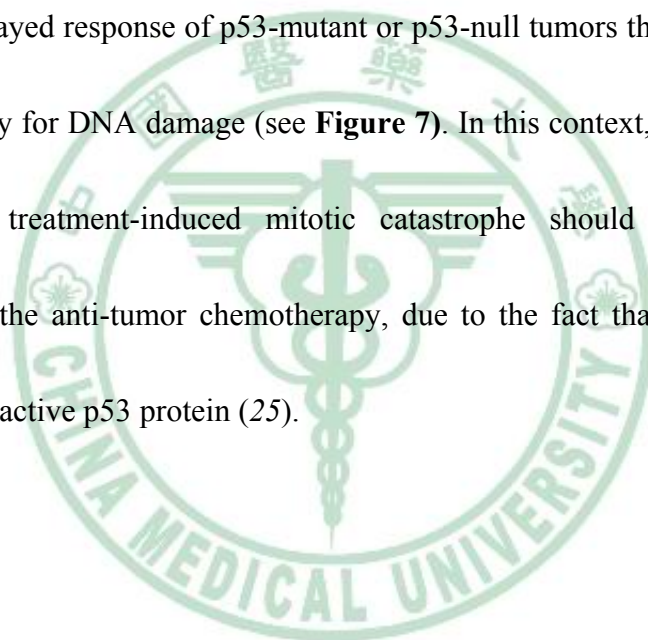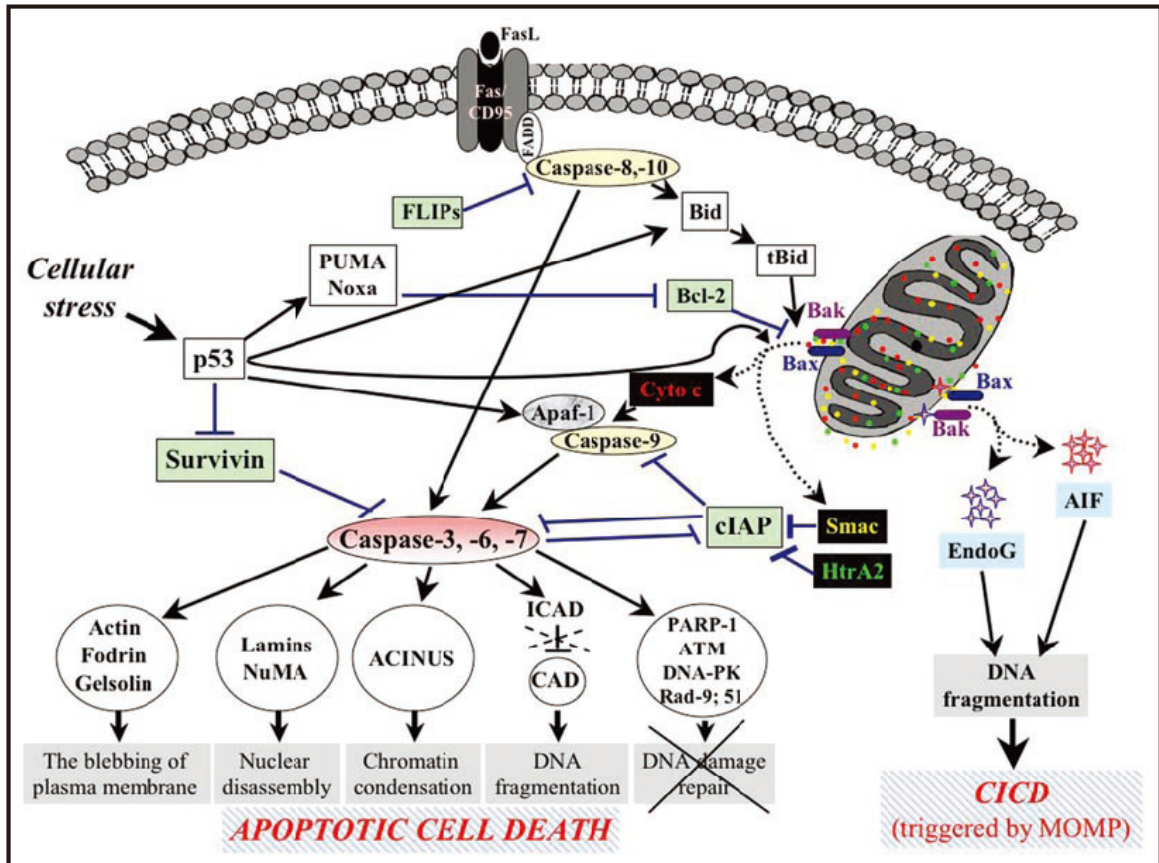
Figure 5. Schematic representation of detailed mechanisms that govern the extrinsic and intrinsic apoptotic pathways and caspase-independent cell death.

Essentially, the common denominator in apoptotic cell death processes is permeabilization of the outer mitochondrial membrane and the release into the cytosol of proteins that trigger death programs. The apoptotis-related caspases appear in yellow and red circles, respectively. Inhibitors of apoptosis are shown in green boxes. [Adopted from Blank et al.(*18*)]

Table 4. Comparison of major cell death pathways observed in drug-treated cells

	Apoptosis	Mitotic catastrophe	Necrosis
Definition and characteristics	* Programmed cell death. * Cells shrink with blebbing of cell membranes. * Condensed chromatin and DNA fragmentation.	* Cell death occurring during or after a faulty mitosis. * Giant cells with two or more nuclei and partially condensed chromatin. * Can lead to necrosis or apoptosis-like death (p53-independent).	*Identifies, in a negative fashion, cell death lacking the features of apoptosis or autophagy. * Cells visible swell with breakdown of cell membrane. * Typical nuclei with vacuolization, and disintegrated cell organelles.
Associated genetic changes	* Stimulated by cyclin D1 activation and by Myc. * Can be inhibited by loss of wild-type p53. * Caspase activation.	* Stimulated by deficiencies in proteins involved in G1 and G2 checkpoints and in mitotic spindle assembly: p53, p21, Cdk1, Chk1, Chk2, etc. * Can follow caspase-dependent or –independent routes.	* In general, it is not considered genetically determined (this is open to debate).
Detection methods	*Sub-G1 peak in flow cytometry. *Annexin-V-staining. *Internucleosomal laddering, etc.	* Cells with two or more nuclei detected by Microscopy or *Laser Scanning Cytometry*. *Accumulation in G2/M and polyploidy.	*Early permeability to vital dyes. * Staining with propidium iodide. *Electron microscopy.

[Adopted from Portugal et al.(*25*)]
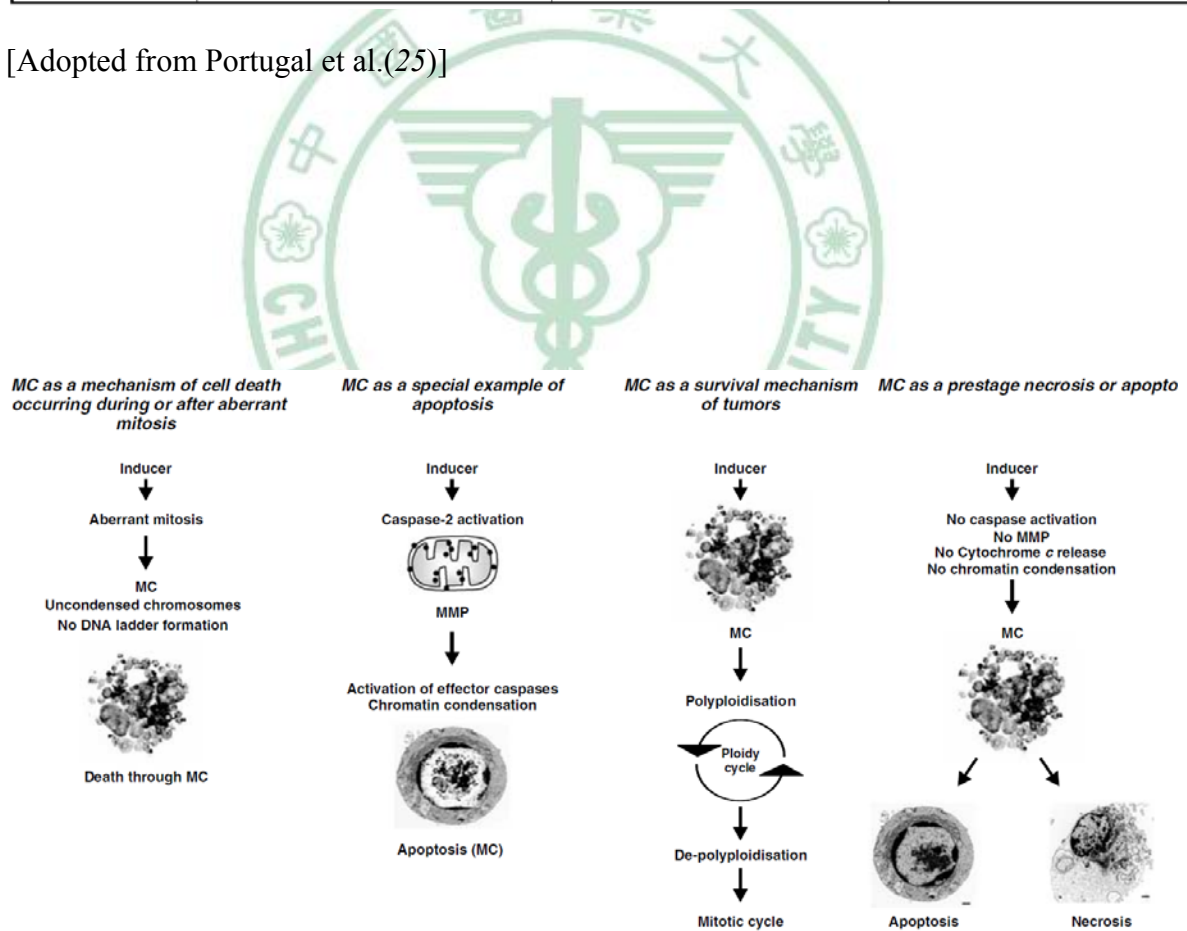
Figure 6. Schematic representation of current concepts of mitotic catastrophe.

[Adopted from Vakifahmetoglu et al. (*26*)]

Table 5. Specific inducers of mitotic catastrophe (MC) and associated events

Inducers	Mechanism of action	Effects	Outcome
DNA damaging agents Doxorubicin, cisplatin Irradiation	Induce DSBs by: Interfering with DNA synthesis Direct DNA damage	Premature segregation into mitosis Defect in maintaining cell arrest	Aneuploidy Tetraploidy Polyploidy Micronucleation Multi/mono-nucleation
Replication fork Checkpoint inhibitors: DBH Checkpoint adaptation Prolonged mitotic arrest and slippage			
Spindle poisons/mitotic inhibitors Taxanes (paclitaxel, docetaxel) Eleutherobins Epothilones Laulimalide Sarcodictyins Discodermolide	Affect microtubule dynamics by: Hyperpolymerization	Failure or inhibition of mitosis: Spindle assembly defects Chromosome segregation defects Abortive centrosome duplications Multipolar mitosis Uneven chromosomes separation Premature segregation of unaligned chromosome	
Vinca alkaloids (vinblastin, vincristin) Cryptophycins Halichondrins Estramustine Colchicine	Depolymerization	Delayed mitosis Microtubule attachment defects Monopolar and monoastral spindles	
Inhibition of mitotic proteins: Thiazole compounds, Monastrol (kinesin spindle protein (KSP)) Small-molecule Inhibitor BI 2536 (Polo-like kinase 1 (PLK1)) Hesperadin, ZM447439 and VX-680 (Aurora kinases)	Disturbing mitotic process	Mitotic spindle checkpoint defects	

[Adopted from Vakifahmetoglu et al. (*26*)]

19
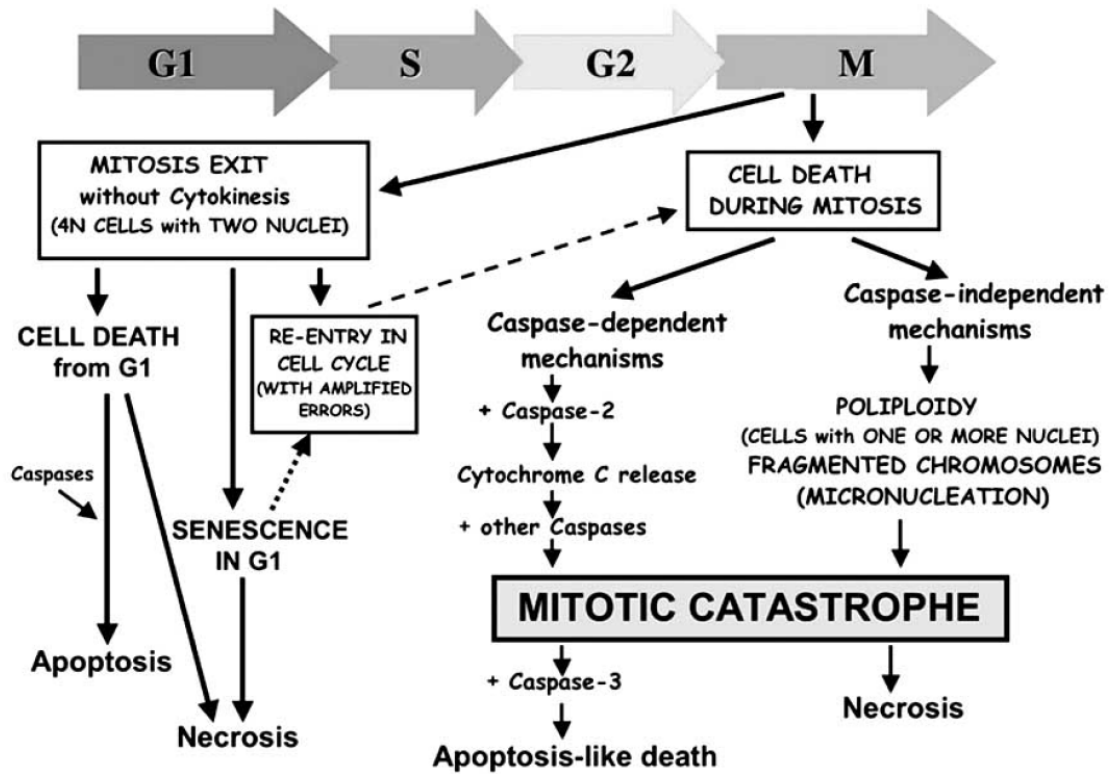
Figure 7. Pathways leading to mitotic catastrophe and cell death after DNA damage.

Several key events occurring after a faulty mitosis are represented. DNA damage in p53-deficient cells can result in an exit from mitosis without cytokinesis, or in cell death occurring during mitosis. The relationship of mitotic catastrophe with apoptosis and/or necrosis is indicated. [Adopted from Portugal et al.(*25*)]

1.4. Relationship between p53 and microtubule-binding agents

Microtubule inhibitors can block the cell cycle at G2/M-phase by damaging the mitotic spindle. However, under certain conditions, specific cells escape these effects and become aneuploid, polyploid and/or micronucleated, or multi-nucleated (*18, 32*). For example, as shown in **Figure 8**, exposure to high doses of the microtubule-depolymerzing agent nocodazole may result in polyploidy due to mitotic slippage in the absence of a functional spindle. Furthermore, it is shown that p53 plays an important role in inducing cell death or ensuring cell survival. Also, different concentrations may cause different types of cell death. The mitotic defect with characteristics of monopolar, pseudo-bipolar, tripolar or multipolar spindles is possibly caused by different microtubule inhibitors including MDAs. As seen in **Figure 9**, these abnormal spindles can result in aneuploidy, polyploidy or other types of aberrant chromosomes. However, depending on whether cells express the p53 gene, cells are likely to die or to survive abnormally (*33*). We therefore hypothesize that cells expressed with or without expression of the p53 gene may be strongly related to different types of cell death or cell survival induced by microtubule inhibitors.
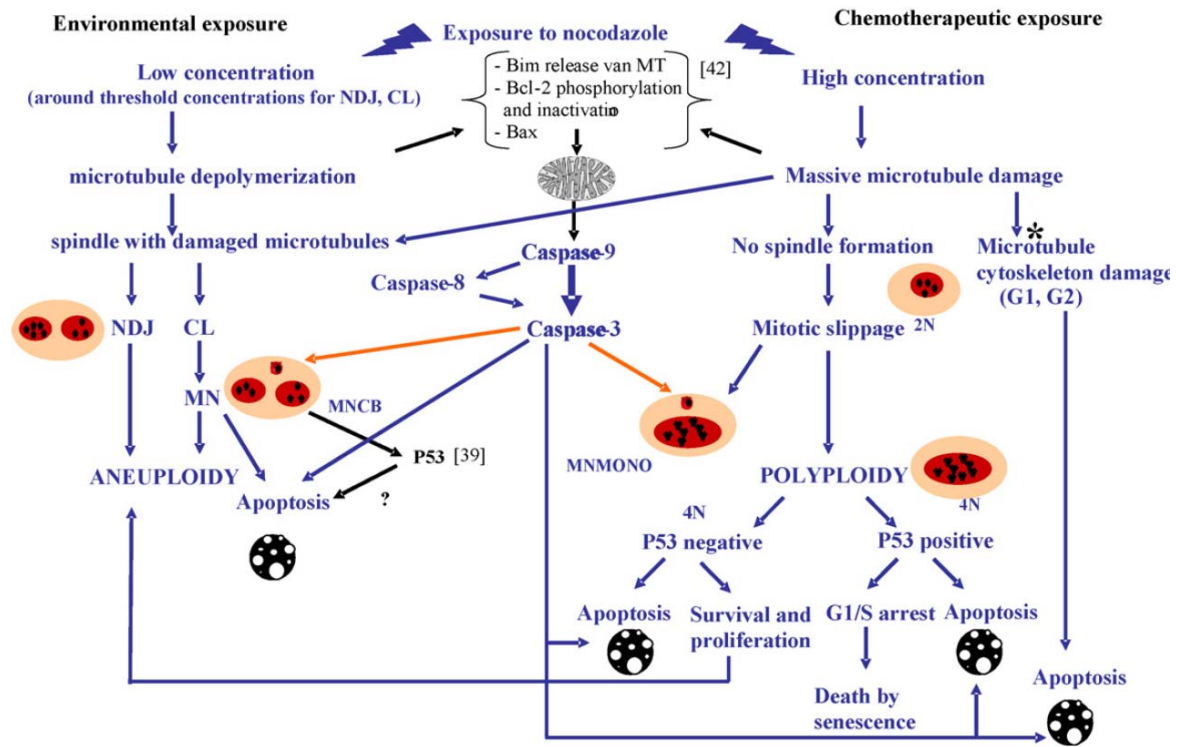
Figure 8. Schematic representation of putative mechanisms of a cell after exposure to low and high concentrations of the microtubule-depolymerizing agents, nocodazole.

[Adopted from Decordier, I. et.al. (*32*).]
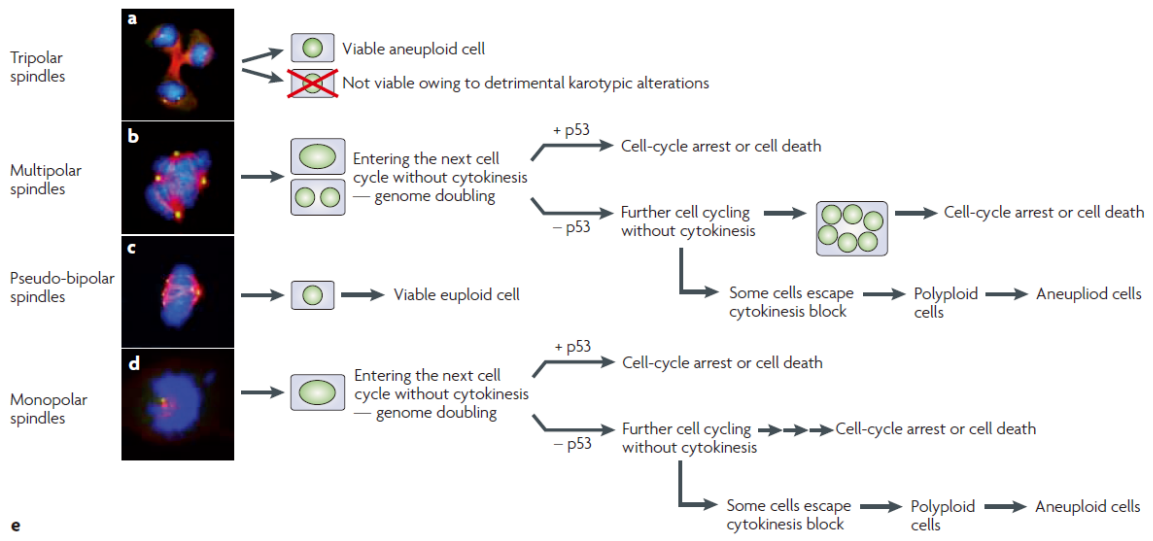
Figure 9. The relationship between mitotic defects with numeral abnormalities of spindles and p53. [Adopted from Fukasawa, K.et.al. (*33*).]
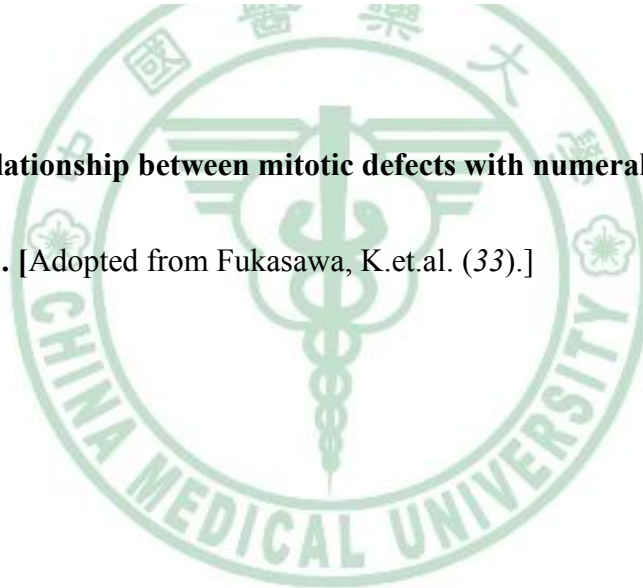
1.5. CMQ as one of 2-phenyl-4-qunolone derivatives with potent anti-tumor activity

As shown in **Table 6**, quinolone, a general structure occurring in natural alkaloids and its derivatives, exhibits several pharmacological activities including antibacterial activity, inhibition of leukotriene biosynthesis and antitumor activity (*34-36*). Furthermore, it has been reported that the 2-phenyl-4-quinolone derivatives exhibited various pharmacological activities including suppression of hind-paw edema and cutaneous vascular plasma extravasation (*37*), regulation of serotonin-mediated changes and permeability of endothelial monolayers (*38*), prevention of serotonin-induced increases in endothelial permeability to albumin (*39*), involvement in cyclic AMP generation in the inhibition of respiratory burst in rat neutrophils (*40*), antiplatelet activity (*41*), potent antagonists for glycine-binding site of the N-Methyl D-aspartate (NMDA) receptor (*42*), potent 5-hydroxytryptamine [5HT(1B)] antagonists (*43*), and especially anti-tumor activities in cancer cell lines by inhibiting polymerization of tubulins (**Table 6**) (*44-52*). Based on the rationale designs and efficacy results for 2-phenyl-4-quinolone derivatives, we found that 2-(3-chlorophenyl)-6, 7-methylenedioxyquinolin-4-one (CMQ) is a good candidate for further investigation of antitumor activities (*45*). Therefore, we investigated the effect of CMQ as a drug candidate for anti-tumor activities in p53-expressing LNCaP cells and p53-null PC-3 cells of prostate cancers.

Table 6. A summarized list of bioactivities of quinolone and 2-phenyl-4- quinolone derivatives.

Compounds	Bioactivities	Reference
quinolones	Antitumor quinolones with mammalian topoisomerase II mediated DNA cleavage activity	Yamashita et al. 1992. (*36*)
2-phenyl-4-quinolone derivatives	Positive inotropic effect in rat cardiac tissues	Su et al. 1993.(*53*)
1,6,7,8-substituted 2-(4'-substituted phenyl)-4-quinolones	Antimitotic agents interacting with tubulin	Kuo et al. 1993.(*44*)
2',3',4',5',5,6,7-substituted 2-phenyl-4-quinolones	Cytotoxicity, and inhibition of tubulin polymerization	Li et al. 1994.(*45*)
2-phenyl-4-quinolone derivatives	Suppress hind-paw edema and cutaneous vascular plasma extravasation in mice	Wang et al. 1994.(*37*)
quinolone derivatives	Antibacterial activity	Kamenska et al. 1996.(*54*) Renau et al. 1996.(*55*) Renau et al. 1996.(*56*) Yoshida et al. 1996.(*57*)
2-phenyl-4-quinolone	Regulate serotonin-mediated changes in the morphology and permeability of endothelial monolayers	Lee et al. 1997.(*38*)
2-phenyl-4-quinolone	Prevents serotonin-induced increases in endothelial permeability to albumin	Lee et al. 1998.(*39*)
2-phenyl-4-quinolone	Involve in cyclic AMP generation in the inhibition of respiratory burst in rat neutrophils	Wang et al. 1998.(*40*)
6,7,2',3',4'-substituted-1,2,3,4-tetrahydro-2-phenyl-4-quinolones	Antimitotic antitumor agents	Xia et al. 1998.(*46*)
2-phenyl-4-quinolone	Antiplatelet activity	Huang et al. 1998.(*41*)

25

fluoroquinolones	Inhibitiobn on DNA gyrase and topoisomerase II & IV	Hooper et al. 1999.(*34*)
Fluorinated 2-phenyl-4-quinolone	Antimitotic antitumor agents	Xia et al. 2001.(*47*)
Alkylation of 2-phenyl-4-quinolones	Synthesis	Hadjeri et al. 2001.(*58*)
2-phenyl-4-quinolone acetic acids and their esters	Antimitotic antitumor agents	Xia et al. 2003.(*59*)
quinolone alkaloids	Inhibition of leukotriene biosynthesis by quinolone alkaloids from the fruits of Evodia rutaecarpa	Adams et al. 2004.(*35*)
5-hydroxy-7-methoxy-2-phenyl-4-quinolones	Antimitotic antitumor agents	Hadjeri et al. 2004. (*60*)
2-phenyl-4-quinolone and 9-oxo-9,10-dihydroacridine derivatives	Antitumor-promoter	Nakamura et al. 2005.(*61*)
3',6-substituted 2-phenyl-4-quinolone-3-carboxylic acid derivatives	Antimitotic antitumor agents	Lai et al. 2005.(*62*)
2-phenyl-4-quinolone	Antimitotic antitumor agents	Chen et al. 2007.(*48*)
quinoline-2-carboxylic acid (4-morpholin-4-yl-phenyl)amides	Potent 5HT(1B) antagonists	Horchler et al. 2007. (*43*)
7-choloro-4-hydroxy-3-[3-(4-methoxybenzyl)phenyl]-2(1H)-quinolone	Antagonist for the glycine-binding site of the N-Methyl D-aspartate (NMDA) receptor	Matsumoto et al. 2007.(*63*)
2-(3-Fluorophenyl)-6-methoxyl-4-oxo-1,4-dihydroquinoline-3-carboxylic acid (YJC-1)	Induces mitotic phase arrest in A549 cells	Hsu et al. 2007.(*64*)
2-(2-fluorophenyl)-6,7-methylenedioxyquinolin-4-one (CHM-1)	Promoted G2/M arrest through inhibition of CDK1 and induced apoptosis through the mitochondrial-dependent pathway in CT-26	Wang et al. 2007.(*65*)

	murine colorectal adenocarcinoma cells	
	Potent and selective antimitotic antitumor activity against human hepatocellular carcinoma in vitro and in vivo	Wang et al. 2008.(*49*)
	Promoted G2/M arrest through inhibition of CDK1 and induced apoptosis through the mitochondrial-dependent pathway in CT-26 murine colorectal adenocarcinoma cells	Chou et al. 2009.(*50*)
	Induces apoptosis and inhibits metastasis in a human osterogenic sarcoma cell line	Hsu et al. 2009.(*52*)
	Induces DNA damage and inhibits DNA repair gene expressions in a human osterogenic sarcoma cell line	Chen et al. 2010.(*66*)
	Induces apoptosis of human umbilical vein endothelial cells via p53-mediated death receptor 5 up-regulation	Tsai et al. 2010.(*51*)
	Inhibits murine WEHI-3 leukemia in BALB/c mice in vivo	Lai et al. 2010.(*67*)
2-(2-fluorophenyl)-6,7-methylenedioxyquinolin-4-one monosodium phosphate (CHM-1-P-Na)	Antimitotic antitumor agents	Chou et al. 2010.(*68*)
2-(3-chlorophenyl)-6,7-methylenedioxyquinolin-4-one (CMQ)	Augment efficacy of dendritic cell-based cancer vaccines	Wen et al. 2011.(*69*)

Chapter 2. Rationale and Significance

The rationale of this study used CMQ as a lead compound for investigating the anti-tumor activity in LNCaP and PC-3 cells are as follows.

It has been reported that derivatives of 2-phenyl-4-quinolone induce cytoxicity and apoptosis in human cancer cell lines by inhibiting the polymerization of tubulins and interfering with microtubule organization (*44-52*). In a previous study, we reported that 2-(3-chlorophenyl)-6,7-methylenedioxyquinolin-4-one (CMQ) holds potential for further research and development into a specific antitumor agent (Fig. 1A) (*45*).

To date, there is no effective treatment for either locally advanced or metastatic prostate cancer. Usually, these cancers are androgen-independent and p53 -null or -mutated. Therefore, various new therapeutic approaches, including new androgen receptor antagonists, antimiotic drugs, antiangiogenic agents, and immune-based therapies are being actively evaluated (*2*).

On the other hand, notably, we understand two key pieces of information as follows: prostrate cancers are androgen dependent [6-7], and TRAIL and p53 play key roles in apoptosis (*18, 23*). However, there is no available research which compares the effects of 2-phenyl-4-quinolone derivatives on cancer cells concurrently with or without the characteristics described above. Therefore, in this study, we evaluated the extent to which CMQ exerts antitumor activities in prostate cancer cells including LNCaP cells

(androgen-sensitive, TRAIL-resistant, p53 wild-type) and PC-3 cells (androgen-independent, TRAIL- sensitive, p53- null). Intriguingly, we found that CMQ could induce G2/M arrest and apoptosis via inhibition of tubulin polymerization in both cell lines, but that it activates a stronger intrinsic apoptotic pathway in the LNCaP cells than in the PC-3 cells, whereas it inhibits phosphorylation of Akt in the PC-3 cells more effectively than in the LNCaP cells. These findings may provide future clinical uses of CMQ or other antimitotic drugs for treatment of different types of prostate cancers.

It was reported recently that specific chemotherapeutic agents, such as microtubule inhibitors and cisplatin, caused mitotic arrest which in turn could induce distinct modes of cell death, including apoptosis and mitotic catastrophe (*32, 70*). Apoptosis has been recognized as a promising focus for cancer therapists (*18*). So far, major apoptotic pathways have been described as distinguishable: the intrinsic pathway, the extrinsic pathway, and the endoplasmic reticulum stress pathway (*18, 19, 23, 24*). Mitotic catastrophe has been recognized as a mode of cell death characterized by the presence of aberrant mitosis with the formation of giant multinucleated cells (*25, 26*). It can be caused by chemical and physical stresses and lead to apoptosis or necrosis but also the survival of tumor cells. Importantly, the p53 tumor suppressor gene not only plays a crucial role as a switch between mitotic catastrophe and apoptosis (*25, 26, 70*), but also functions as a key regulator of both intrinsic and extrinsic apoptotic pathways (*18*). Therefore, it is important

to investigate the possible correlation between p53 expression and the different types of cell death induced by specific chemotherapeutic agents.

Taking the previous researchers' observations together, this study was aimed to address such a possible connection in a prostate cancer cell system. As there is no information available concerning the antitumor effects of 2-phenyl-4-quinolone derivatives on cancer cells with or without p53, we evaluate here whether CMQ exerts significant and differing antitumor activities against specific prostate cancer cell types that differ in p53 expression. Thus, a parallel and comparative study using LNCaP cells (p53 wild-type) and PC-3 cells (p53-null) was conducted. We show that CMQ can induce mitotic arrest and cell death in both cell lines tested, triggering apoptosis in LNCaP cells but causing mitotic catastrophe in p53-lacking PC-3 cells. CMQ activates the intrinsic apoptotic pathway in both LNCaP and PC-3 cells, whereas it did not affect the extrinsic apoptotic pathway in the PC-3 cells. Our findings demonstrate that CMQ may be functionally employed to treat various types of cancer cells by attacking different signaling pathway systems involving distinct modes of cell death. Specifically, CMQ holds potential for future clinical use in the treatment of a variety of prostate cancers.

Chapter 3. Results and Discussion

3.1. Results

3.1.1. CMQ inhibits growth of both LNCaP and PC-3 cells

In order to investigate the cytotoxic effect of CMQ (**Figure 10A)** in LNCaP cells (androgen-sensitive, p53 wild-type) and PC-3 cells (androgen-independent, p53- null), we treated test cells with CMQ in a wide range of concentrations. **Figure 10B** shows that exposure of LNCaP and PC-3 cells to CMQ caused a concentration-dependent inhibition of cancer cell growth as measured by MTT assay. IC_{50} values for LNCaP and PC-3 cells were 2.523μM and >10μM, 0.082 μM and 0.291 μM, and 0.046 μM and 0061 μM, respectively after 24, 48 and 72 hours. CMQ caused approximately 90-95 % cell death in LNCaP cells at high concentrations compared to an approximately 50 % level in PC-3 cells. CMQ conferred an even higher level of cytotoxicity in LNCaP and PC-3 cells than the positive control paclitaxel, for which IC_{50} values of 0.18 μM and 0.51 μM in LNCaP cells and PC-3 cells, respectively, were determined (data not shown). These results suggest that CMQ holds potential for future development as a chemotherapeutic agent. Additional experiments further showed that CMQ displayed a similar cytotoxic effect on other cancer cell types including human breast carcinoma MCF-7 cells and MDA-MB231 cells with IC_{50} values of 1.9 μM and 0.2 μM, respectively (**Figure 10C**). In addition, the cytotoxicity

of CMQ was investigated in non-cancerous cell lines such as human lung fibroblast cells (WI-38) a cell type present in the stromal microenvironment; and resting leukocyte cells, such as primary cultures of human immune cells including CD4$^+$ T cells CD8$^+$ T cells, and human peripheral blood mononuclear cells (PBMC). IC$_{50}$ values of CMQ at 48 h for these cells were significantly higher, ranging from 4.3 and 4.5 μM for PBMC and WI-38, respectively, to >10 μM for CD4$^+$ and CD8$^+$ T cells. It is important to note here that the IC$_{50}$ values of CMQ for the non-cancerous test cells such as WI-38 and PBMC are approximately 52-55-fold and 14-16-fold higher as compared with those for LNCaP and PC-3 cells, respectively, suggesting that CMQ may exert a specific cytotoxicity towards cancerous cells. Together, our results indicate that CMQ can confer different levels of cytotoxicity on the two different prostate cell line tested and that it had a less toxic effect on all non-cancerous cell types investigated.

(A)

2-(3-chlorophenyl)- 6, 7-methylenedioxyquinolin-4-one (CMQ)

(B)

(C)

	MCF-7	MDA-MB231	Wi-38	CD4+ T	CD8+ T	PBMC
IC_{50}	1.9 μM	0.2 μM	4.5 μM	> 10μM	> 10 μM	4.3 μM
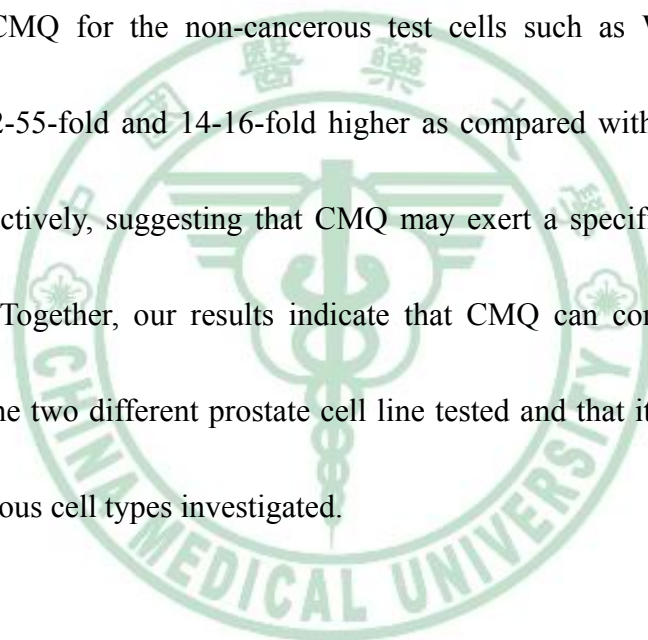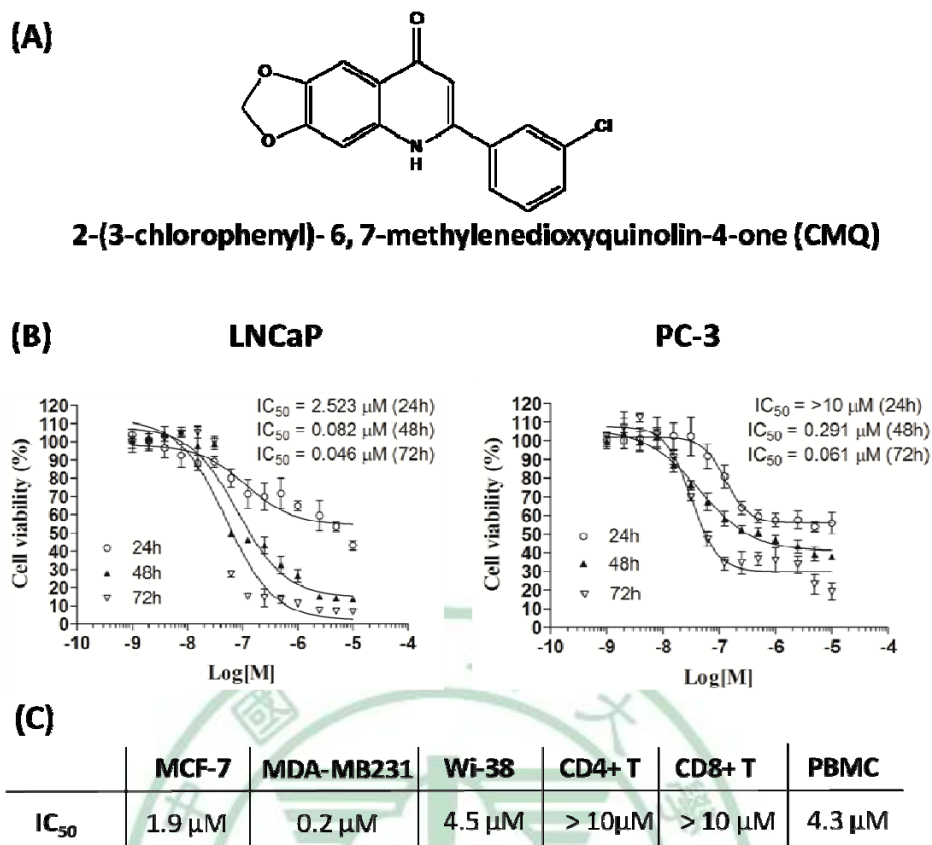
Figure 10. Chemical structure and cytotoxicty of CMQ in human prostate carcinoma and other cells

(A) Chemical structure of 2-(3-chlorophenyl)- 6,7-methylenedioxyquinolin-4-one (CMQ).

(B) Cell viability. LNCaP and PC-3 cells were treated in culture with CMQ at concentrations between 0.0005 and 10 μM for 24, 48 or 72 hours. Data are presented as proportional viability, where viability of vehicle-treated group was regarded as 100%. Cell viability was determined by MTT assay. Data are expressed as mean ± S.D. for triplicate samples. (C) Differential effect of CMQ on cancerous or non-cancerous fibroblast or leukocytes. Cells were cultured in 96-well plates and treated with CMQ for 48h as indicated and IC_{50} values were measured.

3.1.2. CMQ induces G2/M cell cycle arrest that leads to apoptosis in LNCaP cells and endoreduplication in PC-3 cells

To evaluate the possible mechanisms by which CMQ inhibits cell growth, the effect

of CMQ on the progression of cell cycles in LNCaP and PC-3 cells was examined by flow

cytometric analysis. CMQ treatment resulted in a concentration-dependent G2/M cell cycle

arrest with a concomitant reduction in G0-G1 phase population in both LNCaP and PC-3

cells tested at 24 hour treatment (**Figure 11A**). The two agents used as positive control, the

microtubule-stablizing agent paclitaxel (PTX) and the microtubule-destablizing agent

vincristine (V), showed a similar pattern of concomitant accumulation of G2/M phase and

loss of G0-G1 phase populations in both cell lines. Similar data were obtained at prolonged

treatment periods. To examine possible differences between the effects of CMQ on LNCaP

and PC-3 cells, we next investigated the number of cells in subG1 phase which may mark

the apoptosis level in test cells. As seen in Fig. 2B, significant dose-dependent increases in

subG1 phase were detected in LNCaP cells treated with CMQ for 24 to 72 hours. CMQ

treatments for 72 hours increased the cell accumulation at subG1 phase to a level that was

up to 45 % higher than that of cells treated with paclitaxel or vincristine. By contrast, CMQ

induced varying levels of subG1 phase population in PC-3 cells. Increased levels in subG1

phase were found at treatment with 0.1 μM CMQ for 24 to 72 hours. By contrast, at

concentrations of 0.5 and 2.5 μM, CMQ had no effect on subG1 phase accumulation after

24 hours of treatment, and a slightly elevated level in subG1 cell accumulation was

observed at treatment of cells with 2.5 μM CMQ for 48 hours. After 72 hours of treatment

with 0.5 and 2.5 μM CMQ, however, the level of subG1 cells was significantly elevated,

reaching nearly that obtained with 0.1 μM CMQ (**Figure 11B**). Previous studies have

reported that mitotic cell death and high doses of microtubule inhibitors may cause an

endoreduplication (END) effect with polyploidy and the formation of giant

multimicronucleated cells, and that this effect may prolong or decrease apoptosis formation

(*18, 32*). We hence speculated that CMQ could have caused END activity in PC-3 cells at

high concentrations tested. As shown in **Figure 11C**, the levels of END with characteristics

of > 4N in DNA content were significantly increased in PC-3 cells treated with CMQ at

concentrations of 0.5 and 2.5 μM for 24 or 48 hours compared with those of cells treated

with 0.1 μM CMQ or the control group. By contrast, the END activity was less induced in

LNCaP cells by CMQ treatment for 24 or 48 hours. The END activities induced by

treatments with CMQ in both cell lines at 0.5 and 2.5 μM were found to mirror results

from treatment with either of the two reference controls, paclitaxel and vincristine, at 0.5

μM (data not shown). In addition, treatment with CMQ for 24 to 72 hours also increased

the cell size (FSC) and granule content (SSC) with a trend toward an increased level of

polyploidy in PC-3 cells (**Figure 11D**). DNA damage is known to usually contribute to G1

or G2/M cell cycle arrest. The tumor suppressor gene p53 gene plays an important role in

regulating the G2/M checkpoint molecules including ATM, Chk2 and p21 (*33*). We

therefore determined the levels of these molecules in the two cell lines in the absence and presence of treatment with CMQ at different concentrations. After 24 hours treatment with CMQ, expression levels of p-ATM and p21 were found to be elevated (**Figure 12A**). The DNA damage-associated DNA fragmentation induced by CMQ treatment in LNCaP and PC-3 cells was also evaluated (**Figure 12B**). After 24 hours treatment with CMQ, the level of DNA fragmentation was increased in both cell lines. These results suggest that CMQ may induce G2/M arrest via a DNA damage response pathway in test LNCaP and PC-3 cells. However, we also showed that the apoptosis levels were drastically increased in LNCaP cells upon CMQ treatment in contrast to smaller increases in PC-3 cells. The more modest increases of apoptotic cells observed for PC-3 cells, we speculate, may result from the presence of END and lack of p53 expression.

(A) LNCaP (24h)   PC-3 (24h)

(B) LNCaP (24h)   PC-3 (24h)

(C)
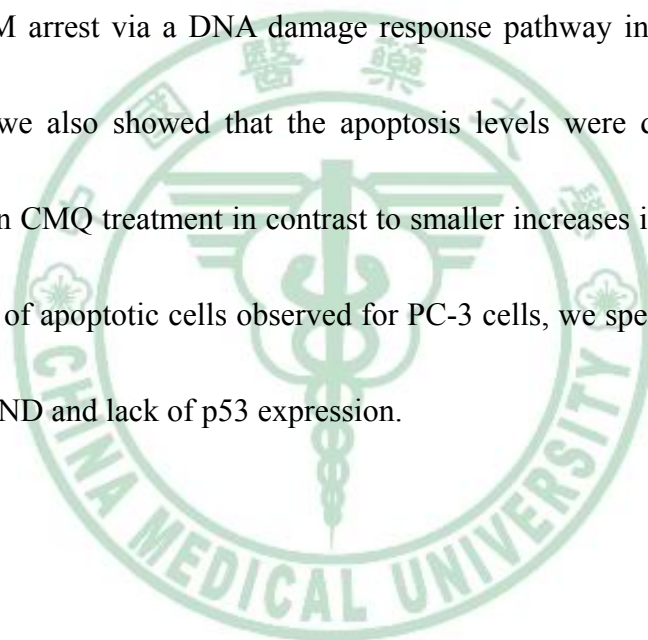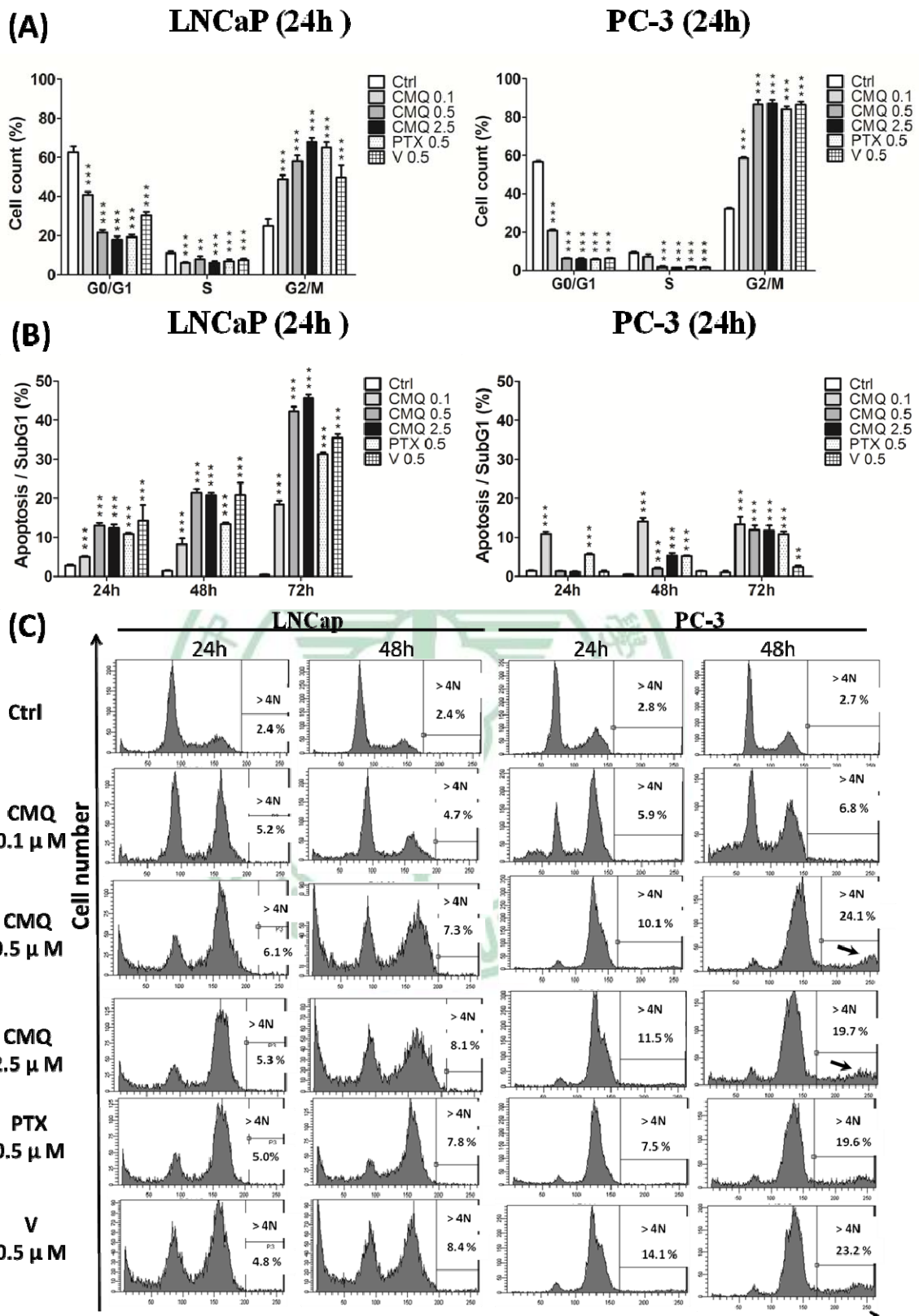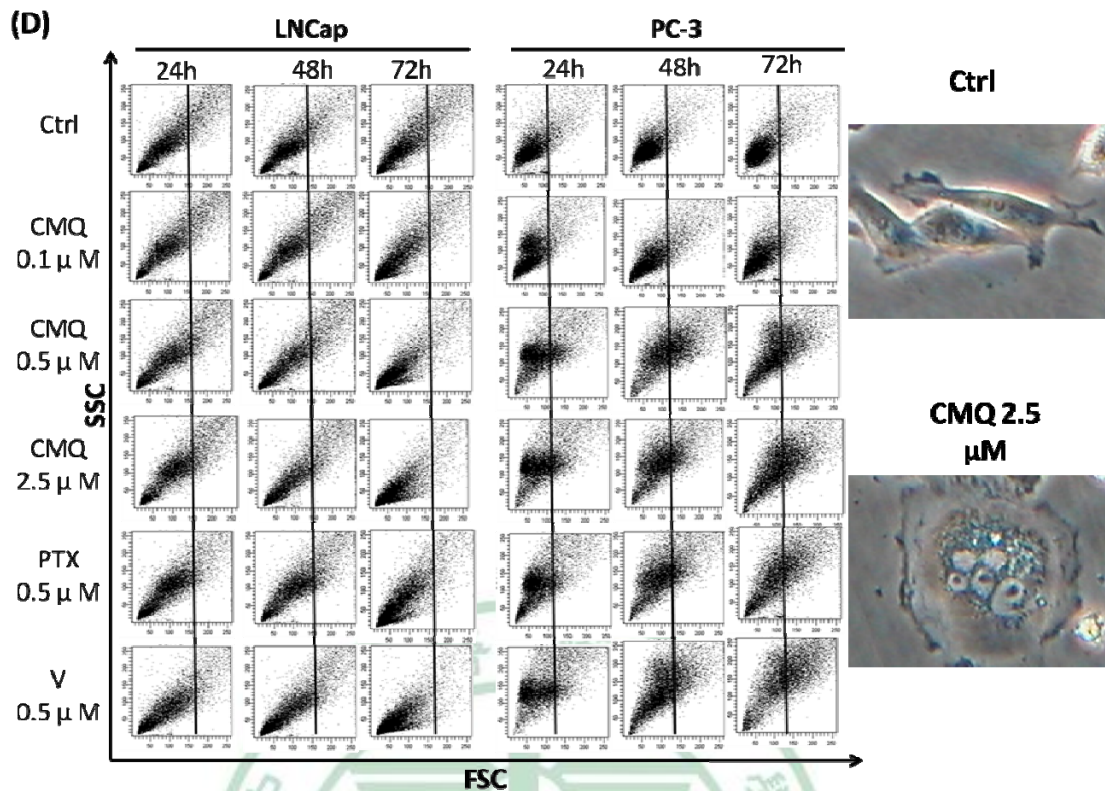
Figure 11. CMQ induces apoptosis and mitotic catastrophe via G2/M cell cycle arrest

(A) Cell cycle analysis for CMQ-treated LNCaP and PC-3 cells. Test cells were treated for

24 hours with CMQ (0.1, 0.5, 2.5 μM) or paclitaxel (PTX, 0.5 μM) and vincristine (V, 0.5

μM) as positive controls, labeled with PI, and analyzed by flow cytometry. Percentages of

cells present in the G0/G1, S and G2/M phases of the cell cycle were quantified. **(B)**

Percentage of apoptotic cells in the sub-G1 phase cell population in LNCaP and PC-3 cells.

Cells were treated as described in (A) for 24, 48, or 72 h. **(C)** CMQ induces apoptosis in

LNCaP cells and endoreduplication in PC-3 cells. Cell-cycle analysis was performed in

test cells as described in (A). Histogram of cell-cycle for specific cells are shown and % of

with DNA content > 4N was quantified. (D) FSC/SSC dot plots obtained from LNCaP and

PC-3 cells treated with indicated compounds.
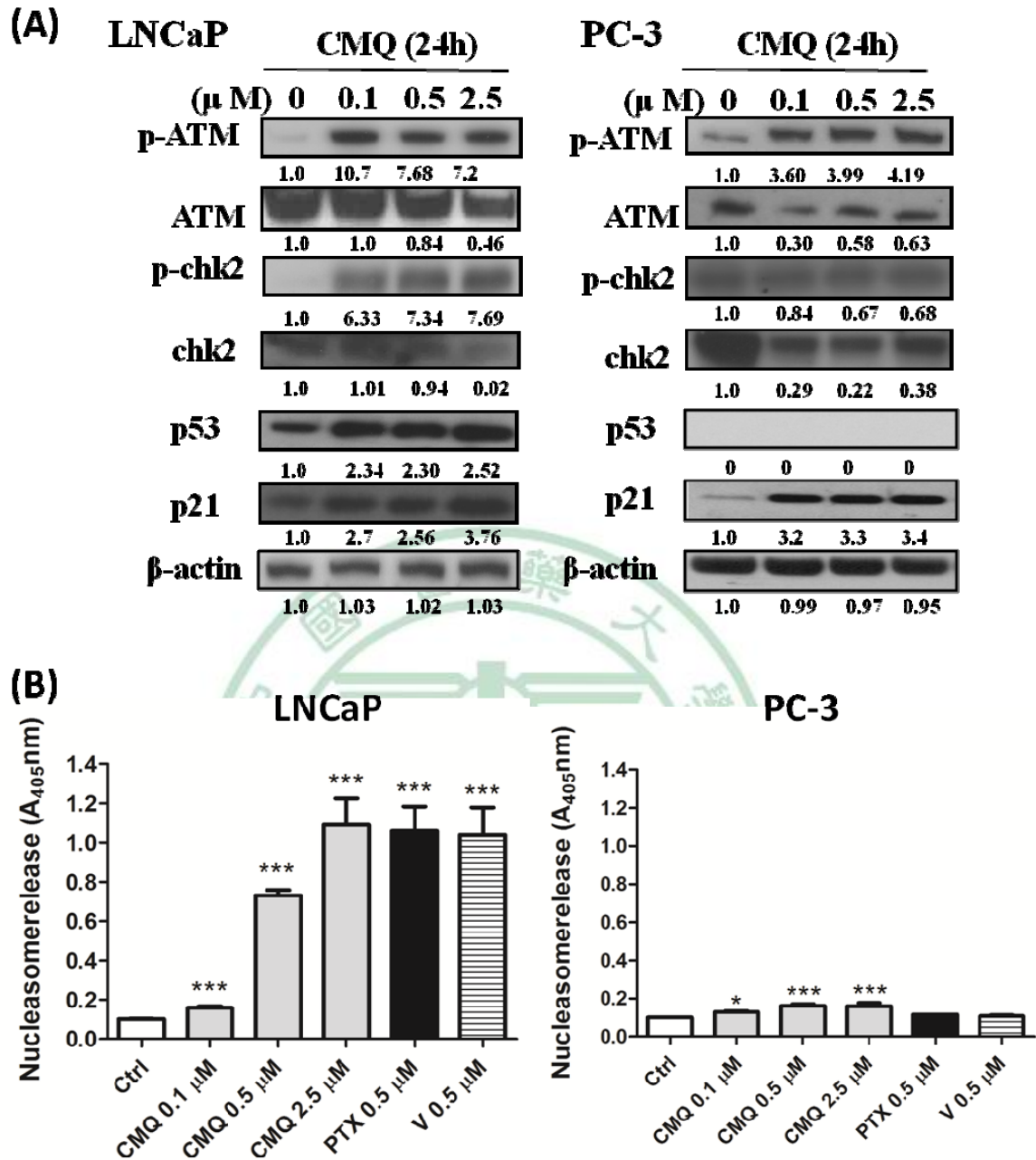
Figure 12. CMQ induces DNA damage and fragmentation

(A) Expression of DNA damage- and G2/M-associated marker proteins. Total cell lysates

(30 μg) from test cell cultures were harvested after treatment with CMQ (0.1, 0.5, 2.5 μM)

for 24 h. Levels of p-ATM, ATM, p-chk2, chk2, p53, p21 and β-actin, were quantitatively

assayed. (B) CMQ induces DNA fragmentation in LNCaP and PC-3 cells. Cell lines were

cultured in 96-well plates and treated with CMQ on the second day as indicated. After 24

hours, DNA fragmentation was measured with the Cell Death Detection ELISA kit (Roche

Molecular Biochemicals). Error bars represent mean S.D. of triplicate determinations.

3.1.3. CMQ suppresses polymerization of microtubules in LNCaP and PC-3 cells

G2/M cell cycle arrest is usually attributed to the disruption of cytoskeleton including microtubules. To evaluate the possible effect of CMQ on the organization of microtubule distribution in LNCaP and PC-3 cells, we further investigated cellular behaviours of the microtubule networks by immunofluorescence microscopy. Paclitaxel, vincristine, and colchicine are microtubule-destablizing agents used as reference controls for the study. As shown in **Figure 13A** and **13B**, in the absence of drug treatment the cellular microtubule network exhibited normal arrangements with a rich and intact structure of cytoplasmic microtubular cytoskeleton in test cells. However, treatment with CMQ at 0.1 to 2.5 μM was found to cause mitotic arrest in both LNCaP and PC-3 cells, with typical characteristics of disorganized microtubules, damaged microtubules and abnormal mitotic spindles. For both cell types, the exposure to CMQ at 0.1 μM resulted in disorganized microtubules that were arranged irregularly into an abnormal spindle status with aster-shaped tubulins, pseudo-bipolarity, tripolarity, or multipolarity. At elevated concentrations of 0.5 μM and 2.5 μM, CMQ treatment provoked massive microtubule damage, and short microtubule fragments were found to be scattered within the cytoplasm, exhibiting depolymerizing properties which are similar to those detected for colchicine- and vinblastine-induced microtubule changes. On the other hand, paclitaxel treatment promoted microtubule polymerization with aster-shaped microtubules, multipolar spindles

and well-organized microtubule structures. To further confirm the observed depolymerizing properties of CMQ, we measured the soluble (monomer) and polymerized forms of tubulin present in untreated PC-3 cells and in cells treated with 0.5 μM CMQ by western blotting. **Figure 13C** shows that CMQ increases the soluble form of tubulin (S) and decreases the polymerized form of tubulin (P) in a time-dependent manner, suggesting strongly that CMQ possesses a microtubule-depolymerizing activity. As shown in **Figure 13B**, high concentrations of CMQ caused mitotic catastrophe-related formation of multinucleated cells (**Figure 11D**). This activity is most notable after DNA damage that causes the fragmentation of chromosomes into pieces (*18, 26, 71*). These findings are consistent with our observations of endoreduplication and increased DNA damage-mediated pathway activity (**Figure 11D** and **13A**). The obtained results illustrate that CMQ can confer strong microtubule-depolymerizing activity which may contribute to G2/M cell cycle arrest and mitotic catastrophe activities detected in PC-3 cells.
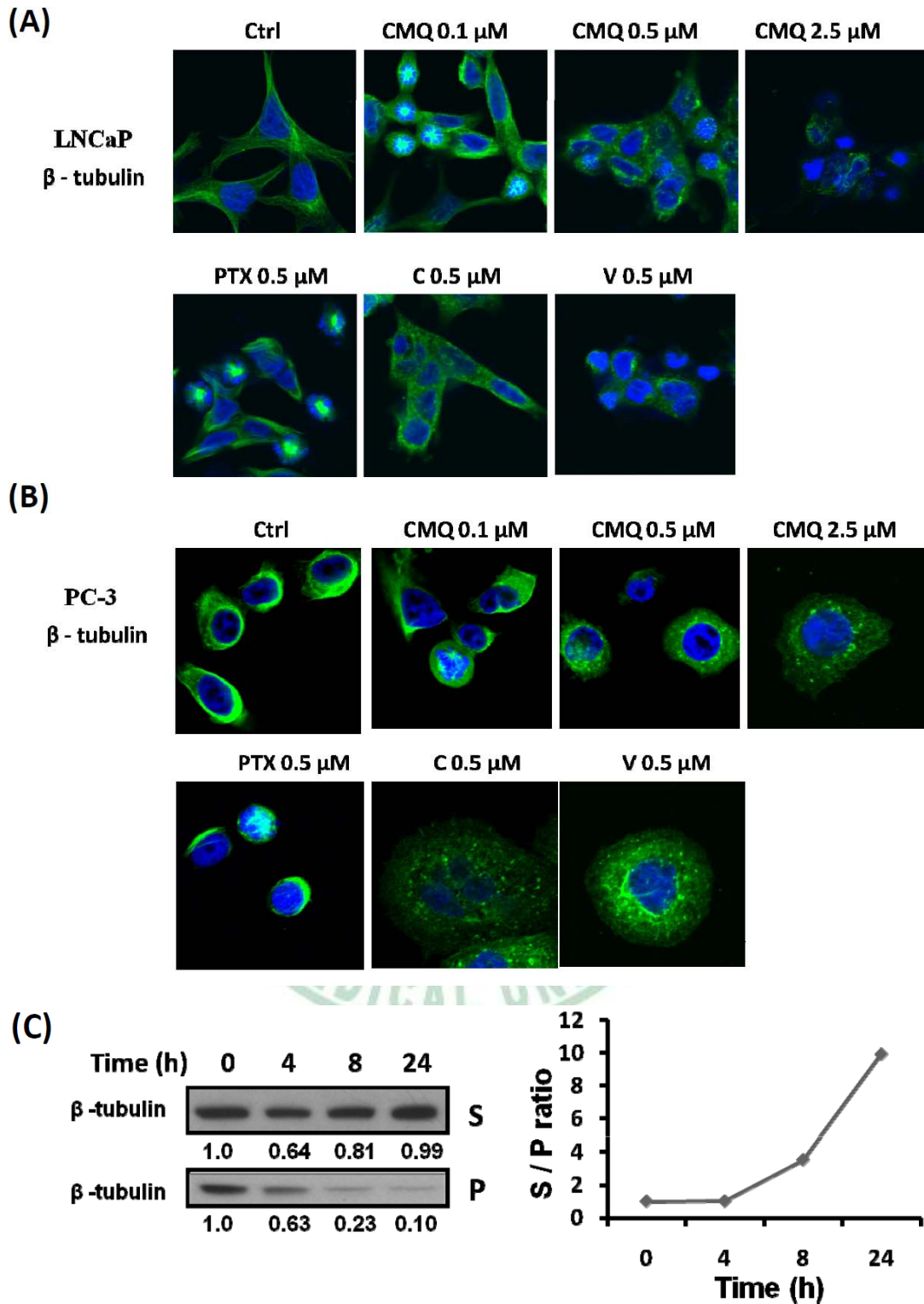
Figure 13. CMQ suppresses polymerization of microtubules in LNCaP and PC-3 cells

(A) Effect of CMQ on the organization of microtubule cytoskeleton. LNCaP and PC-3

cells were grown in medium for 48 h and then treated for 24 h with either 0.1 % DMSO,

various concentrations of CMQ (0.1, 0.5, 2.5 μM), or with 0.5 μM paclitaxel (PTX) and

0.5 μM vincristine (V) as positive controls. Cells were fixed, blocked, and incubated with

polyclonal β-tubulin antibody, then probed with the respective fluorescence-conjugated

secondary antibodies Alexa Fluor 488 and nuclei were stained with DAPI. The samples

and the coverslips were mounted. The immunoflurescent images were visualized by the

confocal microscopy and analyzed using the manufacturer's software. (B) Western blotting

analysis of soluble and polymerized forms of β-tubulin in PC-3 cells treated with CMQ.

After treatment with 0.5 μM CMQ at different time points, the soluble (S) and polymerized

(P) tubulin fractions were separated and immunoblotted with antibody against β-tubulin

(*left*). Plot of S/P ratio as a function of treatment time (*right*) is using the quantified

western blot data.
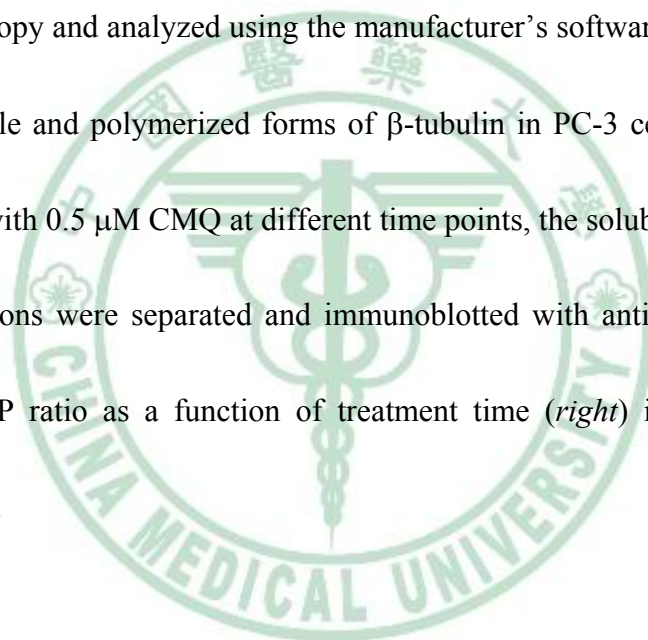
3.1.4. CMQ activates the intrinsic apoptotic pathway in both cell types, but activates the extrinsic pathway only in LNCaP cells

Previous studies have demonstrated that generation of reactive oxygen species (ROS) can initiate the induction of apoptosis and mechanisms for cell death (*72, 73*). We therefore investigated whether ROS can also play a role in the cytotoxic activity of CMQ. As shown in **Figure 14A**, CMQ increased ROS production in a concentration-dependent manner in a range from 40 to 60 (MFI) in LNCaP cells. The ROS production induced by CMQ could be blocked by N-acetyl cysteine (NAC), a thiol compound that serves as a cysteine source for the repletion of intracellular glutathione and act as a direct scavenger of ROS. High levels of ROS activity and mitotic arrest are known to regulate the expression of bcl-2 family proteins that have been shown to be key regulators of the mitochondrial apoptotic pathway (*18, 73*). As shown in **Figure 14B**, treatment with CMQ for 24 hours significantly affected the expression of two kinds of Bcl-2 family proteins in the examined prostate tumor cell lines. In LNCaP cells, CMQ treatment resulted in a 2-3-fold increase in the level of Bax and a maximal ~4-fold decrease in the level of Bcl-2. By contrast, the level of Bax was unchanged or only slightly increased in CMQ-treated PC-3 cells (**Figure 14B**). Based on the positive correlation between bcl-2 family and the mitochondrial pathway (the intrinsic pathway), we next examined whether the pro-apoptotic factors cytochrome c (which can induce caspase-3 and -9 activation), Smac (which can inhibit inhibitors of apoptosis), and apoptosis-inducing factor (AIF) (which can induce caspase-independent

45

cell death) were released from mitochondria into the cytosol to promote cell death of test

tumor cells (*13, 18*). As shown in **Figure 14C**, after treatment for 24 hours, expression

levels of cytochrome c, Smac and AIF were drastically increased in the cytosol fraction of

CMQ-treated LNCaP and PC-3 cells in a dose-dependent manner. By contrast, the

expression of these proteins in the mitochondrial fractions of test cells decreased.

Activation of caspases-8 and -9, important components of the extrinsic and intrinsic

apoptotic pathways, respectively, leads to activation of caspase-3 and subsequent apoptosis

(*18*). We thus measured the effect of CMQ at varying dosage on the activation of

caspases-3, -8 and -9 in LNCaP cells and PC-3 cells. CMQ treatment for 24 hours

effectively induced the expression of the cleaved form of caspases-3 and -9 in LNCaP cells

and PC-3 cells (**Figure 14D**), implying that they could be activated in LNCaP and PC-3

cells. CMQ treatment led also to an increase in the level of the cleaved form of caspase-8

in LNCaP cells; on the contrary, no such increase in the level of caspase-8 was observed in

PC-3 cells. Taken together, these results suggest that CMQ can activate the intrinsic

pathway in both test cell types via mitochondria or ROS activities, whereas the extrinsic

pathway can only be activated by CMQ treatment in the p53-expressing LNCaP cells.

(A)

LNCaP

PC-3

(B)

(C)

	LNCaP (24h)					PC-3 (24h)			
Cytochrome C	CMQ (µM)					CMQ(µM)			
	0	0.1	0.5	2.5		0	0.1	0.5	2.5
Cytosolic fr.	1	3.73	5.17	6.87		1	1.50	2.05	3.70
Mitochodrial fr.	1	0.99	0.74	0.72		1	0.45	0.35	0.33
Smac Cytosolic fr.	1	2.51	2.71	3.11		1	1.67	1.76	2.18
Mitochodrial fr.	1	1.13	0.83	0.72		1	0.98	0.76	0.72
AIF Cytosolic fr.	1	1.63	3.29	3.05		1	4.16	3.74	10.79
Mitochodrial fr.	1	0.94	0.37	0.24		1	0.67	0.82	1.0

(D)

	LNCaP (24h)					PC-3 (24h)			
	CMQ (µM)					CMQ (µM)			
	0	0.1	0.5	2.5		0	0.1	0.5	2.5
Cleaved caspase-3	1	6.0	7.38	3.24		1	1.18	1.37	1.56
Cleaved caspase-9	1	4.55	4.05	4.01		1	1.95	2.16	2.68
Cleaved caspase-8	1	1.68	1.76	1.56		1	1.02	0.61	0.19
β -actin	1	1	1	1		1	1.1	1	1

Figure 14. CMQ triggers the ROS-mediated intrinsic apoptotic pathway in both LNCaP and PC-3 cells, whereas it activates the extrinsic apoptotic pathway only in LNCaP cells

(A) Effect of CMQ on ROS production. LNCaP and PC-3 cells were treated with 0.1, 0.5 and 2.5 μM of CMQ for 24 h with or without 10 mM NAC. Cells were harvested and stained with H_2DCFDA for 30 min at 37^oC. ROS production is presented as mean fluorescence intensity (MFI) *P* values of less than 0.05 were considered statistically significant (**P < 0.01, ***P < 0.001, versus control group). *P* values of less than 0.05 were considered statistically significant (###*P* < 0.001, versus CMQ 0.5 μM group). (B) Effect of CMQ on Bax and Bcl-2 proteins. Test cells were treated with 0.1, 0.5 and 2.5 μM of CMQ for 24 h and lysed to analyze the levels of Bax and Bcl-2 proteins. (C) Effect of CMQ on release of cytochrome c, Smac and AIF proteins from cytosol and mitochondria. The cytosolic and mitochondrial fractions were separated as described in Materials and Methods, and the levels of cytochrome c, Smac and AIF were measured. (D) Effect of CMQ on the activation of capases-3, -8 and -9. Cells were treated and lysed as described in (A) to assay the levels of cleaved and pro-forms of caspases-3, -8 and -9 proteins.

3.1.5. CMQ can confer caspase-dependent and ROS-mediated antitumor activity

In an attempt to evaluate in detail the mechanisms underlying the antitumor activity observed for CMQ, several inhibitors against specific molecules or signaling systems were used to pretreat both types of cells. Cell viability was then measured in the absence and presence of treatment with CMQ. The caspase-9 inhibitor Z-LEHD-FMK, caspase family inhibitor Z-VAD-FMK and the ROS production inhibitor NAC were found to effectively rescue inhibition of tumor-cell growth in both LNCaP (**Figure 15A**) and PC-3 cells (**Figure 15B**). Pretreatment with the caspase-8 inhibitor Z-IETD-FMK reversed the cytotoxicity of CMQ in LNCaP cells but did not have an effect in PC-3 cells. These results suggest that the antitumor activity of CMQ is caspase-dependent and mediated by ROS activity. We also demonstrated here that the activation of caspase-8 may play a role in the antitumor activity of CMQ against LNCaP cells.
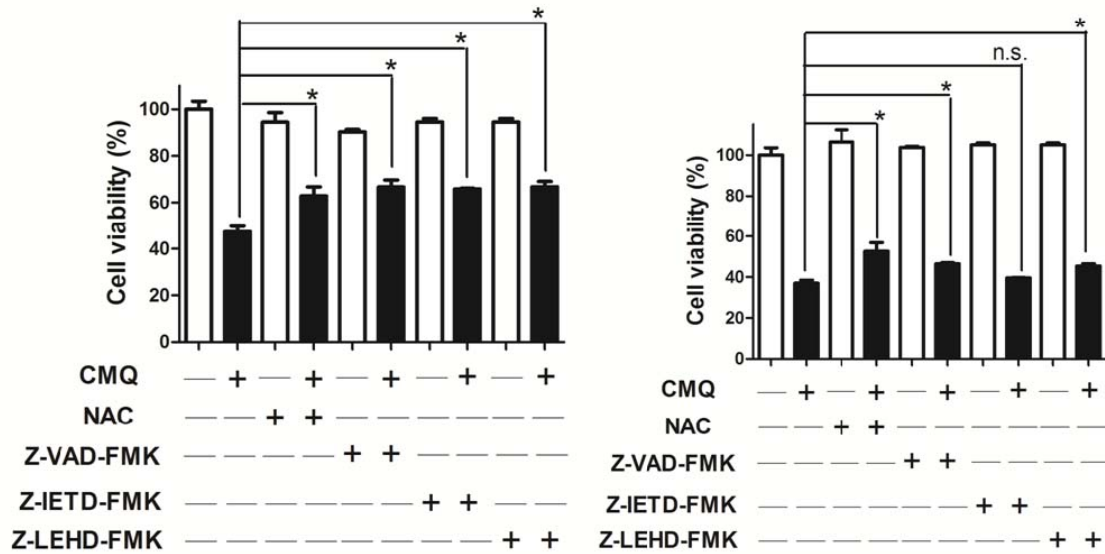
Figure 15. **ROS and caspase plays a role in antitumor activity of CMQ.**

LNCaP (A) and PC-3 cells (B) were pretreated with 10 mM NAC (ROS scavenger), 20 mM CFI (caspase family inhibitor, Z-VAD-FMK), 20 mM C8I (caspase-8 inhibitor, Z-IETD-FMK), 20 mM C9I (caspase-8 inhibitor, Z-LEHD-FMK)or for 30 min prior to treatment with CMQ. P values of less than 0.05 were considered statistically significant (*$P < 0.05$, versus control group).

3.1.6 CMQ suppresses tumor growth in xenograft mouse model

Androgen-dependent prostate cancer cells can often be readily treated with prostatectomy, androgen ablation or chemotherapeutics (*6*), while androgen-independent and p53-null prostate cancers, like PC-3 cells, are more aggressive and less sensitive to treatment with chemotherapeutics. It is therefore important to evaluate *in vivo* the potential antitumor activity of CMQ for both LNCaP and PC-3 cells. Subcutaneous mouse models using CB-17 SCID mice implanted with LNCaP and PC-3 cells, respectively, were employed in this study, and tumor growth in these mice was monitored with and without CMQ treatment. At dosages of 7.5 mg/kg and 15 mg/kg, the intraperitoneal injection of CMQ significantly suppressed LNCaP tumor growth, resulting in a mean tumor size of 394 $\pm$ 127 mm^3 and 353 $\pm$ 151 mm^3, respectively, after 24 days of treatment as compared to 696 $\pm$ 267 mm^3 in the vehicle control-treated mice ($p < 0.05$ for each CMQ treatment group versus vehicle control group, (**Figure 16A** and **16B**). The effect of CMQ was comparable to that of paclitaxel, which resulted in a tumor size of 313 $\pm$ 150 mm^3 when given at a dose of 15 mg/kg (*P < 0.05 versus vehicle control). Like treatment with the reference compound PTX, CMQ treatment did not affect the body weight of test mice (**Figure 16C**). Similar data were obtained in mice xenografted with the PC-3 cell line (**Figure 16D-F**). At a dose of 7.5 mg/kg and 15 mg/kg, CMQ treatment resulted in an average tumor size of 475 $\pm$ 260 mm^3 (*P < 0.05 versus vehicle control with 1152 $\pm$ 390

mm^3) and 367 ± 236 mm^3, respectively, (**P < 0.01 versus vehicle control). Treatment with paclitaxel (15 mg/kg) led to a tumor size of 545 ± 260 mm^3 (*P < 0.05 versus vehicle control). Again, CMQ did not significantly affect the body weight of mice (**Figure 16F**). In the orthotopic xenograft mouse model, as shown in **Figure 16G and Figure 16H**, the doses of 5 mg/kg body weight and 10 mg/kg body weight of CMQ treatment resulted in significant tumor suppression (**P < 0.01 versus vehicle control, ***P < 0.001 versus vehicle control, respectively). The treatment with paclitaxel (10 mg/kg) also led to decreased tumor weight (**P < 0.01 versus vehicle control).

(A) LNCaP
Ctrl
PTX (15 mg/kg)
CMQ (15 mg/kg)
CMQ (7.5 mg/kg)
2 cm

(B) LNCaP

(C) LNCaP

(D) PC-3
Ctrl
PTX (15 mg/kg)
CMQ (15 mg/kg)
CMQ (7.5 mg/kg)
2 cm

(E) PC-3

(F) PC-3

(G)
Ctrl
KY (10 mg/kg)
KY (5 mg/kg)
PTX (10 mg/kg)
2 cm

(E)

54
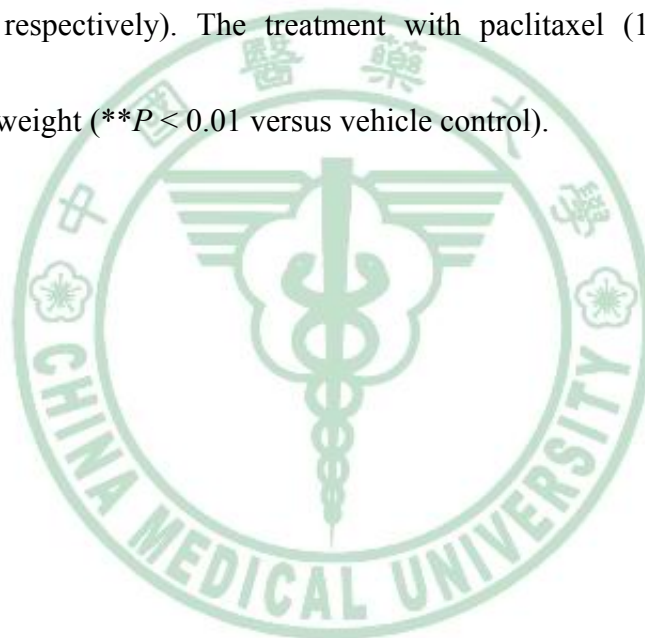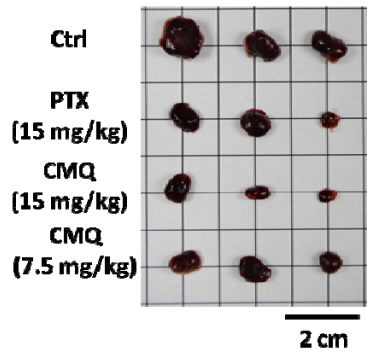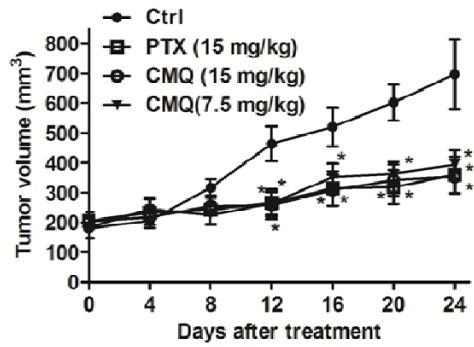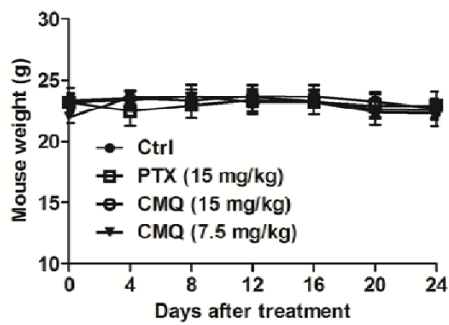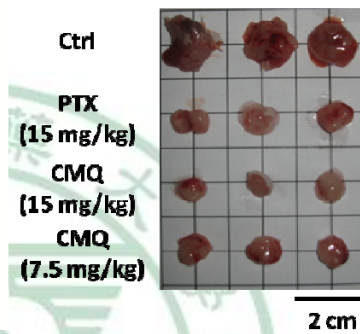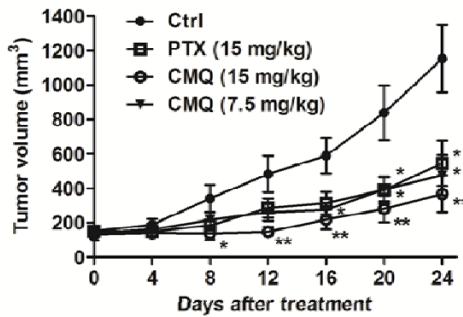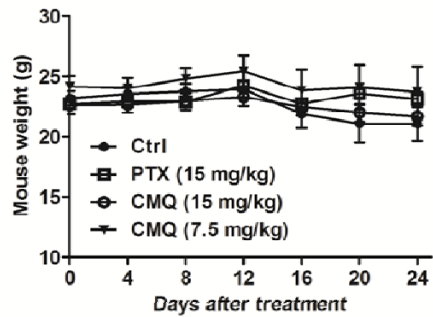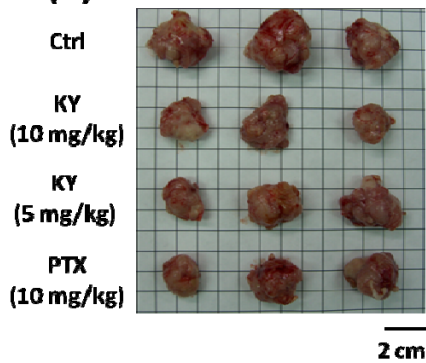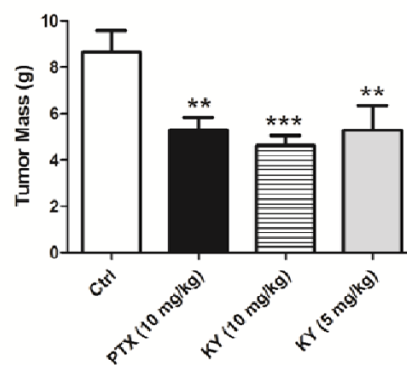
Figure 16. CMQ suppressed PC-3 and LNCaP tumor growth in subcutaneous and orthotopic xenograft SCID mice

(A-F) For subcutaneous xenograft mouse model, each mouse was inoculated s.c. in the right flank with LNCaP cells (4×10^6 cells) or PC-3 cells (2×10^6 cells) in a total volume of 0.2 ml serum-free medium containing 50 % Matrigel (BD Bioscience). As tumors reached an approximate size with a mean tumor volume of 150-200 mm^3, mice were randomly divided into three groups (n=6) that received the following treatments: (a) vehicle only, i.p., twice a week; (b) CMQ at 15 mg/kg, i.p., twice a week; (c) CMQ at 7.5 mg/kg, i.p., twice a week; and (d) paclitaxel at 15mg/kg, i.p., twice a week. Tumors sizes were measured twice a week using a caliper and tumor volumes were calculated using the following formula: Length $\times$ Width^2/ 2. Body weight was measured every four days. Test mice per group were sacrificed on day 40 and the tumors excised. **(G-H)** For orthotopic xenograft mouse model, PC-3 cells (2×10^5) in 20 μl were injected into the left side of the prostate. Two weeks after implantation, mice were randomly assigned to four groups (n = 6) that received vehicle control or CMQ (10 mg/kg and 5 mg/kg) and paclitaxel (10 mg/kg), i.p., twice a week for 3 weeks. All the mice were sacrificed on day 40 and the tumors were excised. Tumor weight was measured. (*$P < 0.05$,**$P < 0.01$, ***$P < 0.001$, versus vehicle control)

3.2. Discussion

Interference with microtubule assembly provides a promising approach for developing cancer therapy agents (*13, 14*). Even though taxanes and vinca alkaloids are currently commonly used as chemotherapeutic agents in clinics, severe toxic side effects and tumor cells developed drug resistance limit their therapeutic utility (*11*). For these and other clinical needs, efforts to find new, alternative therapeutic agents have become imperative for improving cancer treatments. One approach toward achieving this goal is to target molecular signaling systems. The p53 tumor-suppressor protein is well recognized as a key regulator in DNA repair and programmed cell death after DNA damage (*33, 74*). In this regard, aggressive prostate cancers are usually found as p53-null or -mutated. Recently, an increasing body of evidence suggests that 2-phenyl-4-quinolone derivatives possess potent antitumor activities and may offer advantages over current chemotherapeutic agents against certain cancers (*45, 48-50, 65, 68*). Therefore, we investigated in this study the 2-phenyl-4-quinolone derivative CMQ as a possible candidate by evaluating its *in vitro* and *in vivo* antitumor activities against two specific human prostate cancer lines carrying p53-wild type or a p53-null mutation, respectively.

Our results clearly demonstrated here that CMQ effectively inhibits cell proliferation of LNCaP cells and PC-3 cells in a concentraion-dependent manner, with very appreciable IC_{50} values of 0.082 μM and 0.291 μM, respectively at 48 hr (**Figure 10B**). These values

were even lower than those determined for the positive control tested in parallel, namely

paclitaxel, which exhibited an IC_{50} value of 0.18 μM and 0.51 μM, respectively (**Figure**

10). Interestingly, CMQ induced a higher proportion of apoptotic cells in LNCaP cells than

in PC-3 cells (**Figure 11B**). This result was also verified by quantitative assessment of

oligonucleosomal DNA fragmentation in both cell lines (**Figure 12B**). These results show

that distinguishable differences were detectable between LNCaP and PC-3 cells as a

response to CMQ treatment.

It is important to note that, in terms of selective cytotoxicity of CMQ on

non-cancerous or apparently "normal" cells and on tumor cells, we obtained considerably

higher IC_{50} values for non-cancerous WI-38 cells (4.3 μM) and the resting PBMCs (4.5 μM)

(**Figure 10C**). These values are approximately 52-55-fold and 14-16-fold higher as

compared with that for LNCaP and PC-3 cells, respectively. This result suggests that CMQ

could be selectively more cytotoxic to prostate tumor cells *in vitro* than to the surrounding

normal "stromal" cells. Related to this consideration, we showed that CMQ treatment did

not result in an obvious toxicity, as the body weight of test mice remained unchanged

(**Figure 16C** and **16F**). Furthermore, in **Figure 16B** and **16E**, CMQ suppressed tumor

growth in both LNCaP and PC-3 tumor-bearing SCID mice as effectively as paclitaxel. In

the orthotopic model (**Figure 16G** and **16H**), we speculated that intraperitoneal injection of

CMQ would elicit the certain cytotoxicity on implanted orthotopic prostate cancer. We

therefore use lower dose of CMQ (5 and 10 mg/kg body weight) treatments in this model. The results also that CMQ suppressed tumor growth in this model as effectively as paclitaxel. Based on these findings, we suggest that CMQ may be considered as a candidate for further development as a chemotherapeutic agent against prostate cancers.

Cell cycle analyses of LNCaP and PC-3 cells showed that CMQ promoted differentially a stronger G2/M cell cycle arrest in PC-3 cells than in LNCaP cells (Fig. 2A). Interestingly, our results also show that CMQ triggered a higher level of apoptosis in LNCaP cells than in PC-3 cells (**Figure 11B**). By analysis of the detailed cell cycle distribution, we found that with high doses of CMQ treatment, PC-3 cells showed a reduced level in cytotoxicity, delayed cell death, and induced several characteristics of mitotic catastrophe such as endoreduplication and enlarged cell size, as compared with these features in CMQ-treated LNCaP cells (**Figure 11C**). However, a low dose of CMQ (0.1 μM) caused minor apoptosis in PC-3 cells, but high doses of CMQ (0.5 μM and 2.5 μM) promoted endoreduplication, delayed cell death and resulted in mitotic catastrophe. According to these observations and considering the different p53 expression pattern in LNCaP and PC-3 cells, we hypothesized that p53 plays a role in coordinating the activity of G2/M arrest, apoptosis and mitotic catastrophe.

Previous studies reported that an impaired or deficient p53-mediated G2/M checkpoint is an important requisite for the massive damage of microtubules that cause the

activation of mitotic catastrophe (*18, 32*). The DNA damage-induced G2/M checkpoint

activation, which involves interactive activities of p21, p53, ATM and chk-2, has been

shown to be associated with apoptosis and mitotic catastrophe caused by microtubule

damage (*18, 27, 33, 70*). By measuring the expression of some proteins activated by DNA

damage, we found that CMQ increased the expression of ATM, chk-2 and p21 proteins in

both LNCaP and PC-3 cells, suggesting that CMQ can activate a DNA damage pathway

that contributes to apoptosis or mitotic catastrophe (**Figure 11D**). The elevated expression

of p53 gene in CMQ-treated LNCaP cells indicates that p53 may indeed promote apoptosis

rather than mitotic catastrophe. Inhibition of microtubule assembly may contribute to the

G2/M phase arrest, DNA damage, endoreduplication and mitotic catastrophe (*18, 26, 71*).

Thus, we conducted a comparison of the microtubule networks and the soluble (monomer)

and polymerized forms of tubulin in LNCaP and PC-3 cells as a response to treatment with

CMQ, paclitaxel, colchicines and vinchristine. Our results clearly demonstrated a

microtubule-depolymerizing activity of CMQ (**Figure 13A** and **13B**.). This finding is

consistent with the results from a previous study in which it was implied that microtubule

damage may result in G2/M phase arrest and facilitate a high level of subsequent apoptosis

or endoreduplication (*45*). Taking these results together, we suggest that p53 activity may

facilitate excessive G2/M arrest and polyploidy, which then leads to apoptosis. A

hypothesis of the differential cell death modes induced by CMQ in LNCaP cells and PC-3 cells is schematically outlined in **Figure 17A**.

Reactive oxygen species (ROS) are well known to mediate various intracellular signaling cascades (*73*). Oxidative stress regulated by the mitochondria-mediated pathway leading to apoptosis or necrosis may result from excessive production of ROS (*73, 75*). Our results found that CMQ can effectively enhance ROS production, whereas the inhibitor NAC can reduce CMQ-mediated ROS production (**Figure 14A**). The Bcl-2 family proteins have been recognized as crucial regulators of the mitochondria-mediated cell death pathway by functioning either as promoters (such as Bax) or inhibitors (such as Bcl-2) of cell death (*73*). We show in this study that CMQ can increase the expression of Bax but decrease the expression of Bcl-2 in both cell lines (**Figure 14B**). Excessive expression of proapoptotic proteins (such as Bax) over anti-apoptotic proteins (such as Bcl-2) usually initiates mitochondrial outer membrane permeabilization which in turn triggers the release of cytochrome c, Smac/Diablo and AIF (Apoptosis-inducing factor) from the mitochondrial intermembrane space to the cytosol (*18*). Cytochrome c released from mitochondria binds to Apaf-1 ATP and procaspase-9 forming a protein complex named apoptosome that activates caspase-3, leading to apoptosis. The Smac/Diablo proapoptotic protein can significantly enhance apoptotic execution via inactivation of various cellular inhibitors of apoptosis (IAPs) which can bind to active forms of caspase-3

and -9 and directly suppress their enzymatic activity (*18*). The AIF protein, which is involved in caspase-independent cell apoptosis, can directly cause DNA fragmentation and apoptosis. To characterize CMQ effects, we examined the expression patterns of cytochrome c, Smac and AIF in cytosolic and mitochondrial fractions. We demonstrated here that CMQ treatment results in increased levels of cytochrome c, Smac and AIF in the cytosolic fraction, while protein levels were decreased in the mitochondrial fraction (**Figure 14C**). We therefore suggest that CMQ may trigger the mitochondria-mediated pathway, leading to caspase-dependent cell death induced by cytochrome c and Smac, and caspase-independent cell death by AIF. Evaluation of the activation of caspase-3 and -9 induced by CMQ in LNCaP and PC-3 cells showed that caspase-3 and caspase-9 were activated by CMQ treatment in both LNCaP and PC-3 cells, but the activation levels were considerably higher in LNCaP cells (**Figure 14D**).

The activation of caspase-8 activity is known to play a pivotal role in the extrinsic pathway to induce apoptosis (*18*). It is interesting for us to find that caspase-8 was significantly activated by CMQ in LNCaP cells, whereas no induction was observed in PC-3 cells (**Figure 14D**). This finding suggests that p53 plays a role in regulating the control of caspase-8 activation (*51*). Taken together, our results demonstrate that CMQ can induce both caspase-dependent and -independent pathways. These findings are different from results previously reported by Wang and co-workers on another 2-phenyl-4-quinolone

derivative, CHM-1 (*49*). In that study, it was demonstrated that CHM-1 induced apoptosis in hepatocellular carcinoma cells only via a caspase-independent pathway. However, other studies demonstrated that CHM-1 only induced a caspase-dependent pathway in endothelial cells (*51*) and in colon adencarcinoma cells (*50*). In comparison, our current results correlate well with those reported by Hsu and co-workers (*52*), who showed that CHM-1 induces both caspase-dependent and caspase-independent pathways in the human osterogenic sarcoma U-2 OS cell line (*52*). We suggest that some of the dissimilarities observed among these studies may be due to the use of multiple cell types, the difference between chemical structures in CHM-1 and CMQ, and the various treatment conditions for test tumors.

In order to further characterize specific key regulators that may be involved in the observed antitumor activity of CMQ, an ROS scavenger (NAC), a caspase family inhibitor (Z-VAD-FMK), and a caspase-8 inhibitor (Z-IETD-FMK) were used to assess their potential interference effects (**Figure 15A** and **15B**). Our results suggest that ROS indeed may play an important role in promoting the CMQ-induced cell death in both LNCaP and PC-3 cells. However, caspase-8 may be involved to a higher extent in regulating CMQ-induced cell death in LNCaP cells than in PC-3 cells. Based on our various results reported in this study, we here proposed a model that may help explain the action of CMQ in the prostate cancer cells tested (**Figure 17B**).
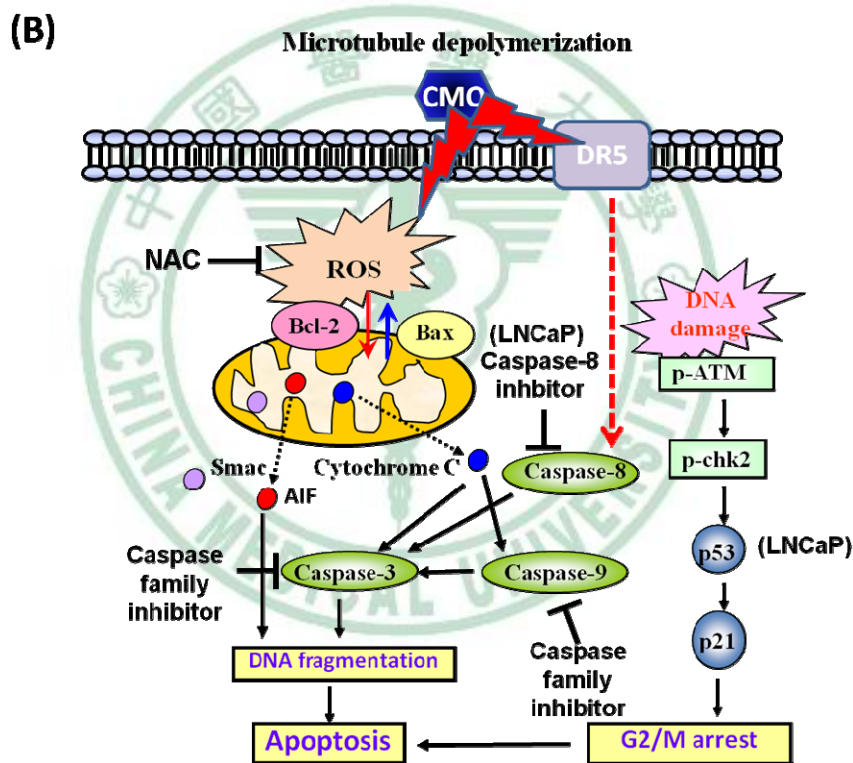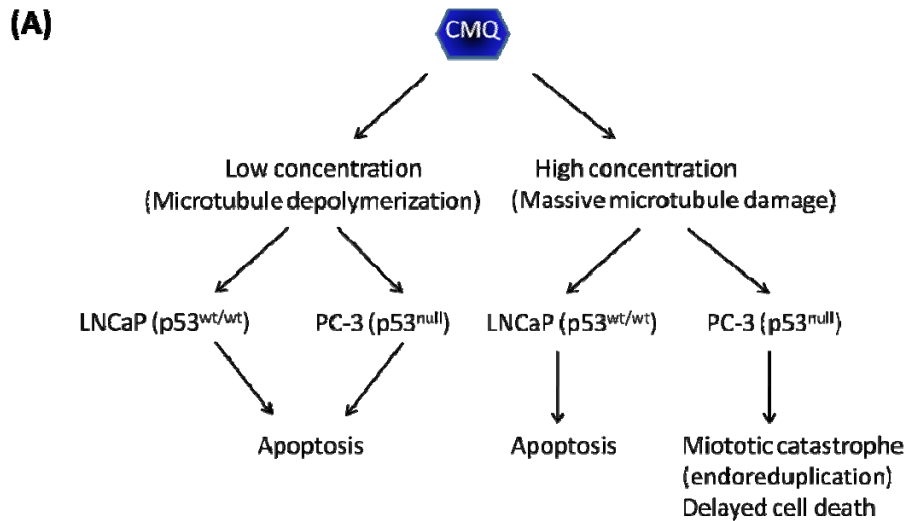
Figure 17. Hypothetical mechanisms for the action mode of CMQ-induced cell cycle arrest and cytotoxicity in LNCaP cells and PC-3 cells

(A) A schematic representation of the hypothetic modes of differential cell death induced by CMQ in LNCaP and PC-3 cells. (B) Hypothetical mechanisms for the action of CMQ on prostate cancer cells.

Chapter 4. Conclusion

In summary, we conclude that CMQ has significant cytoxicity against prostate cancer cells, as shown with LNCaP and PC-3 tumor cells. It may confer relatively low levels of cytoxicity, *in vitro* and *in vivo*, to the tumor-surrounding stromal fibroblast or leukocyte cells. The strong mitotic arrest effect induced by CMQ treatment in both LNCaP and PC-3 cells may be caused by activation of the DNA damage pathway. In addition to ROS, caspase-dependent (especially caspase-9-dependent) and caspase-independent pathways may also play important roles in the antitumor activity of CMQ. Given that LNCaP cells are p53-wild type and PC-3 cells are p53-null and distinguishable patterns were induced by CMQ in LNCaP cells (strong apoptosis and caspase-8 activation) versus PC-3 cells (endoreduplicaiton, mitotic catastrophe and delayed cell death, and caspase-8 inactivation), we suggest that p53 may play a critical role in the action mode of CMQ for tumor suppression. We propose that CMQ may function as a switch between apoptosis and mitotic catastrophe and by fine-tuning the regulation of caspase-8 activation. Our results reported here warrant future systematic evaluations of CMQ for use as a cancer therapy agent.

Chapter 5. Materials and Methods

5.1. Chemicals and reagents

CMQ was synthesized as described (*45*) and was obtained from our laboratory. The compound was dissolved in dimethyl sulfoxide (DMSO) to obtain a stock solution, and a final concentration of 0.1 % DMSO was used in the cell assays. RPMI 1640 medium, DMEM, fetal bovine serum (FBS), penicillin, streptomycin, and all other tissue culture reagents, unless otherwise indicated, were obtained from GIBCO/BRL Life Technologies (Grand Island, NY). DMSO, EGTA, EDTA, leupeptin, dithiothreitol (DTT), propidium iodide (PI), phenylmethylsulfonnylfluoride (PMSF), thiazolyl blue tetrazolium bromide (MTT), and other chemical agents were purchased from Sigma (St Louis, MO). Antibodies to Bcl-2 (sc-7382), Bax (sc-493), smac (sc-22766), cytochrome c (sc-13156), p-ATM (sc-47739), p53 (sc-1311), p21 (sc-469) as well as HRP-labeled anti-mouse (sc-2031) and anti-rabbit (sc-2357) IgGs were obtained from Santa Cruz Biotechnology Inc. (Santa Cruz, CA). Antibodies to apoptosis-inducing factor (AIF) (#4602), caspase 3 (#9662), caspase-8 (#9476), and caspase-9 (#9508) were purchased from Cell Signaling Technologies (Boston, MA). The antibodies to β-tubulin (ab6046) was purchased from Abcam (Cambridge, UK).

5.2. Cell culture and cell viability assay

LNCaP and PC-3 cells (1×10^4 cells/well) were grown in 96-well plates in RPMI and

DMEM medium, respectively, supplemented with non-essential amino acids and 10 %

FBS in 5 % CO_2 at 37^oC. After incubation for 16 h, culture media were removed and cells

treated with different concentrations of CMQ ranging from 0.0005 to 10 μM for 24, 48 or

72 h. Test culture medium was then replaced with 100 μl culture medium containing MTT

at a concentration of 0.5 mg/ml per well for 4 h. Subsequently, light absorbance was

measured with a spectrophotometer at 570 nm (*76, 77*). Cell viability was expressed as the

percentage of vehicle control cells (containing 0.1 % DMSO, as 100 %) cultured in the

absence of any test compounds.

5.3. Cell cycle analysis

After treatment of cells with vehicle or CMQ for the indicated time periods, both of

the floating and adherent cells were harvested by trypsinization, washed with

phosphate-buffered saline (PBS), and then fixed with 70% (v/v) ethanol at 4^oC overnight.

After washing and centrifugation, cells were resuspended in 0.5 ml propidium iodide (PI)

solution containing Triton X-100 (0.01%, v/v), RNase (200 μg/ml) and PI (20 μg/ml) for

30 min at room temperature (*77, 78*). Then, cells were centrifuged and the DNA content

was analyzed by flow cytometry (BD LSR2; BD Bioscience, San Jose, CA).

5.4. Immunofluorescence microscopy

The immunofluorescence assay was performed as described (*4, 79*) with a minor

modification. LNCaP and PC-3 (1×10^5) cells were grown in medium on 12-mm

coverslips for 48 h and then treated either with 0.1 % DMSO, serial concentrations (0.1, 0.5, 2.5 μM) of CMQ, or with the two positive controls, 0.5 μM paclitaxel and 0.5 μM vincristine for 24 h. Cells were fixed with 4% (v/v) paraformaldehyde on ice for 15 min, permeabilized with 0.2% (v/v) Triton X-100/PBS, and then washed three times with PBS. After blocking in 1% (v/v) fish gelatin/PBST (PBS with 0.1% Tween 20) for 1 h, samples were incubated with α-tubulin antibody (clone DM1A, Calbiochem, La Jolla, CA; 1:1000 dilution) and polyclonal β-tubulin antibody (Abcam, Cambridge, UK; 1:1000 dilution) at 4 °C for 18 h, washed thrice with PBST, then probed with the respective Alexa Fluor 488-conjugated secondary antibodies (Invitrogen, Carlsbad, CA; 1:2000 dilution). Nuclei were stained with 4',6-diamidino-2-phenylindole (DAPI, 0.2 μg/mL in PBS; Sigma Chemicals) for 1 h at room temperature. The samples were washed four times and the coverslips were mounted with Prolong Antifade (Invitrogen, Carlsbad, CA, USA). The immunofluorescent images were visualized by confocal microscopy (LSM 510 Meta, Carl Zeiss GmbH).

5.5. Analysis of soluble and polymerized tubulins

Soluble and polymerized tubulins from cell lysates were separated by centrifugation as described previously (*80*). Briefly, PC-3 cell lines (1×10^6 cells) were washed twice with PBS before lysing at 37°C with 100 μL of hypotonic buffer [1 mM $MgCl_2$, 2 mM phenylmethylsulfonyl fluoride, 2 mM EGTA, 0.5% NP40, Roche's Complete Protease

Inhibitor Cocktail, and 20 mM Tris-HCl, (pH 6.8)] in 1.5-ml microfuge tubes for 5 min in the dark. After an additional 100-ml hypotonic buffer was added, the cell lysates were vortexed, and the fractions separated by centrifugation at 16,200 g for 10min at room temperature. The supernatant (200 μL) containing the soluble tubulins was transferred to another tube. The pelleted fraction containing the polymerized tubulins was then resuspended in 200 ml of hypotonic buffer. Proteins were solubilized in 5 X sample buffer and sonicated on ice before heating samples to 99°C for 5 min.

5.6. Preparation of cytosolic and mitochondrial fractions

Fractionation of cystosol and mitochondria was carried out as previously described (*77, 81*). In brief, cells (10^6) were resuspended in 30 μl of homogenization buffer (75 mM KCl, 1 mM NaH$_2$PO$_4$, 8 mM Na$_2$HPO$_4$, 250 mM sucrose, 1 mM EDTA, and 50 μg/ml digitonin) and incubated on ice for 5 min, followed by centrifugation at 16,200 g for 10 min. Supernatants were collected as the cytosolic fraction and the pellets as the mitochondrial fraction. The samples were used for western blot analysis of cytochrome *c*, AIF and Smac.

5.7. Western blotting

After the indicated exposure time to vehicle or to the indicated treatments, cells were washed twice with PBS, and reaction was terminated by the addition of 500 μl ice-cold lysis buffer (20 mM Tris–HCl, pH 7.4, 150 mM NaCl, 1 mM EGTA, 1 mM PMSF, 1 mM

Na$_3$VO$_4$ and 1% Triton X-100) containing Roche's Complete Protease Inhibitor Cocktail and phosphatase inhibitors (Roche Diagnostics Ltd, Mannheim, Germany). For Western blot analysis, equal amounts of total proteins were separated by electrophoresis in a 5–20 % gradient polyacrylamide gel and transferred onto an Immobilon-P PVDF membrane (Millipore Corp., Billerica, MA, USA). After blocking with 5% nonfat milk at room temperature in PBS containing 0.1% Tween 20 (PBST), the membrane was washed with PBST and immuno-reacted with the indicated primary antibody overnight at 4 ^{o}C. After four washings with PBST, anti-mouse or anti-rabbit IgG (dilute 1:10000) secondary antibodies were applied to the membranes for 1 h at room temperature. The membranes were washed with PBST for at least five times and the detection of signals was performed using the Immobilon HRP substrate (Millipore Corp., Billerica, MA, USA) (*79, 82*).

5.8. Subcutaneous and orthotopic xenograft tumor model

CMQ was dissolved in a vehicle mixture of DMSO/10% Cremophor EL/PBS. As a comparison and reference, the positive control paclitaxel was dissolved in the same vehicle solution. For subcutaneous xenograft mouse model, male severe combined immunodeficient (SCID) mice (4-6 weeks of age), were purchased from the National Laboratory Animal Center (Taipei, Taiwan). LNCaP cells (4×10^6) or PC-3 cells (2×10^6) in 50 μl DMEM medium with 50 μl Matrigel (BD Pharmingen, San Diego, CA) were injected subcutaneously (S.C.) into the right flank of each test mouse. When tumors reached an

approximate volume of 150 -200 mm^3, mice were randomly distributed into 4 different test groups (n = 6) receiving vehicle only, CMQ (15 mg/kg and 7.5 mg/kg) or Paclitaxel (15 mg/kg) by intraperitoneal (I.P.) injection twice weekly for 3 weeks. Tumor volumes (V) were determined by measuring the length (L) and the width (W), and tumor volumes were calculated as $V = L \times W^2 / 2$. Body weight was measured every four days. All mice were sacrificed on day 24 post-treatment and the tumors were excised. For the orthotopic implantation, PC-3 cells (2×10^5) in 20 μl were injected into the left side of the mouse prostates. Two weeks after implantation, mice were randomly assigned to four groups (n = 6) that received vehicle control, KY (10 mg/kg and 5 mg/kg) or paclitaxel (10 mg/kg) by I.P. injection twice weekly for 3 weeks. Six mice per group were sacrificed on day 40 and the tumors were excised. Tumor weight was measured.

5.9. Statistical analyses

Data are expressed as mean ± S.D. or ± S.E.M. for the indicated number of separate experiments. Means were analyzed for statistical difference using the Student's *t*-test, and *p* values less than 0.05 were considered significant (*$P < 0.05$; **$P < 0.01$; ***$P < 0.001$).

Part II. CMQ augments efficacy of dendritic cell-based cancer vaccines

Chapter 1. Introduction

1.1. Cancer vaccines and dendritic cells

The term "cancer," which is derived from the Latin word for "crab," was adopted in ancient times to illustrate the way in which malignant tumors seem to grasp the tissues they invade. Cancers may arise due to mutations or epigenetic changes to genes that control cell division, migration, and death, leading to an abnormality in cellular proliferation associated with life-threatening invasive tumor growth and metastases (*83, 84*).

Effective cancer vaccines are sought to treat malignancies by approaches that induce presentation of tumor-associated antigens (TAAs) in contexts that elicit potent CD4$^+$ and CD8$^+$ T-cell responses and break the tolerance of the host immune system to tumor growth (*85, 86*). Immunity, including innate immunity and antigen-specific adaptive immunity, and tolerance toward tumors is orchestrated by a network of antigen-presenting cells, the most crucial of which are dendritic cells (DCs) (*87, 88*). As shown in **Figure 18**, maturation and activation of dendritic cells is critically important for immune response. However, although clinical trials based on DC-based vaccines have been initiated for

certain malignancies (*89*), unlike in pathogen infection, activation of DCs in tumor microenvironments is weak and ineffective (*85, 90*); the challenge, therefore, is to develop DC-based vaccines that can not only induce powerful activation of DCs, but also enhance tumor-specific immunity by breaking tolerance.

The approach to generate *ex vivo* differentiation and activation of DCs for cancer immunotherapy is shown in **Figure 19**. In general, the most common method used to generate DCs in clinical trials is to culture CD14$^+$ monocytes in serum-free media in the presence of GM-CSF and IL-4. After 5–7 days of culture, the monocytes can differentiate into immature DCs with a loss of CD14 expression, the expression of moderate to low levels of CD40 and the costimulatory ligands B7-1 and B7-2. DC maturation is accomplished by culturing the immature DCs for an additional 24–48 hours in the presence of several biological agents, the most popular combination being tumor necrosis factor-α (TNF-α), interleukin-6 (IL-6), interleukin-1β (IL-1β), and prostaglandin E2 (PGE2). Matured DCs further upregulate CD40, B7-1, and B7-2 and induce the expression of the lymph node homing receptor CC chemokine receptor 7 (CCR7). Antigen loading may occur at either the immature or mature DC stage. Later, mature antigen-loaded DCs could be injected into patients subcutaneously, intradermally, or intravenously. They would subsequently migrate to the draining lymph node, where they would encounter and present antigen to the cognate CD4$^+$ T cells. CD40L, which is expressed on the antigen-activated

CD4+ T cell to cross-link CD40 on the DCs, induces the mature DCs to differentiate, a process known as licensing. These licensed DCs upregulate cell surface products, notably the ligands for OX40 and 4-1BB (OX40L and 4-1BBL, respectively). The licensed DCs also present antigen to cognate CD8+ T cells. 4-1BBL–mediated costimulation via 4-1BB on the antigen-activated CD8^{+} T cells elevate the survival and proliferative capacity of the activated CD8^{+} T cells. Similarly, the OX40L-mediated costimulation increases the survival and proliferation of the activated CD4+ T cells. The important factors which influence the efficacy of DC-based vaccines are shown in **Figure 20**.

Numerous dendritic cell-based strategies have been employed for developing anti-cancer vaccines, including defined peptide-loaded DCs (*91, 92*), genetically-modified DCs (*93, 94*), DC-derived exosomes (*89*), apoptotic cell-loaded DCs (*95*), and tumor cell lysate (TCL)-pulsed DCs (*91, 96, 97*). The possible advantage of using whole cell lysates as the source for vaccination is that a full complement of TAAs, including both MHC class I and class II-restricted tumor associated epitopes may be provided, thus reducing the possibility of immune escape by antigen loss variants (*98*). A common technique used to generate tumor cell lysates (TCLs) is the removal of solid cellular debris by centrifugation after repeated cycles of freezing and thawing of target tumor cells (*99-101*). The protective effect of DCs pulsed with TCLs has been proven in animal models (*96, 102*), and reported in a range of clinical trials, summarized in **Table 7** (*91, 97, 103*). Nonetheless, the modest

activities reported thus far for TCL-pulsed DC-based vaccines need to be further improved

and optimized, either in the presence or absence of DC-maturation stimuli (*97, 103*).

a

Peripheral tissue

Apoptotic cell

Immature DC

Antigen uptake

Migration

Inducible regulatory T cells

Antigen presentation in absence of co-stimulation

MHC class II

TCR

Proliferation

Naive T cell

Induction of regulatory phenotype

Deletion

Secondary lymphoid organ

b

Virus infection leading to tissue inflammation

Antigen uptake

Migration and maturation

Killing

ADCC

Cytokines

Virus-infected cell

TCR

MHC class I

Fc receptor

Macrophage

NK cell

T helper cells

CTLs

Antibodies

T_Reg cells

Mature DC

B cell

CD80/CD86

MHC class I/class II

CD28

TCR

Antigen presentation in presence of co-stimulation

Proliferation

T cell

Secondary lymphoid organ

75

Figure 18. The different functions of immature and mature dendritic cells

(a) Immature dendritic cells (DCs) induce tolerance. Tissue DCs always sample their environment, capture specific antigens and migrate in small numbers to the draining lymph nodes. In general, in the absence of inflammation, the DCs usually remain in an immature state, and antigens could be presented to T cells in the lymph node without costimulation, leading to either the deletion of T cells or the induction of regulatory T cells. **(b) Mature DCs induce immunity.** Inflammation of tissue induces the maturation of DCs and triggers the migration of large numbers of them to draining lymph nodes. The mature DCs express peptide–MHC complexes on their surface, and appropriate co-stimulatory molecules. This allows the priming of CD4+ T helper cells and CD8+ cytotoxic T lymphocytes (CTLs), the activation of B cells and the initiation of an adaptive immune response. To control the immune response, CD4+CD25+ regulatory T cell (T_{Reg}) populations are also expanded. ADCC, antibody-dependent cell-mediated cytotoxicity; NK, natural killer; TCR, T-cell receptor. Adopted from Banchereau et al. (*92*).
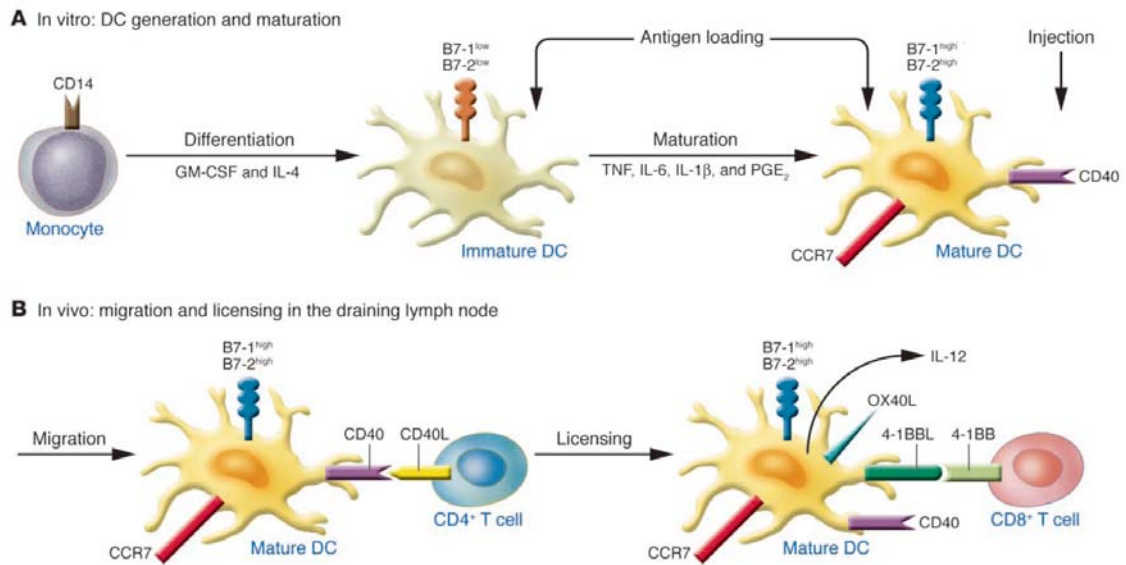
Figure 19. The approach of *ex vivo* differentiation and activation of DCs for cancer immunotherapy. [Adopted from Gilboa, E.et.al. (*90*)]

Generation of DCs
- Direct purification from peripheral blood (± mobilization with Flt3L, ProGP, etc.)
- Monocyte-derived (flask adherence, CD14 bead separation, culture with GM-CSF and IL-4/IL-13)
- CD34$^+$ precursors (CD34 bead separation, culture with Flt3L, IL-3, IL-6, GM-CSF, IL-4)

Antigen loading of DCs
- Peptides (acid-eluted/synthesized, MHC class I/II-restricted)
- Proteins (purified, Ag-Ab immune complexes, coupling with anti-DEC-205 Ab)
- mRNA, DNA (tumor-derived, synthesized single target gene)
- Viral vectors (retrovirus, lentivirus, adenovirus, fowlpox, alphavirus, etc.)
- Tumor cells (apoptotic/necrotic), tumor lysate, DC-tumor cell fusion

Maturation of DCs
- Cytokines (TNF-α alone, TNF-α + IL-1β + IL-6 + PGE2)
- CD40L (±IFN-γ)
- Calcium ionophore
- TLR agonists (CpG ODN, dsRNA, poly I:C, etc.)

DC administration
- Dose
- Frequency
- Route (intravenous, intradermal, subcutaneous, intranodal, intratumoral)

Figure 20. Various factors to be considered in DC-based immunotherapy.

[Adopted from Osada et al. (*104*)]

Table 7. Overview of clinical trials using dendritic cell-based cancer immunotherapy

Tumor type	DC generation	Pulsing	Maturation	Route	Memo	Reference
Soft-tissue sarcoma (STS)	MDDC from GM-CSF (1000 U/ml) & IL-4 (1000 U/ml)	-	-	I.T.	(pilot study)	Finkelstein et al. 2011.(*105*)
Metastatic melanoma	MDDC from GM-CSF (800 U/ml) & IL-4 (500 U/ml)	$gp100_{154-167}$, $gp100_{280-288}$, $tyrosinase_{369-376}$ (25 µg/ml, 60 min)	PGE2 (10 µg/ml), TNF-α (10 ng/ml) (72h)	I.V. (10×10^6 DCs) I.D. (5×10^6 DCs)	Anti-CD25 (Phase I/II)	Jacobs et al. 2010.(*106*)
Colorectal cancer (CRC)	MDDC from GM-CSF (800 U/ml) & IL-4 (500 U/ml)	$CEA_{571-579}$	TNF-α (10 ng/ml), IL-1β (5 ng/ml), IL-6 (15 ng/ml), PGE2 (10 µg/ml)	I.V. (10×10^6 DCs) I.D. (5×10^6 DCs)	Adjuvant: oxaliplatin/c apecitabine (pilot study)	Lesterhuis et al. 2010. (*107*)
Colorectal cancer (CRC)	MDDC from GM-CSF (50 ng/ml) & IL-4 (20 ng/ml)	CEA (20 µg/ml)	OK432, IFN-α (500 U/ml), PGE1 (50 ng/ml)	S.C.	Phase I/II	Sakakibara et al. 2011.(*108*)
Non-small cell lung cancer	MDDC from GM-CSF (50 ng/ml) & IL-4 (30 ng/ml)	WT1 peptide CEA peptide MAGE-1 peptide Her2 peptide	IFN-γ (1000 U/ml) (48h)	S.C. I.V. (5×10^7 DCs)	Maturation, and then loaded with antigens (Phase I)	Perroud et al.2011.(*109*)
Prostate cancer	MDDC from GM-CSF (500 U/ml) & IL-4 (500 U/ml)	PSMA-deriv ed peptide	-	I.V.	Phase II	Lodge et al. 2000.(*110*)
Melanoma	MDDC from GM-CSF (500 U/ml) & IL-4 (500 U/ml)	DNA vaccine: melan A gp100	TNF-α (20 ng/ml), IL-1β (5 ng/ml) (48h)	I.D. S.C. (5×10^6 DCs)	Phase I/II	Steele et al. 2011.(*111*)
Advanced colorectal cancer	MDDC	TCL	-	I.D. ($3\text{-}5 \times 10^6$ DCs)	Pilot study	Burgdorf et al. 2008.(*112*)

(CRC)						
Malignant glioma	MDDC from GM-CSF (800 U/ml) & IL-4 (500 U/ml)	TCL (18h)	-	S.C.	Phase I	Yu et al. 2004.(*113*)
Colorectal cancer (CRC)	MDDC from GM-CSF (800 U/ml) & IL-4 (500 U/ml)	$CEA_{571-579}$ CEA mRNA (electroporation)	TNF-α (10 ng/ml), IL-1β (5 ng/ml), IL-6 (15 ng/ml), PGE2 (10 μg/ml)	I.V. (10×10^6 DCs) I.D. (5×10^6 DCs)	pilot study	Lesterhuis et al. 2010. (*114*)
Metastatic melanoma	MDDC from GM-CSF (1000 U/ml) & IL-4 (250 U/ml)	TCL 100 and 50 μg/ml (F-T)(48h) Peptide (2h)	TNF-α (1000 U/ml), IL-1β (1000 U/ml), IL-6 (1000 U/ml), PGE2 (1 μg/ml)	I.D. I.N. (5×10^6 DCs)	Phase I/II	Trepiakas et al. 2010.(*115*)
Metastatic melanoma	MDDC from GM-CSF (1000 U/ml) & IL-4 (1000 U/ml)	TCL 100 mg/ml	TNF-α (1000 U/ml), IL-1β (1000 U/ml), IL-6 (1000 U/ml), PGE2 (1 μg/ml)	I.V.	Phase I/II	Ridolfi et al. 2006.(*116*)
Metastatic renal cell carcinoma (mRCC)	MDDC from GM-CSF (1000 U/ml) & IL-4 (250 U/ml)	TCL 50 and 100μg/ml (12h)	TNF-α (1000 U/ml), IL-1β (1000 U/ml), IL-6 (1000 U/ml), PGE2 (1 μg/ml)	S.C.	Phase I/II	Soleimani et al. 2009.(*117*)
Colorectal cancer (CRC)	MDDC from GM-CSF (500 U/ml) & IL-4 (20 ng/ml)	TCL	TNF-α (10 ng/ml), IL-1β (10 ng/ml), IL-6 (10 ng/ml), PGE2 (1 μg/ml)	I.D. ($3-5 \times 10^6$ DCs)	Phase II	Toh et al.2009. (*103*)
Medullary thyroid carcinoma (MTC)	MDDC from GM-CSF (1000 U/ml) & IL-4 (500 U/ml)	TCL 200μg/ml (F-T) (12h)	TNF-α (1 μg/ml) , IFN-γ (1000 U/ml) (12h), LPS (50 ng/ml) (4h)	I.V.	Pilot trial	Bachleitner et al. 2009.(*118*)
Hepatocellular carcinoma (HCC)	MDDC from GM-CSF (800 U/ml) & IL-4 (500 U/ml)	TCL (2h)	TNF-α (1 μg/ml)	I.V.	Phase II	Palmer et al. 2009.(*119*)
Metastatic renal cell carcinoma (mRCC)	MDDC from GM-CSF (500 U/ml) & IL-4 (20 ng/ml)	TCL (F-T & Irra) (Tumor : DC =1-3 :1)	TNF-α (50 μg/ml)	I.N.	IL-2 & IFN-α (Phase II)	Schwaab et al.2009.(*97*)

Relapsed glioblastoma multiform (GBM)	MDDC from GM-CSF (500 U/ml) & IL-4 (20 ng/ml)	TCL (F-T & Irra)	TNF-α (120 mg/ml), IL-1β (120 ng /ml), PGE2 (20 μg/ml)	I.D.	Pilot trial	De Vleeschou wer et al. 2008.(*120*)
Pancreatic carcinoma	MDDC from GM-CSF (1000 U/ml) & IL-4 (500 U/ml)	TCL 50 – 150 μg/ml (4h)	TNF-α (1000 U/ml), PGE2 (10 μg/ml)	I.D.	pilot study	Bauer. 2011.(*121*)
Metastatic melanoma	MDDC from GM-CSF (700 U/ml) & IL-13 (136 ng/ml)	TCL	FMKp (1 μg/ml) & IFN-γ (1000 U/ml)	I.D. S.C.	Phase II	Ribas et al. 2010. (*122*)
Glioblastom a multiform (GBM)	MDDC from GM-CSF (1000 U/ml) & IL-4 (1000 U/ml)	TCL (200 μg/10^6 DCs)	TNF-α (120 ng/ml), IL-1β (120 ng/ml), PGE2 (20 ng/ml)	I.D. (5×10^6 DCs)	pilot study	Ardon et al. 2010.(*123*)
Metastatic renal cell carcinoma (mRCC)	MDDC from GM-CSF (750 U/ml) & IL-4 (500 U/ml)	TCL 100 μg /ml (72h)	TNF-α (500 μg /ml), KLH (100 μg /ml)	I.N. S.C.	Phase I/II)	Marten et al. 2002.(*124*)

MDDC, monocyte-derived dendritic cells; CEA,carcinoembryogenic antigen; PSMA, prostate-specific membrane antigen; KLH, keyhole limpet hemocyanin; TCL, Tumor cell lysate; TNF-α, tumor necrosis factor-α; IL-1β, interleukin-1β; IL-6, interleukin-6; PGE2, prostaglandin E2; F-T, 4-6 cycles of freezing-thawing; Irra, irradiation (60 Gray); FMKp, a bacterial membrane fragment of *Klebsiella pneumonia*; I.V., intravenously; I.N.,intranodal; S.C., subcutaneously;, I.D., intradernally; I.T., intratumorally.

1.2 Damage-associated molecular patterns (DAMPs) and immunogenic cell death (ICD)

It is well-recognized that most anticancer chemotherapeutics influence both tumor cells and the associated immune systems (*125, 126*). The conventional chemotherapeutics possibly induce immunogenic cancer cell death or stimulate immune effectors through so-called off-target effects (*126*). However, the nature of the mechanisms underlying the various cellular activities that induce immune response, and whether specific necrotic or apoptotic cells are immunogenic or tolerogenic, remain unclear (*127, 128*).

A key-lock paradigm has been proposed to explain the relationship between immunogenic cell death and DCs (**Figure 21**) (*128*). Immunogenic cell death is characterized by occurring events of damage-associated molecular patterns (DAMPs) including the translocation of calreticulin (CRT), the release of heat shock proteins (HSPs) including HSP70 and HSP90 on the cell surface, and the release of high-mobility group box 1 (HMGB1) proteins (*127, 129-131*). CRT, HSPs and HMGB1 can function as immunological adjuvants for phagocytosis, cross-presentation of tumor-derived antigens and antigen processing as well as presentation by DCs (**Table 8**) (*129*). As seen in **Figure 22**, the induction of tumor cell death results in recognition of cell death by DCs. Perhaps the apoptotic bodies are engulfed by DCs, and tumor-derived antigens are processed and presented along with DAMPs and costimulatory molecules. After DC maturation, they

move to naive T lymphocytes to interact with them. This process is amplified at different steps. Selection of immunogenic cell death inducers allows enhancement of recognition and phagocytosis of apoptotic debris, maturation of DCs, processing and the presentation of tumor-derived antigens. Most importantly, this leads to the induction of a cytotoxic immune response, involving $CD4^+$ and $CD8^+$ T lymphocytes, leading to complete eradication of tumor cells (*126, 127, 130, 131*). Other factors may also involve in the induction of immunogenic cell death via different pathways to enhance the immune response, as summarized in **Figure 23.** The approach of DC-pulsed with tumor cell lysates (TCLs) is clinically used and has the advantage of providing various sources of tumor-associated antigens to DCs; however, TCLs may inhibit the maturation of DCs (*98*). It is, therefore, of importance to investigate the molecular and cellular behaviors of these immunogenic cell death-associated proteins in TCLs with an eye toward improving the efficacy of TCL-pulsed DC-based vaccines.
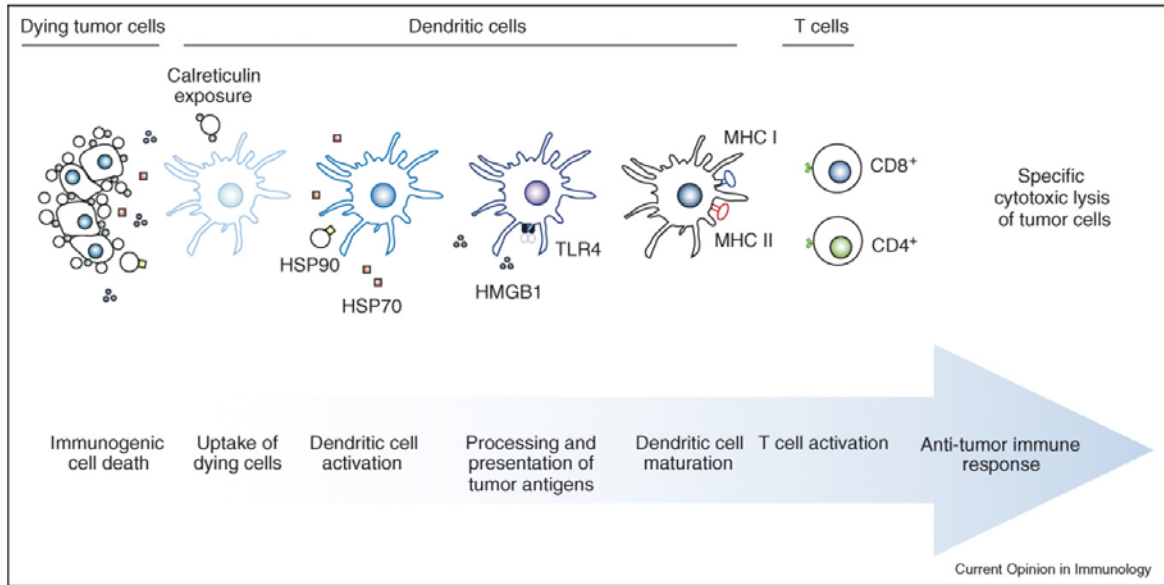
Figure 21. Critical events required to trigger dendritic cell activation by dying tumor cells.

Immunogenic tumor cell death is featured with a temporal sequence of events including translocation of calreticulin (CRT) to the cell surface at the early stage, the release and exposure of heat shock proteins, and the late release of HMGB1, all allowing DC-mediated specific anti tumor immune response. These key components released from or exposed at the surface of dying tumor cells can be said to act at several levels of this immune response: uptake of apoptotic bodies (calreticulin), activation of dendritic cells (heat shock proteins), antigen processing (HMGB1), maturation of dendritic cells, and activation of T lymphocytes. [Adopted from Tesniere et al. (*128*)]

Table 8. Major determinants of immunogenic cancer cell death and their effects on

DCs

Tumor cells	Dendritic cells
Plasma membrane components	
HSP70	Cross presentation of tumor-derived antigens
HSP90	
Calreticulin	Phagocytosis
Phosphatidylserine residues Integrins	Recognition
Proinflammatory mediators	
HSP70 HSP90	DC maturation
HMGB1	Antigen processing and presentation
Uric acid through TLR2 and NALP3 ATP	DC maturation
Late-stage degradation products	
DNA through TLR9 ATP	DC maturation
RNA through TLR3	DC activation
PTX3	Regulation of DC maturation

Adopted from Tesniere et al. (*129*).
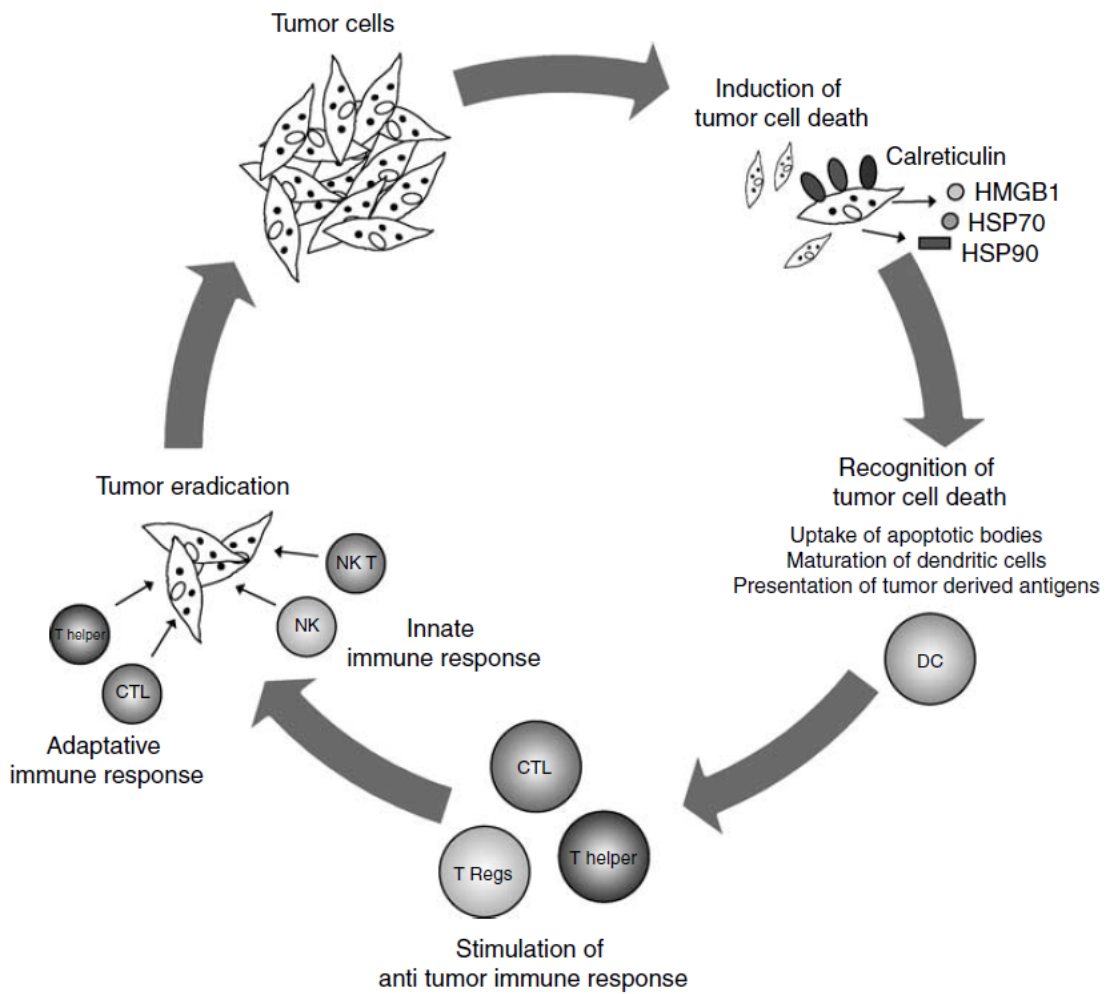
Figure 22. The key steps for the induction of an antitumor immune response triggered by immunogenic cell death. [Adopted from Tesniere et al. (*129*)]
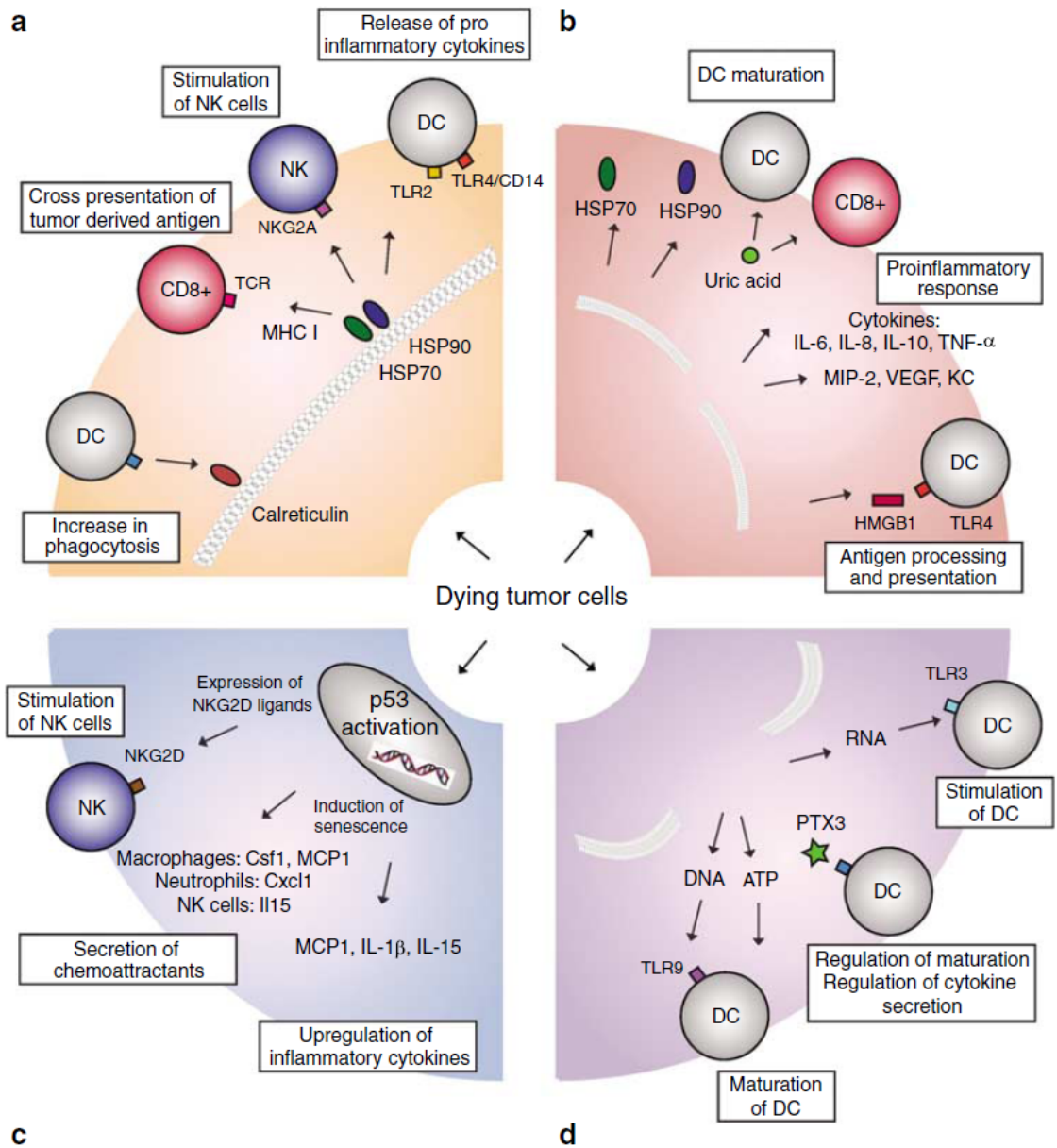
Figure 23. Schematic representation of the main immunogenic determinants of dying tumor cells. [Adopted from Tesniere et al. (*129*))

1.3. The relationship between microtubule-targeting/binding agents (MTAs/MBAs) and immunity

A cornucopia of chemotherapeutic drugs including microtubule-targeting agents can induce cell death (*132*). Recent studies indicate that functional microtubules are required for antigen processing by DCs (*133*) and microtubules mediate NF-κB activation in the TNF-α signaling pathway (*134*). The detailed mechanisms behind this activity are still unclear. Furthermore, in terms of activation of DCs, colchicine was found not only to trigger the maturation of DCs *in vitro* and *in vivo* (*135*), but also promote antigen-cross presentation by murine DCs (*136*). On the other hand, with respect to enhancement of antitumor effect, vincristine increased the antitumor effect of DC-based immunotherapy (*137*), and was also thought to enhance the immunogenicity of chronic lymphocytic leukemia cells (*138*). Taken together, these findings suggest that MDAs may be able to enhance tumor-specific immune response generated by activation of DCs and induce immunogenic cell death. Both, therefore, could conceivably be used in cancer immunotherapy approaches.

Chapter 2. Rationale and Significance

According to the observations and rationale that follow, we hence evaluate the potential MDAs for cancer immunotherapy. First of all, MDAs including 2-phenyl-4 quinolone derivatives such as CMQ, colchicines and vinblastine, and microtubule-polymerizing agents such as paclitaxel have strong anti-tumor activities against various cancers. It is worth investigating whether they possess sufficient strength to induce immunogenic cell death of tumor cells. Secondly, colchicine can trigger the maturation of DCs and promote antigen-cross presentation activity of DCs *in vitro* and *in vivo* (*135, 136*). Vincristine increased the antitumor effect of DC-based immunotherapy (*137, 138*). Thirdly, functional microtubules are essential for antigen processing by DCs (*133, 134*). We therefore hypothesized that MDAs including CMQ can not only activate DCs, but also can induce immunogenic cell death of tumor cells, resulting in a strong tumor-specific immunity.

The metastatic advanced cancer is usually difficult to treat. This cancer also is non-immunogenic and metastatic. B16/F10 cells were derived from the B16/F0 line after 10 successive in vivo passages (*139, 140*). These poorly immunogenic tumor lines only express low MHC class I levels and do not express MHC class II molecules, but both molecules are inducible on IFN-g exposure (*141*). B16/F10 cells are highly aggressive and

metastatic, whereas B16/F0 cells metastasize less and are less aggressive (*139, 142, 143*).

We therefore use B16/F0 cells as a target cancer cell to investigate the effect of MDAs as

adjuvants for cancer immunotherapy.

In this study, we evaluated the effect of colchicine and two 2-pheny-4-quinolone

analogues, which, as MDAs, were shown to confer antitumor effects via inhibition of

tubulin polymerization (*50, 52, 144*) on the activation of DCs and subsequent T-cell

proliferation. We also investigated the effect of these MDAs on mediating immunogenic

cell death in treated B16F10 melanoma cells via induction of DAMP stress proteins.

Possible use of the test MDAs as adjuvants in TCL-pulsed DC vaccines was also evaluated.

Our findings showed that 2-pheny-4-quinolone analogues could induce phenotypic

maturation of DCs. These MDAs were able to augment CD4$^+$ and CD8$^+$ T cell proliferation.

TCLs generated from MDA treatment were further able to improve the efficacy of

TCL-pulsed DC vaccines. Our findings thus provide useful information for potential

clinical application of MDAs in chemotherapy or cancer immunotherapy.

Chapter 3. Results and Discussion

3.1. Results

3.1.1. Effect of various microtubule-depolymerizing agents on growth of B16F10 melanoma cells

Several 2-phenyl-4-quinolone derivatives including CMQ and FMQ have been shown to confer anti-tumor activity via the mitochondria (intrinsic pathway), death receptors (extrinsic pathway), or endoplasmic reticulum (ER) stress (*48, 52, 65*). To evaluate whether CMQ and FMQ and colchicine (chemical structures shown in **Figure 24**) as microtubule-depolymerizing agents can cause cell death leading to immunogenic cell death, we examined their effect along with the effect of doxorubicin as positive control on cell proliferation of B16F10-F10 melanoma cells. Twenty-four hours post-treatment, colchicine effectively inhibited approximately 50% of test cell growth at concentrations greater than 0.05 μM. CMQ and FMQ exerted similar inhibitory patterns in a concentration-dependent manner at concentrations from 0.1 to 2.5 μM, and inhibition reached a plateau at approximately 2.5 μM (**Figure 25**). Doxorubicin inhibited tumor cell growth at all concentrations tested in this study. Our findings suggest that CMQ and FMQ conferred a similar cytotoxic effect on B16F10 tumor cells growth to doxorubicin. Colchicine apparently exerts different cytotoxic patterns on growth of B16F10 melanoma cells.

(A)
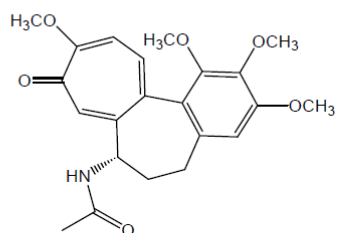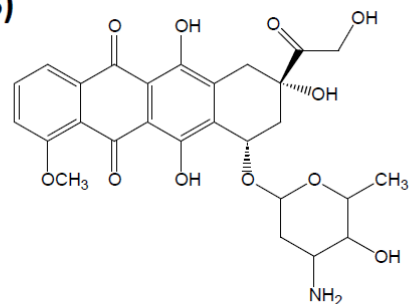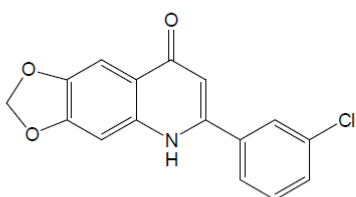
(B)

Colchicine (C)

Doxorubicin (DX)

(C)

(D)

2-(3-chlorophenyl)-6,7-
methylenedioxyquinolin-4-one
(CMQ)
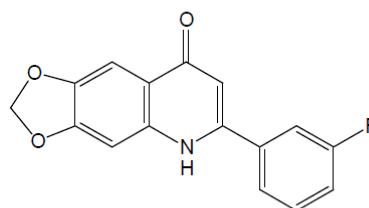
2-(3-fluorophenyl)-6,7-
methylenedioxyquinolin-4-one
(FMQ)

Figure 24. Chemical structures of microtubule-depolymerizing agents and doxorubicin tested in this study
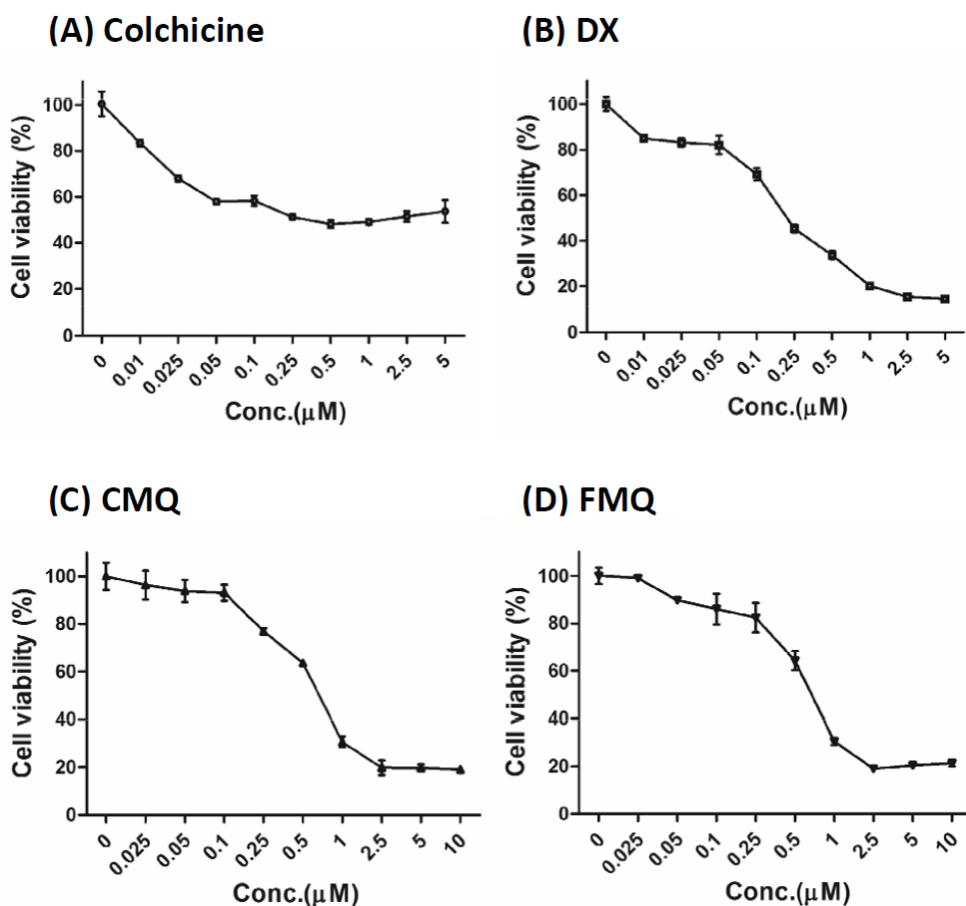
Figure 25. Effect of MDAs and doxorubicin on cell viability of B16F10 melanoma cells

Mouse B16F10 melanoma cells were treated with the indicated concentrations of colchicine, doxorubicin (DX), 2-(3-chlorophenyl)-6,7-methylenedioxyquinolin-4-one (CMQ) and 2-(3-fluorophenyl)-6,7-methylenedioxyquinolin-4-one (FMQ) for 24 h, as shown in A B C and D, respectively. The values are represented as the percentage of viable cells; the vehicle control group was regarded as 100% viable. Cell viability was determined by MTT assay and data were expressed as mean ± S.D. for triplicate culture samples.

3.1.2. Effect of specific microtubule-depolymerizing agents on expression of immunogenic cell death-related proteins and tumor-associated antigens

Recent studies have revealed that increased expression of DAMPs, a characteristic of immunogenic cell death, can boost immunogenicity in cancer vaccines via ER stress or other signaling pathways (*72, 145, 146*). Whether microtubule-depolymerizing agents can induce DAMPs has not, to our knowledge, been previously reported. Therefore, we measured the expression of several DAMPs (HSP70, HSP90, CRT and HMGB1) in TCLs from B16F10 cells after treatment with 2.5 μM colchicine, CMQ, FMQ or doxorubicin. The MDAs colchicine, CMQ and FMQ induced the expression of HSP70, HSP90 and HMGB1 in tumor cells as compared with cells treated with vehicle control, but did not affect the expression of CRT (**Figure 26A**). Doxorubicin induced higher levels of expression of the same DAMPs than the MDAs tested. Specific tumor-associated antigens including glypican-3 and survivin are markers for melanoma and many cancer cell types (*147*). The levels of glypican-3 and survivin in cell lysate were elevated after test tumor cells were treated with colchicine, CMQ, FMQ or doxorubicin (**Figure 26B**). These results suggest that the three MDAs increase the expression of DAMPs as well as the expression of tumor-associated antigens such as survivin and glypican-3, but the expression patterns of these presteins may differ among the MDAs and doxorubicin.

(A)

	Ctrl	C	CMQ	FMQ	DX
HSP70	1	1.91	1.93	2.12	4.17
HSP90	1	2.24	2.28	2.28	2.76
CRT	1	0.91	1.0	0.89	1.33
HMGB1	1	1.54	2.69	1.96	2.06
β - actin	1	1.05	1.18	1.04	1.32

(B)

	Ctrl	C	CMQ	FMQ	DX
Glypican-3	1	1.70	2.49	2.28	6.12
Survivin	1	1.23	1.66	2.40	2.27
β - actin	1	1.05	1.18	1.04	1.32
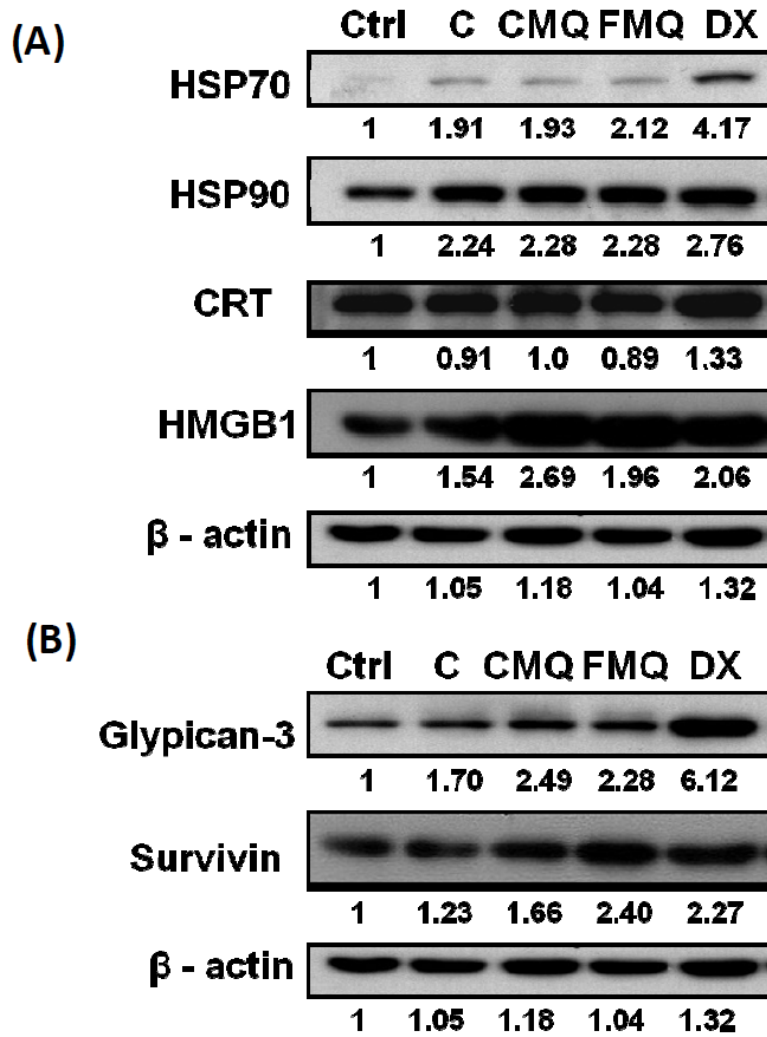
Figure 26. Expression of damage-associated molecular patterns (DAMPs) and tumor-associated antigens in tumor cell lysates of B16F10 melanoma treated with different MDAs

B16F10 tumor cells were treated for 24 h with vehicle control, colchicine (C), CMQ, FMQ or DX, at a concentration of 2.5 μM. After treatment, TCLs were obtained through four freeze-thaw cycles. Western blot analysis for protein expression of damage-associated molecular patterns (DAMPs), heat shock protein 70 (HSP70), heat shock protein 90

(HSP90), calreticulin (CRT) and high-mobility group box-1 (HMGB1), is shown in **(A)**,

and expression of tumor-associated antigens including glypican-3 and survivin, is shown in

(B). Expression of β-actin was used as an internal control. The results show one

representative experiment of three independently performed experiments.

3.1.3. Microtubule-depolymerizing agents can enhance the efficacy of therapeutic immunity provided by tumor cell lysate-pulsed dendritic cell vaccines

The results described above suggest that MDA-conditioned TCLs may induce an immunogenic response *in vivo* and thus augment the efficacy of specific dendritic cell-based vaccines. A mouse model challenged subcutaneously with B16F10 cells and immunized with test DC vaccines intratumorally was used to explore this possibility (**Figure 27A**). Mice receiving PBS only, unpulsed mature DCs, or TCL-DMSO-pulsed DCs showed no significant cytotoxic T lymphocyte (CTL) activity against B16F10 melanoma (**Figure 27B**). However, mice vaccinated with TCL-C-pulsed DCs (DCs pulsed with colchicine-treated tumor cell lysats) ($P = 0.013$ versus TCL-DMSO group) and TCL-CMQ-pulsed DCs ($P = 0.015$ versus TCL-DMSO group) were found to have significantly enhanced CTL activity; the ratio of effector cells to target cells (E:T) increased from 20:1 to 80:1. These CTL activities were comparable with those of the positive control, TCL-DX-pulsed DC vaccine ($P = 0.018$ versus TCL-DMSO group).

With respect to tumor growth, time-course experiments revealed that tumor growth was significantly inhibited in the TCL-DMSO ($P = 0.02$ versus vehicle group) in comparison with the unpulsed DC ($P = 0.02$ versus vehicle group) and vehicle group on day 24 post tumor inoculation (**Figure 27C**). However, treatment with TCL-C ($P = 0.011$

96

versus TCL-DMSO group) and TCL-CMQ ($P = 0.020$ versus TCL-DMSO group) showed

significant tumor suppression, which was comparable to that of the positive control,

TCL-DX ($P = 0.012$ versus TCL-DMSO group). Furthermore, the survival time and

survival rate of test mice in the TCL-C, TCL-CMQ and TCL-DX vaccinated groups (all

with $P < 0.001$) were significantly improved in comparison with those of the TCL-DMSO

group (**Figure 27D**). This trend was in accordance with that for the suppression of tumor

growth (**Figure 27C**). Results for mice vaccinated with TCL-FMQ-pulsed DCs were

similar to those vaccinated with TCL-CMQ pulsed DCs (data not shown). These results

suggest that the efficacy of DC-based vaccines pulsed with TCLs can be effectively

elevated by treating test tumor cells with the MDAs, colchicine, CMQ and FMQ.

(A)

B16 cell
s.c. injection   First   Second   CTL activity
          Priming   boosting   boosting   assay

Day O   Day 7   Day 10   Day 13   Day 23

(B)

(C)

(D)
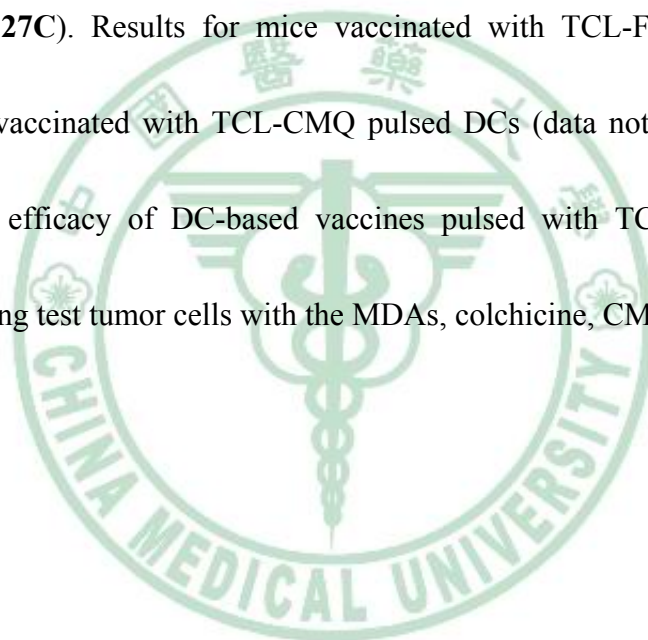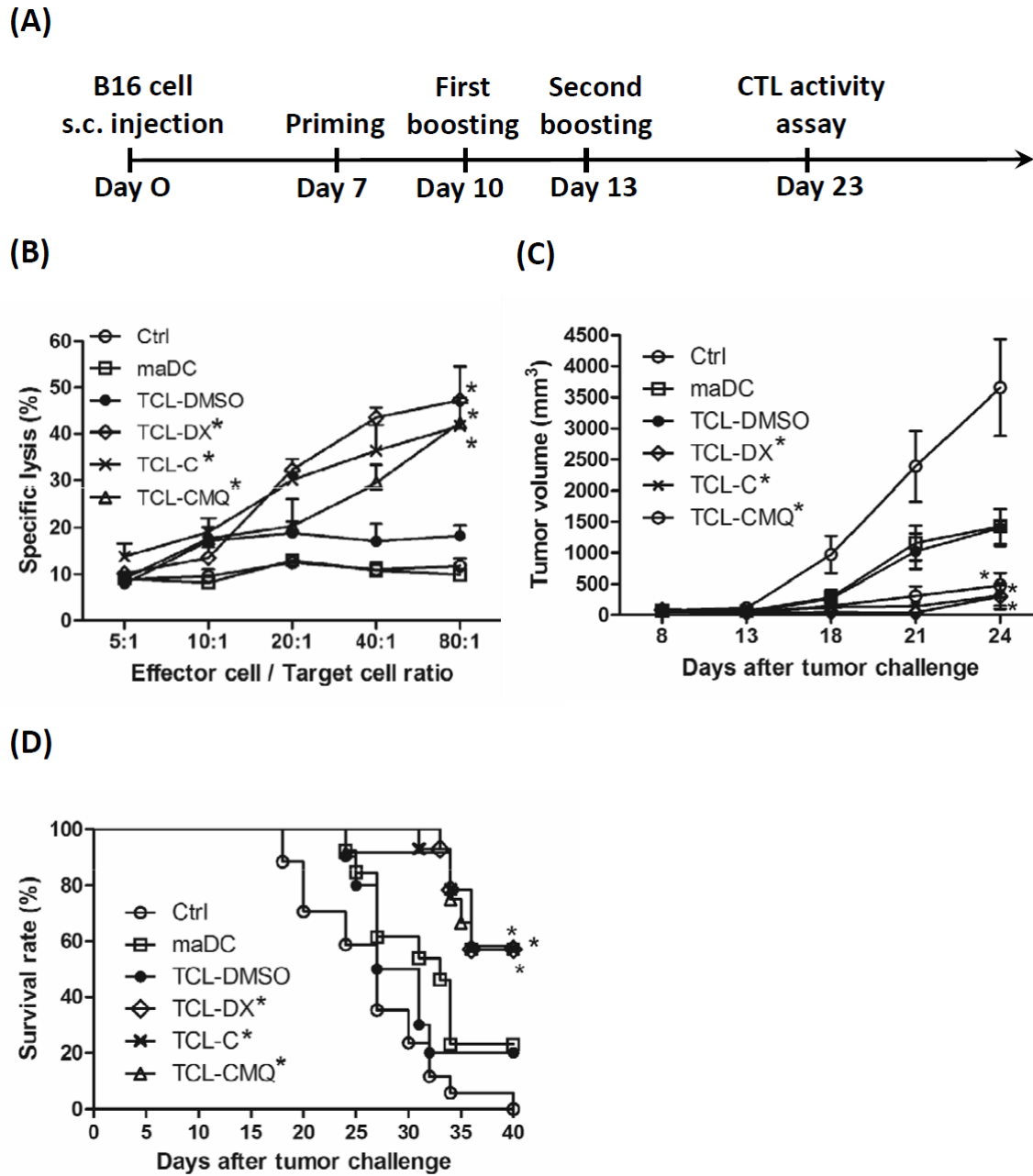
Figure 27. Therapeutic immunity of DC vaccines pulsed with various tumor cell lysates, against B16F10 melanoma

(A) Schematic representation for vaccination. C57BL/6 mice were challenged subcutaneously with 1×10^5 B16F10 cells and vaccinated with different preparations of

98

TCL-pulsed DCs when the tumor volume reached to 50-80 mm^3. On day 10 after the secondary boosting, splenocytes were harvested for cytotoxic T lymphocyte activity (CTL) assay. **(B)** CTL activities in test mice. Splenocytes from vaccinated or control group mice (*n* =8 mice per group) were collected and CTL activity assayed with target tumor cells. Test DCs were pulsed with TCL-DMSO, TLC-DX, TLC-C, or TCL-CMQ. PBS-treated mice (Ctrl) did not receive DC vaccine, only a PBS injection. Test mice in the mature DC group (maDC) were subjected to vaccination with unpulsed mature DCs. **(C)** Tumor growth of treated mice. Tumor size of each group (*n* =8 mice per group) was measured on indicated days. **(D)** Survival rates of treated mice. Survival of mice (*n* = 12 mice per group) was observed after tumor challenge. For all experiments, the TCL-FMQ groups showed a similar pattern of activities as that of TCL-CMQ and hence the data are not shown. All data are expressed as mean ± S.E.M.
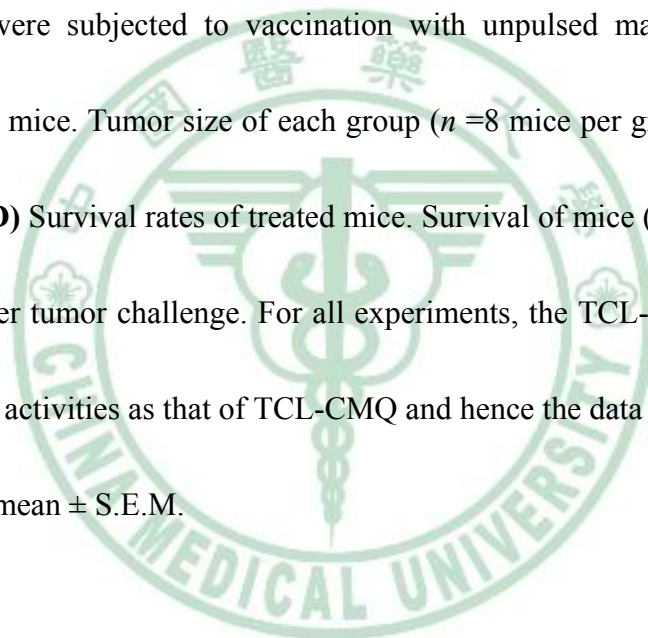
3.1.4. Specific immune cell subsets involved in vaccine efficacy

In order to investigate which immune cell subsets participate in therapeutic immunity of test DC vaccines, mice were injected intraperitoneally with either anti-CD4, -CD8, or -NK1.1 monoclonal antibodies (mAb) to deplete the respective cell types. The vaccinated mice treated with rat-IgG ($P = 0.028$, versus control group) or anti-CD4 mAb ($P = 0.049$, versus control group) showed significantly increased survival rates and times as compared with the control group (**Figure 28**). However, the survival rate of the vaccinated mice injected with anti-CD4 mAb was 40% lower than the rat-IgG group. On the other hand, vaccinated mice treated with anti-CD8 or anti-NK1.1 mAb did not exhibit a statistical change in survival rate and time as compared with control group ($P > 0.05$, versus control group). Depletion of $CD8^+$ T cells and NK cells thus virtually completely blocked the protective activity of DC vaccines pulsed with CMQ-treated TCLs. These results indicate that tumor-specific $CD8^+$ T cells and NK cells play a crucial role in the observed therapeutic immunity induced by DC vaccines pulsed with CMQ-treated TCLs against B16F10 melanoma, whereas $CD4^+$ T cells are only partially involved in the antitumor activity.
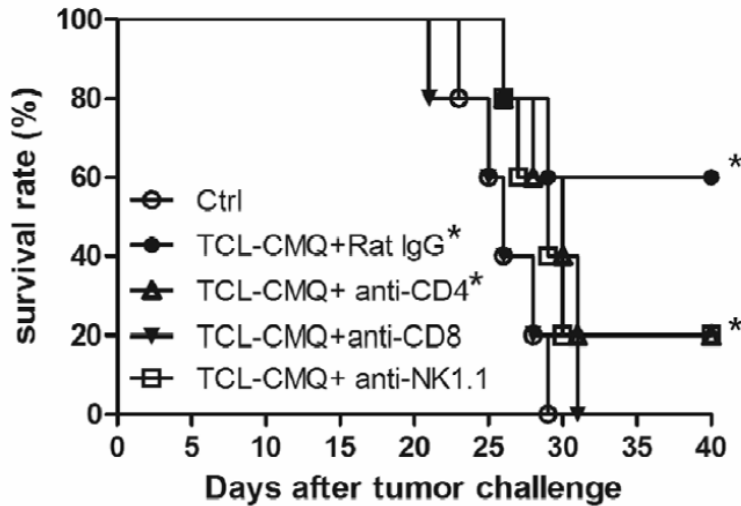
Figure 28. Determination of immune cell subsets responsible for protective immunity induced by test DC vaccines

Preparations of anti-CD4 (GK1.5), anti-CD8 (53–6.7), and anti-NK1.1 (PK136) antibodies were administered by intraperitoneal injection on day 1 in test mice prior to vaccination on days 2, 5 and 8 after tumor challenge as described in Materials and Methods. C57BL/6 mice (n = 5) were immunized intratumorally with test DC vaccines on days 7, 10 and 13 after tumor challenge as described in Materials and Methods and inoculated with B16F10 melanoma cells (10^5 cells/50 μl/mouse) on day 0. Statistical difference was calculated by log-rank (Mantel-Cox) test for mouse survival and P values of less than 0.05 were considered significant as compared with control group (*$P < 0.05$).

3.1.5. Effect of DC culture conditions on vaccine efficacy

Since IL-12p70 is essential to the effective priming of a T_H1 anti-tumor immune response and CTL activities (*148, 149*), and IL-10 has been shown to inhibit the production of IL-12p70 in murine DCs (*150, 151*), we next evaluated the expression and balance of IL-12p70 and IL-10 activities in various TCL-pulsed DC vaccines. To address the possible effect of CMQ on test DCs, we determined the release of IL-12p70 and IL-10 expressed by murine DCs pulsed with or without CMQ-treated TCLs. Experiments were carried out simultaneously by co-treatment or co-incubation for 12 hours and stimulation with or without LPS in the absence of GM-CSF and IL-4 (**Figure 29A**). A higher production of IL-12p70 and a lower production of IL-10 were detected in DCs with LPS stimulation only (maDCs) compared to the pulsed DCs co-cultured with TCL-CMQ and LPS (CTCL-CMQ) or with TCL-CMQ first and stimulated with LPS later (TCL-CMQ) (**Figure 29A**). DCs treated with TCL-CMQ showed increased production of IL-12p70 compared with imDCs and the CTCL-CMQ group, similar to the maDCs group, whereas the production of IL-10 was significantly increased in this group in comparison with other groups. The maDCs were more effective than TCL-CMQ and CTCL-CMQ in increasing production of IL-12, whereas TCL-CMQ was more effective than CTCL-CMQ and maDCs in increasing production of IL-10. Overall, these results suggest that it may be possible to improve IL-12 production and decrease IL-10 production to enhance anti-tumor activity of TCL-CMQ.

Treatment with IL-4 accompanied by GM-CSF can promote IL-12p70 expression and inhibit IL-10 expression in murine or human DCs (*127, 152, 153*). We, therefore, hypothesized that adding GM-CSF and IL-4 to test culture during the pulsing and stimulation period may improve the balance in production of IL-12p70 and IL-10. Accordingly, we cultured DCs without either GM-CSF or IL-4, with GM-CSF only, or with GM-CSF and IL-4 to measure the production of IL-12p70 and IL-10 in test cells treated as above (**Figure 29A)**. Supplement of GM-CSF and IL-4 conferred the highest level of expression of IL-12p70 and lowest level of expression of IL-10 (**Figure 29C**) as compared with the other culture conditions (**Figure 29A** and **29B**). The increase in IL-12p70 and decrease in IL-10 expression levels suggested that TCL-CMQ and CTCL-CMQ treatments could be greatly improved by supplementation with GM-CSF only or by addition of both GM-CSF and IL-4 concomitantly. TCL-CMQ conferred the highest levels of IL-12p70 production and lowest levels of IL-10 in comparison with other test groups. These results suggest that TCL-CMQ treatment combined with culturing in GM-CSF and IL-4 may augment the efficacy of DC-based vaccines pulsed with TCLs.
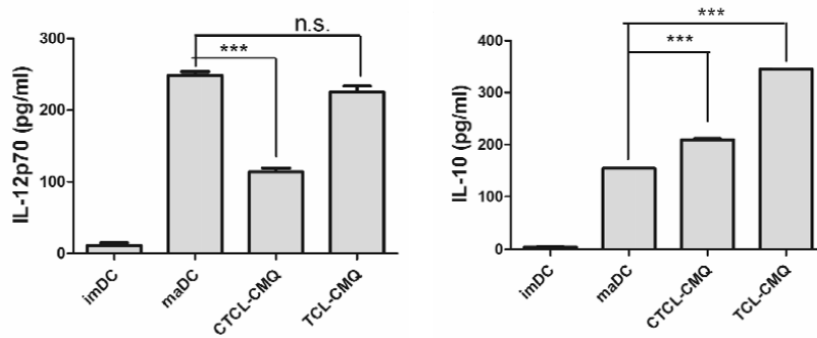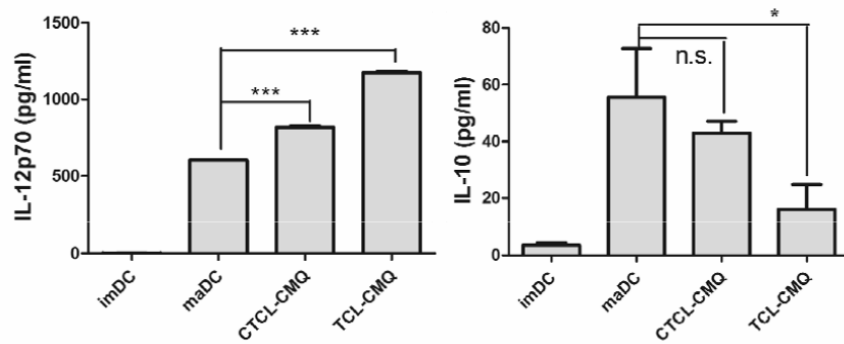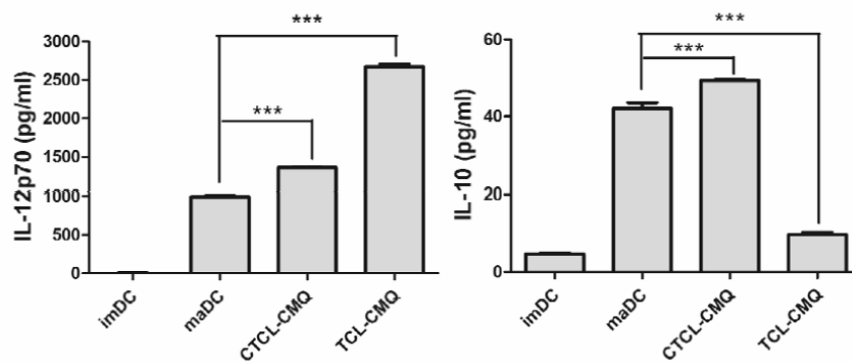
Figure 29. Effect of GM-CSF and IL-4 on IL-12p70 expression in DCs treated with tumor cell lysates

(A-C) IL-12p70 and IL-10 expression in DCs pulsed with CMQ-treated TCLs under

different culture conditions. After harvesting, DCs were incubated in three kinds of culture conditions with or without GM-CSF (20 ng/ml) plus IL-4 (20 ng/ml), and were treated as follows: vehicle (imDC), LPS (maDC), TCL plus LPS for 24 h (CTCL-CMQ) or TCL for 12 h and then LPS for 24 h (TCL-CMQ) as described in Materials and Methods. The level of IL-12p70 released into supernatants of test DC cultures was assayed by ELISA. Statistical difference among test groups was analyzed by Student's t-test. P values less than 0.05 were considered statistically significant (*$P < 0.05$; **$P < 0.01$; ***$P < 0.001$ versus the maDC group).

3.1.6. Effect of different administration routes on therapeutic immunity of DC-based vaccines pulsed with tumor cell lysates

IL-12p70 has been shown to be beneficial when used as an adjuvant with DC-based vaccines, either via systemic or local delivery, especially when administered via intratumoral injection (*150, 154, 155*). It is clinically important to establish optimal methods of administration for effective delivery of TCL-pulsed DC-based vaccines. To evaluate of efficiency of vaccine delivery, test vaccines were injected intratumorally, intranodally, intravenously and subcutaneously into the left flanks of mice. Mice receiving intratumoral injection of TCL-CMQ DC vaccines ($P < 0.01$, versus control group) showed a stronger therapeutic immunity than all the other delivering systems tested (all $P < 0.05$, versus control group) with respect to tumor suppression (**Figure 30A**). Animal survival rate and time, as analyzed by log-rank (Mantel-Cox) test (**Figure 30B**), were also drastically increased by vaccination via intratumoral injection ($P = 0.0011$, versus control group) as compared to vaccination via intranodal injection ($P = 0.0319$ versus control group), intravenous injection ($P = 0.0318$, versus control group) or subcutaneous injection ($P = 0.0355$ versus control group). Nonetheless, it is important to note that the intranodal, intravenous and subcutaneous modes of vaccine delivery also had a significant effect on survival rate and time of test mice in comparison with non-vaccinated (control) mice. These results suggest that the DC-based vaccine pulsed with TCLs delivered by

intratumoral injection may be an efficient experimental mode for laboratory animal and

perhaps human clinical studies.
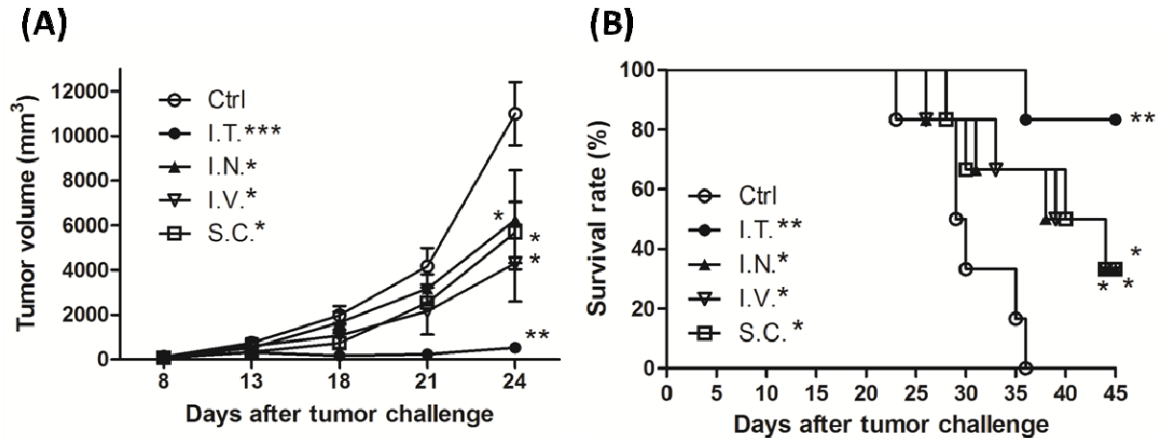
Figure 30. Effect of different administrative routes on DC-based vaccines pulsed with specific tumor cell lysates

C57BL/6 mice (*n* = 6) were immunized by intratumoral (I.T.), intranodal, (I.N.) or subcutaneous (S.C.) injection with DC-based vaccines pulsed with CMQ-treated TCLs on days 7, 10 and 13 after tumor challenge. One week post vaccination, right flanks of mice were subcutaneously inoculated with B16F10 melanoma cells (10^5 cells/50 μl/mouse). During the following 45 days post tumor challenge, tumor volume (**A**) and survival time (**B**) of mice was observed and measured. Analysis of statistical differences among test groups is described in Materials and Methods. P values of less than 0.05 were considered statistically significant (*$P < 0.05$; **$P < 0.01$; ***$P < 0.001$).

3.1.7. Microtubule-depolymerizing agents enhance maturation of dendritic cells and CD4^{+} T and CD8^{+} T cell proliferation

Previous studies reported that some microtubule-targeting agents including colchicine (*135, 136*), vincristine (*156*) and paclitaxel (*157, 158*) induced maturation of DCs and further augmented CD4^{+} T and CD8^{+} T cell activities or antigen cross-presentation activity. However, although 2-phenyl-4-qunilone derivatives have previously been shown to confer strong anti-tumor activity (*45, 48, 49*), whether these CMQ and FMQ phytocompound-derived chemicals could induce maturation of DCs and subsequently enhance CD4^{+} T and CD8^{+} T cell activities has not been reported. As a follow up, we treated DCs with various concentrations of CMQ (0.1, 0.5 and 1 μM), colchicine (2.5 μM) and LPS (1 μg/ml). As shown in **Figure 31A**, expression of DC maturation surface markers such as CD40, CD80, CD86 and MHC-II were greatly increased after treatment with CMQ as compared with those of control group cells. Levels of induction of DC maturation surface markers after treatment with CMQ were comparable to those observed for colchcine, but were less than those observed after LPS treatment. Co-cultivation of CD4^{+} T or CD8^{+} T with DCs showed that CMQ could significantly augment CD4^{+} T and CD8^{+} T cell proliferation (**Figure 31B**). Treatment with FMQ showed similar effects (data not shown). Our findings thus suggest that CMQ and FMQ can induce maturation of DCs and in turn enhance CD4^{+} T and CD8^{+} T cell proliferation.
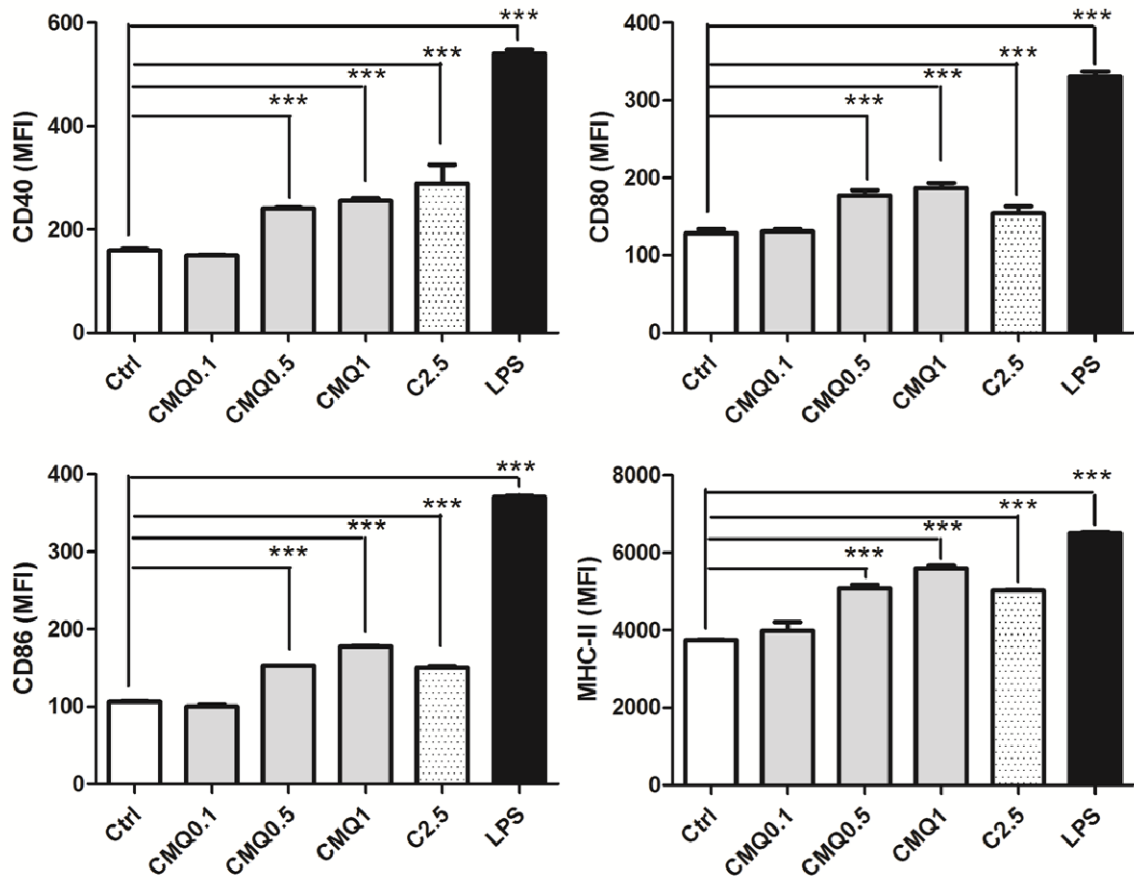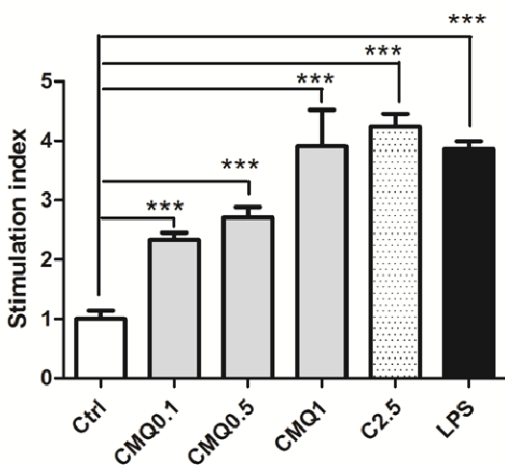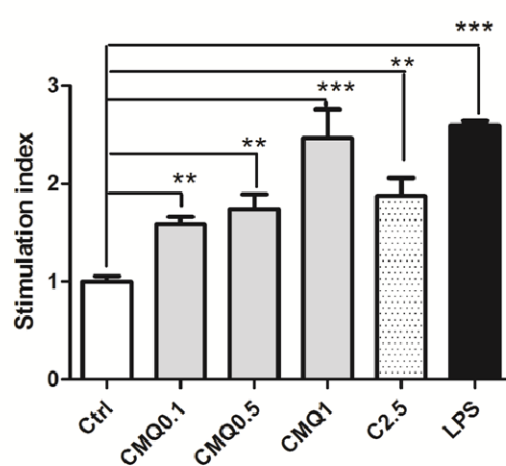
Figure 31. Effect of treatment with different MDAs on expression of cell-surface

markers in mouse bone marrow-derived dendritic cells and CD4⁺ and CD8⁺ T-cell

proliferation

(A) Expression of surface markers on DCs. Cells were treated for 24 h with CMQ (0.1, 0.5 and 1 μM), colchicine (2.5 μM) and LPS (1 μg/ml), and harvested. Examination for the expression of CD40, CD80, CD86, MHC class II and CD11c markers was performed by flow-cytometry. The levels of CD40, CD80, CD86, MHC class II were expressed as mean fluorescence intensity (MFI). **(B)** CD4$^+$ and CD8$^+$ T-cell proliferation. After indicated treatments, treated DCs were co-cultured with CD4$^+$ T cells or CD8$^+$ T cells in a ratio of 1:20 (DCs versus CD4$^+$ T cells or CD8$^+$ T cells) for 72 h. T-cell proliferation was determined in vitro using a BrdU proliferation ELISA kit (Roche, Heidelberg, Germany) according to the manufacturer's instructions. The T-cell proliferation was expressed as the stimulation index, the OD$_{450}$ value of co-culture of treated-DCs and T cells was divided by the value of co-culture of DMSO-treated-DCs co-cultured with T cells. All data were expressed as mean ± S.D. P values less than 0.05 were considered statistically significant (*$P < 0.05$; **$P < 0.01$; ***$P < 0.001$).

3.2. Discussion

The first therapeutic cancer vaccine, Sipuleucel-T (Provenge®), which uses antigen-presenting cell (APC) technology involving dendritic cells (DCs) for cancer immunotherapy, was approved by the FDA in 2010 (*159*). This success highlights the potential of *ex-vivo*-treated DCs as therapeutic vectors for various cell-based cancer vaccines. Immunization of cancer patients using their own DCs that have been loaded with tumor associated antigens (TAAs) and/or immune-modifiers *ex vivo* is becoming an increasingly popular strategy in the development of cancer vaccines (*90, 160*). Microtubule-depolymerizing agents (MDAs) such as colchicine and vincristine, which are used clinically in cancer chemotherapy, have recently been shown to enhance specific immune functions of DCs (*135, 136, 156*). Whether or not MDAs such as these can be employed for use in DC-based cancer vaccines has, to the best of our knowledge, not previously been reported. To address this possibility, our current study explored the effect of three MDAs – the well-known drug, colchicine, and two 2-phenyl-4-qunilone derivatives (CMQ and FMQ) – on immunogenic tumor cell death when used as "adjuvants" of TCL-pulsed DC vaccines in a therapeutic mouse model. MDAs were able to effectively induce the expression of immunogenic cell death-related proteins in targeted tumor cells, and augment the efficacy of TCL-pulsed DC-based vaccines.

Previous studies have shown that colchicine can elicit $CD4^+$ and $CD8^+$ T cell

responses, induce antibody response, and promote antigen cross-presentation by murine dendritic cells (*135, 136, 161, 162*). In this study, we show that colchicine also induces the expression of DAMPs and tumor-associated antigens (TAAs) in dying B16F10 melanoma cells (**Figure 26A-B**). In addition, DC-based vaccines pulsed with colchicine-treated TCLs were able to enhance therapeutic immunity (**Figure 27B-D**). We also tested two 2-phenyl-4-quinolone derivatives, in parallel with colchicine, and doxorubicin (as a positive control), for their effect on this cancer vaccine approach. CMQ and FMQ showed effects comparable to colchicine; however, the detailed mechanism(s) of action of these MDAs remain unclear. Optimization of dosage and improvement in formulation of this MDA-TCL combination will be important for future use in DC-vaccines.

It has been put forth that DCs pulsed with TAA preparations derived from freeze-thaw cycle treatment of autologous TCLs are a promising approach to cancer immunotherapy as a wide repertoire of different TAAs are present in the lysate (*149, 163-165*). Based on knowledge of antigen-processing and cell trafficking of DC activities *in vivo*, it is generally believed to be important to optimize the *in vitro/ex vitro* culture conditions to generate efficacious vaccines for cancer immunotherapy. In cytokine-regulated anti-tumor immunity, IL-12p70 is recognized as a key cytokine in the promotion T_H1 immune response (*155*). IL-10 inhibits the releases of IL-12p70, and is often considered unfavorable for promoting anti-tumor immunity. We showed here (**Figure 29A-C**) that a supplement of GM-CSF only

or GM-CSF plus IL-4 into the culture medium of a DC-based vaccine can drastically alter the balance of IL-12p70 versus IL-10 levels in TCL-pulsed, LPS-activated DCs. Hatfield and his colleagues reported that DCs pretreated with TCLs and then activated by LPS treatment expressed a substantially reduced level of IL-12p70 and a substantially increased level of IL-10 (*99*). Interestingly, here we show that supplement of the cytokines GM-CSF and IL-4 to the culture medium throughout the entire TCL-pulse/LPS-activation incubation period can drastically reverse such IL-12p70/IL-10 expression ratio (**Figure 29A-C**). We therefore believe that this protocol could increase the potency of DC vaccines for use in anti-tumor vaccination (*99*).

Studies on DC-vaccines against cancers have used a number of different modes of administration for delivery (**Table 7**). Unfortunately, little comparative analysis of those delivery systems is available. For future potential clinical application, we consider it important to investigate which delivery system(s) is practical and desirable for such vaccines. Intratumoral injection of test vaccines elicited the best therapeutic effects among all tested administrative routes (**Figure 30A -B**) in this study. In cancer patients, DCs often present in an immature or dysfunctional state, especially tumor-infiltrating DCs, thereby preventing stimulation of tumor-specific T cells (*90*). Our findings suggest that, for large size tumors, intratumoral injection of DC vaccines, may be the most efficacious delivery mode. However, intratumoral injection has several disadvantages including lack of

promotion of systemic circulation, and inconvenience of delivery into tumor sites in some clinical tumors. Therefore combinations of different administration modes still need to be considered to achieve maximum efficacy.

Previously, we developed particle bombardment/gene gun technology, by which 0.1 to 1 million 1-3 M gold particles (biologically inert) can penetrate epidermal or dermal tissues (*166*). We also reported that such ballistic bombardment can systematically generate evenly distributed, microscopic tissue tracks, creating mild, defined tissue- and microvascular wounding in target skin areas (*167, 168*). We propose that anti-cancer vaccines may be optimized by making use of the particle bombardment technology as a systematic, highly effective and multiple site-delivery mode for the pretreatment of tumor-bearing mice areas (especially for the high number, metastasized, microscopic melanoma nodules), before administration of DC-based vaccines. In possible future applications, melanoma patients might be administered TCL-DC anti-cancer vaccines using a combination of gene gun and intratumoral injection of TCL-DCs by simultaneous administration or sequential administration of these two cancer vaccines.

Apoptotic cell death was previously recognized mainly as being tolerogenic, whereas necrosis was considered immunogenic. Recently, it was found that apoptotic cell death also induces immunogenic cell death via expression of DAMPs (*72, 169-172*). A number of studies have also shown that DCs pulsed with apoptotic tumor cells can induce immunity

against tumors (*169, 170*). Whether human DCs pulsed with MDA-treated tumor cells could elicit a strong immunity against human cancers needs to be investigated in future clinical studies. In this study, we for the first time found that the expression of DAMPs increased in the tumor cell lysates of B16F10 cells prepared by a necrotic way with freeze-thaw cycles after treatment with MDAs.

Regardless of which pathways are targeted by DC-based vaccines to treat tumor cells, apoptotic or necrotic, it is generally agreed that treatment needs to result in immunogenic cell death, especially in expression of DAMPs (*72, 145, 146, 173*). Currently, physical methods including irradiation (*174*), heat stress (*99*) and UV (*175*) are used to enhance expression of DAMPs, hence generating strong tumor-specific immunity. Chemotherapeutic agents including doxorubicin, mitoxanthrone, oxaliplatin have been shown to confer these activities (*176-178*). Here, we show that MDAs can also induce immunogenic cell death and confer immunity against test tumors. We speculate that a combination of physical and chemical methods may help upgrade efficacy of either the TCL- or apoptotic tumor cell-pulsed DC vaccines. Future research is required to address these possibilities.

Recent studies have suggested that microtubules play a role in antigen-presenting presentation of dendritic cells (*74, 161*). An increasing body of evidence has also shown that microtubule-targeted agents including vincristine, colchicine and palitaxel can

promote DC-mediated immune responses or enhance efficacy of combined chemotherapy (*135, 136, 156, 157, 179*). The binding site of 2-pheny-4-quinolone derivatives on microtubule proteins was reported to be likely the same as the binding site of colchicine (*45*). Our current findings revealed that 2-phenyl-4-quniolone derivatives can enhance the maturation of DC and mediate promotion of CD4^{+} and CD8^{+} T cell proliferation (**Figure 31A-B**). The specific microtubule-depolymerizing agents we studied here may thus have potential for use as adjuvants for DC-mediated vaccines for infectious diseases or melanoma cancers.
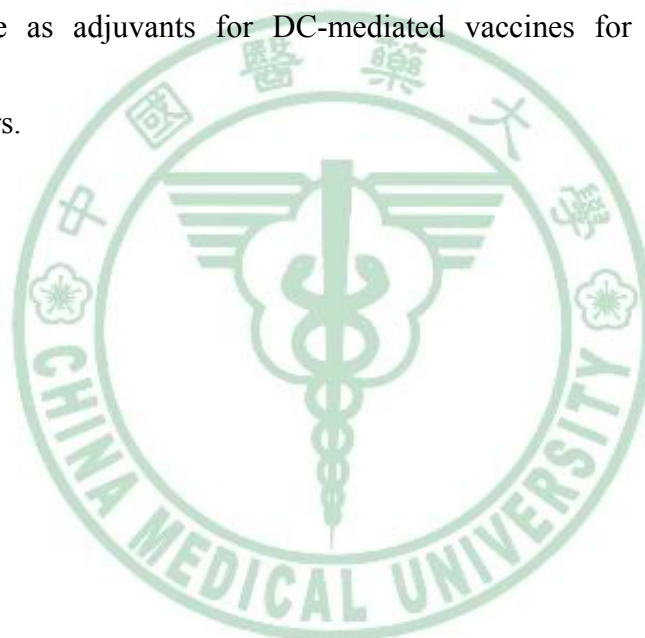
Chapter 4. Conclusion

Three specific microtubule-depolymerizing agents – colchicine, 2-(3-chlorophenyl)-6,7-methylenedioxyquinolin-4-one (CMQ) and 2-(3-fluorophenyl)-6,7-methylenedioxyquinolin-4-one (FMQ) – were found to effectively induce expression of DAMPs proteins and augment the therapeutic efficacy of DC-based vaccines pulsed with TCLs. In test B16F10 melanoma mouse systems, CD8$^+$ T cells and NK cells were found to be involved in the observed therapeutic immunity. Further, supplementing culture media with GM-CSF and IL-4 culture prior to and during pulsing of MDA-treated DCs may enhance the efficacy of vaccines. CMQ and FMQ also induced maturation of DCs and increased CD4$^+$ T and CD8$^+$ T cell proliferation. Our findings show conclusively that colchicines, CMQ and FMQ offer bifunctional anti-tumor protection in a B16F10 melanoma model in rodents: First, these chemicals upregulate tumor DAMP, and cause immunogenic cell death of tumors; second these MDAs strongly augment tumor antigen presenting function of mature DCs, which in turn orchestrate CD4- and CD8-mediated tumor destruction. The synergy of immunogenic cell death at level of tumor cells, coupled with their subsequent adjuvant effect for tumor antigen presentation at level of DCs lend a significant implication for cancer vaccine development. Thus our findings strongly suggest that specific microtubule-depolymerizing agents, especially colchicine,

may be suitable for clinical applications as adjuvants in TCL-pulsed DC vaccines. In the

future, clinical studies on patients with advanced melanoma should be considered.

Chapter 5. Materials and Methods

5.1. Chemicals and reagents

2-(3-chlorophenyl)-6,7-methylenedioxyquinolin-4-one (CMQ) and 2-(3-fluorophenyl)-6,7-methylenedioxyquinolin-4-one (FMQ) were synthesized as previously described (*45*). Each compound was dissolved in dimethyl sulfoxide (DMSO) to obtain a stock solution, and a final concentration of 0.1% DMSO was used in the cell assays. RPMI 1640 medium, DMEM, fetal bovine serum (FBS), penicillin, streptomycin, and all other tissue culture reagents were obtained from GIBCO/BRL Life Technologies (Grand Island, NY) unless otherwise indicated. Colchicine, DMSO, thiazolyl blue tetrazolium bromide (MTT), and other chemical agents were purchased from Sigma (St Louis, MO). Antibodies to β-actin (sc-1616-R) and HRP-labeled anti-mouse (sc-2031) and anti-rabbit (sc-2357) IgGs were obtained from Santa Cruz Biotechnology Inc. (Santa Cruz, CA). Antibodies to HSP70 (#4876), HMGB1 (#6893) and survivin (#2808) were purchased from Cell Signaling Technologies (Boston, MA). Antibodies to calreticulin (ab2907) and glypican-3 (ab66596) were purchased from Abcam (Cambridgeshire, UK), and antibodies to HSP90 (AB3466) were purchased from Millipore (Billerica, MA).

5.2. Mice

Male C57BL/6JNarl mice (6–8-weeks old) were purchased from the National Laboratory Animal Breeding and Research Center, Taipei, Taiwan. All mice were

maintained in a laminar airflow cabinet in a room kept at $24 \pm 2°C$ and 40–70% humidity with a 12 h light/dark cycle under specific pathogen-free conditions. All facilities were approved by the Academia Sinica Institutional Animal Care and Utilization Committee, and all animal experiments were conducted according to institutional guidelines.

5.3. Cell lines and Antibodies

The mouse B16F10F10 (B16F10) melanoma cells were obtained from American Type Culture Collection (ATCC; Manassas, VA, USA). Cell cultures were maintained in Dulbecco's modified Eagle's medium with 1.5 g/l sodium bicarbonate, 10% fetal bovine serum (FBS), 100 mg/ml streptomycin and penicillin, and 2 mM L-glutamine. Mouse bone marrow cells and bone marrow-derived dendritic cells (BMDCs) were cultured in RPMI 1640 containing 10% FBS, 50 mM 2-mercaptoethanol, 100 mg/ml streptomycin and penicillin, and 2 mM L-glutamine.

5.4. Cell viability determined by MTT assays

B16F10F10 cells (1×10^4/well) were grown in 96-well plates in DMEM supplemented with 10% FBS in a 5% CO_2 incubator at 37°C. After incubation for 16 hours, culture media were removed and treated with 14 specified concentrations of CMQ (0.00049-10 μM) for 24, 48 and 72 hours. Test culture medium was then replaced with 100 μl culture medium containing 3-(4,5-dimethylthiozole-2-yl)-2,5-biphenyl tetrazolium bromide (MTT) at a concentration of 0.5 mg/ml per well for 4 hours; then light absorbance

was measured with a spectrophotometer at 570 nm. Cell viability was expressed as percentage of vehicle control cells (containing DMSO 0.1% as 100%) cultured in the absence of any test compounds.

5.5. Preparation of tumor cell lysates (TCLs)

B16F10 cell lysates were prepared as described previously with slight modification (*180*). Cells (5×10^6) were seeded onto a 15-cm dish maintained for 16 hours, and then treated with DMSO (0.1%), doxorubicin (2.5 μM), colchicine (2.5 μM), CMQ (2.5 μM) or FMQ (2.5 μM) for 24 hours. After scraping, centrifuging and rinsing twice with PBS, cells were suspended at a concentration of 1×10^7 cell/ml in PBS, then frozen in liquid nitrogen for 2 minutes. Cells were then thawed in a 37°C water bath for 4 minutes and sonicated for 4 minutes to further disrupt the cell suspension. The freeze–thaw-sonicated cycle was repeated four times in rapid succession. The suspension was then centrifuged at 17,000 × g for 15 minutes and the supernatant (tumor cell lysate) was stored at -80°C.

5.6. Western blot analysis

Tumor cell lysate samples were prepared as previously described. In order to determine the expression levels of DAMPs and tumor-associated antigens, B16F10 tumor cells were harvested after treatment with indicated test compounds, followed by four freeze-thaw cycles. Samples were subsequently resolved by SDS-PAGE using 8%, 10% or 15% gels. The resolved proteins were transferred to a PVDF Immobilon-P membrane

(Millipore, Bedford, CA.), and the membrane was blocked with 5% non-fat dry milk in PBST buffer [phosphate-buffered saline (PBS) containing 0.1% Tween 20] for 60 minutes at room temperature. The membranes were then incubated overnight at 4°C with commercially available antibodies (1:1000 dilutions). Loading of equal amounts of protein was assessed using mouse β-actin. The blots were rinsed three times with PBST buffer for 5 minutes. Washed blots were incubated with HRP-conjugated secondary antibody (1:100,000 dilution) and then washed again three times with PBST buffer. The transferred proteins were visualized with an enhanced chemiluminescence (ECL) detection kit (Amersham Pharmacia Biotech, Buckinghamshire, UK). Quantification of bands was performed using Image J software.

5.7. Generation of mouse bone marrow-derived dendritic cells (BMDCs)

BMDCs were generated as previously described with slight modification (*181*). Briefly, on Day 0, the bone marrow was collected from femurs and tibiae after euthanasia and then flushed with RPMI-1640 medium using a syringe with a 0.45-mm needle. Red blood cells in suspension were lysed with ACK lysing buffer (150 mM NH_4Cl, 1.0 mM $KHCO_3$, 0.1 mM EDTA) for 5 min. Bone marrow cells were suspended at a density of 1×10^7 cells/30 ml in RPMI-1640 containing 10% FBS, 2 mM L-glutamine, 1% of nonessential amino acids and 100 U/mL penicillin and 100 μg/mL streptomycin supplemented with 20

ng/mL of GM-CSF (Peprotech, RocCMQ Hill, NJ) in 15-cm dishes at 37°C with 5% CO_2.

On day 2, two-thirds of the medium was removed and 30 mL fresh medium with GM-CSF

was introduced. On day 5, culture plates were gently swirled and the floating and loosely

adherent cells were discarded. Aliquots of 75% culture media were replenished with 20

ng/mL GM-CSF (PeproTech EC, London, UK) and 20 ng/mL IL-4 (PeproTech, London,

UK). On day 7, non-adherent cells were collected and used as the immature DC population

for subsequent tests and analyses. More than 92% cells were CD11c^{+} as measured by flow

cytometry.

5.8. Dendritic cells pulsed with tumor cell lysates

DCs were suspended in RPMI-1640 medium at a concentration of 2×10^6 cells/3 ml

in 6-well plate. Tumor cell lsysates (TCL, 400 μg) from the various treatments described in

"Preparation of TCLs" above were added to the DC culture for 12 hours and then 1μg/ml

of lipopolysaccharides (LPS) was added as a maturation stimulus. After incubation with

LPS for 12 hours, TCLs-pulsed DCs were harvested as DC vaccines for immunization.

5.9. Different culture conditions for tumor cell lysate-pulsed DCs

DCs generated from bone marrow were incubated under culture conditions: (i)

without GM-CSF (20 ng/ml) and IL-4 (20 ng/ml), (ii) GM-CSF (20 ng/ml), (iii) GM-CSF

(20 ng/ml) and IL-4 (20 ng/ml). These DCs were then further treated with: vehicle only

without any treatment (imDCs), LPS for 24 hours (maDCs), TCL plus LPS for 24 hours (CTCL-CMQ) or TCL for 12 hours and then LPS for 24 hours (TCL-CMQ).

5.10. Measurement of expression of IL-12p70 and IL-10

Expressions of IL-12p70 and IL-10 were measured using a commercial ELISA kit (R&D Systems, Minneapolis, MN) according to the manufacturer's instructions. Briefly, flat-bottomed 96-well plates were coated with capture antibodies, incubated with samples for 2 hours, washed four times with PBS, developed with appropriate biotinylated secondary antibodies for 2 hours and washed a further four times with PBS. Subsequently, plates were incubated with streptavidin conjugate HRP for 30 minutes, washed five times, TMB substrate solution was then added and stopped by 0.2 M sulfuric acid. The OD values were measured at 450 nm.

5.11. *In vivo* B16F10 melanoma tumor model

For the tumor challenge, B16F10 tumor cells were collected at 80% confluence, washed, resuspended in PBS, and injected subcutaneously (10^5 cells/50 μl/mouse) into the right flanks of mice. On day 8 post-tumor cell inoculation (the tumor volume having reached 50-80 mm^3), test mice were vaccinated with different preparations of TCL-pulsed DCs by intratumoral injection. C57BL/6 mice were divided into seven experimental groups (eight mice per group). The seven treatments were: (i) PBS (control, Ctrl), (ii) mature DCs (maDC), (iii) TCL-DMSO, (iv) TCL-DX, (v) TCL-C, (vi) TCL-CMQ, (vii) TCL-FMQ.

These vaccination sets were used for priming and booster vaccination of mice. Two boosters were performed, one on day 10 and one on day 13. Ten days after the second booster (on day 23), splenocytes were harvested from immunized mice and assayed for cytotoxic T lymphocyte (CTL) activity. Tumor volumes were determined from the length (L) and width (W) of test tumors, as measured with a caliper in a blinded manner, by the formula: $V = L \times W^2/2$. Survival of mice was recorded over 40 days following tumor challenge.

5.12. Tumor cell lysis by cytotoxic T lymphocyte (CTL)

Cytotoxicity assays for specific cell lysis were performed using the DELFIA EuTDA cytotoxicity method (*152*). B16F10 cells were trypsinized and suspended at a of density of 1×10^6 cells/ml, then 5 μl BATDA labeling agent was added to each 4 ml of cells for 15 minutes at 37°C. After labeling, cells were centrifuged, washed in PBS, and resuspended at a density of 5×10^4 cells/ml in DMEM. Next, 5×10^3 BATDA-labeled B16F10 target cells in 100 μl of medium were plated into each well of 96-well V-bottomed plates. Splenocytes (effector cells) from vaccinated animals 7 days after second boosting were added to the target cells with ratios ranging from 1:5 to 1:80 for 3 hours at 37°C. Conditions were also established to measure the background level, spontaneous release and maximal lysis. After incubation and centrifugation, 20 μl of supernatant containing released BATDA was transferred to 200 μl of europium solution in a 96-well flat-bottomed plate which was then

shaken for 15 minutes at 25°C. Plates were analyzed on a time-resolved DELFIA fluorometer (Wallac Victor^3, Perkins– Elmer, Shelton, Connecticut, USA). The percentage of specific cell lysis was calculated as follows: (experimental release − spontaneous release)/(maximum release - spontaneous release) × 100. Maximum release was determined from 5 × 10^3 labeled target cells lysed with DELFIA lysis buffer (Perkin–Elmer) in triplicate wells. Spontaneous release was measured by incubating 5 × 10^3 target cells in the absence of effector cells in triplicate wells. Results are reported as mean values of triplicate wells.

5.13. *In vivo* depletion of immune cell subsets

In vivo Ab ablation of rat anti-CD4 (GK1.5), anti-CD8 (53-6.7), and anti- NK1.1 (PK136) monoclonal antibodies (100 μg/ injection/ mice) (all from BioLegend, San Diego, CA) were performed by intraperitoneal injection to deplete CD4+ T cells, CD8+ T cells, and NK cells, respectively, on day 1 before vaccination and on days 2, 5 and 8 after tumor challenge. Normal rat IgG (Sigma) was used as a negative control. C57BL/6 mice (*n* = 5) were immunized by intratumoral injection with DC-based vaccine pulsed with CMQ-treated TCLs on days 7, 10 and 13 after tumor challenge.. Survival of mice was observed up to 40 days after tumor challenge.

5.14. Different delivery systems of DC-based vaccines pulsed with CMQ-treated tumor cell lysates

C57BL/6 mice (n = 6) were immunized by intratumoral, intranodal, or subcutaneous injection with DC-based vaccine pulsed with CMQ-treated TCLs on days 7, 10 and 13 after tumor challenge. One week after immunization, right flanks of mice were subcutaneously inoculated with B16F10 tumor cells (10^5 cells/50 μl/mouse). Tumor volumes were determined from the length (L) and width (W) of test tumors, as measured with a caliper in a blinded manner by the formula: $V = L \times W^2/2$. Survival of mice was recorded over 44 days following tumor challenge.

5.15. Analysis of DC phenotype

DCs were harvested and washed in staining buffer (sterile PBS, 1% FBS) before addition of antibodies. Nonspecific binding was blocked with anti-CD16/CD32 (BD Pharmingen, San Diego, CA) for 15 minutes at 4°C. Cells were then stained with anti-CD11c-phycoerythrin (PE) (BD Pharmingen, San Diego, CA) and related phenotypic maturation markers of DCs [anti-CD40-fluorescein isothiocyanate (FITC), anti-CD80-FITC, anti-CD86-FITC, and anti- I-A/I-E -FITC, all from BD, Pharmingen]. Cells were incubated for 30 minutes at 4°C before washing with staining buffer twice. Cells were then resuspended and fixed in 200 mL 2% formaldehyde solution before analysis with a FACS LSR2 flow cytometer using DIVA software (BD Biosciences, San Diego, CA).

5.16. Mixed lymphocyte reaction induced by DCs

Responder CD4$^+$ T cells and CD8$^+$ T cells, used for the allogeneic T-cell reaction, were isolated by being passed through mononuclear cells in a MACS column (Miltenyi Biotec). DCs were treated for 24 hours with CMQ (0.1, 0.5 and 1 μM) or colchince (2.5μM). After harvesting, DCs (5×10^3 cells) were added to 1×10^5 allogeneic T cells in flat-bottomed 96-well microtiter culture plates. During the last 16 of the 72 hours of culturing, proliferation of T cells was determined using a 5-bromo-2-deoxyuridine (BrdU)-based Cell Proliferation ELISA kit (Roche, Heidelberg, Germany) according to the manufacturer's instructions. The T-cell proliferation was expressed as the stimulation index: the OD$_{450}$ value of co-culture of treated-DCs and T cells divided by the value of co-culture of DMSO-treated-DCs co-cultured with T cells. Results are presented as means of the values of triplicate cultures.

5.17. Statistical analysis

Data are presented as mean ± SEM or ± SD. Statistical analyses were carried out with GraphPad Prism 5.0 (San Diego, CA). Statistical difference between groups was compared by Student's *t*-test. Differences in survival time and rate were evaluated by a log-rank (Mantel-Cox) test of the Kaplan–Meier survival curves. All statistical tests were two-sided. *P* values less than 0.05 were considered statistically significant (*$P < 0.05$; **$P < 0.01$; ***$P < 0.001$).

Part III. Evaluating natural products as candidate anti-severe acute respiratory syndrome (SARS) drug lead.

Chapter 1. Introduction

1.1. Severe acute respiratory syndrome (SARS) and treatment of SARS

Severe acute respiratory syndrome (SARS) is a highly infectious, life-threatening disease caused by a novel coronavirus, severe acute respiratory syndrome coronavirus (SARS-CoV) (**Figure 32**) (*182-184*). In 2003, SARS spread quickly in over 25 countries and caused 8098 probable SARS cases and 774 SARS-related deaths. Although various candidate drugs have subsequently been reported to attenuate the disease (*185-187*), as yet there are no clinically approved or recommended antiviral drugs specific for SARS use. Currently, the most frequently used countermeasure in SARS cases is an antiviral and supportive treatment using a combination of ribavirin and corticosteroids (**Figure 33**) (*188, 189*). Ribavirin, however, is only marginally effective against the SARS virus, and shows serious adverse side effects (*147, 190*). The combination therapy of HIV protease inhibitor drugs (lopinavir/ritonavir) plus ribavirin plus corticosteroids may improve some clinical outcomes, but only when administrated in the early phase of the illness (*191, 192*).
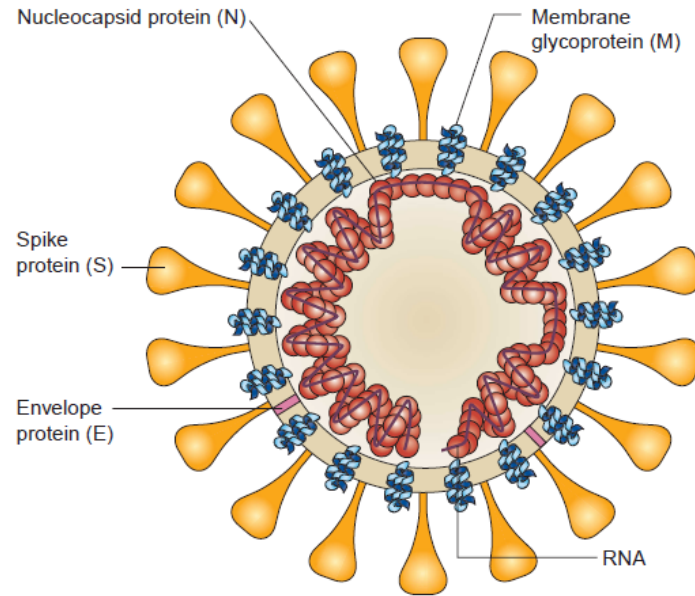
Figure 32. Schematic diagram of the SARS coronavirus structure

[Adopted from Peiris et al. (*146*)]
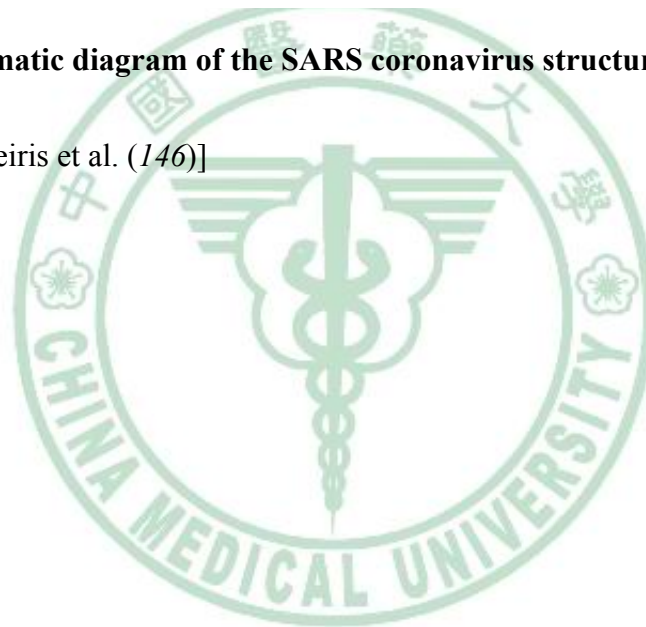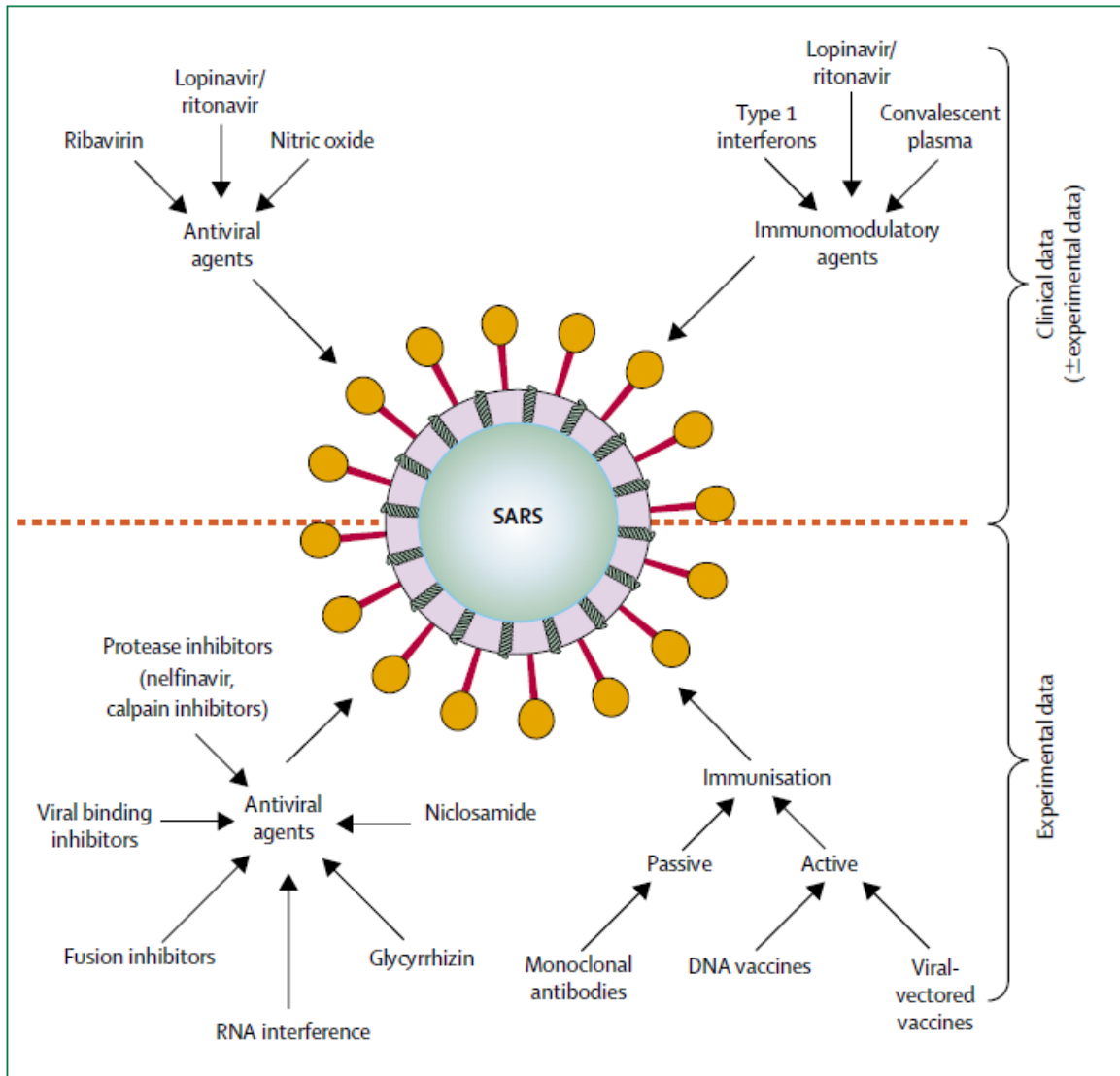
Figure 33. A summary of the agents used clinically and studied experimentally regarding the pharmacological treatment and prevention of SARS

[Adopted from Groneberg et al. (*193*))

1.2. Key steps in SARS-CoV replication as potential targets for anti-SARS-CoV drugs

As shown in **Figure 34,** a number of protein molecules encoded by SARS-CoV genome are potential targets for chemotherapeutic inhibition of viral infection and replication. These intriguing targets include: the spike protein (S), which mediates the entry of the virus; the SARS-CoV main protease (3CL protease); the NTPase/helicase; the RNA-dependent RNA polymerase; the membrane protein (M) required for virus budding; the envelope protein (E) which plays a role in coronavirus assembly; (*187, 193-197*) and the nucleocapsid phosphoprotein (N) that relates to viral RNA inside the virion and other possibly viral protein-mediated processes (*198*). Anti-SARS-CoV agents that can inhibit SARS-CoV replication may be involved in inhibition of one or more of the above protein targets including SARS-CoV 3CL protease. This important protease regulates the proteolytic processing of replicase polypeptides into functional proteins, playing an essential role in viral replication (*199, 200*). SARS-CoV 3CL protease is thus an attractive target for drug candidates against SARS. With such a drastic increase in molecular and biochemical information about various components of the SARS-CoV and their cellular targets, it is practical and timely to reevaluate anti-SARS-CoV activities using alternative experimental approaches.
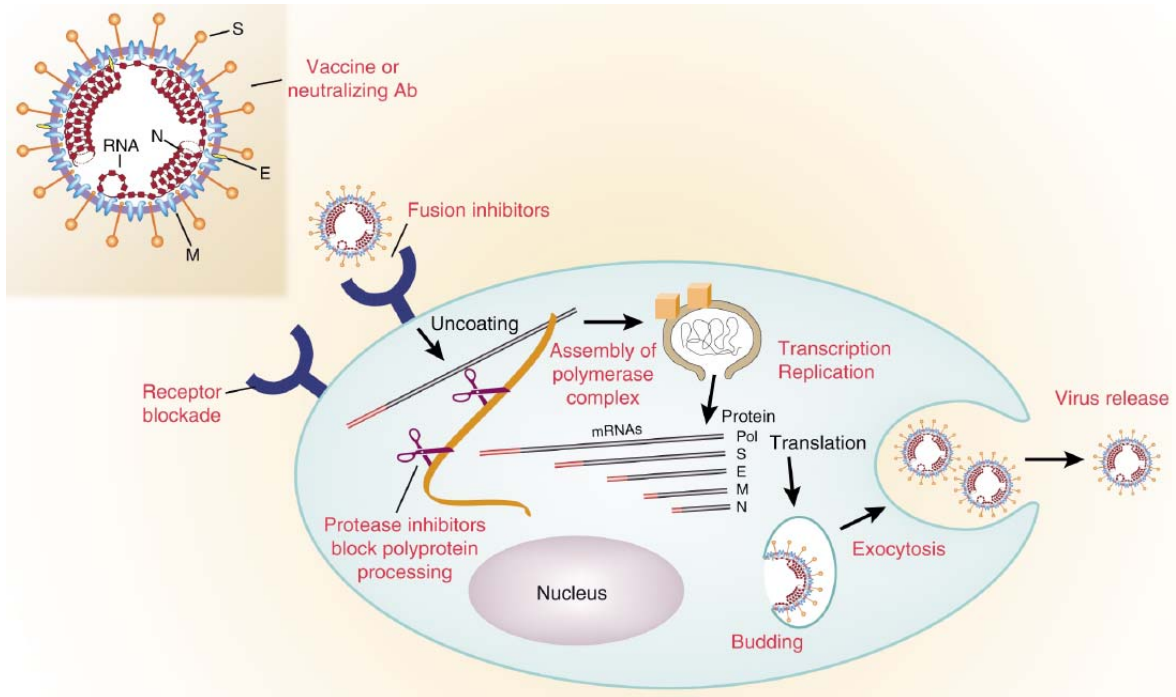
Figure 34. Different drug targets in the life cycle of SARS-CoV

[Adopted from Holmes et al. (*187*)]
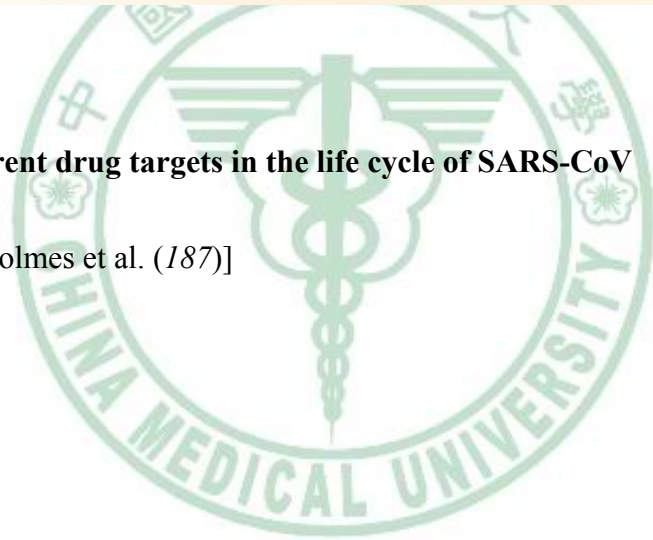
1.3. SARS and anti-SARS drug development

In an attempt to prevent a re-emergence of the disease, considerable effort has gone into screening and evaluating compounds to combat SARS-CoV.. Calpain inhibitors such as Val-Leu-CHO (calpain inhibitor VI) and Z-Val-Phe-Ala-CHO (calpain inhibitor III), have also been shown to be potent inhibitors of SARS-CoV replication (*201*). The non-steroidal anti-inflammatory drug, indomethacin, was also found to confer potent antiviral activity against SARS-CoV (*202*).

A number of traditional herbal medicines have also been reported to possess antiviral activity against SARS-CoV (*203-206*). Glycyrrhizin from licorice roots has been shown to inhibit SARS-CoV replication with a 50% effective concentration (EC_{50}) of 365 μM (*147*), and a number of glycyrrhizin derivatives have shown modestly higher anti-viral bioactivity (*186, 207*).

Based on this understanding, we hence selected potential phytocomponds and herbal extracts from traditional Chinese medicinal herbs to evaluate their anti-SARS-CoV activity.

Chapter 2. Rationale and Significance

The several reasons as follows urge us to do this study. First, SARS is a highly infectious, life-threatening disease and there are thus far no clinically approved or recommended antiviral drugs specific to SARS. Although its appearance was delayed for several years, we need to investigate potential drugs for prevention of its re-emergence. Second, traditional Chinese medicines (TCM) including various herbal medicines have been used for long history. The phytocompounds or phtoextracts derived from TCM may hold valuable potential as anti-SARS drugs. Therefore, in this study, we investigated the effects of specific phytocompounds extracts of traditional Chinese medicinal (TCM) herbs on SARS virus using a Vero E6 cell-based cytopathogenic effect (CPE) assay. A total of 221 compounds with several specific chemical skeletons isolated from a number of medicinal plants were tested, of which a group of 22 compounds and six herbal extracts were chosen to further characterize their anti-SARS-CoV bioactivities using ELISA. In parallel, these 22 compounds were also evaluated for inhibition of SARS-CoV 3CL protease activity. Structural modeling analysis was undertaken to interpret the intermolecular interactions in the compound–SARS-CoV 3CL protease complex. We demonstrate that some specific diterpenoids and lignoids and six herbal extracts have firm potential as lead compounds for future development as anti-SARS therapeutics.

Chapter 3. Results and Discussion

3.1. Results

3.1.1. Anti-SARS-CoV activity of test phytocompounds and extracts as measured by cell-based cytopathogenic effect (CPE) assay

The cell-based assay of cytopathogenic effect on Vero E6 cells infected with SARS virus was adopted to investigate the anti-SARS-CoV activity of 221 selected phytocompounds and test extracts as described previously (*208*). **Figure 35**, panel **A** shows the original morphology of the Vero E6 cells without treatment (negative control), and panel **B** shows the cytopathic morphology of Vero E6 cells after infection with SARS viruses (positive control). The inhibition of CPE of SARS virus on Vero E6 cells was expressed as levels +++, ++, and + (where +++ represented most inhibition and + represented least inhibition) as shown in panels **C**, **D**, and **E**, respectively, in **Figure 35**. Glycyrrhizin and 18*β*-glycyrrhetinic acid, previously been reported to have anti-SARS bioactivity, were employed in this study as reference control samples (*147, 186*). Valinomycin (VAL), which has previously been reported to exhibit strong anti-SARS bioactivity *in vitro* (*207*), was also employed as a reference control with high inhibition (level +++) (**Table 9**). Among the tested compounds, 22 compounds with structures depicted in **Figure 36**, comprising terpenoids (compounds **1-8** as abietane-type diterpenes, compounds **9-10** as labdane-type diterpenes, compounds **11-12** as sesquiterpenes and

compounds **13-14** as triterpenes), lignoids (compounds **15-19**), curcumin (**20**), niclosamide (**21**) and valinomycin (**22**), showed high inhibition (level ++ or +++) activity in the CPE assays at concentrations between 3.3 and 20 μM (**Table 9**). Moreover, compounds **12**, **15**, **21** and **22** also exhibited significant inhibitory effects at concentrations as low as 1 μM. Interestingly, glycyrrhizin and 18*β*-glycyrrhetinic acid were found to exhibit little or no activity in CPE reduction at a concentration of 20 μM. Among all tested extracts, none of the W fractions from test plant materials conferred significant anti-SARS activity. For E, M and H fractions from all herbal extracts, only six extracts, CBE and CBM from *Cibotium barometz*, GSH from *Gentiana scabra*, DBM from *Dioscorea batatas*, CTH from *Cassia tora*, and TCH from *Taxillus chinensis*, showed inhibitiory activity (at levels + to +++) in the CPE assays at concentrations between 25 and 200 μg/ml (**Table 10**). To evaluate whether the used vehicle solvent (0.2-0.4% DMSO) in this report would cause any possible cytotoxic or negative effect on test Vero E6 cells, MTT assay and microscopic examination were performed. Our result showed that little or no cytotoxic effect was observed in 0.2-0.4% DMSO-treated cells, as 93 to 96% cells were viable (data not shown), in addition, there was no morphological changes of test cells observed in the same tested DMSO concentrations.
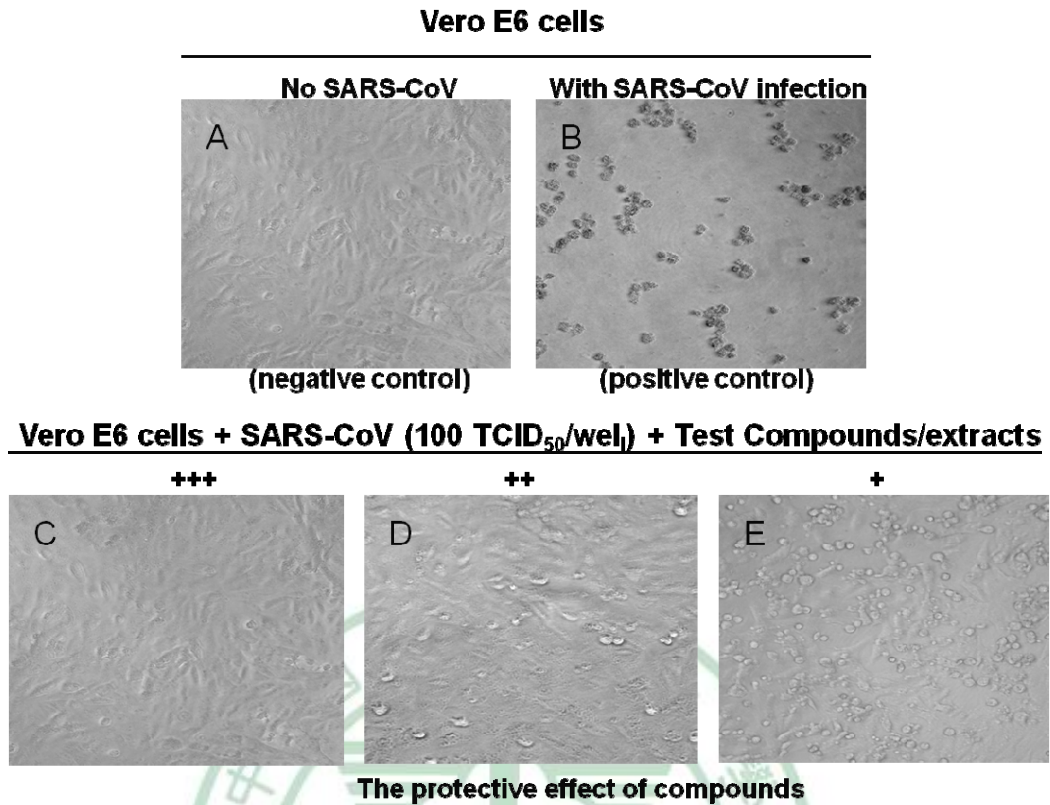
Figure 35. Characterization of compound inhibition of cytopathogenic effect (CPE) of SARS-CoV on Vero E6 cells using a cell-based assay

(A) and (B) represent cell culture phenotypes or behavior of Vero E6 cells with or without infection with SARS-CoV. (C), (D) and (E) represent semi-quantitatively the three levels (high **+++**, moderate **++,** and low **+**, respectively) of CPE inhibition, as evaluated by phase contrast microscopy.

A Terpenoids

1

2 R₁= H   R₂= H
3 R₁= H   R₂= OH
4 R₁= OH R₂= OCH₃

5

6

7

8

9

10

11

12

13

14

B Lignoids

15

16

17

18 R₁= H   R₂= OH
19 R₁= OH R₂= H

C Miscellaneous

20

21

22
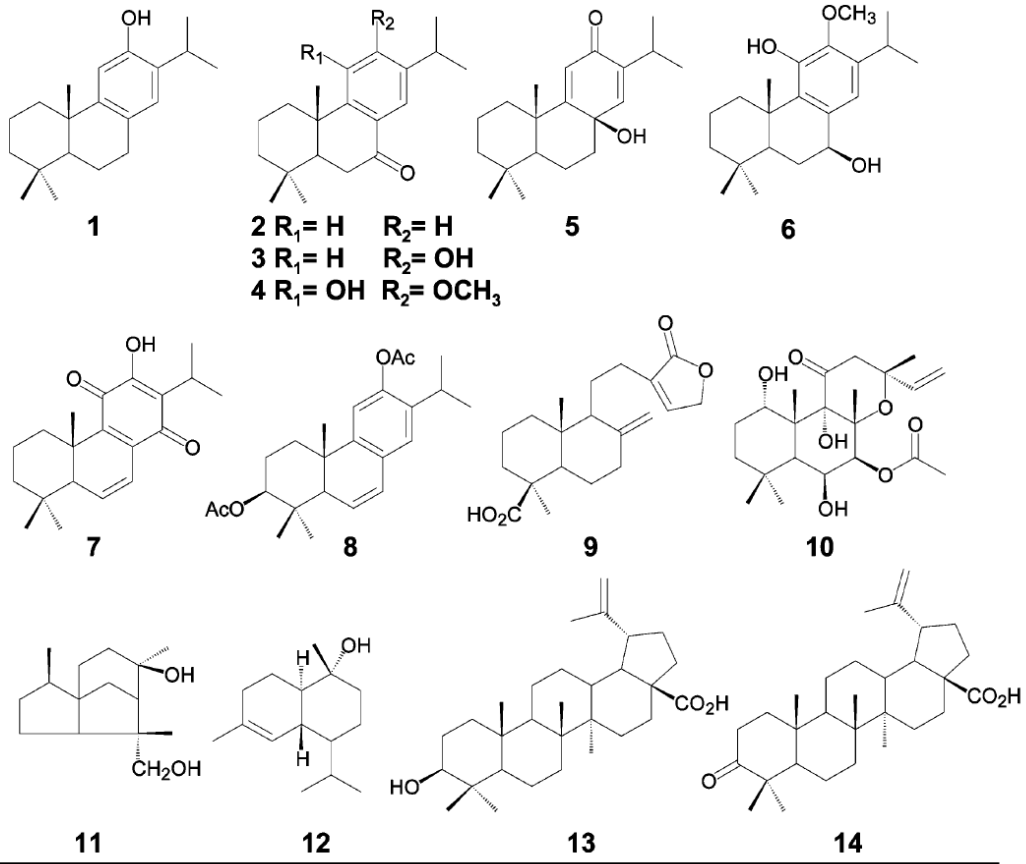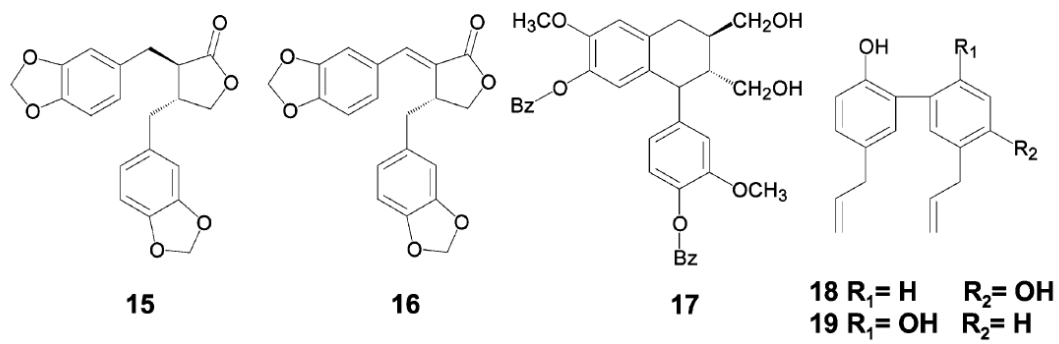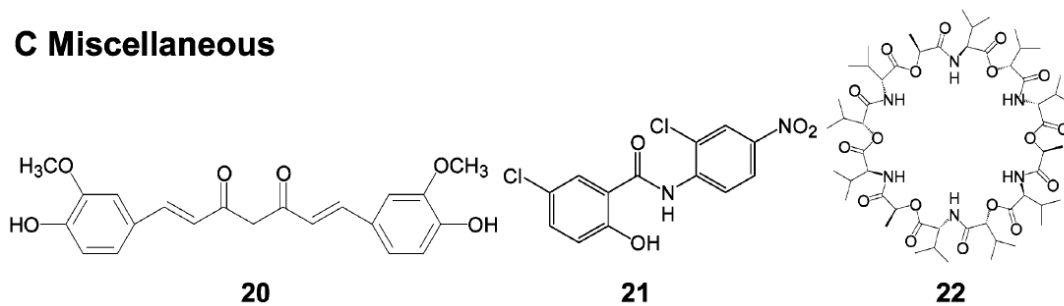
Figure 36. Chemical structures of the 22 compounds that exhibit significantly inhibitory activity against cytopathogenic effect of SARS-CoV on Vero E6 cells

(A) Terpenoids. The 14 terpenoids were 10 diterpenes, including 8 abietane derivatives (**1-8**) and two labdane derivatives (**9**, **10**), two sesquiterpenes (**11**, **12**), and two triterpenes (**13**, **14**). (B) Lignoids. The 5 lignoids were three lignan derivatives (**15-17**) and two neolignans (**18**, **19**). (C) Miscellaneous. This group includes one phenolic compound (**20,** curcumin) and two known anti-SARS-CoV compounds used as positive controls (**21**, **22**). Individual compound names are: **1:** ferruginol, **2:** dehydroabita-7-one, **3:** suginol, **4:** cryptojaponol, **5:** [8β-hydroxyabieta-9(11),13-dien-12-one)], **6:** 7β-hydroxydeoxycrptojaponol, **7:** 6,7-dehydroroyleanone, **8:** 3β,12-diacetyoabieta-6,8,11,13-tetraene, **9:** pinusolidic acid, **10**: forskolin, **11:** cedrane-3β,12-diol, **12:** α-cadinol, **13:** betulinic acid, **14:** betulonic acid, **15:** hinokinin, **16:** savinin, **17:** 4,4'-*O*-benzoylisolariciresinol**, 18:** honokiol, **19:** magnolol, **20:** curcumin, **21:** niclosamide, and **22:** valinomycin.

Table 7. Phytocompounds tested as effective against CPE of SARS-CoV on Vero E6 cells

Compounds		Concentration (μM)				
		20	10	3.3	1	0
Diterpenoids	**1**	+++	+++	++	—	—
(Abietane-type)	**2**	+++	+++	N.T.[a]	N.T.[a]	—
	3	+++	+++	N.T.[a]	N.T.[a]	—
	4	+++	+++	N.T.[a]	N.T.[a]	—
	5	+++	+++	+	—	—
	6	+++	+++	N.T.[a]	N.T.[a]	—
	7	+++	++	—	—	—
	8	+++	++	++	—	—
Diterpenoids	**9**	+++	+++	N.T.[a]	N.T.[a]	—
(Labdane-type)	**10**	+++	++	+	—	—
Sesquiterpenoids	**11**	+++	++	+	—	—
	12	+++	++	++	+	—
Triterpenoids	**13**	+++	++	+	—	—
(Lupane-type)	**14**	+++	+++	N.T.[a]	N.T.[a]	—
Lignoids	**15**	+++	++	++	+	—
	16	+++	+++	N.T.[a]	N.T.[a]	—
	17	+++	+++	N.T.[a]	N.T.[a]	—
	18	+++	+++	++	—	—
	19	+++	+++	+	—	—
Curcumin	**20**	++	+	—	—	—
Niclosamide	**21**	+++	++	++	+	—
Valinomycin	**22**	+++	++	++	+	—
Glycyrrhizin	**GL**	—	—	—	—	—
18β-glycyrrhetinic acid		—	—	—	—	—

[a] N.T., not tested.

+++, ++, + represents approximately <25%, 30-50%, and 50-70 % reduction CPE reduction, repectively.

—: no effect was observed.

Table 8. Effect of traditional Chinese medicine extracts on cytopathogenic effect (CPE) of SARS-CoV on Vero E6 cells

Sample	Extract code	Concentration (μg/ml)				
		200	100	50	25	0
Cibotium barometz	CBE	+++	++	+	+	−
Cibotium barometz	CBM	+++	+	+	−	−
Gentiana scabra	GSH	+++	++	+	+	−
Dioscorea batatas	DBM	+++	++	+	+	−
Cassia tora	CTH	++	++	+	+	−
Taxillus chinensis	TCH	+++	+++	++	+	−
Valinomycin	VAL	N.T.	N.T.	N.T.	+++	−

[a] N.T., not tested

3.1.2. Inhibition of SARS-CoV replication evaluated using ELISA

In order to investigate whether the 22 compounds and the six herbal extracts that exhibited potent inhibitory activity on cytopathogenic effect of SARS-CoV could also inhibit viral replication, levels of spike proteins in SARS-CoV infected Vero E6 cells, with or without treatment with test compounds or extracts, were measured by ELISA. As examples, the anti-SARS-CoV replication activity of four selected compounds at indicated concentrations (0.1-10 μM) are shown in **Figure 37A**. As seen in **Figure 38A** the six extracts showed anti-SARS-CoV replication activities at concentrations of 0.1 - 10 μg/ml as detected by ELISA. The concentration of each test compound or extract which was able to inhibit 50% of viral replication (EC_{50}) was calculated and summarized in **Table 11** and **Table 12**. In contrast to compounds **4**, **11**, **13**, **15** and **20** which had EC_{50} values higher than 10 μM, the EC_{50} values of are listed as follows: the four abietane-type diterpenes (compound **1**, 1.39 μM**;** compound **5**, 1.47 μM; compound **6**, 1.15 μM**;** compound **8**, 1.57 μM), one triterpene (compound **14**, 0.63 μM), one lignan (compound **16**, 1.13 μM) and niclosamide (compound **21**, < 0.1 μM). These values are similar to or even lower than that of the reference compound valinomycin (**22**) (EC_{50} = 1.63 μM). A number of other tested compounds (**2**, **7**, **9**, **10**, **12**, **18** and **19**) also showed appreciable levels of anti-SARS virus bioactivity with EC_{50} values ranging from 3.8 to 7.5 μM. On the other hand, in contrast to CBM which had EC_{50} values higher than 10 μg/ml, the EC_{50} values of CBE, GSH, DBM,

144

CTH and TCH were determined at 8.42, 8.70, 8.06, 8.42 and, 5.39 μg/ml, respectively.

Although these values are 2-3 fold higher than that of the reference compound valinomycin

(VAL) (EC_{50} = 1.87 μg/ml), the considerably low EC_{50} values (< 10 μg/ml) of these

extracts are very interesting, and may suggest that these test extracts apparently can

significantly inhibit SARS-CoV replication with specificities. Taken together, we suggest

that these specific phytocompounds and herbal extracts can significantly inhibit

SARS-CoV replication.

A Inhibition of SARS-CoV replication   **B**   Cytotoxic assay
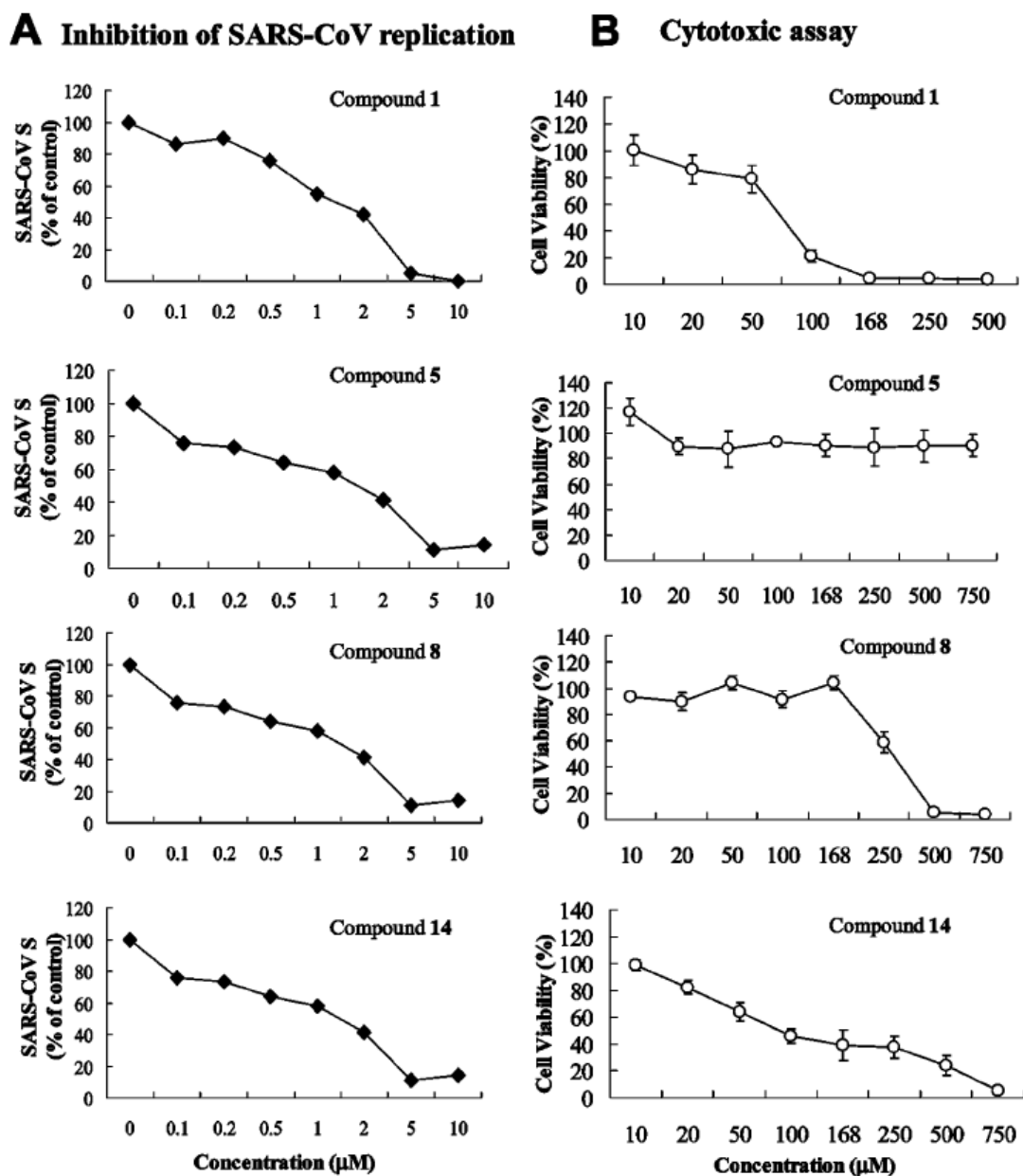
Figure 37. The inhibitory effects of test compounds on replication of SARS-CoV and on proliferation of Vero E6 cells

(A) Inhibition of SARS-CoV replication in response to treatment with specific compounds, as measured by the level of SARS-CoV spike protein (SARS-CoV S) in test Vero E6 cell cultures using ELISA. % of Control = (OD_{492} of SARS-CoV infection − OD_{492} of Mock

146

infection [Conc. X])/ (OD$_{492}$ of SARS-CoV infection – OD$_{492}$ of Mock infection [Conc. 0]).

(B) Anti-cell proliferation or cytotoxic effects of test compounds on Vero E6 Cells determined using MTT assay. Each data point represents the mean ± S.D. (n = 3). Cell viability (%) = (OD$_{570}$ of treated cells/OD$_{570}$ of vehicle cells) × 100.

Figure 38. Inhibitory effect of test extracts on replication of SARS-CoV and on proliferation of Vero E6 cells

(A) Inhibition of SARS-CoV replication in response to treatment with specific extracts is measured by the level of SARS-CoV spike protein (SARS-CoV S) in test Vero E6 cell cultures using ELISA. % of Control = (OD_{492} of SARS-CoV infection $-$ OD_{492} of mock infection [concn X]) / (OD_{492} of SARS-CoV infection - OD_{492} of Mock infection [concn 0]). (B) Cytotoxic effects of test compounds on Vero E6 cells were determined using MTT assay. Each data point represents the mean ± SD ($n = 3$). Cell viability (%) = (OD_{570} of treated cells / OD_{570} of vehicle cells) × 100.

Table 11. Inhibition of Vero E6 cell proliferation and SARS-CoV replication by test phytocompounds

compound	CC_{50} $(\mu M)^a$	EC_{50} $(\mu M)^b$	selective index^c
	Diterpenoids (Abietane-type)		
1	80.4	1.39	58.0
2	305.1	4.00	76.3
3	N.T.^{d}	N.T.^{d}	N.C.^{e}
4	78.5	>10	<7.9
5	>750	1.47	>510
6	127	1.15	111
7	89.7	5.55	16.2
8	303.3	1.57	193
	Diterpenoids (Labdane-type)		
9	>750	4.71	>159
10	674	7.5	89.8
	Sesquiterpenoids		
11	>750	>10	N.C.^{e}
12	76.8	4.44	17.3
	Triterpenoids (Lupane-type)		
13	150	>10	<15
14	112	0.63	180
	Lignoids		
15	>750	>10	N.C.^{e}
16	>750	1.13	>667
17	N.T.^{d}	N.T.^{d}	N.C.^{e}
18	88.9	6.50	13.7
19	68.3	3.80	18.0
curcumin, **20**	>250	>10	N.C.^{e}
niclosamide, **21**	22.1	<0.1	>221
valinomycin, **22**	67.5	1.63	41.4

^{a} Determined as the cytotoxic concentration (CC_{50}) of test compounds that reduced cell viability to 50% of the untreated (control) cell cultures. Each value was calculated with data obtained from triplicate samples.

^{b} Determined as the effective concentration (EC_{50}) for the inhibition of viral replication to

50% of the untreated (control) cell cultures. Each value was calculated with data obtained

from triplicate samples.

^{C} Selective index was the ratio of CC_{50} to EC_{50} (CC_{50}/EC_{50})

^{d} N.T., not tested

^{e} N.C., not calculable

Table 12. Effect of test extracts on Vero E6 cell proliferation and

SARS-CoV replication

Sample	CC_{50} (µg/ml)[a]	EC_{50} (µg/ml)[b]	Selective Index[c]
CBE	>500	8.42	>59.4
CBM	>500	>10	N.C [d]
GSH	>500	8.70	>57.5
DBM	>500	8.06	>62.0
CTH	>500	8.43	>59.3
TCH	>500	5.39	>92.8
VAL [e]	75.01	1.81	41.4

[a] Determined as the cytotoxic concentration of test compounds that reduced

cell viability to 50% of the control (i.e., cells with a treated equal volume of

vehicle control).

[b] Determined as the effective concentration at which inhibition of viral

replication was reduced to 50% of the untreated (control) cell cultures.

[c] Selective index was taken to be the ratio of CC_{50} to EC_{50} (CC_{50}/EC_{50})

[d] N.C., not calculable

[e] VAL., valinomycin

3.1.3. Cytotoxic effects of test compounds on Vero E6 cells

Since the anti-SARS-CoV activity observed using test compounds might have resulted from a direct inhibition on the growth of test cells, MTT assay was conducted to evaluate potential cytotoxic effect of test compounds at concentrations ranging from 20 to 750 µM and test phytoextracts in concentrations ranging from 10 to 500 µg/ml on Vero E6 cells. The experiment was performed with test compounds prepared in DMEM supplemented with 2% FBS. **Figure 37B** showed the results for the cytotoxic effects of compounds **1**, **5**, **8** and **14** as examples of this study. As seen in **Table 12** and **Figure 38B**, the cytotoxic concentrations of individual compounds or extracts that reduced the cell viability to 50% of the untreated control (CC_{50}) were calculated and compared with each other. The CC_{50} values (summarized in **Table 11**) for most of the test compounds (**1**, **4**, **7**, **12**, **13**, **14**, **18** and **19**), except **21** (niclosamide, $CC_{50} = 22.1$ µM), were > 65 µM, indicating that these compounds might interfere only slightly with the growth of Vero E6 cells. In addition, compounds **2**, **5**, **8**, **9**, **10**, **11**, **15**, **16** and **20** had a CC_{50} of > 250 µM; these chemicals can thus be considered biologically safe for the host cells. On the basis of the results in **Table 9**, we suggest that it is quite unlikely that the observed inhibitory effects of compounds 1-22 on viral replication of SARS-CoV were due to the inhibitory effect on the growth of host cells. Among the test extracts, the CC_{50} values were detected as higher than 500 µg/ml; interestingly, however, the positive control valinomycin had in fact a relatively

low CC $_{50}$ value (75.01 μg/ml). This result suggests that these extracts had little or no interference with the growth of Vero E6 cells; they can be considered generally biologically safe for the host cells. We hence suggest that it is quite unlikely that the inhibitory effects detected for the compounds or herbal extracts tested on viral replication of SARS-CoV were due to the inhibitory effect on cell growth or viability of host cells. The selective index (SI), the ratio of CC_{50} to EC_{50}, was also calculated in order to demonstrate the potency of anti-SARS-CoV activity of test compounds (**Table 11** and **Table 12**). The SI of the five abietane-type diterpenes (**1**, **2**, **5**, **6** and **8**), two labdane-type diterpenes (**9** and **10**), one triterpene (**14**) and one lignan (**16**) were determined to be 58, 76.3, >510, 111, 193, >159, 89.8, 180 and >667, respectively. These SI values are all remarkably higher than the value of the reference control valinomycin (SI = 41.4), determined in parallel in this study and previously reported (*207*). These SI values, with the exception of CBM, are all higher than the value of the reference control valinomycin (SI = 41.4) as determined in parallel in this study and as we previously reported (*207*).

3.1.4. Inhibitory effects of test phytocompounds or extracts on SARS-CoV 3CL protease activity

The proteolytic cleavage of viral polyproteins at specific sites by 3CL protease plays an important role in SARS-CoV replication (*199, 200*). For a better understanding of possible sites targeted by the specific anti-SARS compounds, all of the 22 compounds and six herbal extracts were evaluated in a 3CL protease inhibition assay. The principle of this assay is shown in **Figure 39**. IC_{50} values of compounds were measured by a quenched fluorescence energy transfer (FRET) method (*200*). None of the diterpenoids tested inhibited SARS-CoV 3CL protease at concentrations of less than 100 μM. Betulinic acid (**13**), savinin (**16**), curcumin (**20**), and niclosamide (**21**) showed inhibitory effects on 3CL protease activity with IC_{50} values of 10, 25, 40, and 40 μM, respectively. By contrast, betulonic acid (**14**) and hinokinin (**15**), analogues of compounds **13** and **16**, respectively, inhibited 3CL-protease activity with IC_{50} values > 100 μM (**Table 13**). We then further characterized the inhibitory mechanism of the two most potent compounds, **13** and **16**, against SARS-CoV 3CL protease activity. The K_i values of betulinic acid (**13**) and savinin (**16**) were determined at 8.2 ± 0.7 and 9.1 ± 2.4 μM, with a competitive inhibition mode of action (**Figure 40**). Niclosamide (NIC) has been reported to be an inhibitor of SARS-CoV 3CL protease activity and was used as a reference control: NIC had an IC_{50} value of 13 μg/ml in this study. As seen in **Figure 41** and **Table 14**, among these extracts tested, only

CBM and DBM conferred a considerable inhibition of SARS-CoV 3CL protease activity,

with IC_{50} values of 39 μg/ml and 44 μg/ml, respectively. The IC_{50} values of the other test

extracts were all higher than 50 μg/ml.
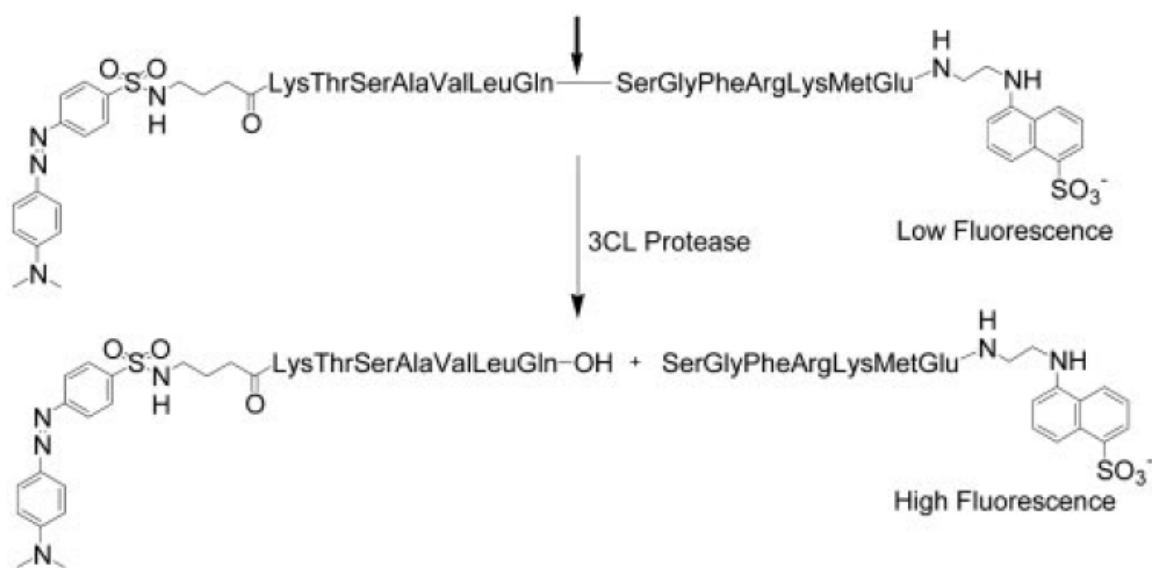
Figure 39. The principle of the SARS-CoV 3CL protease inhibition assay using

fluorogenic substrate

Enhanced fluorescence caused by 3CL protease-specific cleavage of the fluorogenic

substrate peptide was monitored at 538 nm with excitation at 355 nm.

Table 13. Kinetic properties of specific compounds that inhibit the enzymatic activity

of SARS-CoV 3CL protease

Compound	IC$_{50}$ (μM)	Ki^{a}
Betulinic acid (**13**)	10	8.2 ± 0.7
Betulonic acid (**14**)	>100	N. T.[b]
Hinokinin (**15**)	>100	N. T.[b]
Savinin (**16**)	25	9.1 ± 2.4
Curcumin **(20)**	40	N. T.[b]
Niclosamide **(21)**	40	N. T.[b]

[a] The measurement of K_i value was performed using two fixed

compound concentrations and varying substrate concentrations containing

50 nM SARS-CoV protease.

[b] N.T., not tested.
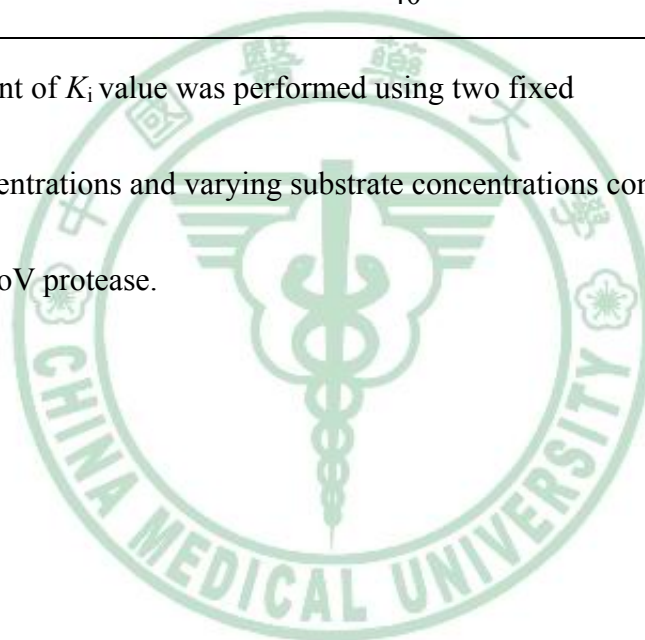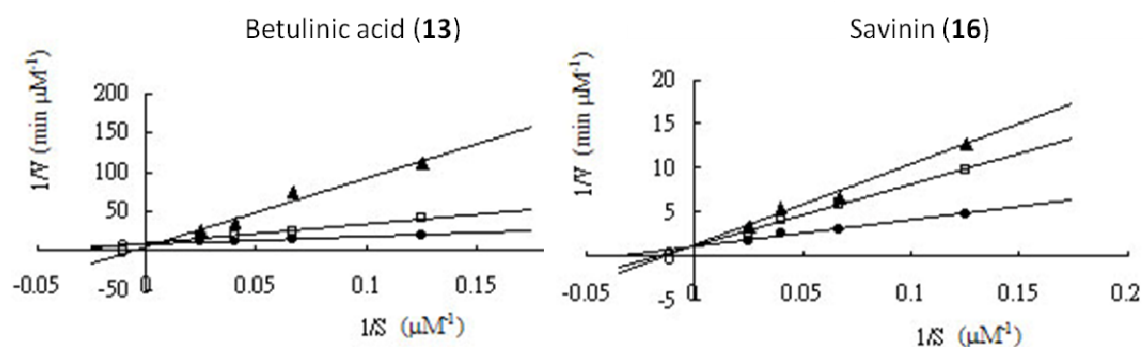
Figure 40. The inhibitory properties of betulinic acid (13) and savinin (16) on the enzymatic activity of SARS-CoV 3CL protease

Protease enzyme activity was measured using 8-80μM of fluorogenic substrate in the absence (●) or presence of 25 μM (□) and 50 μM (▲) compounds. The data were fitted with Equation 1 using KinetAsyst II program to calculate the K_i values of betulinic acid (**13**) and savinin (**16**). The inhibition pattern indicates that compound **13** and **16** are competitive inhibitors with respect to the substrate.

Table 14. IC$_{50}$ values of test extracts on the enzymatic activities of SARS-CoV 3CL protease

Sample	IC$_{50}$ (µg/ml)
CBE	>50
CBM	39 ± 3
GSH	>50
DBM	44 ± 2
CTH	>50
TCH	>50
NIC [a]	13. ± 0.7

[a] NIC, niclosamide
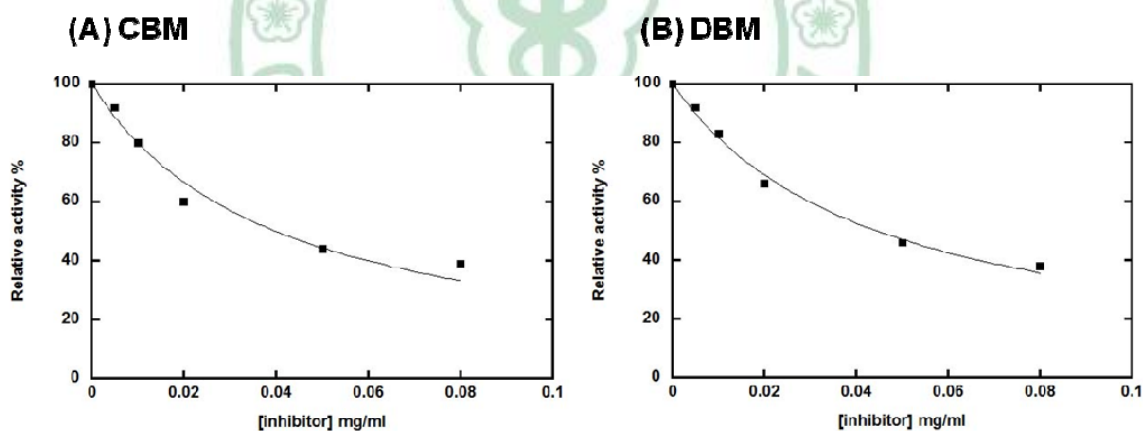
Figure 41. Inhibition of the enzymatic activity of SARS-CoV 3CL protease by CBM and DBM

The initial velocities of the inhibitory activities on 50 nM SARS 3CL-protease using 6 µM fluorogenic substrate were plotted against the different inhibitor concentrations (0 − 0.08 mg/ml) of CBM (A) and DBM (B) to obtain the IC$_{50}$ values.

3.1.5. Structural modeling of compounds 13-15 with SARS-CoV 3CL protease

Structural modeling was employed to examine the differential inhibition of SARS-CoV 3CL protease by compound analogues. Previous X-ray diffraction study showed that SARS-CoV 3CL protease has a Cys-His catalytic dyad (Cys145 and His41) located and formed between the domain I (residues 8-101) and domain II (residues 102-184) of the 3CL protease (*209*). Computer docking analysis revealed that betulinic acid (**13**) can be nicely fitted into the substrate-binding pocket of SARS-CoV 3CL protease. In addition, the hydroxyl group of C3 of **13** formed a hydrogen bond with the oxygen atom of the carbonyl group of Thr24 located in the N-terminus of domain I (residues 8-101) of the 3CL protease to strengthen the binding. In contrast, betulonic acid (**14**) did not form additional intermolecular bonds with the enzyme besides the hydrophobic interaction (**Figure 42A**). For hinokinin (**15**) and savinin (**16**), the computer modeling analyses (**Figure 42B**) suggested savinin fits into the active site cavity better by forming hydrogen bonds with the NHs of Gly143, Ser144 and Cys145 via the *O* atoms located at C9, and with the NHs of Glu166 and Gln189 via oxygen atoms attached to C3' and C4', respectively. However, hinokinin only forms a H-bond between the *O* atom located at C9 and the NH of Ser144. Moreover, only the C4' *O* atom on hinokinin forms a H-bond with Gln189. These differences of intermolecular interaction apparently are reflected by the

160

4-fold smaller K_i value of savinin compared with that of hinokinin in inhibiting the 3CL

protease (**Table 13**). In fact, the only difference in the chemical structures of hinokinin and

savinin is the single vs. double bond between C7 and C8. The more rigid structure from the

double bond found in savinin (forming a planar structure in the C7, C8 and the lactone ring)

ensures its proper binding with the 3CL protease.
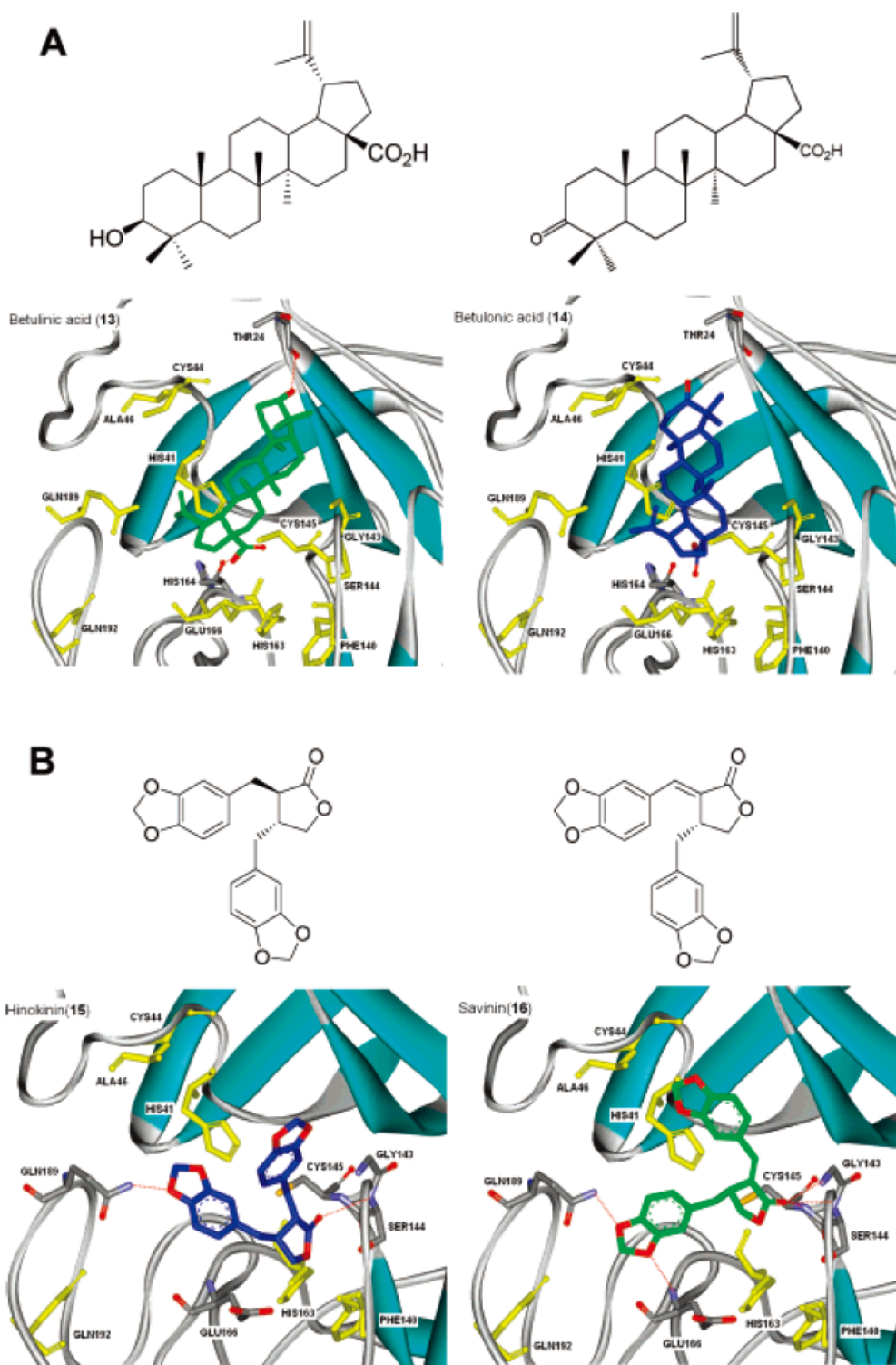
Figure 42. Structural modeling of the binding of compounds 13-16 to SARS-CoV 3CL protease.

(A) Ribbon plots of compounds **13** and **14** complex with SARS-CoV 3CL protease,

respectively. (B) Ribbon plots of compounds **15** and **16** complex with SARS-CoV 3CL protease, respectively. The figures depict the predicted intermolecular interactions of compounds in binding to the SARS-CoV 3CL protease. The oxygen atoms in the compounds are indicated in red, and hydrogen bonds are shown in dotted-lines.

3.2. Discussion

Since the outbreak of SARS in 2003, a large number of efforts have been put into research of the disease; however, to date, there is as yet no laboratory proven or clinically defined treatment for the significant public health risk posed by severe acute respiratory syndrome (SARS) (*210*). To assure adequate public safety and control of infection in the event of a re-emergence of this illness, effective anti-SARS-CoV agents may still be highly desirable or even necessary. Plant materials, especially for those that were previously used in traditional Chinese medicines, we believe are rich resources for development of the related therapeutic agents or drug candidates. In this study, we have employed a cell-based cytopathogenic effect (CPE) assay in SARS-CoV-infected Vero E6 cells for screening more than of 200 herbal extracts and more than 200 phytocompounds for potential anti-SARS-CoV activity. In the CPE assay, twenty tested phytocompounds exhibited significant levels (++ to +++) of anti-SARS-CoV activity at 10 μM, and these unique features of test compounds have not been previously reported (**Table 7**). The newly identified bioactive compounds with anti-SARS-CoV activity in the μM range include abitane-type (**1-8**) and labdane-type diterpenes (**9-10**), sesquiterpenes (**11-12**), lupane-type triterpenes (**13-14**), lignoids (**15-19**), and curcumin (**20**). Although α-cadinol (**12**) has previously been shown to exhibit strong antifungal (*211*), antitermitic (*211, 212*), and antitumoral (*213*) activities, this is the first time it has been shown to possess antiviral

activity. Six herbal extracts from traditional Chinese medicinal herbs were found to exhibit

significant levels (+ to +++) of anti-SARS-CoV activity at concentrations of 25 and 100

μg/ml (**Table 8**). As measured and compared by results from the CPE assays, this level of

anti-SARS-CoV activity is better than that reported for glycyrrhizin (*147*), a compound

with known anti-SARS-CoV activity, and extracts of other traditional herbs previously

reported to confer anti-SARS-CoV activity (*204, 214*).

Because CPE of viral infection include complex interactions of several mechanisms

between the SARS-CoV and test Vero E6 cells (*194*), we then evaluated the effect of

phytocompounds and extracts specifically on viral replication, by quantification of the

amount of spike proteins present in cultures of SARS-CoV infected Vero E6 cells (EC_{50}).

In addition, a MTT assay was used to determine the CC_{50} of the test compounds to

eliminate any possible cytotoxic or anti-cell proliferation effect of the phytocompounds on

the host cells as a cause of a low observed EC50. Once these values were established, the

SI (selective index) value was calculated from the ratio of CC50 to EC50 as an indicator of

the potency of these compounds. In comparison to the positive controls, niclosamide

(**21**)(*213, 215*) and valinomycin (**22**),(*207*) most of the compounds with potent activity

against CPE also exhibited marked inhibitory effects on SARS-CoV replication. The SI

values (Table 2) for ferruginol (**1**), dehydroabieta-7-one (**2**),

8*β*-hydroxyabieta-9(11),13-dien-12-one) (**5**), 7*β*-hydroxydeoxycrptojaponol (**6**),

165

3β,12-diacetyoabieta-6,8,11,13-tetraene (**8**), pinusolidic acid (**9**), forskolin (**10**), betulonic

acid (**14**) and savinin (**16**) are in fact substantially higher than the SI value of the positive

control valinomycin (**22**) (SI = 41.4). These compounds with high SI values apparently

inhibit SARS-CoV replication with little or no cytotoxicity against Vero E6 cells, and thus

have good potential as lead compounds in the future development of anti-SARS drugs.

Pinusolidic acid (**9**) has been reported as a platelet-activating factor inhibitor,30 and

forskolin (**10**), a well-known labdane-type diterpene, was reported to activate adenylate

cyclase and increase cyclic AMP levels in several cell types.31 In this report, we observed

potent anti-SARS virus activity for these two compounds.

By quantification of the amount of spike protein present in SARS-CoV-infected Vero

E6 cells (EC_{50}), we showed that the anti-SARS-CoV activity of these extracts may act

specifically on the inhibition of viral replication (**Table 11** and **Figure 37A**). In addition, a

MTT assay was adopted to determine the CC_{50} of test extracts, and our data led us to

suggest that the anti-viral activities we detected were apparently not due to the effects of

cytotoxicity of test extracts on the host cells, as evidenced by the low EC_{50} of the extracts.

The selective index (SI) value was calculated as the ratio of CC_{50} to EC_{50} as an indicator of

the potency of test phytoextracts. In comparison to the positive control, valinomycin (VAL)

(*207*), CBE, GSH, DBM, CTH and TCH showed potent activities against CPE, and they

also exhibited marked inhibitory effects on SARS-CoV replication. The SI values (**Table**

166

12) for these five bioactive extracts are significantly higher even than the SI value of the positive control valinomycin (SI = 41.4). The SI values (all > 55) of these five extracts are also higher than two other traditional Chinese herbs previously reported to inhibit SARS-CoV infection; *Cinnamomi cortex* was shown to inhibit SARS-CoV infection at a SI value of 23.4, and *Toona sinensis* extract was shown to inhibit SARS-CoV replication with an SI value of (12 to 17) (*203*). Taken together, we hence suggest that the six TCM phytoextracts reported here can inhibit SARS-CoV replication with little or no cytotoxicity to Vero E6 cells, and are may thus serve as useful candidates for future development of anti-SARS therapeutics.

The SARS-CoV main protease, 3CL protease is involved in the viral maturation process to cleave the virus-encoded polyproteins. Due to its pivotal role in the SARS-CoV life cycle, the 3CL protease is a key target for discovery of anti-SARS-CoV agents. In this report, the inhibitory effects of compounds **1**-**22** on SARS-CoV 3CL protease activity were investigated. Only betulinic acid (**13**) (K_i = 8.2 ± 0.7 μM) and savinin (**16**) (K_i = 9.1 ± 2.4 μM) exhibited significant inhibition on 3CL protease. On the basis of structural modeling results (**Figure 42**), the competitive inhibition of betulinic acid and savinin on 3CL protease activity was due to the formation of multiple hydrogen bonding between the compound and specific amino acid residues located at the active site pocket of the enzyme. So far, a number of efforts have contributed to the identification of inhibitors of

SARS-CoV 3CL protease (*216, 217*). However, this is the first report to demonstrate that natural lupane-type triterpenes (**13**) and a lignan (**16**) block 3CL protease activity by competitive inhibition.

The anti-SARS activity of these two compounds could be the result of a combination of two antiviral mechanisms. One of these is protease inhibition, as demonstrated in the present study. Additionally, evidence from several reports (*218-221*) has demonstrated that in the low micromolar range betulinic acid derivatives could effectively interfere with HIV-1 virus entry in test cells at a post-bonding, envelope-dependent step apparently related with the fusion of the incoming virus to the host cell membrane. Because of the similarity between the gp41 of the retrovirus HIV-1 and the S2 subunit of the spike protein of SARS-CoV, both of which are responsible for virus-induced membrane fusion, we speculate that a further anti-SARS-CoV mechanism might be the blocking of SARS-CoV entry at the post-binding step during the fusion of virus particle to host cell membrane. The other molecular virological mechanisms apparently affected by these compounds certainly warrant future study.

Various studies have also reported that abietane-type diterpenes exhibited various anti-viral activities against Herpes simplex virus (HSV) (*222, 223*), varicella-zoster virus (VZV), cytomegalovirus (CMV) (*224*), influenza virus (*225*), and human immunodeficiency virus-1 (HIV-1) (*226, 227*). In addition, some abietane-type diterpenes

were also found to inhibit HIV-1 protease (*226, 227*). We observed that the specific abietane-type diterpenes (**1-8**) possessed potent anti-SARS viral activities, but that these activities apparently did not involve action on 3CL protease because no 3CL protease inhibition was observed (data not shown). The molecular mechanism(s) by which these compounds operate needs to be investigated further.

The activity of lignans against HSV-I, measles virus, HIV-1 and other types of viruses has been studied 43-45. The antiviral mechanisms identified include interference with tubulin binding, inhibition of reverse transcriptase and inhibition of integrase and topoisomerase activities (*228-230*). The five lignoids (**15-19**) studied here possessed marked anti-SARS-CoV activity. Among them, savnin (**16**) (IC_{50} = 25 μM, Ki = 9.1 ± 2.4 μM) also showed much greater specific protease inhibition than the other lignans tested. This may correlate with its better anti-SARS-CoV proliferation activity in the ELISA test than other compounds (**Table 11**). Curcumin (**20**), a known phytocompound from *Curcuma longa*, has been reported to exhibit anti-inflammatory, antioxidant, anti-carcinogenic and anti-HIV activities (*231*). In this study, mild activity against SARS-CoV replication and inhibition of 3CL protease were observed.

Regarding the delivery strategy for the identified bioactive phytocompounds in this study that can or may result in an appropriate bioavailability for the specific type of compounds against SARS virus, we proposed here that diterpenes compounds (**1-10**) can

be considered for oral or intravenous administration in future clinical practice. Although

we have not found researches that directly address the bioavailability of diterpenes with the

structural features identical to compounds **1-10** in animals or humans, a previous

pharmacokinetics study of a diterpene triptolide in male Sprague-Dowley rats after oral

and *i.v.* administration showed that a high oral absolute bioavailability (72.08%) was

observed at the dose of 0.6 mg/kg (*232*). Previous pharmacokinetics and plasma and tissue

distribution study results of butulinic acid (**13**) in mice, rat or dog suggested that

intraperitoneal (*i.p.*) or dermal administration was efficacious for the compound with no

observed toxic response in test animals at the dose of 500 mg/kg body weight (*233*).

However, low oral bioavailability (0.7%) for oleanolic acid, an analog of butulinic acid,

was observed, implying a poor absorption and extensive metabolite clearance (*234*). These

results indicate that butulinic acid can be used *i.p.* or dermal administration without a

major problem. On the other hand, oral or *i.v.* route for the lignoids compounds (**15-18**)

administration can be considered as novel because previous studies showed that

retrojusticidin B, an analog of **15-17**, suspended in corn oil was observed with a good oral

bioavailability (33.1%) in rats (*235*), and *i.v.* administration of honokiol (**18**) exhibited a

linear pharmacokinetics in rats (*236*). Specific enteric-coated or tablet-coated formulations

may be employed in future clinical or pharmacokinetics study to enhance the efficacy of

oral delivery of specific compound. Alternatively, nasal spray or oral mucosal delivery

may also take advantage of the new approaches in making good use of new drug formulation materials that are compatible with drug stability and/or bioavailability, and the use of nanoparticles or slow-released delivery strategies.

The SARS-CoV 3CL protease is involved in the viral maturation process by cleaving the virus-encoded polyproteins (199). Because of its pivotal role in the SARS-CoV life cycle, the 3CL protease is recognized as an important target for discovery of anti-SARS-CoV agents. Among the extracts tested for inhibition of SARS-CoV 3CL protease activity, the IC_{50} values of CBM (39 μg/ml) and DBM (44 μg/ml) suggest that these two extracts can exhibit significant inhibitory activity against 3CL protease. A number of studies have contributed to the identification of inhibitors of SARS-CoV 3CL protease [15, 28-29]. However, the IC_{50} values of CBM and DBM for inhibition of SARS-CoV 3CL protease are also similar or higher than extracts from other anti-SARS-CoV medicinal herbs reported to date, including *Isatis indigotica* ($IC_{50} = 53.8$ μg/ml) (*204*), *Torreya nucifera* ($IC_{50} = 100$ μg/ml), tea extract ($IC_{50} = 125$ μg/ml) (*237*) and *Houttuynia cordata* ($IC_{50} = 1000$ μg/ml) (*214*). We therefore suggest that these two herbal extracts may also be useful drug candidates against SARS-CoV 3CL protease and may have potential for use as alternative herbal therapies against SARS.

Recently, phytochemicals or extracts derived from traditionally used medicinal plants or herbs have been contemplated or clinically evaluated as alternative or complementary

treatments for various diseases. Previous reports showed that *Cibotium barometz* inhibited

osteoclast formation and has antioxidative, tyrosinase inhibiting and antibacterial activities

(*150, 238*). In this study, *Cibotium barometz* was found to possess good anti-SAR-CoV

activity and effectively inhibit SARS-3CL protease activity. The bioactive components

responsible for these activities should therefore warrant further investigations. *Gentiana*

scabra has previously been shown to confer a hepatoprotective effect (*239*) and contains

triterpenoids of secoiridoid and its glycosides (*240-242*). Based on our previous study on

anti-SARS-CoV phytocompounds (*208*), specific triterpenoids have been shown to inhibit

SARS-CoV replication. We therefore suggest here that secoiridoid and its glycosides may

contribute to the anti-SARS activity detected for *Gentiana scabra*extract, and secoiridoid

and its glycosiedes may have potential for further evaluation as anti-SARS lead

compounds. In our previous study (*243, 244*), two specific polysaccharide-containing

fractions from *Dioscorea batatas* tuber extracts significantly increased GM-CSF promoter

activity in normal and inflamed skin, enhanced murine splenocyte proliferation ex vivo and

improved regeneration of bone marrow cells *in vivo*. Other studies also revealed that the

ethanolic extract from *Dioscorea batatas* can exert anti-inflammatory effect through the

inhibition of NF-κB-mediated inducible nitric oxide synthase (iNOS) and

cyclooxygenase-2 (COX-2) expressions (*245*). Inhibition of COX-2 expression is known to

be positively correlated with anti-SARS-CoV and other antiviral activities (*202, 246*). We

therefore hypothesize that the anti-SARS-CoV activities we demonstrated here may result from inhibition of COX-2 activity. *Cassia tora* has been found to confer anti-hypertensive (*247*), anti-hyperlipidemia (*248*), anti-bacterial (*249*), and anti-fungal properties (*250*). Anthraquinones including emodin, physcion, and rhein may be the active phytocompounds that confer these activities (*250, 251*). Because emodin has already been found to exhibit anti-SARS-CoV activity via inhibition of the viral entry by binding with the spike proteins and interfering with the SARS-CoV 3CL protease activity, we hypothesize that the active phytochemical components responsible for anti-SARS-CoV activity of CTH may be contributed by emodin or another anthraquinone(s) suggested or known to present in CTH. *Taxillus chinensis* was shown to inhibit fatty acid synthase (*252, 253*). Based on the previous study (*254*), which showed luteolin and quercetin can interfere with the entry of the virus to its host cells, we therefore hypothesize that specific glycosylated flavonoid and quercetin may play an effective role in this activity. Whether these flavonoids can also contribute to the detected anti-SARS activity warrants future investigation.

Chapter 4. Conclusion

In conclusion, in this study, twenty phytocompounds including the abietane-type and labdane-type diterpenes, lupane-type triterpenes, liganoids and curcumin, were selected from 221 compounds to undergo a more detailed characterization of their anti-SARS-CoV activity. Six phytoextracts from *Cibotium barometz*, *Gentiana scabra*, *Dioscorea batatas*, *Cassia tora*, and *Taxillus chinensis* also confer effective anti-SARS-CoV activity *via* inhibition of SARS-CoV replication. These phytocompounds and these phytoextracts were shown for the first time to exhibit significant and specific anti-SARS CoV activity, and thus provide us with a new direction for development of anti-SARS-CoV agents.
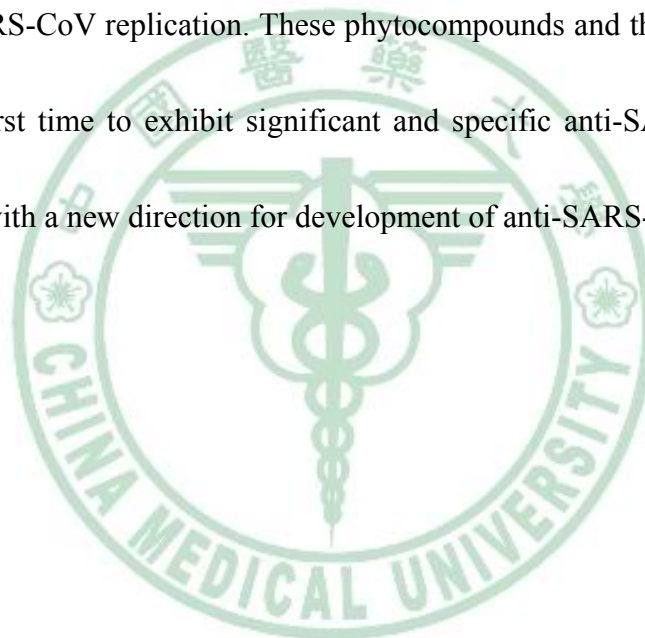
Chapter 5. Materials and Methods

5.1. Sources of compounds tested against SARS-CoV

More than two hundred compounds were selected, tested and grouped based on their chemical structures and natural sources. Compounds **1** (ferruginol), **2** (dehydroabita-7-one), **3** (suginol), **5** [8β-hydroxyabieta-9(11),13-dien-12-one)], **7** (6,7-dehydroroyleanone), **9** (pinusolidic acid), **12** (α-cadinol), **15** (hinokinin) and **16** (savinin) were purified from the ethyl acetate extracts of the heartwood of *Taiwania cryptomerioides*; and compounds **8** (3β,12-diacetyoabieta-6,8,11,13-tetraene), **11** (cedrane-3β,12-diol) and **14** (betulonic acid) were isolated from the ethyl acetate extracts of the heartwood of *Juniperus formosana*. Compounds **4** (cryptojaponol) and **6** (7β-hydroxydeoxycrptojaponol) were isolated from the heartwood of *Cryptomeria japonica*. Compound **17** (4,4'-*O*-benzoylisolariciresinol) is a synthetic liganoid. Compounds **10** (forskolin), **13** (betulinic acid), **20** (curcumin), **21** (niclosamide) and **22** (valinomycin) were purchased from Sigma (St. Louis, MO, USA) and compounds **18** (honokiol) and **19** (magnolol) came from the Pharmaceutical Industry Technology Development Center in Taiwan. The remaining test compounds were laboratory chemical stocks stored as specialty compounds in the five participating research laboratories of this study.

Test compounds were first dissolved in 100% dimethyl sulphoxide (DMSO, Hybrix-Max®, SIGMA), and then transferred to 96 well microtiter plates for assay of

activity against SARS-CoV-induced CPE, cytotoxicity in Vero E6 cells, inhibition of viral

replication activity, and inhibition of 3CL protease activity. The final DMSO concentration

in each assay was kept below 0.4%.

5.2. Preparation of extracts from traditional Chinese medicinal herbs

More than 50 traditional Chinese medicinal herbs were prepared and used as shown in

Chart 1. Briefly, plant materials were ground into a powder, immersed in 10-fold volume

of water in a sonicator for 1 hour, and filtered. Three-fold volume of 95% ethanol was

further added to the filtrate left for 1 hour and centrifuged at 10000g for 20 minutes, at 4°C

to obtain a supernatant (E) and a precipitate (W). The previous residue was mixed with

5-fold volume of methanol, left for 1 hour, and filtered again to obtain two fractions, the

filtrate (M) and the residue. The residue was then mixed with 5-fold volume of n-hexane in

a sonicator for 1 hour, kept overnight, and filtered to obtain a further filtrate (H). All plant

materials were coded as the first letters of the name of the genus and species followed by

the abbreviation for the preparative method. For example, the W, E, M and H extracts of

Cibotium barometz were abbreviated as CBW, CBE, CBM and CBH, respectively.

Chinese herbal medicines

↓ grind

10 X H$_2$O / ultrasonic extraction for 1 hr

↓

Filter

```
        Filtrate                              Residues
           ↓                                     ↓
3X 95 ﹪ ethanol extraction for 1 hr    5X 100% methanol extraction
           ↓                                     ↓
Cfg. 10000 g / 20min / 4℃              ultrasonic extraction for 1 hr
           ↓                                     ↓
   Supernatant（E）                          Filter

   Precipitate（W）
```

```
        Filtrate          residues
           ↓                 ↓
         （M）    5X 98% n-hexane extraction
                             ↓
                  ultrasonic extraction for 1 hr
                          Overnight
                             ↓
                           Filter
                             ↓
                           （H）
```
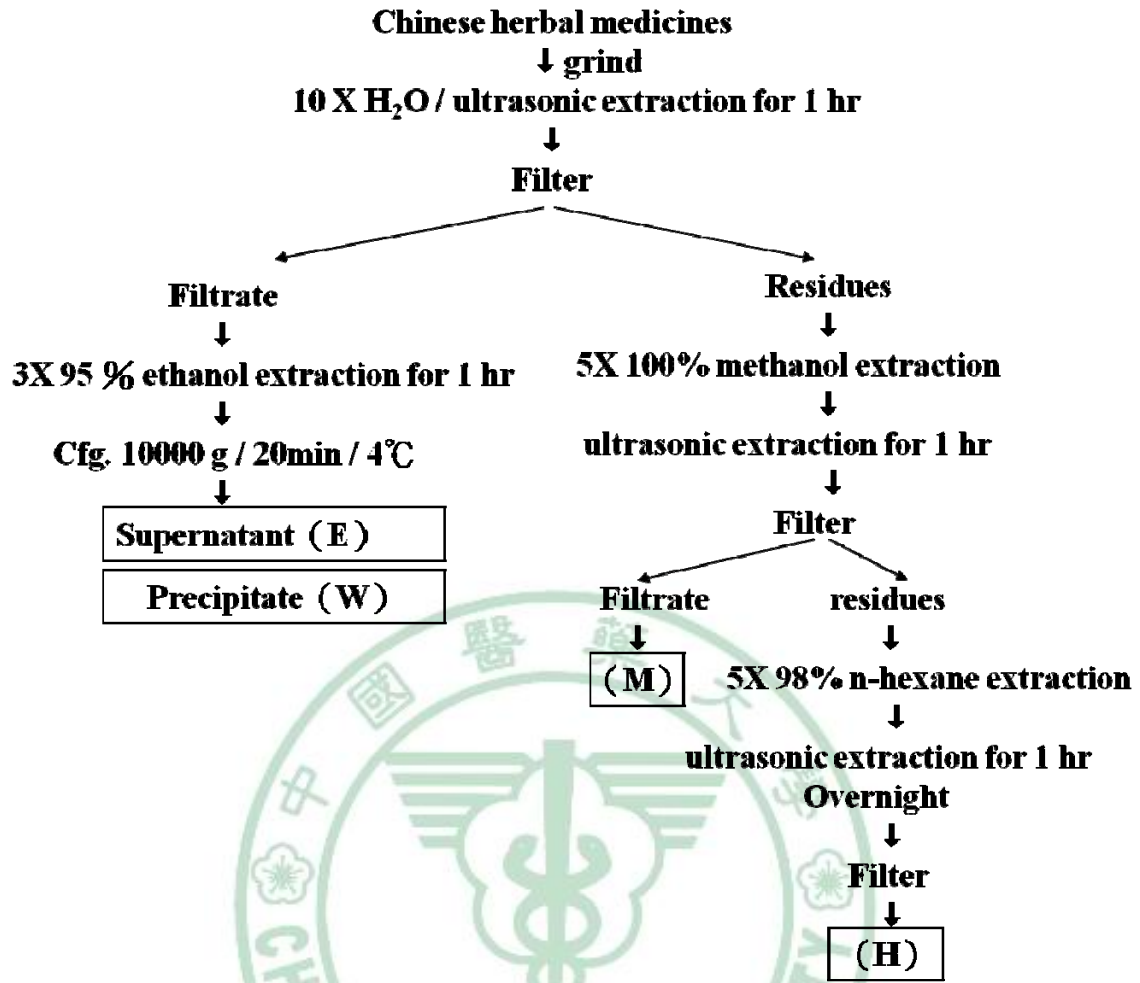
Figure 43. Schematic representation of different preparations of test herbal extracts

177

5.3. Cell-based assay utilizing CPE on Vero E6 Cells via SARS-CoV infection.

For each compound or extract treatment, eight wells were used for a complete set of assays, with three wells for virus-infection only (as positive control for CPE), three wells for virus-infection with compound treatment, and two wells with compound treatment only without viral infection. Briefly, Vero E6 cells (2×10^4/well) were cultured in 96-well plates in Dulbecco's modified Eagle's medium (DMEM) supplemented with 10% fetal bovine serum (FBS) at 37°C in 5% CO_2 incubator for one day. Before cells in culture reached a 80-90% confluence, the cell culture medium was removed and replenished with 100 μL DMEM supplemented with 2% FBS. Test cell cultures at $\geqq$ 90% confluence were treated with or without tested compounds in a DMEM + 2% FBS medium. After incubation for 2 h in a 5%CO_2 incubator at 37°C, test cells were inoculated with SARS-CoV (Hong Kong strain) in 50 μL at a dose of 100 $TCID_{50}$ (50% tissue culture infectious doses) per well. The cytopathic morphology of cells was then observed and evaluated at 72 h post infection by use of inverted phase contrast microscopy.

The inhibition by the tested compounds of SARS-CoV mediated CPE was classified into three different levels (+++, ++, +) as previously reported by other laboratories (*255*). When less than 25% of Vero E6 cells in the culture showed cytopathogenic morphology in response to SARS-CoV after treatment with compound, the inhibition was scored as level

+++. The cultures showing 25-50% and 50-70% cells as cytopathogenic are scored as level ++ and +, respectively.

5.4. Cytotoxic effects of test compounds or test extracts on Vero E6 cells

The assay protocol was as reported previously (*208*). Vero E6 cells (2×10^4/well) were grown in a 96-well plates in DMEM supplemented with nonessential amino acids and 10% FBS in a 5%CO_2 incubator at 37°C. After one day of incubation where cells in culture reached 90% confluence, the culture medium was replaced by 100 μL fresh DMEM medium containing 2% FBS and test compounds or test extracts varying at concentrations and placed into microwells and incubated for 3 days. The test culture medium was then replaced with 100 μL fresh culture medium containing 3-(4,5-dimethylthiozole-2-yl)-2,5-biphenyl tetrazolium bromide (MTT) at a concentration of 0.5 mg/mL per well for 4 h. Optical density (OD) was then measured with a spectrophotometer at 570 nm. Survival of Vero E6 cells after treatment was calculated using the formula: viable cell number (%) = [$OD_{570 \text{ (treated cells)}}$]/$OD_{570 \text{ (vehicle control cells)}}$] × 100. CC_{50} represented the level at which 50% of cell viability was reduced by 50%.

5.5. Inhibition of Viral Replication in SARS-CoV–infected Vero E6 Cells

The inhibitory effects of test extracts or test compounds on SARS-CoV replication were measured as previously described (*208*). After the Vero E6 cells with test compounds added had been incubated for 3 days with SARS-CoV, the cells were gently rinsed with PBS three times and then fixed with 10% formalin for 5 min at room temperature. The 10% formalin was removed and the cells fixed again in methanol/acetone (v/v, 1:1) solution for 5 min at room temperature. Cells were then blocked with 3% skim milk in PBS for 2 h at room temperature, rinsed three times with PBS, and then incubated for 1 h at 37°C with 1:2,000 dilution of monoclonal antibody against the spike protein of SARS-CoV. All samples were then rinsed with three changes of PBS containing 0.05% Tween 20 (PBS-T buffer) twice with fresh PBS at room temperature; and finally rinsed with 3% skim milk in PBS-T buffer. Cells were then incubated with a horseradish peroxidase-conjugated goat anti-mouse IgG for 30 min at room temperature. After rinsing three times with PBS-T buffer, a substrate solution containing *o*-phenylenediamine dihydrochloride, citrate buffer (pH 5.0), and hydrogen peroxide was added to each well. Plates were covered and gently shaken at room temperature for 10 min in the dark. The reaction was stopped by addition of 2N sulfuric acid and absorbance was read immediately

at 492 nm with an ELISA reader. The EC_{50} value for each test compound was calculated from a linear regression plot of compound concentration versus OD_{492}.

5.6. SARS-CoV 3CL protease inhibition assay

As previously reported (*200, 256*), the gene encoding the SARS-CoV main protease was cloned from the whole viral genome by polymerase chain reaction (PCR) and primer insertion (forward primer 5'-GGTATTGAGGGTCGCAGTGGTTTTAGG-3' and reverse primer 5'-AGAGGAGAGTTAGAGCCTTATTGGAAGGTAACACC-3') into the pET32Xa/Lic vector. The recombinant 3CL protease plasmid was then transformed into *E. coli* JM109 competent cells that were streaked on a Luria–Bertani (LB) agar plate containing 100 μg/mL ampicillin. The correct construct was subsequently transformed into *E. coli* BL21 host cells for expression of the His-tagged protein, which was then digested with FXa protease to remove the tag. The purified protein was confirmed by N-terminal sequencing and mass spectrometry analysis. The enzyme concentration used in all experiments was determined from the absorbance at 280 nm.

All kinetic measurements were performed in a solution containing 20 mM bis[(2-hydroxyethyl)amino]tris(hydroxymethyl)methane (pH 7.0) at 25°C. Enhanced fluorescence due to cleavage of the fluorogenic substrate peptide (Dabcyl-KTSAVLQ-SGFRKME-Edans) of SARS 3CL-protease was monitored at 538 nm with excitation at 355 nm on a fluorescence plate reader. The initial velocities of the

inhibiting activities on 50 nM SARS 3CL-protease using 6 μM fluorogenic substrate were

plotted against the different inhibitor concentrations to obtain the IC_{50} values using

Equation 1 (Eq. 1):

$$A[I] = A[0] \times \{1 - [[I]/([I] + IC_{50})]\} \qquad (Eq. 1)$$

where $A[I]$ is the enzyme activity with inhibitor concentration $[I]$; $A[0]$ is the enzyme

activity without interference from an inhibitor. K_i measurements were performed at two

fixed inhibitor concentrations and various substrate concentrations ranging from 8 to 80

μM in a reaction mixture containing 50 nM SARS protease. Lineweaver–Burk plots of

kinetic data were fitted using the computer program KINETASYST II (IntelliKinetics,

State College, PA, USA) by nonlinear regression to obtain the K_i value for competitive

inhibition from the following Equation 2 (Eq. 2).

$$1/V = K_m/V_m (1 + [I]/K_i) 1/[S] + 1/V_m \qquad (Eq. 2)$$

where K_m is the Michaelis constant of the substrate, K_i is the inhibition constant, V_m is

maximal velocity, and $[I]$ and $[S]$ represent the inhibitor and substrate concentrations in the

reaction mixture, respectively.

5.7. Computer modeling of SARS-CoV 3CL protease inhibition

Molecular docking was performed with the computer program Discovery Studio Modeling

1.2 SBD, (Accelrys, Inc., San Diego, CA). The core domain in subunit A of the X-ray

structure of the SARS-CoV 3CL protease in complex with a substrate-analog inhibitor

(coded 1uk4)(*209*) obtained from the Protein Data Bank (PDB; http://www.rcsb.org/pdb/)

was used for modeling analysis. Docking experiments were performed using an automated

ligand-docking sub-program of the computer program (Discovery Studio Modeling 1.2

SBD) that uses a genetic algorithm to fit ligands into the active site of the SARS protease

in 3-D mode. A number of parameters were chosen to control the precise operation of the

genetic algorithm via defined binding sites, specified ligand conformations, energy grid

parameter, variable numbers of Monte Carlo trials, and selected score type. Docking runs

were carried out using standard default settings ("grid resolute" of 5 Å, "site opening" of

12 Å, "binding site" selected) of the active site cavity which are similar to those used when

fitting the inhibitors in a previous report (*216*). The interaction energy was calculated from

Dreiding/Gasteiger forcefield, and poses with DockScore below 0 were rejected. 1000

iterations were performed in the "in situ ligand minimization algorithm" of the Smart

Minimization program.

References

1. Jemal, A., Siegel, R., Ward, E., Hao, Y., Xu, J., Murray, T., and Thun, M. J. (2008) Cancer statistics, 2008, *CA Cancer J Clin 58*, 71-96.

2. Lassi, K., and Dawson, N. A. (2010) Update on castrate-resistant prostate cancer: 2010, *Curr Opin Oncol 22*, 263-267.

3. Jemal, A., Siegel, R., Xu, J., and Ward, E. (2010) Cancer statistics, 2010, *CA Cancer J Clin 60*, 277-300.

4. Lin, F. M., Tsai, C. H., Yang, Y. C., Tu, W. C., Chen, L. R., Liang, Y. S., Wang, S. Y., Shyur, L. F., Chien, S. C., Cha, T. L., and Hsiao, P. W. (2008) A novel diterpene suppresses CWR22Rv1 tumor growth in vivo through antiproliferation and proapoptosis, *Cancer Res 68*, 6634-6642.

5. Albertsen, P. C., Hanley, J. A., Barrows, G. H., Penson, D. F., Kowalczyk, P. D., Sanders, M. M., and Fine, J. (2005) Prostate cancer and the Will Rogers phenomenon, *J Natl Cancer Inst 97*, 1248-1253.

6. Roth, B. J. (2005) Prostate cancer chemotherapy: emerging from the shadows, *J Clin Oncol 23*, 3302-3303.

7. Chen, A. C., and Petrylak, D. P. (2005) Complications of androgen-deprivation therapy in men with prostate cancer, *Curr Urol Rep 6*, 210-216.

8. Petrylak, D. P. (2005) Future directions in the treatment of androgen-independent prostate cancer, *Urology 65*, 8-12.

9. Jordan, M. A., and Wilson, L. (2004) Microtubules as a target for anticancer drugs, *Nat Rev Cancer 4*, 253-265.

10. Dumontet, C., and Jordan, M. A. (2010) Microtubule-binding agents: a dynamic field of cancer therapeutics, *Nat Rev Drug Discov 9*, 790-803.

11. Kavallaris, M. (2010) Microtubules and resistance to tubulin-binding agents, *Nat Rev Cancer 10*, 194-204.

12. Walczak, C. E., Cai, S., and Khodjakov, A. (2010) Mechanisms of chromosome behaviour during mitosis, *Nat Rev Mol Cell Biol 11*, 91-102.

13. Bhalla, K. N. (2003) Microtubule-targeted anticancer agents and apoptosis, *Oncogene 22*, 9075-9086.

14. Morris, P. G., and Fornier, M. N. (2008) Microtubule active agents: beyond the taxane frontier, *Clin Cancer Res 14*, 7167-7172.

15. Giannakakou, P., Sackett, D., and Fojo, T. (2000) Tubulin/microtubules: still a promising target for new chemotherapeutic agents, *J Natl Cancer Inst 92*, 182-183.

16. Kroemer, G., Galluzzi, L., Vandenabeele, P., Abrams, J., Alnemri, E. S., Baehrecke, E. H., Blagosklonny, M. V., El-Deiry, W. S., Golstein, P., Green, D. R., Hengartner, M., Knight, R. A., Kumar, S., Lipton, S. A., Malorni, W., Nunez, G., Peter, M. E., Tschopp,

J., Yuan, J., Piacentini, M., Zhivotovsky, B., and Melino, G. (2009) Classification of cell death: recommendations of the Nomenclature Committee on Cell Death 2009, *Cell Death Differ 16*, 3-11.

17.   Fesik, S. W. (2005) Promoting apoptosis as a strategy for cancer drug discovery, *Nat Rev Cancer 5*, 876-885.

18.   Blank, M., and Shiloh, Y. (2007) Programs for cell death: apoptosis is only one way to go, *Cell Cycle 6*, 686-695.

19.   Fulda, S., Galluzzi, L., and Kroemer, G. (2010) Targeting mitochondria for cancer therapy, *Nat Rev Drug Discov 9*, 447-464.

20.   Ziegler, D. S., and Kung, A. L. (2008) Therapeutic targeting of apoptosis pathways in cancer, *Curr Opin Oncol 20*, 97-103.

21.   Vizirianakis, I. S., Chatzopoulou, M., Bonovolias, I. D., Nicolaou, I., Demopoulos, V. J., and Tsiftsoglou, A. S. (2010) Toward the development of innovative bifunctional agents to induce differentiation and to promote apoptosis in leukemia: clinical candidates and perspectives, *J Med Chem 53*, 6779-6810.

22.   Fulda, S., and Debatin, K. M. (2006) Extrinsic versus intrinsic apoptosis pathways in anticancer chemotherapy, *Oncogene 25*, 4798-4811.

23.   Johnstone, R. W., Frew, A. J., and Smyth, M. J. (2008) The TRAIL apoptotic pathway in cancer onset, progression and therapy, *Nat Rev Cancer 8*, 782-798.

24.   Kim, I., Xu, W., and Reed, J. C. (2008) Cell death and endoplasmic reticulum stress: disease relevance and therapeutic opportunities, *Nat Rev Drug Discov 7*, 1013-1030.

25.   Portugal, J., Mansilla, S., and Bataller, M. (2010) Mechanisms of drug-induced mitotic catastrophe in cancer cells, *Curr Pharm Des 16*, 69-78.

26.   Vakifahmetoglu, H., Olsson, M., and Zhivotovsky, B. (2008) Death through a tragedy: mitotic catastrophe, *Cell Death Differ 15*, 1153-1162.

27.   Castedo, M., Perfettini, J. L., Roumier, T., Andreau, K., Medema, R., and Kroemer, G. (2004) Cell death by mitotic catastrophe: a molecular definition, *Oncogene 23*, 2825-2837.

28.   Mansilla, S., Priebe, W., and Portugal, J. (2006) Mitotic catastrophe results in cell death by caspase-dependent and caspase-independent mechanisms, *Cell Cycle 5*, 53-60.

29.   Ngan, C. Y., Yamamoto, H., Takagi, A., Fujie, Y., Takemasa, I., Ikeda, M., Takahashi-Yanaga, F., Sasaguri, T., Sekimoto, M., Matsuura, N., and Monden, M. (2008) Oxaliplatin induces mitotic catastrophe and apoptosis in esophageal cancer cells, *Cancer Sci 99*, 129-139.

30.   Strauss, S. J., Higginbottom, K., Juliger, S., Maharaj, L., Allen, P., Schenkein, D., Lister, T. A., and Joel, S. P. (2007) The proteasome inhibitor bortezomib acts

independently of p53 and induces cell death via apoptosis and mitotic catastrophe in B-cell lymphoma cell lines, *Cancer Res 67*, 2783-2790.

31. Eom, Y. W., Kim, M. A., Park, S. S., Goo, M. J., Kwon, H. J., Sohn, S., Kim, W. H., Yoon, G., and Choi, K. S. (2005) Two distinct modes of cell death induced by doxorubicin: apoptosis and cell death through mitotic catastrophe accompanied by senescence-like phenotype, *Oncogene 24*, 4765-4777.

32. Decordier, I., Cundari, E., and Kirsch-Volders, M. (2008) Survival of aneuploid, micronucleated and/or polyploid cells: crosstalk between ploidy control and apoptosis, *Mutat Res 651*, 30-39.

33. Fukasawa, K. (2007) Oncogenes and tumour suppressors take on centrosomes, *Nat Rev Cancer 7*, 911-924.

34. Hooper, D. C. (1999) Mode of action of fluoroquinolones, *Drugs 58 Suppl 2*, 6-10.

35. Adams, M., Kunert, O., Haslinger, E., and Bauer, R. (2004) Inhibition of leukotriene biosynthesis by quinolone alkaloids from the fruits of Evodia rutaecarpa, *Planta Med 70*, 904-908.

36. Yamashita, Y., Ashizawa, T., Morimoto, M., Hosomi, J., and Nakano, H. (1992) Antitumor quinolones with mammalian topoisomerase II mediated DNA cleavage activity, *Cancer Res 52*, 2818-2822.

37. Wang, J. P., Hsu, M. F., Raung, S. L., and Kuo, S. C. (1994) Suppressive effect of 2-phenyl-4-quinolone (YT-1) on hind-paw edema and cutaneous vascular plasma extravasation in mice, *Naunyn Schmiedebergs Arch Pharmacol 349*, 324-330.

38. Lee, H. Z. (1997) Inhibitory effect of 2-phenyl-4-quinolone on serotonin-mediated changes in the morphology and permeability of endothelial monolayers, *Eur J Pharmacol 335*, 245-254.

39. Lee, H. Z., Lin, W. C., Yeh, F. T., and Wu, C. H. (1998) 2-Phenyl-4-quinolone prevents serotonin-induced increases in endothelial permeability to albumin, *Eur J Pharmacol 354*, 205-213.

40. Wang, J. P., Raung, S. L., Huang, L. J., and Kuo, S. C. (1998) Involvement of cyclic AMP generation in the inhibition of respiratory burst by 2-phenyl-4-quinolone (YT-1) in rat neutrophils, *Biochem Pharmacol 56*, 1505-1514.

41. Huang, L. J., Hsieh, M. C., Teng, C. M., Lee, K. H., and Kuo, S. C. (1998) Synthesis and antiplatelet activity of phenyl quinolones, *Bioorg Med Chem 6*, 1657-1662.

42. Leung, K. (2004) 4-Acetoxy-7-chloro-3-(3-(-4-[11C]methoxybenzyl)phenyl)-2(1H)-quinolone.

43. Horchler, C. L., McCauley, J. P., Jr., Hall, J. E., Snyder, D. H., Craig Moore, W., Hudzik, T. J., and Chapdelaine, M. J. (2007) Synthesis of novel quinolone and quinoline-2-carboxylic acid (4-morpholin-4-yl-phenyl)amides: a late-stage diversification approach to potent 5HT1B antagonists, *Bioorg Med Chem 15*,

939-950.

44.   Kuo, S. C., Lee, H. Z., Juang, J. P., Lin, Y. T., Wu, T. S., Chang, J. J., Lednicer, D., Paull, K. D., Lin, C. M., Hamel, E., and et al. (1993) Synthesis and cytotoxicity of 1,6,7,8-substituted 2-(4'-substituted phenyl)-4-quinolones and related compounds: identification as antimitotic agents interacting with tubulin, *J Med Chem 36*, 1146-1156.

45.   Li, L., Wang, H. K., Kuo, S. C., Wu, T. S., Lednicer, D., Lin, C. M., Hamel, E., and Lee, K. H. (1994) Antitumor agents. 150. 2',3',4',5',5,6,7-substituted 2-phenyl-4-quinolones and related compounds: their synthesis, cytotoxicity, and inhibition of tubulin polymerization, *J Med Chem 37*, 1126-1135.

46.   Xia, Y., Yang, Z. Y., Xia, P., Bastow, K. F., Tachibana, Y., Kuo, S. C., Hamel, E., Hackl, T., and Lee, K. H. (1998) Antitumor agents. 181. Synthesis and biological evaluation of 6,7,2',3',4'-substituted-1,2,3,4-tetrahydro-2-phenyl-4-quinolones as a new class of antimitotic antitumor agents, *J Med Chem 41*, 1155-1162.

47.   Xia, Y., Yang, Z. Y., Xia, P., Hackl, T., Hamel, E., Mauger, A., Wu, J. H., and Lee, K. H. (2001) Antitumor Agents. 211. Fluorinated 2-phenyl-4-quinolone derivatives as antimitotic antitumor agents, *J Med Chem 44*, 3932-3936.

48.   Chen, Y. C., Lu, P. H., Pan, S. L., Teng, C. M., Kuo, S. C., Lin, T. P., Ho, Y. F., Huang, Y. C., and Guh, J. H. (2007) Quinolone analogue inhibits tubulin polymerization and induces apoptosis via Cdk1-involved signaling pathways, *Biochem Pharmacol 74*, 10-19.

49.   Wang, S. W., Pan, S. L., Huang, Y. C., Guh, J. H., Chiang, P. C., Huang, D. Y., Kuo, S. C., Lee, K. H., and Teng, C. M. (2008) CHM-1, a novel synthetic quinolone with potent and selective antimitotic antitumor activity against human hepatocellular carcinoma in vitro and in vivo, *Mol Cancer Ther 7*, 350-360.

50.   Chou, L. C., Yang, J. S., Huang, L. J., Wu, H. C., Lu, C. C., Chiang, J. H., Chen, K. T., Kuo, S. C., and Chung, J. G. (2009) The synthesized 2-(2-fluorophenyl)-6,7-methylenedioxyquinolin-4-one (CHM-1) promoted G2/M arrest through inhibition of CDK1 and induced apoptosis through the mitochondrial-dependent pathway in CT-26 murine colorectal adenocarcinoma cells, *J Gastroenterol 44*, 1055-1063.

51.   Tsai, A. C., Pan, S. L., Sun, H. L., Wang, C. Y., Peng, C. Y., Wang, S. W., Chang, Y. L., Kuo, S. C., Lee, K. H., and Teng, C. M. (2010) CHM-1, a new vascular targeting agent, induces apoptosis of human umbilical vein endothelial cells via p53-mediated death receptor 5 up-regulation, *J Biol Chem 285*, 5497-5506.

52.   Hsu, S. C., Yang, J. S., Kuo, C. L., Lo, C., Lin, J. P., Hsia, T. C., Lin, J. J., Lai, K. C., Kuo, H. M., Huang, L. J., Kuo, S. C., Wood, W. G., and Chung, J. G. (2009) Novel quinolone CHM-1 induces apoptosis and inhibits metastasis in a human osterogenic sarcoma

cell line, *J Orthop Res 27*, 1637-1644.

53. Su, M. J., Chang, G. J., and Kuo, S. C. (1993) Mechanical and electrophysiological studies on the positive inotropic effect of 2-phenyl-4-oxo-hydroquinoline in rat cardiac tissues, *Br J Pharmacol 110*, 310-316.

54. Kamenska, V., Mekenyan, O., Sterev, A., and Nedjalkova, Z. (1996) Application of the dynamic quantitative structure-activity relationship method for modeling antibacterial activity of quinolone derivatives, *Arzneimittelforschung 46*, 423-428.

55. Renau, T. E., Gage, J. W., Dever, J. A., Roland, G. E., Joannides, E. T., Shapiro, M. A., Sanchez, J. P., Gracheck, S. J., Domagala, J. M., Jacobs, M. R., and Reynolds, R. C. (1996) Structure-activity relationships of quinolone agents against mycobacteria: effect of structural modifications at the 8 position, *Antimicrob Agents Chemother 40*, 2363-2368.

56. Renau, T. E., Sanchez, J. P., Gage, J. W., Dever, J. A., Shapiro, M. A., Gracheck, S. J., and Domagala, J. M. (1996) Structure-activity relationships of the quinolone antibacterials against mycobacteria: effect of structural changes at N-1 and C-7, *J Med Chem 39*, 729-735.

57. Yoshida, T., Yamamoto, Y., Orita, H., Kakiuchi, M., Takahashi, Y., Itakura, M., Kado, N., Mitani, K., Yasuda, S., Kato, H., and Itoh, Y. (1996) Studies on quinolone antibacterials. IV. Structure-activity relationships of antibacterial activity and side effects for 5- or 8-substituted and 5,8-disubstituted-7-(3-amino-1-pyrrolidinyl)-1-cyclopropyl-1, 4-dihydro-4-oxoquinoline-3-carboxylic acids, *Chem Pharm Bull (Tokyo) 44*, 1074-1085.

58. Hadjeri, M., Mariotte, A. M., and Boumendjel, A. (2001) Alkylation of 2-phenyl-4-quinolones: synthetic and structural studies, *Chem Pharm Bull (Tokyo) 49*, 1352-1355.

59. Xia, Y., Yang, Z. Y., Xia, P., Bastow, K. F., Nakanishi, Y., Nampoothiri, P., Hamel, E., Brossi, A., and Lee, K. H. (2003) Antitumor agents. Part 226: synthesis and cytotoxicity of 2-phenyl-4-quinolone acetic acids and their esters, *Bioorg Med Chem Lett 13*, 2891-2893.

60. Hadjeri, M., Peiller, E. L., Beney, C., Deka, N., Lawson, M. A., Dumontet, C., and Boumendjel, A. (2004) Antimitotic activity of 5-hydroxy-7-methoxy-2-phenyl-4-quinolones, *J Med Chem 47*, 4964-4970.

61. Nakamura, S., Kozuka, M., Bastow, K. F., Tokuda, H., Nishino, H., Suzuki, M., Tatsuzaki, J., Morris Natschke, S. L., Kuo, S. C., and Lee, K. H. (2005) Cancer preventive agents, Part 2: Synthesis and evaluation of 2-phenyl-4-quinolone and 9-oxo-9,10-dihydroacridine derivatives as novel antitumor promoters, *Bioorg Med Chem 13*, 4396-4401.

62.   Lai, Y. Y., Huang, L. J., Lee, K. H., Xiao, Z., Bastow, K. F., Yamori, T., and Kuo, S. C. (2005) Synthesis and biological relationships of 3',6-substituted 2-phenyl-4-quinolone-3-carboxylic acid derivatives as antimitotic agents, *Bioorg Med Chem 13*, 265-275.

63.   Matsumoto, R., Haradahira, T., Ito, H., Fujimura, Y., Seki, C., Ikoma, Y., Maeda, J., Arakawa, R., Takano, A., Takahashi, H., Higuchi, M., Suzuki, K., Fukui, K., and Suhara, T. (2007) Measurement of glycine binding site of N-methyl-D-asparate receptors in living human brain using 4-acetoxy derivative of L-703,717, 4-acetoxy-7-chloro-3-[3-(4-[11c] methoxybenzyl) phenyl]-2(1H)-quinolone (AcL703) with positron emission tomography, *Synapse 61*, 795-800.

64.   Hsu, M. H., Chen, C. J., Kuo, S. C., Chung, J. G., Lai, Y. Y., Teng, C. M., Pan, S. L., and Huang, L. J. (2007) 2-(3-Fluorophenyl)-6-methoxyl-4-oxo-1,4-dihydroquinoline-3-carboxylic acid (YJC-1) induces mitotic phase arrest in A549 cells, *Eur J Pharmacol 559*, 14-20.

65.   Wang, S. W., Pan, S. L., Peng, C. Y., Huang, D. Y., Tsai, A. C., Chang, Y. L., Guh, J. H., Kuo, S. C., Lee, K. H., and Teng, C. M. (2007) CHM-1 inhibits hepatocyte growth factor-induced invasion of SK-Hep-1 human hepatocellular carcinoma cells by suppressing matrix metalloproteinase-9 expression, *Cancer Lett 257*, 87-96.

66.   Chen, H. Y., Lu, H. F., Yang, J. S., Kuo, S. C., Lo, C., Yang, M. D., Chiu, T. H., Chueh, F. S., Ho, H. C., Ko, Y. C., and Chung, J. G. (2010) The novel quinolone CHM-1 induces DNA damage and inhibits DNA repair gene expressions in a human osterogenic sarcoma cell line, *Anticancer Res 30*, 4187-4192.

67.   Lai, T. Y., Yang, J. S., Wu, P. P., Huang, W. W., Kuo, S. C., Ma, C. Y., Gibson Wood, W., and Chung, J. G. (2010) The quinolone derivative CHM-1 inhibits murine WEHI-3 leukemia in BALB/c mice in vivo, *Leuk Lymphoma 51*, 2098-2102.

68.   Chou, L. C., Chen, C. T., Lee, J. C., Way, T. D., Huang, C. H., Huang, S. M., Teng, C. M., Yamori, T., Wu, T. S., Sun, C. M., Chien, D. S., Qian, K., Morris-Natschke, S. L., Lee, K. H., Huang, L. J., and Kuo, S. C. (2010) Synthesis and preclinical evaluations of 2-(2-fluorophenyl)-6,7-methylenedioxyquinolin-4-one monosodium phosphate (CHM-1-P-Na) as a potent antitumor agent, *J Med Chem 53*, 1616-1626.

69.   Wen, C. C., Chen, H. M., Chen, S. S., Huang, L. T., Chang, W. T., Wei, W. C., Chou, L. C., Arulselvan, P., Wu, J. B., Kuo, S. C., and Yang, N. S. (2011) Specific microtubule-depolymerizing agents augment efficacy of dendritic cell-based cancer vaccines, *J Biomed Sci 18*, 44.

70.   Vakifahmetoglu, H., Olsson, M., Tamm, C., Heidari, N., Orrenius, S., and Zhivotovsky, B. (2008) DNA damage induces two distinct modes of cell death in ovarian carcinomas, *Cell Death Differ 15*, 555-566.

71.   Margittai, E., Banhegyi, G., Kiss, A., Nagy, G., Mandl, J., Schaff, Z., and Csala, M.

(2005) Scurvy leads to endoplasmic reticulum stress and apoptosis in the liver of Guinea pigs, *J Nutr 135*, 2530-2534.

72.   Dhanasekaran, D. N., and Reddy, E. P. (2008) JNK signaling in apoptosis, *Oncogene 27*, 6245-6251.

73.   Singh, S. V., Srivastava, S. K., Choi, S., Lew, K. L., Antosiewicz, J., Xiao, D., Zeng, Y., Watkins, S. C., Johnson, C. S., Trump, D. L., Lee, Y. J., Xiao, H., and Herman-Antosiewicz, A. (2005) Sulforaphane-induced cell death in human prostate cancer cells is initiated by reactive oxygen species, *J Biol Chem 280*, 19911-19924.

74.   Green, D. R., and Kroemer, G. (2009) Cytoplasmic functions of the tumour suppressor p53, *Nature 458*, 1127-1130.

75.   Zhang, R., Humphreys, I., Sahu, R. P., Shi, Y., and Srivastava, S. K. (2008) In vitro and in vivo induction of apoptosis by capsaicin in pancreatic cancer cells is mediated through ROS generation and mitochondrial death pathway, *Apoptosis 13*, 1465-1478.

76.   Wu, P. P., Liu, K. C., Huang, W. W., Ma, C. Y., Lin, H., Yang, J. S., and Chung, J. G. (2011) Triptolide induces apoptosis in human adrenal cancer NCI-H295 cells through a mitochondrial-dependent pathway, *Oncol Rep 25*, 551-557.

77.   Yang, J. S., Hour, M. J., Huang, W. W., Lin, K. L., Kuo, S. C., and Chung, J. G. (2010) MJ-29 inhibits tubulin polymerization, induces mitotic arrest, and triggers apoptosis via cyclin-dependent kinase 1-mediated Bcl-2 phosphorylation in human leukemia U937 cells, *J Pharmacol Exp Ther 334*, 477-488.

78.   Wu, S. H., Hang, L. W., Yang, J. S., Chen, H. Y., Lin, H. Y., Chiang, J. H., Lu, C. C., Yang, J. L., Lai, T. Y., Ko, Y. C., and Chung, J. G. (2010) Curcumin induces apoptosis in human non-small cell lung cancer NCI-H460 cells through ER stress and caspase cascade- and mitochondria-dependent pathways, *Anticancer Res 30*, 2125-2133.

79.   Chiang, J. H., Yang, J. S., Ma, C. Y., Yang, M. D., Huang, H. Y., Hsia, T. C., Kuo, H. M., Wu, P. P., Lee, T. H., and Chung, J. G. (2011) Danthron, an Anthraquinone Derivative, Induces DNA Damage and Caspase Cascades-Mediated Apoptosis in SNU-1 Human Gastric Cancer Cells through Mitochondrial Permeability Transition Pores and Bax-Triggered Pathways, *Chem Res Toxicol 24*, 20-29.

80.   Izdebskaya, Y., Shvedov, V., and Volyar, A. (2005) Focusing of wedge-generated higher-order optical vortices, *Opt Lett 30*, 2530-2532.

81.   Chen, M., Guerrero, A. D., Huang, L., Shabier, Z., Pan, M., Tan, T. H., and Wang, J. (2007) Caspase-9-induced mitochondrial disruption through cleavage of anti-apoptotic BCL-2 family members, *J Biol Chem 282*, 33888-33895.

82.   Lu, C. C., Yang, J. S., Huang, A. C., Hsia, T. C., Chou, S. T., Kuo, C. L., Lu, H. F., Lee, T. H., Wood, W. G., and Chung, J. G. (2010) Chrysophanol induces necrosis through the production of ROS and alteration of ATP levels in J5 human liver cancer cells,

Mol Nutr Food Res 54, 967-976.

83. Hanahan, D., and Weinberg, R. A. (2000) The hallmarks of cancer, *Cell 100*, 57-70.

84. Vogelstein, B., and Kinzler, K. W. (2004) Cancer genes and the pathways they control, *Nat Med 10*, 789-799.

85. Melief, C. J. (2008) Cancer immunotherapy by dendritic cells, *Immunity 29*, 372-383.

86. Smyth, M. J., Godfrey, D. I., and Trapani, J. A. (2001) A fresh look at tumor immunosurveillance and immunotherapy, *Nat Immunol 2*, 293-299.

87. Banchereau, J., Briere, F., Caux, C., Davoust, J., Lebecque, S., Liu, Y. J., Pulendran, B., and Palucka, K. (2000) Immunobiology of dendritic cells, *Annu Rev Immunol 18*, 767-811.

88. Banchereau, J., and Steinman, R. M. (1998) Dendritic cells and the control of immunity, *Nature 392*, 245-252.

89. Viaud, S., Thery, C., Ploix, S., Tursz, T., Lapierre, V., Lantz, O., Zitvogel, L., and Chaput, N. (2010) Dendritic cell-derived exosomes for cancer immunotherapy: what's next?, *Cancer Res 70*, 1281-1285.

90. Gilboa, E. (2007) DC-based cancer vaccines, *J Clin Invest 117*, 1195-1203.

91. Nestle, F. O., Alijagic, S., Gilliet, M., Sun, Y., Grabbe, S., Dummer, R., Burg, G., and Schadendorf, D. (1998) Vaccination of melanoma patients with peptide- or tumor lysate-pulsed dendritic cells, *Nat Med 4*, 328-332.

92. Banchereau, J., and Palucka, A. K. (2005) Dendritic cells as therapeutic vaccines against cancer, *Nat Rev Immunol 5*, 296-306.

93. Aravindaram, K., Yu, H. H., Lan, C. W., Wang, P. H., Chen, Y. H., Chen, H. M., Yagita, H., and Yang, N. S. (2009) Transgenic expression of human gp100 and RANTES at specific time points for suppression of melanoma, *Gene Ther 16*, 1329-1339.

94. Smits, E. L., Anguille, S., Cools, N., Berneman, Z. N., and Van Tendeloo, V. F. (2009) Dendritic cell-based cancer gene therapy, *Hum Gene Ther 20*, 1106-1118.

95. Goldszmid, R. S., Idoyaga, J., Bravo, A. I., Steinman, R., Mordoh, J., and Wainstok, R. (2003) Dendritic cells charged with apoptotic tumor cells induce long-lived protective CD4+ and CD8+ T cell immunity against B16 melanoma, *J Immunol 171*, 5940-5947.

96. Fields, R. C., Shimizu, K., and Mule, J. J. (1998) Murine dendritic cells pulsed with whole tumor lysates mediate potent antitumor immune responses in vitro and in vivo, *Proc Natl Acad Sci U S A 95*, 9482-9487.

97. Schwaab, T., Schwarzer, A., Wolf, B., Crocenzi, T. S., Seigne, J. D., Crosby, N. A., Cole, B. F., Fisher, J. L., Uhlenhake, J. C., Mellinger, D., Foster, C., Szczepiorkowski, Z. M., Webber, S. M., Schned, A. R., Harris, R. D., Barth, R. J., Jr., Heaney, J. A., Noelle, R. J., and Ernstoff, M. S. (2009) Clinical and immunologic effects of intranodal

autologous tumor lysate-dendritic cell vaccine with Aldesleukin (Interleukin 2) and IFN-{alpha}2a therapy in metastatic renal cell carcinoma patients, *Clin Cancer Res 15*, 4986-4992.

98.   Hatfield, P., Merrick, A. E., West, E., O'Donnell, D., Selby, P., Vile, R., and Melcher, A. A. (2008) Optimization of dendritic cell loading with tumor cell lysates for cancer immunotherapy, *J Immunother 31*, 620-632.

99.   Kusunoki, S. (2003) Diagnosis, pathogenesis and treatment of Miller Fisher syndrome and related disorders: clinical significance of antiGQ1b IgG antibody, *Expert Rev Neurother 3*, 133-140.

100. Omar, S., Zhang, J., MacKinnon, S., Leaman, D., Durst, T., Philogene, B. J., Arnason, J. T., Sanchez-Vindas, P. E., Poveda, L., Tamez, P. A., and Pezzuto, J. M. (2003) Traditionally-used antimalarials from the Meliaceae, *Curr Top Med Chem 3*, 133-139.

101. Hemida, M. H., Mahmoud, N. S., El, M. M., Ammar el, S. G., Kilany, Y. F., El, T. D., and El, D. T. (2010) Interleukin (Il)-12, Il-5 and total IgE in hepatosplenic schistosomiasis with or without asthma, *J Egypt Soc Parasitol 40*, 367-376.

102. Asavaroengchai, W., Kotera, Y., and Mule, J. J. (2002) Tumor lysate-pulsed dendritic cells can elicit an effective antitumor immune response during early lymphoid recovery, *Proc Natl Acad Sci U S A 99*, 931-936.

103. Toh, H. C., Wang, W. W., Chia, W. K., Kvistborg, P., Sun, L., Teo, K., Phoon, Y. P., Soe, Y., Tan, S. H., Hee, S. W., Foo, K. F., Ong, S., Koo, W. H., Zocca, M. B., and Claesson, M. H. (2009) Clinical Benefit of Allogeneic Melanoma Cell Lysate-Pulsed Autologous Dendritic Cell Vaccine in MAGE-Positive Colorectal Cancer Patients, *Clin Cancer Res 15*, 7726-7736.

104. Osada, T., Clay, T. M., Woo, C. Y., Morse, M. A., and Lyerly, H. K. (2006) Dendritic cell-based immunotherapy, *Int Rev Immunol 25*, 377-413.

105. Finkelstein, S. E., Iclozan, C., Bui, M. M., Cotter, M. J., Ramakrishnan, R., Ahmed, J., Noyes, D. R., Cheong, D., Gonzalez, R. J., Heysek, R. V., Berman, C., Lenox, B. C., Janssen, W., Zager, J. S., Sondak, V. K., Letson, G. D., Antonia, S. J., and Gabrilovich, D. I. (2011) Combination of External Beam Radiotherapy (EBRT) with Intratumoral Injection of Dendritic Cells as Neo-Adjuvant Treatment of High-Risk Soft Tissue Sarcoma Patients, *Int J Radiat Oncol Biol Phys*, (In press).

106. Jacobs, J. F., Punt, C. J., Lesterhuis, W. J., Sutmuller, R. P., Brouwer, H. M., Scharenborg, N. M., Klasen, I. S., Hilbrands, L. B., Figdor, C. G., de Vries, I. J., and Adema, G. J. (2010) Dendritic cell vaccination in combination with anti-CD25 monoclonal antibody treatment: a phase I/II study in metastatic melanoma patients, *Clin Cancer Res 16*, 5067-5078.

107. Lesterhuis, W. J., de Vries, I. J., Aarntzen, E. A., de Boer, A., Scharenborg, N. M., van

de Rakt, M., van Spronsen, D. J., Preijers, F. W., Figdor, C. G., Adema, G. J., and Punt, C. J. (2010) A pilot study on the immunogenicity of dendritic cell vaccination during adjuvant oxaliplatin/capecitabine chemotherapy in colon cancer patients, *Br J Cancer 103*, 1415-1421.

108. Sakakibara, M., Kanto, T., Hayakawa, M., Kuroda, S., Miyatake, H., Itose, I., Miyazaki, M., Kakita, N., Higashitani, K., Matsubara, T., Hiramatsu, N., Kasahara, A., Takehara, T., and Hayashi, N. (2011) Comprehensive immunological analyses of colorectal cancer patients in the phase I/II study of quickly matured dendritic cell vaccine pulsed with carcinoembryonic antigen peptide, *Cancer Immunol Immunother*.

109. Perroud, M. W., Jr., Honma, H. N., Barbeiro, A. S., Gilli, S. C., Almeida, M. T., Vassallo, J., Saad, S. T., and Zambon, L. (2011) Mature Autologous Dendritic Cell Vaccines in Advanced Non-Small Cell Lung Cancer: a Phase I Pilot Study, *J Exp Clin Cancer Res 30*, 65.

110. Lodge, P. A., Jones, L. A., Bader, R. A., Murphy, G. P., and Salgaller, M. L. (2000) Dendritic cell-based immunotherapy of prostate cancer: immune monitoring of a phase II clinical trial, *Cancer Res 60*, 829-833.

111. Steele, J. C., Rao, A., Marsden, J. R., Armstrong, C. J., Berhane, S., Billingham, L. J., Graham, N., Roberts, C., Ryan, G., Uppal, H., Walker, C., Young, L. S., and Steven, N. M. (2011) Phase I/II trial of a dendritic cell vaccine transfected with DNA encoding melan A and gp100 for patients with metastatic melanoma, *Gene Ther 18*, 584-593.

112. Burgdorf, S. K., Fischer, A., Myschetzky, P. S., Munksgaard, S. B., Zocca, M. B., Claesson, M. H., and Rosenberg, J. (2008) Clinical responses in patients with advanced colorectal cancer to a dendritic cell based vaccine, *Oncol Rep 20*, 1305-1311.

113. Yu, J. S., Liu, G., Ying, H., Yong, W. H., Black, K. L., and Wheeler, C. J. (2004) Vaccination with tumor lysate-pulsed dendritic cells elicits antigen-specific, cytotoxic T-cells in patients with malignant glioma, *Cancer Res 64*, 4973-4979.

114. Lesterhuis, W. J., De Vries, I. J., Schreibelt, G., Schuurhuis, D. H., Aarntzen, E. H., De Boer, A., Scharenborg, N. M., Van De Rakt, M., Hesselink, E. J., Figdor, C. G., Adema, G. J., and Punt, C. J. (2010) Immunogenicity of dendritic cells pulsed with CEA peptide or transfected with CEA mRNA for vaccination of colorectal cancer patients, *Anticancer Res 30*, 5091-5097.

115. Trepiakas, R., Berntsen, A., Hadrup, S. R., Bjorn, J., Geertsen, P. F., Straten, P. T., Andersen, M. H., Pedersen, A. E., Soleimani, A., Lorentzen, T., Johansen, J. S., and Svane, I. M. (2010) Vaccination with autologous dendritic cells pulsed with multiple tumor antigens for treatment of patients with malignant melanoma: results from a phase I/II trial, *Cytotherapy 12*, 721-734.

116. Ridolfi, R., Petrini, M., Fiammenghi, L., Stefanelli, M., Ridolfi, L., Ballardini, M., Migliori, G., and Riccobon, A. (2006) Improved overall survival in dendritic cell vaccination-induced immunoreactive subgroup of advanced melanoma patients, *J Transl Med 4*, 36.

117. Soleimani, A., Berntsen, A., Svane, I. M., and Pedersen, A. E. (2009) Immune responses in patients with metastatic renal cell carcinoma treated with dendritic cells pulsed with tumor lysate, *Scand J Immunol 70*, 481-489.

118. Bachleitner-Hofmann, T., Friedl, J., Hassler, M., Hayden, H., Dubsky, P., Sachet, M., Rieder, E., Pfragner, R., Brostjan, C., Riss, S., Niederle, B., Gnant, M., and Stift, A. (2009) Pilot trial of autologous dendritic cells loaded with tumor lysate(s) from allogeneic tumor cell lines in patients with metastatic medullary thyroid carcinoma, *Oncol Rep 21*, 1585-1592.

119. Palmer, D. H., Midgley, R. S., Mirza, N., Torr, E. E., Ahmed, F., Steele, J. C., Steven, N. M., Kerr, D. J., Young, L. S., and Adams, D. H. (2009) A phase II study of adoptive immunotherapy using dendritic cells pulsed with tumor lysate in patients with hepatocellular carcinoma, *Hepatology 49*, 124-132.

120. De Vleeschouwer, S., Fieuws, S., Rutkowski, S., Van Calenbergh, F., Van Loon, J., Goffin, J., Sciot, R., Wilms, G., Demaerel, P., Warmuth-Metz, M., Soerensen, N., Wolff, J. E., Wagner, S., Kaempgen, E., and Van Gool, S. W. (2008) Postoperative adjuvant dendritic cell-based immunotherapy in patients with relapsed glioblastoma multiforme, *Clin Cancer Res 14*, 3098-3104.

121. Bauer, C., Dauer, M., Saraj, S., Schnurr, M., Bauernfeind, F., Sterzik, A., Junkmann, J., Jakl, V., Kiefl, R., Oduncu, F., Emmerich, B., Mayr, D., Mussack, T., Bruns, C., Ruttinger, D., Conrad, C., Jauch, K. W., Endres, S., and Eigler, A. (2011) Dendritic cell-based vaccination of patients with advanced pancreatic carcinoma: results of a pilot study, *Cancer Immunol Immunother*, (In press).

122. Ribas, A., Camacho, L. H., Lee, S. M., Hersh, E. M., Brown, C. K., Richards, J. M., Rodriguez, M. J., Prieto, V. G., Glaspy, J. A., Oseguera, D. K., Hernandez, J., Villanueva, A., Chmielowski, B., Mitsky, P., Bercovici, N., Wasserman, E., Landais, D., and Ross, M. I. (2010) Multicenter phase II study of matured dendritic cells pulsed with melanoma cell line lysates in patients with advanced melanoma, *J Transl Med 8*, 89.

123. Ardon, H., Van Gool, S., Lopes, I. S., Maes, W., Sciot, R., Wilms, G., Demaerel, P., Bijttebier, P., Claes, L., Goffin, J., Van Calenbergh, F., and De Vleeschouwer, S. (2010) Integration of autologous dendritic cell-based immunotherapy in the primary treatment for patients with newly diagnosed glioblastoma multiforme: a pilot study, *J Neurooncol 99*, 261-272.

124. Marten, A., Flieger, D., Renoth, S., Weineck, S., Albers, P., Compes, M., Schottker, B.,

Ziske, C., Engelhart, S., Hanfland, P., Krizek, L., Faber, C., von Ruecker, A., Muller, S., Sauerbruch, T., and Schmidt-Wolf, I. G. (2002) Therapeutic vaccination against metastatic renal cell carcinoma by autologous dendritic cells: preclinical results and outcome of a first clinical phase I/II trial, *Cancer Immunol Immunother 51*, 637-644.

125. Casares, N., Pequignot, M. O., Tesniere, A., Ghiringhelli, F., Roux, S., Chaput, N., Schmitt, E., Hamai, A., Hervas-Stubbs, S., Obeid, M., Coutant, F., Metivier, D., Pichard, E., Aucouturier, P., Pierron, G., Garrido, C., Zitvogel, L., and Kroemer, G. (2005) Caspase-dependent immunogenicity of doxorubicin-induced tumor cell death, *J Exp Med 202*, 1691-1701.

126. Zitvogel, L., and Kroemer, G. (2009) Anticancer immunochemotherapy using adjuvants with direct cytotoxic effects, *J Clin Invest 119*, 2127-2130.

127. Zitvogel, L., Apetoh, L., Ghiringhelli, F., and Kroemer, G. (2008) Immunological aspects of cancer chemotherapy, *Nat Rev Immunol 8*, 59-73.

128. Tesniere, A., Apetoh, L., Ghiringhelli, F., Joza, N., Panaretakis, T., Kepp, O., Schlemmer, F., Zitvogel, L., and Kroemer, G. (2008) Immunogenic cancer cell death: a key-lock paradigm, *Curr Opin Immunol 20*, 504-511.

129. Tesniere, A., Panaretakis, T., Kepp, O., Apetoh, L., Ghiringhelli, F., Zitvogel, L., and Kroemer, G. (2008) Molecular characteristics of immunogenic cancer cell death, *Cell Death Differ 15*, 3-12.

130. Kepp, O., Tesniere, A., Schlemmer, F., Michaud, M., Senovilla, L., Zitvogel, L., and Kroemer, G. (2009) Immunogenic cell death modalities and their impact on cancer treatment, *Apoptosis 14*, 364-375.

131. Garg, A. D., Nowis, D., Golab, J., Vandenabeele, P., Krysko, D. V., and Agostinis, P. (2010) Immunogenic cell death, DAMPs and anticancer therapeutics: an emerging amalgamation, *Biochim Biophys Acta 1805*, 53-71.

132. Kroemer, G., and Zitvogel, L. (2007) Death, danger, and immunity: an infernal trio, *Immunol Rev 220*, 5-7.

133. Peachman, K. K., Rao, M., Palmer, D. R., Zidanic, M., Sun, W., Alving, C. R., and Rothwell, S. W. (2004) Functional microtubules are required for antigen processing by macrophages and dendritic cells, *Immunol Lett 95*, 13-24.

134. Jackman, R. W., Rhoads, M. G., Cornwell, E., and Kandarian, S. C. (2009) Microtubule-mediated NF-kappaB activation in the TNF-alpha signaling pathway, *Exp Cell Res 315*, 3242-3249.

135. Mizumoto, N., Gao, J., Matsushima, H., Ogawa, Y., Tanaka, H., and Takashima, A. (2005) Discovery of novel immunostimulants by dendritic-cell-based functional screening, *Blood 106*, 3082-3089.

136. Mizumoto, N., Tanaka, H., Matsushima, H., Vishwanath, M., and Takashima, A.

(2007) Colchicine promotes antigen cross-presentation by murine dendritic cells, *J Invest Dermatol 127*, 1543-1546.

137. Shin, J. Y., Lee, S. K., Kang, C. D., Chung, J. S., Lee, E. Y., Seo, S. Y., Lee, S. Y., Baek, S. Y., Kim, B. S., Kim, J. B., and Yoon, S. (2003) Antitumor effect of intratumoral administration of dendritic cell combination with vincristine chemotherapy in a murine fibrosarcoma model, *Histol Histopathol 18*, 435-447.

138. Shaha, S. P., Tomic, J., Shi, Y., Pham, T., Mero, P., White, D., He, L., Baryza, J. L., Wender, P. A., Booth, J. W., and Spaner, D. E. (2009) Prolonging microtubule dysruption enhances the immunogenicity of chronic lymphocytic leukaemia cells, *Clin Exp Immunol 158*, 186-198.

139. Fidler, I. J. (1973) Selection of successive tumour lines for metastasis, *Nat New Biol 242*, 148-149.

140. Brown, D. M., Fisher, T. L., Wei, C., Frelinger, J. G., and Lord, E. M. (2001) Tumours can act as adjuvants for humoral immunity, *Immunology 102*, 486-497.

141. Seliger, B., Wollscheid, U., Momburg, F., Blankenstein, T., and Huber, C. (2001) Characterization of the major histocompatibility complex class I deficiencies in B16 melanoma cells, *Cancer Res 61*, 1095-1099.

142. Nakamura, K., Yoshikawa, N., Yamaguchi, Y., Kagota, S., Shinozuka, K., and Kunitomo, M. (2002) Characterization of mouse melanoma cell lines by their mortal malignancy using an experimental metastatic model, *Life Sci 70*, 791-798.

143. DiLillo, D. J., Yanaba, K., and Tedder, T. F. (2010) B cells are required for optimal CD4+ and CD8+ T cell tumor immunity: therapeutic B cell depletion enhances B16 melanoma growth in mice, *J Immunol 184*, 4006-4016.

144. Li, L., Wang, H. K., Kuo, S. C., Wu, T. S., Mauger, A., Lin, C. M., Hamel, E., and Lee, K. H. (1994) Antitumor agents. 155. Synthesis and biological evaluation of 3',6,7-substituted 2-phenyl-4-quinolones as antimicrotubule agents, *J Med Chem 37*, 3400-3407.

145. Bohnenkamp, H. R., Coleman, J., Burchell, J. M., Taylor-Papadimitriou, J., and Noll, T. (2004) Breast carcinoma cell lysate-pulsed dendritic cells cross-prime MUC1-specific CD8+ T cells identified by peptide-MHC-class-I tetramers, *Cell Immunol 231*, 112-125.

146. Peiris, J. S., Guan, Y., and Yuen, K. Y. (2004) Severe acute respiratory syndrome, *Nat Med 10*, S88-97.

147. Cinatl, J., Morgenstern, B., Bauer, G., Chandra, P., Rabenau, H., and Doerr, H. W. (2003) Glycyrrhizin, an active component of liquorice roots, and replication of SARS-associated coronavirus, *Lancet 361*, 2045-2046.

148. Shah, V. A., and Chalam, K. V. (2009) Values for macular perimetry using the MP-1 microperimeter in normal subjects, *Ophthalmic Res 41*, 9-13.

149. Shi, Y. L., Li, L. H., Sun, Z. H., Chen, J. Y., Liao, Y., Zeng, L. L., Zhang, W., Chen, X. D., and Cao, C. (2010) [Study on the changing regularity of special antibody and expression of stomach and enteric involvement on SARS-coronavirus infection in the recovery period of severe acute respiratory syndrome.], *Zhonghua Liu Xing Bing Xue Za Zhi 31*, 795-799.

150. Lai, H. Y., Lim, Y. Y., and Tan, S. P. (2009) Antioxidative, tyrosinase inhibiting and antibacterial activities of leaf extracts from medicinal ferns, *Biosci Biotechnol Biochem 73*, 1362-1366.

151. Xu, Z., Chen, Z., Ge, F., and Zhang, K. (2001) [Determination of phospholipid in Cibotium barometz by supercritical fluid extraction and RP-HPLC], *Zhong Yao Cai 24*, 174-175.

152. Patel, A. K., and Boyd, P. N. (1995) An improved assay for antibody dependent cellular cytotoxicity based on time resolved fluorometry, *J Immunol Methods 184*, 29-38.

153. Nakamura, S., Akiguchi, I., and Kimura, J. (1995) Topographic distributions of monoamine oxidase-B-containing neurons in the mouse striatum, *Neurosci Lett 184*, 29-31.

154. Raevuori, A., Keski-Rahkonen, A., Hoek, H. W., Sihvola, E., Rissanen, A., and Kaprio, J. (2008) Lifetime anorexia nervosa in young men in the community: five cases and their co-twins, *Int J Eat Disord 41*, 458-463.

155. Li, Y. Y., Zhang, Y. J., Zhou, Y., Yang, J. L., and Zheng, S. J. (2009) Protecting cell walls from binding aluminum by organic acids contributes to aluminum resistance, *J Integr Plant Biol 51*, 574-580.

156. Formarier, M., Poirier Coutansais, G., and Psiuk, T. (1999) [The organizing concepts of science, their application to nursing care], *Rech Soins Infirm*, 6-18.

157. Jackson, J. R., Patrick, D. R., Dar, M. M., and Huang, P. S. (2007) Targeted anti-mitotic therapies: can we improve on tubulin agents?, *Nat Rev Cancer 7*, 107-117.

158. Maecker, H. L., Koumenis, C., and Giaccia, A. J. (2000) p53 promotes selection for Fas-mediated apoptotic resistance, *Cancer Res 60*, 4638-4644.

159. Jeong, Y. J., Hong, S. W., Kim, J. H., Jin, D. H., Kang, J. S., Lee, W. J., and Hwang, Y. I. (2011) Vitamin C-treated murine bone marrow-derived dendritic cells preferentially drive naive T cells into Th1 cells by increased IL-12 secretions, *Cell Immunol 266*, 192-199.

160. Liang, S., Krauss, J. L., Domon, H., McIntosh, M. L., Hosur, K. B., Qu, H., Li, F., Tzekou, A., Lambris, J. D., and Hajishengallis, G. (2011) The C5a receptor impairs IL-12-dependent clearance of Porphyromonas gingivalis and is required for induction of periodontal bone loss, *J Immunol 186*, 869-877.

161. Emerson, R. E., and Ulbright, T. M. (2010) Intratubular germ cell neoplasia of the testis and its associated cancers: the use of novel biomarkers, *Pathology 42*, 344-355.

162. Lo, S. L., Cai, C. Z., Chen, Y. Z., and Chung, M. C. (2005) Effect of training datasets on support vector machine prediction of protein-protein interactions, *Proteomics 5*, 876-884.

163. Peterson, D., Kaakko, T., Smart, E., Jorgenson, M., and Herzog, C. (2007) Dental students attitudes regarding online education in pediatric dentistry, *J Dent Child (Chic) 74*, 10-20.

164. Labeur, M. S., Roters, B., Pers, B., Mehling, A., Luger, T. A., Schwarz, T., and Grabbe, S. (1999) Generation of tumor immunity by bone marrow-derived dendritic cells correlates with dendritic cell maturation stage, *J Immunol 162*, 168-175.

165. Counihan, T. C., Roberts, P. L., Schoetz, D. J., Jr., Coller, J. A., Murray, J. J., and Veidenheimer, M. C. (1994) Fertility and sexual and gynecologic function after ileal pouch-anal anastomosis, *Dis Colon Rectum 37*, 1126-1129.

166. Egilmez, N. K., and Kilinc, M. O. (2010) Tumor-resident CD8+ T-cell: the critical catalyst in IL-12-mediated reversal of tumor immune suppression, *Arch Immunol Ther Exp (Warsz) 58*, 399-405.

167. van de Kerkhof, P. C. (2010) Novel biologic therapies in development targeting IL-12/IL-23, *J Eur Acad Dermatol Venereol 24 Suppl 6*, 5-9.

168. Nagai, T., Yanagida, T., and Hirohata, S. (2011) Anti-ribosomal P protein antibody induces Th1 responses by enhancing the production of IL-12 in activated monocytes, *Mod Rheumatol 21*, 57-62.

169. Hiroishi, K., Eguchi, J., Baba, T., Shimazaki, T., Ishii, S., Hiraide, A., Sakaki, M., Doi, H., Uozumi, S., Omori, R., Matsumura, T., Yanagawa, T., Ito, T., and Imawari, M. (2010) Strong CD8(+) T-cell responses against tumor-associated antigens prolong the recurrence-free interval after tumor treatment in patients with hepatocellular carcinoma, *J Gastroenterol 45*, 451-458.

170. Li, Y. R., Zhang, H. Y., Jin, Z. J., Li, Y. L., and Wang, L. (2010) [Gene therapy based on inducible IL-12 gene in a mouse model of orthotopically transplanted H22 hepatoma], *Zhonghua Zhong Liu Za Zhi 32*, 487-491.

171. Koutruba, N., Emer, J., and Lebwohl, M. (2010) Review of ustekinumab, an interleukin-12 and interleukin-23 inhibitor used for the treatment of plaque psoriasis, *Ther Clin Risk Manag 6*, 123-141.

172. Sakamoto, M., Mori, T., Masugi, Y., Effendi, K., Rie, I., and Du, W. (2008) Candidate molecular markers for histological diagnosis of early hepatocellular carcinoma, *Intervirology 51 Suppl 1*, 42-45.

173. Weger, W. (2010) Current status and new developments in the treatment of

psoriasis and psoriatic arthritis with biological agents, *Br J Pharmacol 160*, 810-820.

174. Tourret, M., Guegan, S., Chemin, K., Dogniaux, S., Miro, F., Bohineust, A., and Hivroz, C. (2010) T cell polarity at the immunological synapse is required for CD154-dependent IL-12 secretion by dendritic cells, *J Immunol 185*, 6809-6818.

175. Lavoie, P. M., Huang, Q., Jolette, E., Whalen, M., Nuyt, A. M., Audibert, F., Speert, D. P., Lacaze-Masmonteil, T., Soudeyns, H., and Kollmann, T. R. (2010) Profound lack of interleukin (IL)-12/IL-23p40 in neonates born early in gestation is associated with an increased risk of sepsis, *J Infect Dis 202*, 1754-1763.

176. Xu, M., Mizoguchi, I., Morishima, N., Chiba, Y., Mizuguchi, J., and Yoshimoto, T. (2010) Regulation of antitumor immune responses by the IL-12 family cytokines, IL-12, IL-23, and IL-27, *Clin Dev Immunol 2010*.

177. Filmus, J., Capurro, M., and Rast, J. (2008) Glypicans, *Genome Biol 9*, 224.

178. Nagai, H., Oniki, S., Fujiwara, S., Yoshimoto, T., and Nishigori, C. (2010) Antimelanoma immunotherapy: clinical and preclinical applications of IL-12 family members, *Immunotherapy 2*, 697-709.

179. Sukumaran, S., Pittman, K. B., Patterson, W. K., Dickson, J., Yeend, S., Townsend, A., Broadbridge, V., and Price, T. J. (2010) A phase I study to determine the safety, tolerability and maximum tolerated dose of green-lipped mussel (Perna canaliculus) lipid extract, in patients with advanced prostate and breast cancer, *Ann Oncol 21*, 1089-1093.

180. Pavelko, K. D., Heckman, K. L., Hansen, M. J., and Pease, L. R. (2008) An effective vaccine strategy protective against antigenically distinct tumor variants, *Cancer Res 68*, 2471-2478.

181. Inaba, K., Inaba, M., Romani, N., Aya, H., Deguchi, M., Ikehara, S., Muramatsu, S., and Steinman, R. M. (1992) Generation of large numbers of dendritic cells from mouse bone marrow cultures supplemented with granulocyte/macrophage colony-stimulating factor, *J Exp Med 176*, 1693-1702.

182. Drosten, C., Gunther, S., Preiser, W., van der Werf, S., Brodt, H. R., Becker, S., Rabenau, H., Panning, M., Kolesnikova, L., Fouchier, R. A., Berger, A., Burguiere, A. M., Cinatl, J., Eickmann, M., Escriou, N., Grywna, K., Kramme, S., Manuguerra, J. C., Muller, S., Rickerts, V., Sturmer, M., Vieth, S., Klenk, H. D., Osterhaus, A. D., Schmitz, H., and Doerr, H. W. (2003) Identification of a novel coronavirus in patients with severe acute respiratory syndrome, *N Engl J Med 348*, 1967-1976.

183. Ksiazek, T. G., Erdman, D., Goldsmith, C. S., Zaki, S. R., Peret, T., Emery, S., Tong, S., Urbani, C., Comer, J. A., Lim, W., Rollin, P. E., Dowell, S. F., Ling, A. E., Humphrey, C. D., Shieh, W. J., Guarner, J., Paddock, C. D., Rota, P., Fields, B., DeRisi, J., Yang, J. Y., Cox, N., Hughes, J. M., LeDuc, J. W., Bellini, W. J., and Anderson, L. J. (2003) A novel

coronavirus associated with severe acute respiratory syndrome, *N Engl J Med 348*, 1953-1966.

184.   Kuiken, T., Fouchier, R. A., Schutten, M., Rimmelzwaan, G. F., van Amerongen, G., van Riel, D., Laman, J. D., de Jong, T., van Doornum, G., Lim, W., Ling, A. E., Chan, P. K., Tam, J. S., Zambon, M. C., Gopal, R., Drosten, C., van der Werf, S., Escriou, N., Manuguerra, J. C., Stohr, K., Peiris, J. S., and Osterhaus, A. D. (2003) Newly discovered coronavirus as the primary cause of severe acute respiratory syndrome, *Lancet 362*, 263-270.

185.   Cinatl, J., Jr., Michaelis, M., Hoever, G., Preiser, W., and Doerr, H. W. (2005) Development of antiviral therapy for severe acute respiratory syndrome, *Antiviral Res 66*, 81-97.

186.   Hoever, G., Baltina, L., Michaelis, M., Kondratenko, R., Baltina, L., Tolstikov, G. A., Doerr, H. W., and Cinatl, J., Jr. (2005) Antiviral activity of glycyrrhizic acid derivatives against SARS-coronavirus, *J Med Chem 48*, 1256-1259.

187.   Holmes, K. V. (2003) SARS coronavirus: a new challenge for prevention and therapy, *J Clin Invest 111*, 1605-1609.

188.   Peiris, J. S., Yuen, K. Y., Osterhaus, A. D., and Stohr, K. (2003) The severe acute respiratory syndrome, *N Engl J Med 349*, 2431-2441.

189.   So, L. K., Lau, A. C., Yam, L. Y., Cheung, T. M., Poon, E., Yung, R. W., and Yuen, K. Y. (2003) Development of a standard treatment protocol for severe acute respiratory syndrome, *Lancet 361*, 1615-1617.

190.   Stroher, U., DiCaro, A., Li, Y., Strong, J. E., Aoki, F., Plummer, F., Jones, S. M., and Feldmann, H. (2004) Severe acute respiratory syndrome-related coronavirus is inhibited by interferon- alpha, *J Infect Dis 189*, 1164-1167.

191.   Chan, K. S., Lai, S. T., Chu, C. M., Tsui, E., Tam, C. Y., Wong, M. M., Tse, M. W., Que, T. L., Peiris, J. S., Sung, J., Wong, V. C., and Yuen, K. Y. (2003) Treatment of severe acute respiratory syndrome with lopinavir/ritonavir: a multicentre retrospective matched cohort study, *Hong Kong Med J 9*, 399-406.

192.   Chu, C. M., Poon, L. L., Cheng, V. C., Chan, K. S., Hung, I. F., Wong, M. M., Chan, K. H., Leung, W. S., Tang, B. S., Chan, V. L., Ng, W. L., Sim, T. C., Ng, P. W., Law, K. I., Tse, D. M., Peiris, J. S., and Yuen, K. Y. (2004) Initial viral load and the outcomes of SARS, *Cmaj 171*, 1349-1352.

193.   Groneberg, D. A., Poutanen, S. M., Low, D. E., Lode, H., Welte, T., and Zabel, P. (2005) Treatment and vaccines for severe acute respiratory syndrome, *Lancet Infect Dis 5*, 147-155.

194.   Stadler, K., Masignani, V., Eickmann, M., Becker, S., Abrignani, S., Klenk, H. D., and Rappuoli, R. (2003) SARS--beginning to understand a new virus, *Nat Rev Microbiol 1*, 209-218.

195. Lai, S. T. (2005) Treatment of severe acute respiratory syndrome, *Eur J Clin Microbiol Infect Dis 24*, 583-591.

196. Kliger, Y., Levanon, E. Y., and Gerber, D. (2005) From genome to antivirals: SARS as a test tube, *Drug Discov Today 10*, 345-352.

197. De Clercq, E. (2004) Antivirals and antiviral strategies, *Nat Rev Microbiol 2*, 704-720.

198. Gallagher, T. M., and Buchmeier, M. J. (2001) Coronavirus spike proteins in viral entry and pathogenesis, *Virology 279*, 371-374.

199. Chen, Y. H., Chen, A. P., Chen, C. T., Wang, A. H., and Liang, P. H. (2002) Probing the conformational change of Escherichia coli undecaprenyl pyrophosphate synthase during catalysis using an inhibitor and tryptophan mutants, *J Biol Chem 277*, 7369-7376.

200. Kuo, C. J., Chi, Y. H., Hsu, J. T., and Liang, P. H. (2004) Characterization of SARS main protease and inhibitor assay using a fluorogenic substrate, *Biochem Biophys Res Commun 318*, 862-867.

201. Barnard, D. L., Hubbard, V. D., Burton, J., Smee, D. F., Morrey, J. D., Otto, M. J., and Sidwell, R. W. (2004) Inhibition of severe acute respiratory syndrome-associated coronavirus (SARSCoV) by calpain inhibitors and beta-D-N4-hydroxycytidine, *Antivir Chem Chemother 15*, 15-22.

202. Amici, C., Di Coro, A., Ciucci, A., Chiappa, L., Castilletti, C., Martella, V., Decaro, N., Buonavoglia, C., Capobianchi, M. R., and Santoro, M. G. (2006) Indomethacin has a potent antiviral activity against SARS coronavirus, *Antivir Ther 11*, 1021-1030.

203. Chen, C. J., Michaelis, M., Hsu, H. K., Tsai, C. C., Yang, K. D., Wu, Y. C., Cinatl, J., Jr., and Doerr, H. W. (2008) Toona sinensis Roem tender leaf extract inhibits SARS coronavirus replication, *J Ethnopharmacol 120*, 108-111.

204. Li, S. Y., Chen, C., Zhang, H. Q., Guo, H. Y., Wang, H., Wang, L., Zhang, X., Hua, S. N., Yu, J., Xiao, P. G., Li, R. S., and Tan, X. (2005) Identification of natural compounds with antiviral activities against SARS-associated coronavirus, *Antiviral Res 67*, 18-23.

205. Lin, C. W., Tsai, F. J., Tsai, C. H., Lai, C. C., Wan, L., Ho, T. Y., Hsieh, C. C., and Chao, P. D. (2005) Anti-SARS coronavirus 3C-like protease effects of Isatis indigotica root and plant-derived phenolic compounds, *Antiviral Res 68*, 36-42.

206. Ryu, Y. B., Jeong, H. J., Kim, J. H., Kim, Y. M., Park, J. Y., Kim, D., Nguyen, T. T., Park, S. J., Chang, J. S., Park, K. H., Rho, M. C., and Lee, W. S. (2010) Biflavonoids from Torreya nucifera displaying SARS-CoV 3CL(pro) inhibition, *Bioorg Med Chem 18*, 7940-7947.

207. Wu, C. Y., Jan, J. T., Ma, S. H., Kuo, C. J., Juan, H. F., Cheng, Y. S., Hsu, H. H., Huang, H. C., Wu, D., Brik, A., Liang, F. S., Liu, R. S., Fang, J. M., Chen, S. T., Liang, P. H., and

Wong, C. H. (2004) Small molecules targeting severe acute respiratory syndrome human coronavirus, *Proc Natl Acad Sci U S A 101*, 10012-10017.

208. Wen, C. C., Kuo, Y. H., Jan, J. T., Liang, P. H., Wang, S. Y., Liu, H. G., Lee, C. K., Chang, S. T., Kuo, C. J., Lee, S. S., Hou, C. C., Hsiao, P. W., Chien, S. C., Shyur, L. F., and Yang, N. S. (2007) Specific plant terpenoids and lignoids possess potent antiviral activities against severe acute respiratory syndrome coronavirus, *J Med Chem 50*, 4087-4095.

209. Yang, H., Yang, M., Ding, Y., Liu, Y., Lou, Z., Zhou, Z., Sun, L., Mo, L., Ye, S., Pang, H., Gao, G. F., Anand, K., Bartlam, M., Hilgenfeld, R., and Rao, Z. (2003) The crystal structures of severe acute respiratory syndrome virus main protease and its complex with an inhibitor, *Proc Natl Acad Sci U S A 100*, 13190-13195.

210. Cleri, D. J., Ricketti, A. J., and Vernaleo, J. R. (2010) Severe acute respiratory syndrome (SARS), *Infect Dis Clin North Am 24*, 175-202.

211. Cheng, S. S., Wu, C. L., Chang, H. T., Kao, Y. T., and Chang, S. T. (2004) Antitermitic and antifungal activities of essential oil of Calocedrus formosana leaf and its composition, *J Chem Ecol 30*, 1957-1967.

212. Chang, S. T., Cheng, S. S., and Wang, S. Y. (2001) Antitermitic activity of essential oils and components from Taiwania (Taiwania cryptomerioides), *J Chem Ecol 27*, 717-724.

213. Zhang, X. W., and Yap, Y. L. (2004) Old drugs as lead compounds for a new disease? Binding analysis of SARS coronavirus main proteinase with HIV, psychotic and parasite drugs, *Bioorg Med Chem 12*, 2517-2521.

214. Lau, K. M., Lee, K. M., Koon, C. M., Cheung, C. S., Lau, C. P., Ho, H. M., Lee, M. Y., Au, S. W., Cheng, C. H., Lau, C. B., Tsui, S. K., Wan, D. C., Waye, M. M., Wong, K. B., Wong, C. K., Lam, C. W., Leung, P. C., and Fung, K. P. (2008) Immunomodulatory and anti-SARS activities of Houttuynia cordata, *J Ethnopharmacol 118*, 79-85.

215. Wu, C. J., Jan, J. T., Chen, C. M., Hsieh, H. P., Hwang, D. R., Liu, H. W., Liu, C. Y., Huang, H. W., Chen, S. C., Hong, C. F., Lin, R. K., Chao, Y. S., and Hsu, J. T. (2004) Inhibition of severe acute respiratory syndrome coronavirus replication by niclosamide, *Antimicrob Agents Chemother 48*, 2693-2696.

216. Shie, J. J., Fang, J. M., Kuo, C. J., Kuo, T. H., Liang, P. H., Huang, H. J., Yang, W. B., Lin, C. H., Chen, J. L., Wu, Y. T., and Wong, C. H. (2005) Discovery of potent anilide inhibitors against the severe acute respiratory syndrome 3CL protease, *J Med Chem 48*, 4469-4473.

217. Liang, P. H. (2006) Characterization and inhibition of SARS-coronavirus main protease, *Curr Top Med Chem 6*, 361-376.

218. Mayaux, J. F., Bousseau, A., Pauwels, R., Huet, T., Henin, Y., Dereu, N., Evers, M., Soler, F., Poujade, C., De Clercq, E., and et al. (1994) Triterpene derivatives that

block entry of human immunodeficiency virus type 1 into cells, *Proc Natl Acad Sci U S A 91*, 3564-3568.

219. Reissman, P. (1996) Significance of anal canal ultrasound before sphincterotomy in multiparous women with anal fissure, *Dis Colon Rectum 39*, 1060.

220. Soler, F., Poujade, C., Evers, M., Carry, J. C., Henin, Y., Bousseau, A., Huet, T., Pauwels, R., De Clercq, E., Mayaux, J. F., Le Pecq, J. B., and Dereu, N. (1996) Betulinic acid derivatives: a new class of specific inhibitors of human immunodeficiency virus type 1 entry, *J Med Chem 39*, 1069-1083.

221. Ito, J., Chang, F. R., Wang, H. K., Park, Y. K., Ikegaki, M., Kilgore, N., and Lee, K. H. (2001) Anti-AIDS agents. 48.(1) Anti-HIV activity of moronic acid derivatives and the new melliferone-related triterpenoid isolated from Brazilian propolis, *J Nat Prod 64*, 1278-1281.

222. Batista, O., Simoes, M. F., Duarte, A., Valdeira, M. L., de la Torre, M. C., and Rodriguez, B. (1995) An antimicrobial abietane from the root of Plectranthus hereroensis, *Phytochemistry 38*, 167-169.

223. Gigante, B., Santos, C., Silva, A. M., Curto, M. J., Nascimento, M. S., Pinto, E., Pedro, M., Cerqueira, F., Pinto, M. M., Duarte, M. P., Laires, A., Rueff, J., Goncalves, J., Pegado, M. I., and Valdeira, M. L. (2003) Catechols from abietic acid synthesis and evaluation as bioactive compounds, *Bioorg Med Chem 11*, 1631-1638.

224. Fonseca, T., Gigante, B., Marques, M. M., Gilchrist, T. L., and De Clercq, E. (2004) Synthesis and antiviral evaluation of benzimidazoles, quinoxalines and indoles from dehydroabietic acid, *Bioorg Med Chem 12*, 103-112.

225. Staschke, K. A., Hatch, S. D., Tang, J. C., Hornback, W. J., Munroe, J. E., Colacino, J. M., and Muesing, M. A. (1998) Inhibition of influenza virus hemagglutinin-mediated membrane fusion by a compound related to podocarpic acid, *Virology 248*, 264-274.

226. Paris, A., Strukelj, B., Renko, M., Turk, V., Pukl, M., Umek, A., and Korant, B. D. (1993) Inhibitory effect of carnosic acid on HIV-1 protease in cell-free assays [corrected], *J Nat Prod 56*, 1426-1430.

227. Aruoma, O. I., Spencer, J. P., Rossi, R., Aeschbach, R., Khan, A., Mahmood, N., Munoz, A., Murcia, A., Butler, J., and Halliwell, B. (1996) An evaluation of the antioxidant and antiviral action of extracts of rosemary and Provencal herbs, *Food Chem Toxicol 34*, 449-456.

228. Charlton, J. L. (1998) Antiviral activity of lignans, *J Nat Prod 61*, 1447-1451.

229. Eich, E., Pertz, H., Kaloga, M., Schulz, J., Fesen, M. R., Mazumder, A., and Pommier, Y. (1996) (-)-Arctigenin as a lead structure for inhibitors of human immunodeficiency virus type-1 integrase, *J Med Chem 39*, 86-95.

230. Hara, H., Fujihashi, T., Sakata, T., Kaji, A., and Kaji, H. (1997) Tetrahydronaphthalene

lignan compounds as potent anti-HIV type 1 agents, *AIDS Res Hum Retroviruses 13*, 695-705.

231. Joe, B., Vijaykumar, M., and Lokesh, B. R. (2004) Biological properties of curcumin-cellular and molecular mechanisms of action, *Crit Rev Food Sci Nutr 44*, 97-111.

232. Shao, F., Wang, G., Xie, H., Zhu, X., Sun, J., and A, J. (2007) Pharmacokinetic study of triptolide, a constituent of immunosuppressive chinese herb medicine, in rats, *Biol Pharm Bull 30*, 702-707.

233. Cheng, X., Shin, Y. G., Levine, B. S., Smith, A. C., Tomaszewski, J. E., and van Breemen, R. B. (2003) Quantitative analysis of betulinic acid in mouse, rat and dog plasma using electrospray liquid chromatography/mass spectrometry, *Rapid Commun Mass Spectrom 17*, 2089-2092.

234. Jeong, D. W., Kim, Y. H., Kim, H. H., Ji, H. Y., Yoo, S. D., Choi, W. R., Lee, S. M., Han, C. K., and Lee, H. S. (2007) Dose-linear pharmacokinetics of oleanolic acid after intravenous and oral administration in rats, *Biopharm Drug Dispos 28*, 51-57.

235. Wang, C. Y., Sun, S. W., and Lee, S. S. (2004) Pharmacokinetic and metabolic studies of retrojusticidin B, a potential anti-viral lignan, in rats, *Planta Med 70*, 1161-1165.

236. Tsai, T. H., Chou, C. J., Cheng, F. C., and Chen, C. F. (1994) Pharmacokinetics of honokiol after intravenous administration in rats assessed using high-performance liquid chromatography, *J Chromatogr B Biomed Appl 655*, 41-45.

237. Chen, C. N., Lin, C. P., Huang, K. K., Chen, W. C., Hsieh, H. P., Liang, P. H., and Hsu, J. T. (2005) Inhibition of SARS-CoV 3C-like Protease Activity by Theaflavin-3,3'-digallate (TF3), *Evid Based Complement Alternat Med 2*, 209-215.

238. Cuong, N. X., Minh, C. V., Kiem, P. V., Huong, H. T., Ban, N. K., Nhiem, N. X., Tung, N. H., Jung, J. W., Kim, H. J., Kim, S. Y., Kim, J. A., and Kim, Y. H. (2009) Inhibitors of osteoclast formation from rhizomes of Cibotium barometz, *J Nat Prod 72*, 1673-1677.

239. Jiang, W. X., and Xue, B. Y. (2005) [Hepatoprotective effects of Gentiana scabra on the acute liver injuries in mice], *Zhongguo Zhong Yao Za Zhi 30*, 1105-1107.

240. Chueh, F. S., Chen, C. C., Sagare, A. P., and Tsay, H. S. (2001) Quantitative determination of secoiridoid glucosides in in vitro propagated plants of Gentiana davidii var. formosana by high performance liquid chromatography, *Planta Med 67*, 70-73.

241. Kakuda, R., Iijima, T., Yaoita, Y., Machida, K., and Kikuchi, M. (2001) Secoiridoid glycosides from Gentiana scabra, *J Nat Prod 64*, 1574-1575.

242. Kim, J. A., Son, N. S., Son, J. K., Jahng, Y., Chang, H. W., Jang, T. S., Na, M., and Lee, S. H. (2009) Two new secoiridoid glycosides from the rhizomes of Gentiana scabra

Bunge, *Arch Pharm Res 32*, 863-867.

243. Su, P. F., Staniforth, V., Li, C. J., Wang, C. Y., Chiao, M. T., Wang, S. Y., Shyur, L. F., and Yang, N. S. (2008) Immunomodulatory effects of phytocompounds characterized by in vivo transgenic human GM-CSF promoter activity in skin tissues, *J Biomed Sci 15*, 813-822.

244. Su, P. F., Li, C. J., Hsu, C. C., Benson, S., Wang, S. Y., Aravindaram, K., Chan, S. I., Wu, S. H., Yang, F. L., Huang, C. H., Shyur, L. F., and Yang, N. S. (2011) Dioscorea phytocompounds enhance murine splenocyte proliferation ex vivo and improve regeneration of bone marrow cells in vivo, *Evidence-Based Complementary and Alternative Medicine 2011*, 1-11.

245. Jin, M., Suh, S. J., Yang, J. H., Lu, Y., Kim, S. J., Kwon, S., Jo, T. H., Kim, J. W., Park, Y. I., Ahn, G. W., Lee, C. K., Kim, C. H., Son, J. K., Son, K. H., and Chang, H. W. (2010) Anti-inflammatory activity of bark of Dioscorea batatas DECNE through the inhibition of iNOS and COX-2 expressions in RAW264.7 cells via NF-kappaB and ERK1/2 inactivation, *Food Chem Toxicol 48*, 3073-3079.

246. Kim, H. Y., Eo, E. Y., Park, H., Kim, Y. C., Park, S., Shin, H. J., and Kim, K. (2010) Medicinal herbal extracts of Sophorae radix, Acanthopanacis cortex, Sanguisorbae radix and Torilis fructus inhibit coronavirus replication in vitro, *Antivir Ther 15*, 697-709.

247. Hyun, S. K., Lee, H., Kang, S. S., Chung, H. Y., and Choi, J. S. (2009) Inhibitory activities of Cassia tora and its anthraquinone constituents on angiotensin-converting enzyme, *Phytother Res 23*, 178-184.

248. Cho, I. J., Lee, C., and Ha, T. Y. (2007) Hypolipidemic effect of soluble fiber isolated from seeds of Cassia tora Linn. in rats fed a high-cholesterol diet, *J Agric Food Chem 55*, 1592-1596.

249. Hatano, T., Uebayashi, H., Ito, H., Shiota, S., Tsuchiya, T., and Yoshida, T. (1999) Phenolic constituents of Cassia seeds and antibacterial effect of some naphthalenes and anthraquinones on methicillin-resistant Staphylococcus aureus, *Chem Pharm Bull (Tokyo) 47*, 1121-1127.

250. Kim, Y. M., Lee, C. H., Kim, H. G., and Lee, H. S. (2004) Anthraquinones isolated from Cassia tora (Leguminosae) seed show an antifungal property against phytopathogenic fungi, *J Agric Food Chem 52*, 6096-6100.

251. Wu, C. H., and Yen, G. C. (2004) Antigenotoxic properties of Cassia tea (Cassia tora L.): mechanism of action and the influence of roasting process, *Life Sci 76*, 85-101.

252. Wang, Y., Deng, M., Zhang, S. Y., Zhou, Z. K., and Tian, W. X. (2008) Parasitic loranthus from Loranthaceae rather than Viscaceae potently inhibits fatty acid synthase and reduces body weight in mice, *J Ethnopharmacol 118*, 473-478.

253. Wang, Y., Zhang, S. Y., Ma, X. F., and Tian, W. X. (2006) Potent inhibition of fatty

acid synthase by parasitic loranthus [Taxillus chinensis (dc.) danser] and its constituent avicularin, *J Enzyme Inhib Med Chem 21*, 87-93.

254. Yi, L., Li, Z., Yuan, K., Qu, X., Chen, J., Wang, G., Zhang, H., Luo, H., Zhu, L., Jiang, P., Chen, L., Shen, Y., Luo, M., Zuo, G., Hu, J., Duan, D., Nie, Y., Shi, X., Wang, W., Han, Y., Li, T., Liu, Y., Ding, M., Deng, H., and Xu, X. (2004) Small molecules blocking the entry of severe acute respiratory syndrome coronavirus into host cells, *J Virol 78*, 11334-11339.

255. Tan, E. L., Ooi, E. E., Lin, C. Y., Tan, H. C., Ling, A. E., Lim, B., and Stanton, L. W. (2004) Inhibition of SARS coronavirus infection in vitro with clinically approved antiviral drugs, *Emerg Infect Dis 10*, 581-586.

256. Okamura-Ikeda, K., Kameoka, N., Fujiwara, K., and Motokawa, Y. (2003) Probing the H-protein-induced conformational change and the function of the N-terminal region of Escherichia coli T-protein of the glycine cleavage system by limited proteolysis, *J Biol Chem 278*, 10067-10072.